Mechanisms Underlying Neurovascular Interactions:

Blood-Brain Barrier and Neurovascular Coupling

A dissertation presented

by

Brian Wai Chow

to

The Division of Medical Sciences

in partial fulfillment of the requirements

for the degree of

Doctor of Philosophy

in the subject of

Neurobiology

Harvard University

Cambridge, Massachusetts

April 2019

Dissertation Advisor: Dr. Chenghua Gu Brian Wai Chow

Mechanisms Underlying Neurovascular Interactions: Blood-Brain Barrier and Neurovascular Coupling

Abstract

To continuously compute neural activity for perception, motor movements and cognition, the central nervous system (CNS) requires a homeostatic microenvironment that is not only enriched in nutrients to meet its high metabolic demands but also devoid of toxins to prevent harm to the sensitive neural tissue. To establish and maintain this highly regulated microenvironment, the CNS has induced its vasculature to evolve two functions that are absent in the vasculature of peripheral organs: 1) blood-CNS barrier formation and 2) neurovascular coupling. Blood-CNS barriers partition the circulating blood from the CNS and regulate the selective trafficking of substances between the blood and the CNS. Neurovascular coupling ensures that following local neural activation, regional blood flow increases quickly to supply more nutrients and dispel metabolic waste.

The goal of this dissertation is to show how the CNS vasculature acquires, maintains and executes these two functions for optimal neural function. First, we provide a mechanism of how the CNS vasculature forms the blood-CNS barrier during development. Using a combination of mouse genetics, light and electron microscopy, we showed that nascent CNS vessels initially lack a blood-CNS barrier. However, through development, they gradually acquire barrier properties from the neural environment. Specifically, we identified that nascent CNS vessels already have functional tight junctions but display bulk transcytosis, resulting in the immature

barrier. However, through development, nascent CNS vessels gradually suppress transcytosis and eventually form a functional blood-CNS barrier.

Second, we demonstrate that CNS arteriolar endothelial cells (aECs), a segment of the CNS vasculature, play an active role to mediate neurovascular coupling. Using mouse genetics, two-photon imaging, electron and light microscopy, we find that aECs, unlike other segments of endothelial cells in the CNS vasculature, have abundant caveolae. CNS aECs use caveolae to mediate neurovascular coupling, as ablation of caveolae specifically in aECs disrupts neurovascular coupling. Furthermore, this caveolae-mediated pathway is independent of the eNOS-mediated pathway. Finally, we find that Mfsd2a, a suppressor of caveolae in capillary endothelial cells to ensure functional blood-CNS barrier integrity, is absent in aECs. Ectopic expression of Mfsd2a in CNS aECs deters caveolae formation and concurrently, impairs neurovascular coupling.

Table of Contents

Acknowledgments

There are many people who have supported and guided me through my graduate studies. First, I thank Chenghua for providing me the opportunities to develop my creativity, curiosity and independence. I am grateful that she had faith in my scientific development to pioneer a new research program in her lab, specifically neurovascular coupling. She has also been a great mentor, providing both personal and professional advice. I will miss chatting and working with her.

Chenghua is deft in assembling an amazing team of talented scientist. I thank all the Gu lab members for their support and advice. I had the unique opportunity to be sandwich between two different generations of Gu lab colleges. First, I thank Ayal Ben-Zvi, Aleks Tata and Baptiste Lacoste, who would great mentors when I first joined the lab. Second, I thank Ben Andreone who not only supported me as a fellow graduate student but also as a best friend. Third, I thank my co-author colleague, Vince Nunez, on my second thesis project. It has been fun developing the neurovascular coupling platform with him and I will miss working with him.

I would like to thank the Program in Neuroscience and Department of Neurobiology at Harvard Medical School for their providing an intimate community to learn. Thank you to Liz Benecchi, Maria Ericsson, Louise Trakimas and Peg Coughlin for their help with electron microscopy support! Thank you to Drs. David Ginty, Parica D'Amore and Jonathan Cohen for their invaluable guidance and support as DAC members throughout my graduate training and career development! I am grateful to Drs. Gary Yellen, Chuck Weitz and David Boas for their time to serve on my exam committee.

The ascent of my scientific training began with Dr. Ardem Patapoutian's lab at The Scripps Research Institute. Thank you Ardem, Sanjeev Ranade and Elena Gastelum for the

support and guidance as an undergraduate researcher. You all really inspired my interest and curiosity in life science.

Also, I would like to thank my family and friends. Thanks to my college friends, Kim Nguyen and Rachel Cheong. You made UC San Diego unique, fun and special for me. Thanks to all my amazing graduate school friends, especially Aurora Zhang, Chris Tzeng, Ben Andreone, Chester Chia and Shan Shan Wang. You guys have made graduate school and these past six years the most memorable parts of my life. Finally, thank you, Baba and Mom, for their unconditional support and love. You have sacrificed so much to provide amazing opportunities for me. Also, thank you to the MacDonald family for their generosity and love. You have welcomed me to the family and I am so grateful. Finally, thank you to Shane Macdonald, who has been my rock and inspiration during graduate school. I cannot wait to make more memories with you!

CHAPTER 1

Introduction

A part of Chapter 1 is adopted from a publication in *Trends in Neuroscience* (August 20, 2015)

The Molecular Constituents of the Blood-Brain Barrier

Brian Wai Chow[1] and Chenghua Gu[1,*]

[1]Department of Neurobiology, Harvard Medical School, 220 Longwood Avenue, Boston, Massachusetts, 02115, USA

[*]Correspondence: Chenghua_gu@hms.harvard.edu

Our central nervous system (CNS) grants us the abilities to sense our environment, move our body and learn new knowledge. To continuously execute these functions, the CNS has a high metabolic demand (Zlokovic, 2008). For example, although the brain comprises just 2% of our total body mass, it consumes 20% of our body's energy at rest (Andreone et al., 2015). However, unlike other metabolically costly organs such as the liver and muscle, the brain has a negligible energy storage (Zlokovic, 2011). Instead, to satisfy the brain's high metabolic consumption, the CNS vasculature has evolved two unique functions absent in the vasculature of peripheral organs. These two functions are 1) neurovascular coupling, a process where increased local neural activation accelerates local blood flow to replenish nutrients as well as clear waste, and 2) formation of the Blood-CNS Barrier, a physiological barrier that regulates the selective trafficking of substances between the blood and the CNS, such as importing desirable nutrients but excluding harmful toxins (Andreone et al., 2015). Here, I will first highlight the formation of blood-CNS barrier and then summarize our current understanding of neurovascular coupling.

1.1. History and location of the Blood-CNS Barriers

Blood-CNS Barriers, which includes the blood-brain barrier (BBB), blood-spinal cord barrier and blood-retinal barrier, were first observed over a century ago (Ehrlich, 1885). Studying the cerebrospinal fluid, pioneering physiologists experimented in rodents and observed that water-soluble dyes injected intravenously in the peripheral circulation stained several peripheral organs except for the brain, spinal cord or retinas (Ehrlich, 1904). Initially, Paul Ehrlich, who won the Nobel Prize in Physiology or Medicine in 1908, argued that this phenomenon occurred because the CNS had low affinity for the dye (Ehrlich, 1904). However, his student, Edwin Goldmann, refuted Ehrlich's argument as injection of the same dyes into the subarachnoid space

equally stained the brain but not peripheral tissues, demonstrating that the CNS and the peripheral circulation were partitioned (Goldmann, 1909). Continuing from these studies, Lina Stern and colleagues performed experiments in which they injected several different dyes into the brain parenchyma and blood. These studies prompted Stern to introduce the term "blood-brain barrier" and suggest its physiological function in maintaining brain homeostasis (Vein, 2008). Over the years, the concept of the BBB fascinated physiologists but the anatomical site of the BBB was highly disputed. Many speculated that Blood-CNS Barriers were located either at the CNS endothelium, at the pericytes that wrapped the endothelium, at the astrocytic end-feet, or at the basement membrane, which collectively is known as the neurovascular unit (**Figure 1.1**). With the advent of electron microscopy (EM), Thomas Reese and Morris Karnovsky resolved that the CNS endothelium is the site of the Blood-CNS Barriers (Reese and Karnovsky, 1967). In their seminal study, Reese and Karnovsky injected horseradish peroxidase (HRP) tracers into the peripheral circulation of rodents. After providing DAB (3,3'-diaminobenzidine) substrate for HRP enzymatic reaction, ultrastructural localization of the HRP tracer will appear electron dense under EM. Using these methods, Reese and Karnovsky identified that HRP was confined to the lumen of the CNS endothelium and with no extravasation of the tracer to the brain parenchyma (Reese and Karnovsky, 1967). Furthermore, EM analysis revealed that the CNS endothelial cells are joined continuously by tight junction complexes and have limited intracellular vesicles (Reese and Karnovsky, 1967). These two subcellular properties prevent the tracer from moving past the brain endothelium to the brain. In contrast, HRP tracer readily diffused past the endothelium in peripheral organs such as the heart

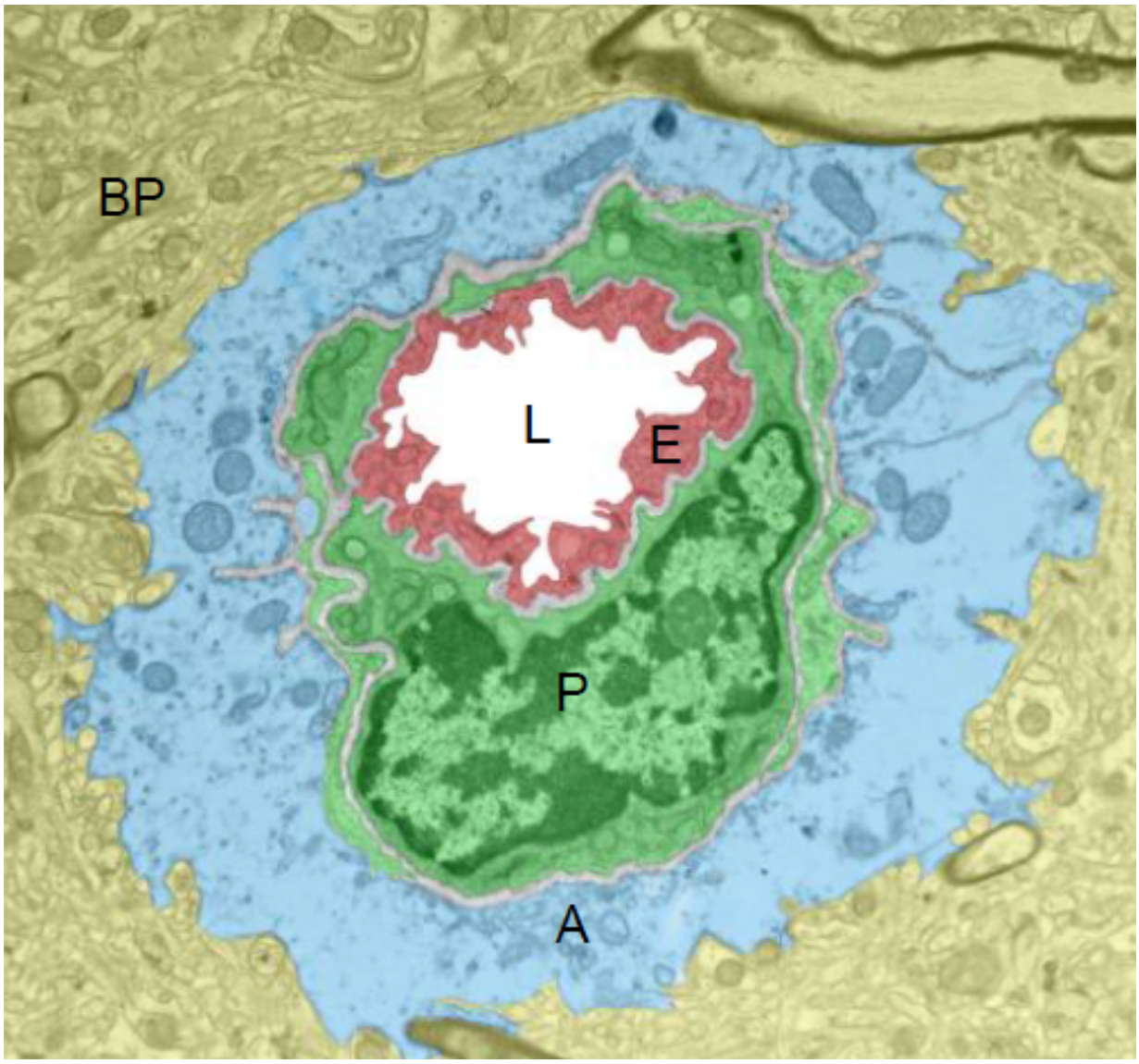

Figure 1.1. The neurovascular unit. A cross-section of a brain capillary visualized under electron microscopy and color-coded to illustrate the cell types of the neurovascular unit. Abbreviations: L, lumen; E, endothelial cell; P, pericyte; A, astrocyte end-feet; gray, basement membrane. Figure from Andreone, B.

and skeletal muscles (Karnovsky, 1967). EM analysis revealed that the HRP tracers leaked between peripheral endothelial cells and were endocytosed in vesicles in the peripheral endothelium (Karnovsky, 1967). Finally, analogous to Goldman's experiments, HRP injection directly into the brain parenchyma diffused past astrocytic end-feet and halted at the abluminal membrane of the endothelium, demonstrating that astrocytic end-feet do not significantly contribute to the physical barrier and instead, the brain endothelium is the bone-a-fide site of the blood-CNS barrier (Brightman and Reese, 1969). Thus, the site of the blood-CNS barrier is at the CNS capillaries, comprising single layer of non-fenestrated, continuous endothelial cells.

1.2. Molecular properties of the Blood-CNS Barriers

CNS endothelial cells are highly polarized with distinct luminal (apical) and abluminal (basolateral) compartments (Betz and Goldstein, 1978). The polarized nature of CNS endothelial cells is reflected in their four fundamental barrier properties that contribute to Blood-CNS Barrier function and integrity (**Figure 1.2**) (Blanchette and Daneman, 2015). First, tight junction complexes at the lateral, luminal membrane between CNS endothelial cells establish a high-resistance paracellular barrier to small hydrophilic molecules and ions (Brightman and Reese, 1969; J R Pappenheimer, 1951). Tight junction complexes are comprised of i) tight junction proteins such as claudins and occludin, ii) adhesion molecules such as VE-cadherin and E-cadherin and iii) junctional adhesion molecules (Liu et al., 2012; Siegenthaler et al., 2013). These transmembrane proteins are further linked and stabilized to the cytoskeleton via multiple cytoplasmic adaptor proteins such as zonula occludens proteins (Balda and Matter, 2009). Emerging studies have demonstrated that there is significant crosstalk among these tight junction

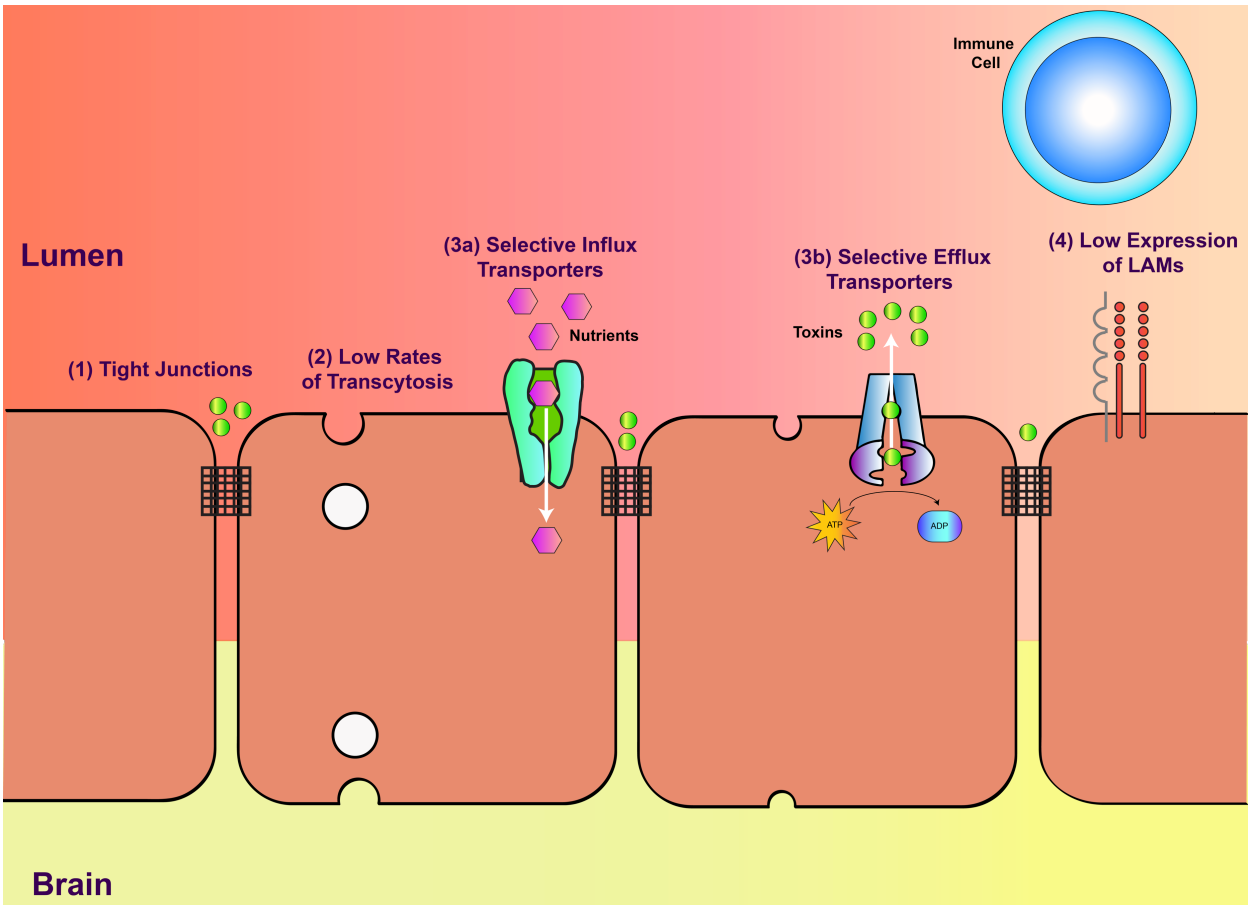

Figure 1.2. The four fundamental molecular properties of CNS endothelial cells that contribute to integrity and function. (1) Specialized tight junction complexes between endothelial cells prevent paracellular flux. (2) CNS endothelial cells have low rates of transcytosis, limiting transcellular flux. (3a) CNS endothelial cells mediate the selective uptake of nutrients (purple hexagons) from the blood using selective influx transporters and (3b) efflux of toxins (green circles) against their concentration gradient with ATP-dependent selective efflux transporters. (4) The low expression of leukocyte adhesion molecules (LAMs) contributes to the low level of immune surveillance in the CNS.

complex proteins to regulate the restrictive barrier junction (Tietz and Engelhardt, 2015). Second, in contrast to the endothelium in peripheral organs, CNS endothelial cells display minimal vesicular trafficking, limiting the vesicle-mediated transcellular movement of cargo known as transcytosis (Tuma and Hubbard, 2003). Although CNS endothelial cells display limited transcytosis, it is still the preferred pathway for the selective transport of plasma macromolecules such as albumin and low-density lipoprotein (Xiao and Gan, 2013). Third, the establishment of the restrictive paracellular and transcellular barriers allows CNS endothelial cells to use highly polarized cellular transporters to selectively regulate the influx of nutrients and efflux of metabolic waste and toxins between the blood and the brain parenchyma. The major class of known efflux transporters is the ATP-binding cassette (ABC) transporters- including Pgp, BCRP and MRP- mostly localized at the luminal membrane (Löscher and Potschka, 2005; Schinkel et al., 1994; 1995). These efflux transporters hydrolyze ATP to transport a wide array of substrates against their concentration gradients into the blood (Löscher and Potschka, 2005; Schinkel et al., 1994). CNS endothelial cells also express specialized nutrient transporters that facilitate the transport of ions, macromolecules and proteins from the blood to the brain. Many of these transporters belong to the superfamily solute carrier proteins (SLC) of facilitative transporters that includes sugar transporters such as SLC2A1 (GLUT1), and cationic amino acid transporters such as SLC7A1 (Saunders et al., 2013; Simpson et al., 2007). It is surprising to note that although SLCs play a vital role in metabolism and nutrition, they are particularly understudied (César-Razquin et al., 2015). Fourth, CNS endothelial cells lack the expression of leukocyte adhesion molecules (LAMs) such as E-selectin and Icam1(Engelhardt and Ransohoff, 2012). The lack of these luminal surface molecules prevents the entry of immune

cells from the blood into the parenchyma, resulting in a paucity of immune cells in the brain microenvironment (Ransohoff and Engelhardt, 2012). As a result, the healthy brain is "immune privileged", where introduced antigens do not elicit the development of adaptive immune responses (Muldoon et al., 2013). These fundamental molecular characteristics confer BBB properties on CNS endothelial cells to regulate brain homeostasis.

1.3. Known molecular regulators of Blood-CNS Barrier function in CNS endothelial cells

The four fundamental Blood-CNS Barrier properties listed above are not intrinsic to CNS endothelial cells but are induced and regulated by the neural environment (Hagan and Ben-Zvi, 2014). Transplantation studies using chick/quail chimeras have demonstrated that non-vascularized brain fragments transplanted into the coelomic cavity were soon vascularized by abdominal vessels that developed BBB characteristics, such as the exclusion of circulating dye and the low number of vesicles (Stewart and Wiley, 1981). In contrast, non-vascularized embryonic mesoderm tissues grafted in the CNS were soon vascularized by neural vessels that failed to displayed BBB properties (Stewart and Wiley, 1981). This seminal experiment demonstrated that: 1) BBB properties are not inherent to CNS endothelial cells and 2) the neural environment provides inductive cues to CNS endothelial cells to activate genetic programs in order to acquire BBB properties. Although the identities of these signals and genetic programs have been elusive, recent advances in purification and gene expression profiling of CNS endothelial cells have elucidated novel molecular mediators that confer barrier properties upon CNS endothelial cells.

The most well-characterized genetic program inducing Blood-CNS Barrier properties in CNS endothelial cells is β-catenin signaling (Daneman et al., 2009; Liebner et al., 2008; Stenman et al., 2008). Daneman *et al*. purified CNS and peripheral endothelial cells using fluorescence-activated cell sorting (FACS) from Tie2GFP mice, a transgenic GFP reporter for endothelial cells (Daneman et al., 2009). Microarray analysis indicated that many downstream effectors of Wnt/ β-catenin signaling are enriched in CNS endothelial cells, suggesting that β-catenin signaling may mediate CNS vasculature functions. Indeed, various studies have demonstrated that canonical Wnt signaling is essential for both CNS-specific angiogenesis and barriergenesis. For example, endothelial cell specific deletion of *β-catenin* disrupts CNS-angiogenesis, resulting in gross vascular malformations and hemorrhages whereas peripheral angiogenesis remains largely undisrupted (Daneman et al., 2009; Stenman et al., 2008). In addition, endothelial cell-specific deletion of *β-catenin* disrupts barriergenesis, downregulating Glut1 expression, a marker commonly used for BBB formation, in CNS vasculature (Daneman et al., 2009; Liebner et al., 2008; Stenman et al., 2008). Zhou *et al*. demonstrated that postnatal, endothelial cell-specific deletion of *β*-catenin results in BBB breakdown, exemplified by extravasation of dyes and downregulation of tight junction protein expression, showing that barrier dysfunction is not a consequence of disrupted angiogenesis. Recently, many of the receptors upstream of β-catenin - including Frizzled receptors, co-receptors LRP5 /LRP6 and auxiliary receptor GPR124 - as well as the Wnt ligands necessary for β-catenin activation have been identified (Anderson et al., 2011; Chen et al., 2012; Cho et al., 2017; Cullen et al., 2011; Kuhnert et al., 2010; Posokhova et al., 2015; Vanhollebeke et al., 2015; Wang et al., 2018; 2012; Zhou and Nathans, 2014; Zhou et al., 2014). Loss-of-functions of these genes results in CNS vasculature dysfunction and largely resembles *β*-catenin mutants.

A recent study identified novel downstream targets of β-catenin signaling that mediate both CNS angiogenesis and barriergenesis. Tam *et al*. used antibody-based FACS to isolate endothelial cells from CNS and non-CNS tissues at three developmental ages (Tam et al., 2012). Microarray analysis indicated *dr6*, *troy* and *spock2* are highly enriched in CNS endothelial cells. Indeed, these genes are essential for CNS vasculature function as *dr6*, *troy* and *spock2* knockdown in zebrafish resulted in vascular malformation and barrier dysfunction. In contrast, loss-of-function of other genes enriched in CNS endothelial cells, *abcyap1r1* and *tspn5*, resulted in vascular morphogenesis defects but exhibited no barrier dysfunction. The authors demonstrated that *in vitro* activation of β-catenin with recombinant Wnt ligands upregulates the expression of *dr6* and *troy*, suggesting that these genes are downstream effectors of β-catenin. However, it is difficult to determine if these genes specifically regulate barriergenesis or if barrier dysfunction is a consequence of vascular malformations. Temporal deletion of these genes after CNS angiogenesis can clarify this point.

Genes that specifically regulate BBB function and integrity independent of CNS angiogenesis have been identified via gene profiling of purified CNS endothelial cells. Ben-Zvi et al. mapped the development of mouse cortical barriergenesis at E15.5 and performed microarray analysis from FACS purified Tie2GFP+ CNS and lung endothelial cells at E13.5, a time when barrier properties are actively forming (Ben-Zvi et al., 2014). The microarray analysis indicated that major facilitator domain containing protein 2A (Mfsd2a) is enriched in CNS endothelial cells. *Mfsd2a* is expressed specifically in CNS vasculature and not in the choroid plexus, a structure that lacks BBB. *Mfsd2a* knockout mice display BBB dysfunction due to unregulated bulk flow of transcytosis. However, vascular development and patterning remain unaffected, suggesting *Mfsd2a* specifically regulates BBB integrity independent of angiogenesis.

Surprisingly, Mfsd2a has dual physiological functions (Betsholtz, 2014; Nguyen et al., 2014; Zhao and Zlokovic, 2014). Not only is Mfsd2a essential for the CNS endothelium to maintain low rates of transcytosis, but also Mfsd2a is a transporter for omega-3 fatty acids across the CNS endothelium (Betsholtz, 2014; Nguyen et al., 2014; Zhao and Zlokovic, 2014). Lipidomics revealed that brains of *Mfsd2a* knockout mice exhibit decreased docosahexaenoic acid (DHA), an omega-3 fatty acid essential for neuronal function, and elevated arachidonic acid, an omega-6 fatty acid. Furthermore, *Mfsd2a* knockout mice display fewer neurons in the hippocampus and cerebellum, microcephaly and other neurological deficits. These altered brain fatty acids and behavioral abnormalities are reminiscent of omega-3 fatty acid deficiency (Lafourcade et al., 2011). In fact, human genetics studies identified hypomorph missense mutations in *MFSD2A* as a recessive cause of microcephaly (Alakbarzade et al., 2015; Guemez-Gamboa et al., 2015). One study identified two different *MFSD2A* missense mutations that result in severe intellectual disability, seizures and early lethality, whereas a second study identified a milder *MFSD2A* missense mutation that results in patients with intellectual disability alone and without lethality. Interestingly, a recent study identified siblings with shared parental ancestral with homozygous null mutations of *MFSD2A.* Although both siblings displayed microcephaly, intellectual impairments and ataxia, both siblings survived, suggesting that the other factors, including environmental or nutrition can impact the severity of the phenotype (Harel et al., 2018). Interestingly, Similar to GLUT1, Mfsd2a has dual physiological functions at the BBB, maintaining barrier integrity and transporting nutrients, across the barrier (Winkler et al., 2015; Zheng et al., 2010). It will be essential for future studies to determine if Mfsd2a's dual physiological functions of (1) maintaining BBB integrity and (2) transporting essential nutrients act independently or if one function is required for the other.

Another recently discovered gene that mediates barriergenesis independent of angiogenesis is lipolysis-stimulated lipoprotein receptor (LSR). Sohet and Daneman *et al.* also purified TIE2GFP+ CNS and peripheral endothelial cells and performed microarray analysis to identify *lsr*, another gene enriched in CNS endothelial cells (Daneman et al., 2010; Sohet et al., 2015). Although *lsr* is expressed in many cell-types in peripheral tissues, it is expressed specifically in endothelial cells in the brain. Initially, LSR was reported to mediate clearance of triglyceride-rich lipoproteins and low-density lipoproteins (Yen et al., 2008). *Lsr* knockout mice were reported not to display any vascular malformations or hemorrhage but still display BBB dysfunction. Indeed, LSR is essential for BBB integrity, as *lsr* knockout embryos exhibit extravasation of small molecular weight tracers (Sohet et al., 2015) but not larger molecular weight tracers, a phenotype that is reminiscent of the *claudin5* knockout mouse (Nitta et al., 2003). This size selective permeability dysfunction may be a common phenotype observed when disrupting tight junction molecules. The extravasation of small tracers is most likely mediated via paracellular entry. In contrast, larger molecules most likely leak out through transcytosis, such as observed in Mfsd2a knockout mice, where HRP (44 kDa) and 70 kDa dextran tracers leak out of the CNS vasculature. However, the molecular mechanism underlying LSR regulation of BBB integrity is still unknown. Although LSR is localized at the tricellular tight junctions (where two bicellular tight junctions meet) in the functional BBB, *lsr* knockout mice display no obvious disruption in TJ complexes by EM.

1.4. Inductive signals that confer BBB properties

Recent studies have identified key inductive signals in the CNS microenvironment that confer CNS endothelial cells with Blood-CNS Barrier properties. It is evident that these inductive signals originate from the neurovascular unit. As mentioned above, the most well-characterized signal that mediates BBB function is canonical Wnt signaling (Cho et al., 2017; Daneman et al., 2009; Liebner et al., 2008; Stenman et al., 2008; Wang et al., 2012; 2018; Zhou and Nathans, 2014; Zhou et al., 2014). Neural progenitors in the neuroepithelium secrete Wnt7a/Wnt7b, whereas in the cerebellum, Bergmann glia secrete Norrin. These secreted ligands bind to classical components of canonical Wnt signaling such as the Frizzled receptors and co-receptors LRP5 /LRP6 that are expressed on CNS endothelial cells to drive β-catenin signaling. Disruption of these Wnt ligands phenocopies *β-catenin* mutants, impairing CNS angiogenesis and displaying loss of vessel numbers, vascular malformations, hemorrhages, and BBB dysfunction (Cho et al., 2017; Daneman et al., 2009; Liebner et al., 2008; Stenman et al., 2008; Wang et al., 2012; 2018; Zhou and Nathans, 2014; Zhou et al., 2014).

Another inductive signal essential for barriergenesis is Sonic hedgehog (Shh) signaling. Although Hedgehog signaling has been well-characterized for neuronal development and angiogenesis, Alvarez et al. demonstrated that astrocyte-secreted Shh is essential for BBB integrity and CNS immune quiescence (Alvarez et al., 2011; Martí and Bovolenta, 2002). Astrocytes express *shh* whereas CNS endothelial cells robustly express Hedgehog signaling components- Patched-1, Smoothened and Gil. Astrocyte-conditioned medium or recombinant Shh were sufficient to (a) elevate tight junction protein expression and transendothelial electrical resistance (TEER), a technique used to measure the integrity of tight junction dynamics in cell culture, and (b) suppress permeability of various tracers *in vitro*. Furthermore, endothelial cell-

specific disruption of Hedgehog signaling *in vivo* results in normal vascular formation but BBB dysfunction through the suppressed expression of tight junction proteins and extravasation of plasma proteins. Hedgehog signaling is also essential to establish immune quiescence in the CNS. For example, Hedgehog signaling is sufficient to suppress chemokines and LAM expression in ECs *in vitro*. Furthermore, Hedgehog signaling in leukocytes suppresses the expression of proinflammatory cytokines, such as Tumor Necrosis Factor (TNF), reducing neuroinflammatory processes. Hedgehog signaling has a protective role in neuroinflammatory diseases such as Multiple Sclerosis (MS). MS patients display elevated Hedgehog signaling components in the CNS and pharmacological blockade of Hedgehog signaling in Experimental autoimmune encephalomyelitis (EAE) models results in greater severity of the disease, with increases in proinflammatory cytokines, leukocyte accumulation in the CNS and demyelination. It should be noted that the above studies focus on Hedgehog signaling as essential for BBB maintenance, not necessarily induction, as astrocytes are born and manifest in the NVU around birth. Although Shh is robustly expressed in the CNS during embryonic development and Shh knockout mice display reduced tight junction expression at E13.5, shortly before BBB maturation, the early roles of Hedgehog signaling during barriergenesis is still not well-characterized. Therefore, it will be interesting to explore the early inductive roles of Shh during BBB development before the onset of astrocyte-mediated Shh signaling to maintain BBB integrity.

Although it is well established that the neural microenvironment contains factors that induce CNS endothelial cells to manifest BBB properties, recent studies demonstrate that environmental cues and factors extrinsic to the CNS can impact BBB development and integrity as well. Braniste et al. demonstrated that gut microbiota influences the regulation of the BBB

through epigenetic control of tight junction expression in CNS endothelial cells (Braniste et al., 2014). Emerging studies have demonstrated that an organism's microbiota influences many physiological functions, including behavior (Hsiao et al., 2013). Furthermore, the gut microbiota has been reported to influence tissue barrier systems (Al-Asmakh and Hedin, 2015). Comparing pathogen-free (control) and germ-free mice (altered microbiota), these authors discovered that germ-free mice display BBB dysfunction in both embryonic development and postnatal life, due to downregulation of tight junction protein expression. Indeed, unlike pathogen-free mice, germ-free mice display extravasation of Evans blue dye. Consistent with low tight junction expression, ultrastructure analysis by EM revealed disruption of tight junction complexes. Remarkably, transplanting fecal matter from pathogen-free mice to recolonize the intestinal microbiota of germ-free mice can restore the dysfunctional BBB observed in germ-free adult mice. Indeed, germ-free mice with recolonized microbiota have restored tight junction protein expression in the CNS with accompanying restriction of dye tracers to CNS endothelium. The molecular determinants from microbiota impacting BBB integrity in these experiments were short-chain fatty acids such as butyrate, which has been reported to strengthen the integrity of the intestinal epithelial barrier. Indeed, treatment with butyrate was sufficient to elevate tight junction protein expression and restore the BBB integrity in the germ-free mice. The authors suggest that butyrate epigenetically regulates tight junction expression in the CNS by increasing histone acetylation. This crosstalk between microbiota and the BBB is intriguing and provocative. It will be interesting to explore if short-chain fatty acids directly increase BBB integrity or cause secondary effects on other signaling pathways throughout the body. Furthermore, it will be of clinical interest to explore how the use of strong antibiotics that eliminate gut microbiota influences the BBB.

Another recent study highlighted how foreign microbes impact the BBB. Acute bacterial meningitis is an infection in the CNS that causes neural damage and can result in mental impairment, seizures, paralysis and death if untreated (Brouwer et al., 2010). To induce meningitis, bacteria must first breach the BBB (van Sorge and Doran, 2012). However, it is unclear how bacteria penetrate through the BBB. Kim et al. demonstrated that blood-borne bacteria such as group B *Streptococcus* (GBS) can weaken BBB integrity by upregulating the expression of *Snail1,* a zinc finger transcription factor, in host CNS endothelial cells that subsequently suppresses tight junction protein expression (Kim et al., 2015). Exposure of GBS to CNS endothelial cells *in vitro* and *in vivo* upregulates *Snail1* expression and downregulates tight junction protein expression, with accompanying increases in GBS counts in the brain. Furthermore, transgenic dominant-negative *Snai1* zebrafish are more resistant to GBS-mediated lethality. It is interesting that bacteria can manipulate the gene expression in host CNS endothelial cells to weaken the integrity of the BBB. It will be of clinical interest for future studies to explore what bacterial molecules interact with host CNS endothelial cells to alter gene expression and to determine if bacteria breach the BBB via weakened tight junctions.

1.5. Acquisition of the two structural properties for BBB integrity

Despite our ever-increasing understanding of the inductive factors for BBB development and function, how and when CNS endothelial cells acquire the two structural properties- tight junctions and suppression of transcytosis- for BBB integrity have been unclear. Do developing CNS vessels acquire these two structural properties sequentially or synchronously? What is the contribution of these two structural properties in regulating the impermeability of the BBB?

These gaps of knowledge have been difficult to address given the complex development and architecture of brain vasculature (Hagan and Ben-Zvi, 2014). Addressing these questions requires the unambiguous identification of nascent vessels from mature vessels to determine which structural properties are present (or absent) in nascent and mature vessels. In the first half of my thesis (Chapter 3), I will show using the retinal vasculature, a more tractable CNS vasculature that forms the physiologically analogous blood-retinal barrier, we can unequivocally discern nascent and mature vessels to assess the acquisition of tight junctions and suppression of transcytosis within these two developmentally distinct vessels and. Using the blood-retinal barrier, we can address these fundamental barrier questions and we anticipate these findings can apply to other blood-CNS barriers.

1.6. Strategies for drug delivery across the BBB

A comprehensive understanding of the molecular constituents and mechanisms of BBB function and integrity would offer novel strategies for CNS therapeutics. Although the functional BBB is essential for proper neuronal function, the restrictive BBB is an impediment to deliver therapeutics, including recombinant proteins, antibodies and even small molecules, to the brain parenchyma (Pardridge, 2012). Thus, a major focus of BBB research is identifying strategies to enhance the delivery of therapeutics across the BBB. There are three promising methods to manipulate BBB properties to deliver drugs. First, several groups have demonstrated that hijacking receptor-mediated transcytosis pathways could deliver large, genetically engineered proteins across barrier endothelium (Pardridge, 2012). The transferrin receptor (TfR), which binds to its ligand transferrin-bound iron and undergoes clathrin-mediated transcytosis to

facilitate iron delivery to the brain, has been the main target of this work (Jones and Shusta, 2007; Yu and Watts, 2013). For example, chimeric monoclonal antibodies with α-Tfn fused to α-Aβ antibodies have been successful in hijacking the TfR pathway to reduce Aβ in an Alzheimer's disease mouse model (Niewoehner et al., 2014). Second, scanning ultrasound (SUS), in which systemic injected circulating microbubbles causes the transient opening of tight junctions when activated with ultrasound, has been reported to safely and transiently permeabilize the BBB (McDannold et al., 2012; Samiotaki et al., 2015). Third, as we identify the mediators of BBB function and better understand the molecular and cellular pathway underlying BBB regulation, we could target and manipulate these proteins to enhance therapeutic delivery. For example, functional Frizzled4 blocking antibodies have been shown to permeabilize the blood-retina barrier, offering a temporal opportunity for enhanced drug delivery (Paes et al., 2011). As we further understand the cellular pathways and molecular mechanisms that regulate BBB function and integrity, we can develop creative strategies to manipulate these molecules to enhance drug delivery. Answering fundamental questions in BBB research and identifying molecular constituents of barrier regulation will enhance the development of therapeutics to modulate the BBB for drug delivery and neurologic disorders.

1.7. History of neurovascular coupling

The intimate coupling between increased neuronal activation and subsequent increased local cerebral blood flow, a process now dubbed neurovascular coupling, was first observed for more than a century (Roy and Sherrington, 1890). In the 19th century, there was an ongoing debate about whether the blood flow in the brain is solely regulated by extrinsic factors such as

cardiac output or if there were also intrinsic mechanisms in the brain to regulate the cerebral blood flow (Small, 2004). Physiologists who advocated for the latter hypothesis argued that brain-derived chemical cues could alter cerebral vasodilation and increase blood flow independent of extrinsic factors. However, many dismissed this hypothesis, arguing that the rigidity of the skull would deter intrinsic mechanisms that induce blood vessel volume changes. However, Charles Smart Roy and Charles Scott Sherrington, pioneering British physiologists, were the first to experimentally support the hypothesis of the intrinsic mechanisms. They invented a device placed on the brain surfaces of dogs to measure changes in intracranial volumes and identified fluctuations in cranial volumes (Roy and Sherrington, 1890). From these experiments, they inferred that "the brain possesses an intrinsic mechanism by which its vascular supply can be varied locally in correspondence with local variations of functional activity" (Roy and Sherrington, 1890). However, critics were not satisfied by Roy and Sherrington's experiment and criticized experiment flaws for their interpretations. Criticism included that the experiment used anesthetized subjects, which does not reflect normal physiology. Furthermore, the device was not directly measuring blood volume changes but instead, measuring changes in the volume of the cranium (Small, 2004). In the mid 20th century, Seymour S. Kety and Carl F. Schmidt established a novel method to measure cerebral blood flow in humans by having subjects inhale nitrous oxide and sample various gases in the cerebral arterial and venous circulation (Kety and Schmidt, 1947). Their results bolstered the hypothesis of intrinsic mechanisms governing cerebral blood flow (Kety and Schmidt, 1947), pioneering the field of neurovascular coupling. Significant advances in neurovascular coupling technology began in the 1970s with the advent of the modem neuroimaging techniques, including positron emission tomography (PET) and magnetic resonance imaging (MRI), techniques that are still actively advancing. These

techniques allowed for the visualization of regional blood flow changes in the brain, an advancement that the nitrous oxide method developed by Kety and Schmidt could not detect as their method measured average cerebral blood flow.

Since then, physiologists have strived to understand the mechanisms that govern the increased cerebral blood flow following neural activation. Two hypotheses have emerged to explain neurovascular coupling: 1) the *metabolic hypothesis* was advocated by Roy and Sherrington who postulated that changes in cerebral blood flow are linked to neural metabolism. Thus, given this hypothesis, either dips in O2 and glucose or accumulation of metabolic by-products such as CO2 were the determinant to elicit the increase in cerebral blood flow. 2) *neurogenic hypothesis* postulates that neuronal activity releases synaptic chemicals which can elicit an increase in cerebral blood flow independent of the state of neural metabolism.

1.8. Metabolic hypothesis of neurovascular coupling

In the early part of the 20th century, many physiologists had advocated for the *metabolic hypothesis.* In their seminal study, Roy and Sherrington inferred that the intrinsic mechanisms that elicit cerebral blood flow changes are due to "the chemical products of cerebral metabolism" (Roy and Sherrington, 1890). Furthermore, Kety's and Schmidt's tracer injection experiments also suggested that cerebral blood flow can change by manipulating the substrates and products of oxidative metabolism such as CO2 and O2 (Kety and Schmidt, 1947). However, it was not until the 1980s that there was unequivocal experimental evidence to refute the *metabolic hypothesis.* Peter Fox and Marcus Raichle used radiolabeled oxygen ^{15}O with PET imaging to measure the cerebral metabolic rate of oxygen (CMRO2) in humans (Fox and Raichle, 1986; Fox

et al., 1988). Imaging two different brain systems, the somatosensory and the visual system, the authors identified that following neural activation in these two brain regions, O2 levels actually rose (Fox and Raichle, 1986; Fox et al., 1988). From these seminal studies, the authors made two watershed conclusions: i) increases in cerebral blood flow and glucose utilization during local brain activation are not coupled by oxygen consumption, suggest the cerebral blood flow must be regulated by other factors besides oxygen or glucose and ii) ATP production during neural activation is due to both oxidative and non-oxidative metabolism (Fox and Raichle, 1986; Fox et al., 1988). Indeed, subsequent studies confirmed these two conclusions. Rodents in hyperbaric hyperoxygenation chambers demonstrated that an increase in cerebral blood flow continues normally despite the oversaturation of oxygen in the brain (Lindauer et al., 2009). Furthermore, rodents in a hyperglycemic state also have unaltered neurovascular coupling (Wolf et al., 1997). Conversely, studies examining humans in the hypoglycemic state do not have altered neurovascular coupling (Powers et al., 1996), suggesting that glucose levels do not elicit neurovascular coupling. Finally, subsequent studies identified that exogenous lactate can regulate increase cerebral blood flow (Mintun et al., 2004), confirming that ATP consumption in the brain is partially non-oxidative. Serendipitously, the uncorrelation between neurovascular coupling and CMRO2 is the basis for the widely used technique, blood oxygenation level–dependent (BOLD) functional magnetic resonance imaging (fMRI) contrast imaging (Kwong et al., 1992; Ogawa et al., 1992).

fMRI relies on the basis that deoxyhemoglobin (HbR) is paramagnetic and can be detected by MRI (Hillman, 2014; Ogawa et al., 1990). In the 1990s, Seiji Ogawa et al. demonstrated that the “BOLD signal” increases with the decrease in (HbR) signal and

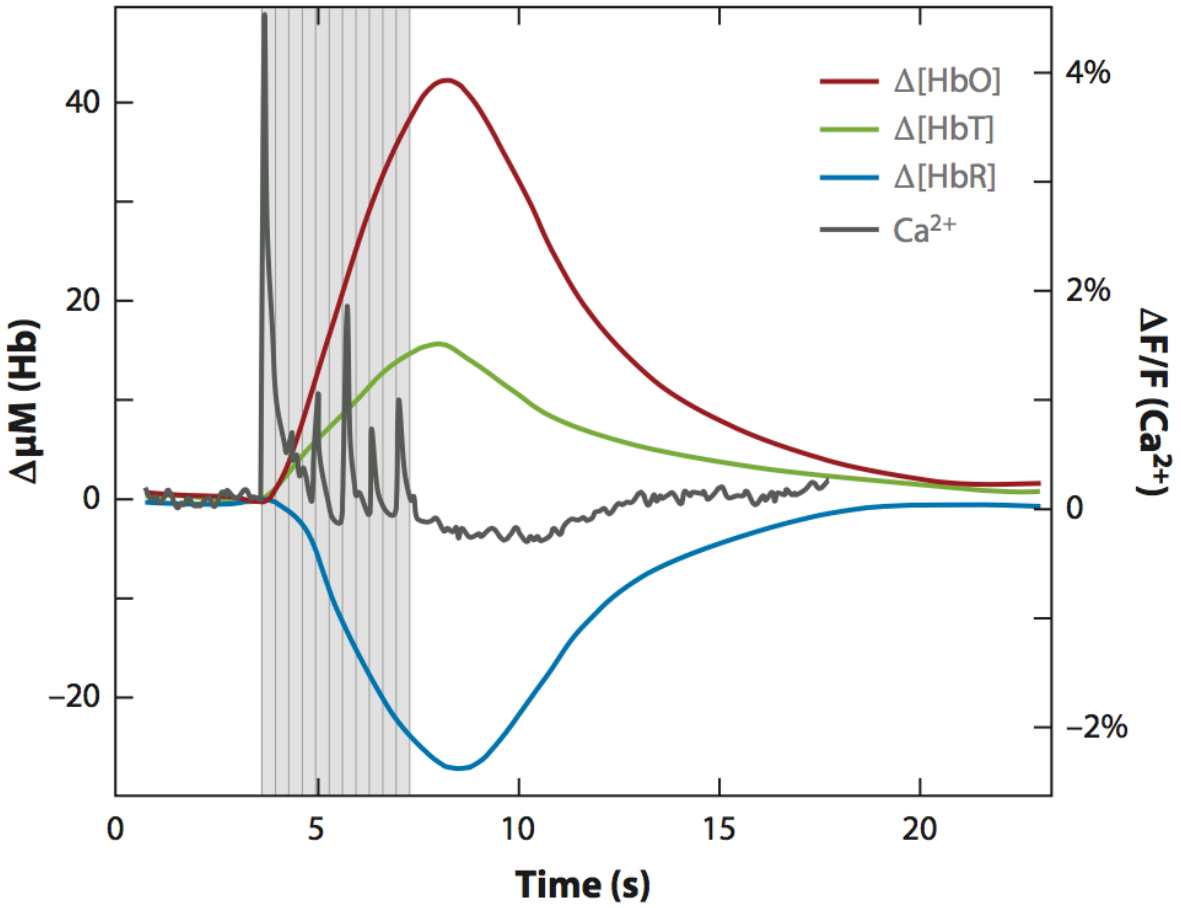

Figure 1.3. The stereotypic dynamics of the BOLD signal. A stereotypic response of the BOLD signal in rat somatosensory cortex. Here, rat skull was exposed and Ca^{2+} indicators were injected into the brain (gray trace) and absorbed by neurons as a proxy to measure neural activity. Upon shock to forepaws (gray hash lines) as a sensory-stimulus, neural activity (gray) increases. The oxygenated hemoglobin (HbO, red) increases, deoxygenated hemoglobin decreases (HbR, blue) and the sum of the two signal, total hemoglobin (HbT, green) increases. Note the overshoot in HbT. Figure is readapted from (Hillman, 2014).

analysis of these signals can produce functional maps for brain activity (Ogawa et al., 1990; 1992). fMRI confirms the finding of Peter Fox and Marcus Raichle that following neural activity, blood oxygenation level overshoots beyond the baseline (Kwong et al., 1992). While fMRI is ubiquitously used as an invaluable method for research and diagnostics to this day, we still do not have a complete understanding on the mechanisms of BOLD signals and more generally, on the mechanisms underlying neurovascular coupling. Thus, it is essential to understand the molecular and cellular mechanisms that govern neurovascular coupling to fully understand our interpretation of the BOLD signal, which has a profound impact on research and medical diagnostic.

1.9. Extrinsic neurogenic hypothesis of neurovascular coupling

Given that neurovascular coupling is not elicited by metabolism, many advocated that neurogenic cues released during synaptic activity must elicit the increase in blood flow. The neural factors that induce and modulate cerebral blood flow have been of high interest in the field of neurovascular coupling. However, controversy exists on whether functional regulation of cerebral blood vessels is regulated by "extrinsic" perivascular nerves with the soma located outside the brain and/or whether neurovascular coupling is regulated by "intrinsic" neurons, with the soma residing inside the brain. Physiologists would argue extrinsic perivascular nerves indeed regulate neurovascular because nerve fibers are found on the surface of the brain. Thomas Willis, the neuroanatomist renowned for his discovery and characterization of the "Circle of Willis", was the first to describe the existence of perivascular nerve innervation on extracerebral vessels at the base and surface of the brain in the late 1600s (Hamel, 2006; Willis, 1664). In

1932, Wilder Penfield described that indeed extracerebral vessels on the brain surface were indeed wrapped by nerve fibers. Furthermore, he also highlighted that intracortical arteries that extended from these extracerebral vessels were also wrapped by nerves (Penfield, 1932). These findings prompted physiologists to speculate that these nerves might regulate cerebral blood flow (Hamel, 2006). Ultrastructural analysis by EM of cerebral arteries from cats suggested that these nerves might originate from the autonomic nervous system, with both sympathetic and parasympathetic innervations (Nielsen et al., 1971). However, the excitement that there could be autonomic regulation on cerebral vessels was quelled when subsequent studies identified that an adrenergic receptor antagonist, phentolamine, had no effect on the tone of extracerebral vessels (Kuschinsky and Wahl, 1975). Furthermore, studies in dogs and cats had discovered that stimulation of superior cervical ganglia, a sympathetic ganglion, or sympathetic nerves had no or negligible effect on extracerebral vascular tone (Busija et al., 1982; Heistad et al., 1977). Yet, many other studies refuted that there are sympathetic innervations on extracerebral vessels. For example, studies on newborn pigs discovered that stimulation of sympathetic nerves induces vasoconstriction, which can be attenuated when extracerebral vessels are pre-treated with an adrenergic antagonist, yohimbine (Busija and Leffler, 1987). Thus, there is a controversy on whether sympathetic innervations play a significant physiological function on extracerebral vasculatures and regulates neurovascular coupling (Purves, 1978).

Parasympathetic and cholinergic regulations of extracerebral vessels have been murkier than sympathetic regulation (Cauli and Hamel, 2010; Purves, 1978). Because parasympathetic ganglia are anatomically inaccessible and encased in bone, it is more difficult to stimulate parasympathetic ganglia. The prevailing view is that parasympathetic perivascular nerves play a minor role in the physiological regulation of extracerebral vessels (Hamel, 2006). Interestingly,

whether extrinsic perivascular nerves function to impact neurovascular coupling has diminished recently but is appropriate to revisit given today's modern technologies in optics and genetics.

1.10. Intrinsic neurogenic regulation of cerebral blood flow

Analogous to the regulation of the BBB, various cell types of the neurovascular unit have been demonstrated to regulate neurovascular coupling (Kisler et al., 2017). However, there are significant caveats in these findings, specifically the use of *ex vivo* paradigms, such as acute brain slices or isolated blood vessels, to model neurovascular coupling. Conclusions obtained from studies using *ex vivo* preparations conflict with many results from studies that use *in vivo* paradigms. Indeed, it is noteworthy that many physiological dimensions of neurovascular coupling are abolished *ex vivo*. For example, *ex vivo* vasodilation in response to pharmacological compounds occurs over minutes, compared to physiological vasodilation in response to natural stimuli *in vivo* that occurs over hundreds of milliseconds (Hillman, 2014) as observed in BOLD signals (**Figure 1.3**). This dramatic difference is due to the artificial conditions of the *ex vivo* settings: it requires immersion of the tissue in solution with non-physiological levels of oxygen to maintain tissue health. Furthermore, *ex vivo* tissues lack blood circulation, causing the blood vessels to over-dilate and thus, requiring pharmacological compounds to re-constrict blood vessels before studying vasodilatory responses. Given the profound caveat for *ex vivo* preparations to study neurovascular coupling, I will highlight whether past findings were performed with *ex vivo* or *in vivo* preparations. Finally, given the advent of single-cell RNA sequencing, we are in the era where we can understand the transcriptome of various cell types in the brain (Klein et al., 2015; Tasic et al., 2016; Vanlandewijck et al., 2018). Thus, using publicly-available unbiased single-cell RNA sequencing data (Klein et al., 2015; Tasic et al.,

2016; Vanlandewijck et al., 2018), we can now reevaluate the past claims of molecular mechanisms and cell types that function in neurovascular coupling.

Excitatory neurons: Many studies have demonstrated that activation of excitatory neurons can evoke vascular responses. Using both viral-injection (Ji et al., 2012; Lee et al., 2010) and transgenic rodents (Lacroix et al., 2015) to express channelrhodopsin in excitatory neurons and then using *in vivo* imaging techniques, many studies identified that following neural activation in excitatory neurons, cerebral blood flow is increased. What are the signals from excitatory neurons that evoke neurovascular coupling? Lacroix et al. identified that excitatory neurons express COX-2 (*ptgs2)* to generate prostaglandin E2 (PgE2). The authors then proposed that PgE2 binds to EP2 (*ptger2)* and EP4 (*ptger4)* receptors on smooth muscle cells to relax them (Lacroix et al., 2015). While single-cell RNA sequencing data indeed demonstrate that *ptgs2* is expressed in excitatory pyramidal neurons and that COX-2 or *ptgs2* knockout mice indeed have impaired neurovascular coupling in response to sensory-evoked neural activity, both *ptger2* and *ptger4* expression are negligible in smooth muscle cells and instead, are mostly expressed in interneurons (Tasic et al., 2018; Vanlandewijck et al., 2018). Given the lack of genetic data for this proposed mechanism, it is unclear if prostaglandins are directly signaling to smooth muscle cells or indirectly signaling to other cell types to mediate or regulate neurovascular coupling.

Inhibitory neurons: It has been unclear if net neural excitation is necessary for neurovascular coupling or if activation of inhibitory neurons could also elicit neurovascular coupling. Interestingly, selective activation of inhibitory neurons can indeed elicit neurovascular coupling as transgenic mice expressing channelrhodopsin specifically in inhibitory neurons (*Vgat:Chr2-*

YFP) also evoked neurovascular coupling (Uhlirova et al., 2016) *in vivo*. Interestingly, net neural activity as measured by electrode recordings is indeed decreased, suggesting that neurovascular coupling can be evoked without net neural activation. Given that there are various subtypes of inhibitory interneurons, which subtypes can evoke and modulate neurovascular coupling? Interestingly, *in vivo* two-photon imaging with optogenetic stimulation of subtypes of interneurons has demonstrated that distinct subtypes of interneurons mediate the dilation phase whereas others mediate the contraction phase. Selective activation of VIP+ or NOS1+ or SST+ interneurons using transgenic mice that express channelrhodopsin specifically in these respective interneurons evoked vasodilation (Granger et al., 2019; Lee et al., 2019). Conversely, selective activation of PV+ and presumably NPY+ interneurons caused constriction (Uhlirova et al., 2016; Urban et al., 2012).

What are the signals released from interneuron subtypes that evoke neurovascular coupling? Presumably, it is the neurotransmitters, neuropeptides or neuromodulators that define the molecular identities of these interneuron subtypes that cause vasodilation. Here, I will highlight the interneurons subtypes and review the function of these neurotransmitters, neuropeptides and neuromodulators in the context of neurovascular coupling. VIP or Vasoactive intestinal peptide was identified over 50 years and is known to have potent vasodilatory effects on peripheral vasculature (Dickson and Finlayson, 2009). However, *Vip* knockout mice have yet to be tested to determine if VIP plays a role in neurovascular coupling *in vivo*.

There are three nitric oxide synthase isoforms, *Nos1* or neuronal NOS (nNOS), *Nos2* or inducible NOS (iNOS), and *Nos3* or endothelial NOS (eNOS). While all three isoforms encode enzymes that use L-Arginine to synthesize nitric oxide, a potent vasodilator, the expression of these isoforms varies across tissue and organs. In the cortex, Nos1 is expressed by SST+

interneurons found in layer 5 (Tasic et al., 2018). *Nos1* germline knockout mice have been assessed for neurovascular coupling defects. Surprisingly, *Nos1* knockout mice have similar sensory-evoked neurovascular coupling as wild-type mice as assessed under anesthesia by laser-doppler flowmetry *in vivo* (Ma et al., 1996). Yet, the authors attributed the lack of observed phenotype in *Nos1* knockout mice to compensation of constitutive germline deletion. Inducible, conditional deletion of *Nos1* could clarify the importance of Nos1 for neurovascular coupling.

NPY or Neuropeptide Y was first extracted from porcine brain and identified in 1982 (Tatemoto et al., 1982) and has been implicated in various roles from cardiovascular regulation to energy homeostasis (Tan et al., 2018). While NPY has been implicated in vasoconstriction via smooth muscle cell constriction (Li et al., 2016; Uhlirova et al., 2016), *Npy* knockout mice have yet to be assessed for neurovascular coupling defects.

Astrocytes: The involvement of astrocytes in neurovascular coupling has been controversial. Many hypothesized that astrocytic intracellular calcium may play a role in neurovascular coupling. Early studies used pharmacology to manipulate astrocytic calcium in *ex vivo* acute brain slices from rats, resulting in contradictory results (Mulligan and MacVicar, 2004; Zonta et al., 2003). Zonta et al. claimed that blockade of metabotropic glutamate receptors 1 and 5 using LY367385 and MPEP, respectively, abolished astrocytic calcium release and impairs neurovascular coupling as assessed by Laser Doppler flowmetry *in vivo* (Zonta et al., 2003). However, given that both excitatory and inhibitory neurons also express metabotropic glutamate receptors 1 and 5 at higher levels than astrocytes (Tasic et al., 2018), it is unclear if these drugs are actually impairing neural function instead of astrocytic function. A later study demonstrated that adult rodents lack metabotropic glutamate receptor 1 and 5 in astrocytes (Sun et al., 2013).

To test if these contradictory results were due to the use of *ex vivo* acute brain slice, Takano et al. manipulated calcium in astrocyte via calcium uncaging with DMNP-EDTA and imaged calcium dynamics with rhod-2/am in anesthetized mice *in vivo* and found that increased calcium evokes vasodilation (Takano et al., 2006). Furthermore, the authors identified that stimulated astrocytes metabolized arachidonic acid to PGE2 via COX-1 (*ptgs1)* that putatively binds to EP4 receptors on smooth muscle cells. This then promotes cAMP levels and cause vasodilation. However, given that both DMNP-EDTA and rhod-2/am were simply incubated on an open craniotomy, other cells besides astrocytes were loaded with these indicators. This could be a caveat as the light stimulation (355 nm) could have uncaged calcium in cells below and above the focal plane and could potentially evoke neurovascular coupling independent of calcium uncaging in astrocytes. Finally, it should be emphasized that COX-1 is more expressed in interneurons, macrophages and microglia than in astrocytes and COX-1 null mice have no impairments in sensory-evoked neural activity as assessed by laser Doppler flowmetry.

Indeed, further evidence from more recent studies questioned whether calcium in astrocytes contributes to neurovascular coupling. The release of calcium from the endoplasmic reticulum is a major source of astrocytic calcium. *Itpr2* encodes for the predominant inositol trisphosphate receptor in astrocytes. Nizar et al., Bonder et al. and Takata et al. identified that although *Itpr2* knockout mice have abolished calcium release in astrocytes, arteriolar dilation persisted upon sensory-evoked neural activity *in vivo* (Bonder and McCarthy, 2014; Nizar et al., 2013; Takata et al., 2013). Bonder et al. also manipulated astrocytic calcium by expressing Gq-DREADDs (Designer Receptors Exclusively Activated by Designer Drugs) to release calcium in astrocytes and found that the release of calcium via DREADDs in astrocytes had no effect on neurovascular coupling (Bonder and McCarthy, 2014). Furthermore, both studies identified that

in wild-type mice, arteriolar dilation precedes the increase in astrocytic calcium upon sensory-evoked neural activity, suggesting the rise in astrocytic calcium does not necessarily trigger vasodilation (Bonder and McCarthy, 2014; Nizar et al., 2013). Consistently, a recent study also identified that the onset of astrocytic calcium release is after arteriolar dilation (Tran et al., 2018). In fact, arteriolar dilation actually triggered the astrocytic calcium (Tran et al., 2018). Collectively, it is becoming clear that astrocytic calcium is not required for neurovascular coupling as arteriolar dilation precedes the release in astrocytic calcium upon neural activity and it is neither sufficient nor necessary. Further *in vivo* and genetic studies will determine the precise role of astrocytes in neurovascular coupling.

Vascular Smooth Muscle Cells: The cellular mechanisms of neurovascular coupling begin with neural activity and end with smooth muscle relaxation to dilate vessels and increase blood flow. Smooth muscle cells ensheathe only arteriolar endothelial cells and morphologically have been described as circumferential bands wrapping along the arteries (Armulik et al., 2011). Furthermore, astrocytic end-feet encase the smooth muscle cells (Iadecola, 2017). As the pial arteries on the brain dive into the brain parenchyma and branch into arterioles and then capillaries, the smooth muscle cells are replaced by pericytes, which wrap around capillary endothelial cells (Armulik et al., 2011). While many have argued recently that pericytes can also relax and contribute to neurovascular coupling (discussed more below), the prevailing view in the field is that smooth muscle cells are indeed the canonical effectors. Many have proposed that various cell types in the brain release vasoactive molecules that modulate smooth muscle relaxation and contraction as discussed in the previous sections. However, the advent of single-

cell RNA sequencing demonstrates that brain smooth muscle cells lack many of the receptors for these vasoactive molecules.

Astrocyte → Smooth Muscle Cells: Many argue that excitatory pyramidal neurons express COX-2 and astrocytes express COX-1 to metabolize arachidonic acid to PGE2 that is released onto smooth muscle cells to target EP2 and EP4 receptors, increasing cAMP levels to mediate relaxation (Lacroix et al., 2015; Takano et al., 2006). However, both EP2 and EP4 receptors, as mentioned above, are undetectable in smooth muscle cells by single-cell RNA sequencing and instead, both are more expressed in GABAergic interneurons (Hrvatin et al., 2018; Tasic et al., 2018; Vanlandewijck et al., 2018). Another putative mechanism is that astrocytes express the BK channel, *Kcnma1,* with calcium activation in astrocyte causing BK channels to release K+ into the extracellular space and hyperpolarize smooth muscle cells (Filosa et al., 2006). However, *Kcnma1* null mice do not have impairments in neurovascular coupling upon sensory-evoked neural activity (Girouard et al., 2010). While astrocytes could certainly still signal to smooth muscle cells to mediate neurovascular coupling, emerging evidence suggests that the proposed mechanisms are questionable and require further investigation.

Inhibitory Neuron → Smooth Muscle Cells: Recently, it has been postulated that interneurons can secrete vasoactive compounds directly onto smooth muscle cells (Iadecola, 2017). As discussed in the *Interneuron* section, it is thought that these subtypes of interneurons release neuromodulators or neuropeptides that could evoke or modulate neurovascular coupling. A recent study suggests that NPY released from interneurons acts to enhance the contractional phase of neurovascular coupling (Uhlirova et al., 2016). Antagonizing NPY type 1 receptor (*Npy1r*) with BIBP 3326 attenuated the magnitude of the constriction (Uhlirova et al., 2016). Single-cell RNA sequencing indeed demonstrates that *Npy1r* is expressed in smooth muscle cells

but also expressed in excitatory and inhibitory neurons (Hrvatin et al., 2018; Tasic et al., 2018; Vanlandewijck et al., 2018). Thus, it is possible that BIBP 3326 could antagonize NPY type 1 receptors on neurons and indirectly impair neurovascular coupling. A cell type conditional deletion of *Npy1r* will determine the role of NPY signaling in smooth muscle cells. VIP stimulates adenylate cyclase to increase cAMP level and induces vasodilation in isolated cerebral vessels *ex vivo* (Edvinsson et al., 1985; Huang and Rorstad, 1983). However, its function has remained elusive in neurovascular coupling *in vivo*. Specifically, VIP receptors, VPAC1 and VPAC2, are lowly expressed in smooth muscle cells and are also found in neurons, mainly excitatory neurons (Hrvatin et al., 2018; Tasic et al., 2018; Vanlandewijck et al., 2018). Again, cell type deletion of these receptors in smooth muscle cell specifically will elucidate the role of VIP signaling in neurovascular coupling *in vivo.* Somatostatin receptors are undetectable by single-cell RNA sequencing in smooth muscle cells (Hrvatin et al., 2018; Tasic et al., 2018; Vanlandewijck et al., 2018). Finally, while it is possible that NO from NOS1+ interneurons could induce smooth muscle cell relaxation, a cell-type specific deletion of NOS1 has not been performed *in vivo.*

Pericytes: While smooth muscle cells wrap around arteriolar endothelial cells, pericytes wrap around capillaries. Pericytes indeed are required for blood-CNS barrier formation (as discussed in the previous section), but their role in neurovascular coupling has been controversial. Specifically, while many accept that smooth muscle cells contract and dilate the arterioles, it has been uncertain whether pericytes play similar roles and modulate capillary vascular tone in response to neural activity.

The dispute about pericytes in regulating blood flow has been largely due to the identification and classification of smooth muscle cells and pericytes. Collectively, both are known as mural cells. However, both cell types share similar molecular markers and their ontogeny in various organs are overlapping (Armulik et al., 2011; 2005). Hall et al. claimed that pericytes can indeed relax and contract in a "branch order" dependent manner with the pial vessel classified as arterioles and any downstream vascular branches are considered capillaries (Hall et al., 2014). However, this classification is somewhat arbitrary. In the subsequent year, Hall et al. used *in vivo* two-photon imaging with molecular reporters to classify smooth muscle cells and pericytes (Hill et al., 2015). Using smooth muscle actin (SMA) as a genetic marker for smooth muscle cells and not pericytes, they found that SMA+ mural cells can relax and contract independent of diameter or their location on branch order (Hill et al., 2015). Furthermore, when Hill et al. expressed channelrhodopsin in all mural cells to depolarize the mural cells, they found that only SMA+ mural cells can contract (Hill et al., 2015). In a subsequent study from the same lab, Damisah et al. reported that Neurotrace 525 when applied *in vivo,* only labeled specifically SMA- mural cells and thus, labeled only "pericytes" (Damisah et al., 2017). Consistently, the dye is mutually exclusive with SMA+ and hydrazide 633+ mural cells and vessels, respectively, which are both markers for arterioles (Hill et al., 2015; Shen et al., 2012). Future studies should adopt a consensus identification for these various mural cells using unequivocal, unique molecular markers. Recent single-cell RNA sequencing studies have clustered various cell types based on SMA+ as smooth muscle cells and SMA- as pericytes. With these clustering, they discovered novel molecular markers to identify unambiguously smooth muscle cells by the expression of *Myh11, Tagln,* and *Cnnn1* and pericytes by the expression *kcnj8* and *abcc9* (Tasic

et al., 2018; Vanlandewijck et al., 2018). Using these novel markers to identify and classify smooth muscle cells, the field should reexamine the role of pericytes in neurovascular coupling.

Endothelial Cells: The prevailing neurovascular coupling model postulates that astrocytes or interneurons sense local neural activity and release vasodilation factors onto the smooth muscle cells of penetrating arterioles to relax and dilate arterioles (Attwell et al., 2010). However, given that changes in neural activity occur deep in the brain while smooth muscle cells only surround upstream arterioles, it is unlikely that locally generated factors, such as nitric oxide, can diffuse over a long distance (up to 200 microns) away to the upstream arterioles to elicit a vasodilatory response in such a short time frame (at hundreds of milliseconds *in vivo*) (Hillman, 2014). Given the spatiotemporal constraint of neurovascular coupling, this proposed model does not match the spatiotemporal criteria dictated by the anatomy of the vascular network.

Recent evidence suggests endothelial cells (ECs) play a pivotal role during neurovascular coupling: capillaries in deeper cortical layers sense neural activity and 'retrogradely' relay this information to dilate upstream arterioles via ionic electrical coupling (Chen et al., 2014; Longden et al., 2017; O'Herron et al., 2016; Silva and Koretsky, 2002). This model fits the spatiotemporal constraints. Capillary ECs (cECs) are ideal for sensing neural activity because they are deep in the brain and close to all neurons (Tsai et al., 2009). In a recent study, using an *ex vivo* and *in vivo* preparation containing both capillaries and upstream arterioles from the mouse brain, Longden et al. found brain cECs specifically express a potassium channel, Kir2.1, which makes cECs highly sensitive to the potassium generated during neural activity. Further supporting this idea, mice lacking Kir2.1 show attenuated neurovascular coupling (Longden et al., 2017). In addition, the spread of electrical signals across ECs is fast and can traverse long distances. In

peripheral vessels, ECs are electrically coupled via gap junctions and can rapidly conduct signals between ECs. These waves of ions, including potassium and calcium, trigger endothelial cell release of vasodilation factors onto smooth muscle cells (Segal, 2015; Tallini et al., 2007). A similar mechanism may exist in the brain vasculature, as micropipette application of 6-10 mM potassium to capillaries generated robust hyperpolarization in ECs that was transmitted retrogradely to penetrating arterioles at the estimated speed of 2 mm/s (Longden et al., 2017). Such hyperpolarization could travel through the endothelium via gap junctions to produce relaxation of smooth muscle cells (Iadecola, 2017; Segal, 2015; Tallini et al., 2007).

However, there is little evidence that gap junctions across the brain endothelium propagate hyperpolarization. Furthermore, once this hyperpolarization signal reaches arteriolar endothelial cells, it is unclear how the arteriolar endothelial cells relay signals to smooth muscle cells to dilate. One molecular player is eNOS or *nos3.* Analogous to nNOS, eNOS uses L-Arginine to generate nitric oxide, a potent vasodilator (Toth et al., 2015). However in contrast to nNOS, which is expressed in neurons, eNOS is expressed in all segments of the brain vasculature (Vanlandewijck et al., 2018). Furthermore, eNOS null mice display defects in neurovascular coupling upon sensory-evoked neural activity as assessed by laser Doppler flowmetry (Toth et al., 2015). Thus, while eNOS is necessary for optimal neurovascular coupling, it is unclear how eNOS is activated to synthesize NO to elicit neurovascular coupling.

Finally, analogous to the mural cells, endothelial cells across the different vascular segments also exhibit molecular heterogeneity (Vanlandewijck et al., 2018). Could arteriolar and capillary endothelial cells expressed differential genes and play distinct roles in mediating neurovascular coupling? In the second part of my thesis (Chapter 4), I will show that arteriolar and capillary endothelial cells exhibit molecular heterogeneity that results in both cellular and

functional heterogeneity. Specifically, my thesis work will highlight for the first time that arteriolar endothelial cells are important for neurovascular coupling.

In conclusion, neurovascular coupling is a complex process involving the coordination of multiple cells and feedback cycles. With the development of single-cell transcriptomics, cell-type conditional loss-of-function approaches, *in vivo* imaging and manipulation paradigms, the field could make a significant breakthrough to our understanding of the mechanisms underlying neurovascular coupling.

Conclusions

Although the neurovascular research community has recently made significant strides in identifying novel molecular regulators and inductive signals that mediate BBB function and neurovascular coupling, the field is still in its infancy, with many fundamental questions waiting to be answered. Further refinements in cell type purification techniques and next-generation sequencing technologies will unravel key molecular regulators and core pathways essential for the two unique functions of the CNS vasculature formation and function. Single-cell RNA sequencing to identify the transcriptome of brain cells and other purified cell types in the NVU at different developmental, physiological, aging and disease contexts will address many questions about its regulation. For example, different brain regions use different Wnt/ β-catenin molecular components for BBB function. Norrin is the Wnt signal in the retina and cerebellum whereas Wnt 7a/7b are the signals in the forebrain. (Zhou et al., 2014). Furthermore, it would be interesting to explore how the molecular signatures of the CNS endothelial cells in circumventricular organs (the regions in the CNS that do not display BBB such as median

eminence) differ from CNS endothelial cells displaying BBB (Broadwell and Brightman, 1976; Gross et al., 1987; Johnson and Gross, 1993).

Transcriptomics has proven invaluable in identifying genes that may regulate BBB function and neurovascular coupling (Huntley et al., 2014). But the genes from these datasets are still merely candidates until validated that they indeed mediate BBB and neurovascular regulation. Therefore, the field needs high-throughput screening to not only validate candidate genes but also to discover drugs that can modulate BBB permeability and neurovascular coupling. The advent of genome editing methods such as CRISPR-Cas9 has facilitated the generation of *in vivo* loss-of-function transgenesis, but this process is still arduous and too low throughput to validate a list of candidates from transcriptomics datasets (Sander and Joung, 2014). Thus, the use of more tractable model organisms with simpler CNS vasculature and robust loss-of-function genetic manipulations could accelerate the validation of candidates.

Although the CNS vasculature field has made significant progress in identifying key molecules that mediate BBB function and neurovascular coupling, the molecular and cellular mechanisms of how these molecules are mediating BBB function and neurovascular coupling are still poorly understood. This gap in knowledge is partly due to the limitations in the current technologies. For example, EM analyses in conjunction with dye tracers are the main techniques to monitor BBB properties (Hagan and Ben-Zvi, 2014). But these techniques only provide a static snapshot of the BBB and do not provide essential information such as kinetics of vesicular trafficking. There is a pressing need to develop an *in vivo* high-resolution technique to monitor BBB properties such as tight junction complexes and transcytosis in real time. As for neurovascular coupling, selective genetic access to manipulate the various steps of neurovascular coupling is needed *in vivo.*

However, these past discoveries mentioned above have greatly expanded our molecular and cellular understanding of this specialized vasculature that has fascinated physiologists for more than a century. Nevertheless, these discoveries open many more fundamental questions waiting to be resolved. There is a pressing demand for refinement in experimental technologies that will certainly accelerate our discoveries for novel molecules and our understanding of their cellular mechanisms that mediate BBB function and neurovascular coupling. Future findings will directly benefit therapeutics for neurological disorders in both drug delivery, repairing the dysfunctional barrier and cerebral blood flow in certain neurological diseases.

References

Maha Al-Asmakh & Lars Hedin (2015) Microbiota and the control of blood-tissue barriers, Tissue Barriers. *1*, 1-7.

Alakbarzade, V., Hameed, A., Quek, D.Q.Y., Chioza, B.A., Baple, E.L., Cazenave-Gassiot, A., Nguyen, L.N., Wenk, M.R., Ahmad, A.Q., Sreekantan-Nair, A., et al. (2015). A partially inactivating mutation in the sodium-dependent lysophosphatidylcholine transporter MFSD2A causes a non-lethal microcephaly syndrome. Nat. Genet. *47*, 814–817.

Alvarez, J.I., Dodelet-Devillers, A., Kebir, H., Ifergan, I., Fabre, P.J., Terouz, S., Sabbagh, M., Wosik, K., Bourbonnière, L., Bernard, M., et al. (2011). The Hedgehog pathway promotes blood-brain barrier integrity and CNS immune quiescence. Science *334*, 1727–1731.

Anderson, K.D., Pan, L., Yang, X.-M., Hughes, V.C., Walls, J.R., Dominguez, M.G., Simmons, M.V., Burfeind, P., Xue, Y., Wei, Y., et al. (2011). Angiogenic sprouting into neural tissue requires Gpr124, an orphan G protein-coupled receptor. Proc. Natl. Acad. Sci. U.S.a. *108*, 2807–2812.

Andreone, B.J., Lacoste, B., and Gu, C. (2015). Neuronal and vascular interactions. Annu. Rev. Neurosci. *38*, 25–46.

Armulik, A., Abramsson, A., and Betsholtz, C. (2005). Endothelial/pericyte interactions. Circulation Research *97*, 512–523.

Armulik, A., Genové, G., and Betsholtz, C. (2011). Pericytes: developmental, physiological, and pathological perspectives, problems, and promises. Developmental Cell *21*, 193–215.

Attwell, D., Buchan, A.M., Charpak, S., Lauritzen, M., MacVicar, B.A., and Newman, E.A. (2010). Glial and neuronal control of brain blood flow. Nature *468*, 232.

Balda, M.S., and Matter, K. (2009). Tight junctions and the regulation of gene expression. Biochim. Biophys. Acta *1788*, 761–767.

Ben-Zvi, A., Lacoste, B., Kur, E., Andreone, B.J., Mayshar, Y., Yan, H., and Gu, C. (2014). Mfsd2a is critical for the formation and function of the blood-brain barrier. Nature *509*, 507–511.

Betsholtz, C. (2014). Physiology: Double function at the blood-brain barrier. *509*, 432–433.

Betz, A.L., and Goldstein, G.W. (1978). Polarity of the Blood-Brain Barrier: Neutral Amino Acid Transport into Isolated Brain Capillaries. Science *202*, 225–227.

Blanchette, M., and Daneman, R. (2015). Formation and maintenance of the BBB. Mech. Dev. *138 Pt 1*, 8–16.

Bonder, D.E., and McCarthy, K.D. (2014). Astrocytic Gq-GPCR-linked IP3R-dependent Ca2+ signaling does not mediate neurovascular coupling in mouse visual cortex in vivo. J. Neurosci. *34*, 13139–13150.

Braniste, V., Al-Asmakh, M., Kowal, C., Anuar, F., Abbaspour, A., Tóth, M., Korecka, A., Bakocevic, N., Guan, N.L., Kundu, P., et al. (2014). The gut microbiota influences blood-brain barrier permeability in mice. Sci Transl Med *6*, 263ra158–263ra158.

Brightman, M.W., and Reese, T.S. (1969). Junctions between intimately apposed cell membranes in the vertebrate brain. J. Cell Biol. *40*, 648–677.

Broadwell, R.D., and Brightman, M.W. (1976). Entry of peroxidase into neurons of the central and peripheral nervous systems from extracerebral and cerebral blood. J. Comp. Neurol. *166*, 257–283.

Brouwer, M.C., Tunkel, A.R., and van de Beek, D. (2010). Epidemiology, diagnosis, and antimicrobial treatment of acute bacterial meningitis. Clin. Microbiol. Rev. *23*, 467–492.

Busija, D.W., and Leffler, C.W. (1987). Postjunctional alpha 2-adrenoceptors in pial arteries of anesthetized newborn pigs. Dev Pharmacol Ther *10*, 36–46.

Busija, D.W., Marcus, M.L., and Heistad, D.D. (1982). Pial Artery Diameter and Blood Flow Velocity during Sympathetic Stimulation in Cats:. Journal of Cerebral Blood Flow & Metabolism *2*, 363–367.

Cauli, B., and Hamel, E. (2010). Revisiting the role of neurons in neurovascular coupling. Front Neuroenergetics *2*, 9.

César-Razquin, A., Snijder, B., Frappier-Brinton, T., Isserlin, R., Gyimesi, G., Bai, X., Reithmeier, R.A., Hepworth, D., Hediger, M.A., Edwards, A.M., et al. (2015). A Call for Systematic Research on Solute Carriers. Cell *162*, 478–487.

Chen, B.R., Kozberg, M.G., Bouchard, M.B., Shaik, M.A., and Hillman, E.M.C. (2014). A Critical Role for the Vascular Endothelium in Functional Neurovascular Coupling in the Brain. J Am Heart Assoc *3*, e000787–e000787.

Chen, J., Stahl, A., Krah, N.M., Seaward, M.R., Joyal, J.-S., Juan, A.M., Hatton, C.J., Aderman, C.M., Dennison, R.J., Willett, K.L., et al. (2012). Retinal expression of Wnt-pathway mediated genes in low-density lipoprotein receptor-related protein 5 (Lrp5) knockout mice. PLoS ONE *7*, e30203.

Cho, C., Smallwood, P.M., and Nathans, J. (2017). Reck and Gpr124 Are Essential Receptor Cofactors for Wnt7a/Wnt7b-Specific Signaling in Mammalian CNS Angiogenesis and Blood-Brain Barrier Regulation. Neuron *95*, 1056–1073.e5.

Cullen, M., Elzarrad, M.K., Seaman, S., Zudaire, E., Stevens, J., Yang, M.Y., Li, X., Chaudhary, A., Xu, L., Hilton, M.B., et al. (2011). GPR124, an orphan G protein-coupled receptor, is required for CNS-specific vascularization and establishment of the blood-brain barrier. Proc. Natl. Acad. Sci. U.S.a. *108*, 5759–5764.

Damisah, E.C., Hill, R.A., Tong, L., Murray, K.N., and Grutzendler, J. (2017). A fluoro-Nissl dye identifies pericytes as distinct vascular mural cells during in vivo brain imaging. Nat. Neurosci. 1–12.

Daneman, R., Agalliu, D., Zhou, L., Kuhnert, F., Kuo, C.J., and Barres, B.A. (2009). Wnt/beta-catenin signaling is required for CNS, but not non-CNS, angiogenesis. Proc. Natl. Acad. Sci. U.S.a. *106*, 641–646.

Daneman, R., Zhou, L., Agalliu, D., Cahoy, J.D., Kaushal, A., and Barres, B.A. (2010). The mouse blood-brain barrier transcriptome: a new resource for understanding the development and function of brain endothelial cells. PLoS ONE *5*, e13741.

Dickson, L., and Finlayson, K. (2009). VPAC and PAC receptors: From ligands to function. Pharmacology & Therapeutics *121*, 294–316.

Edvinsson, L., Fredholm, B.B., Hamel, E., Jansen, I., and Verrecchia, C. (1985). Perivascular peptides relax cerebral arteries concomitant with stimulation of cyclic adenosine monophosphate accumulation or release of an endothelium-derived relaxing factor in the cat. Neurosci. Lett. *58*, 213–217.

Ehrlich, P. (1885). Das Sauerstoff-Bedürfniss des Organismus. Eine Farbenanalytische Studie. Berlin 1–85.

Ehrlich, P. (1904). Ueber die beziehungen von chemischer constitution, verteilung und pharmakologischer wirkung. In Gesammelte Arbeiten Zur Immunitaetsforschung, 1–8.

Engelhardt, B., and Ransohoff, R.M. (2012). Capture, crawl, cross: the T cell code to breach the blood-brain barriers. Trends Immunol. *33*, 579–589.

Filosa, J.A., Bonev, A.D., Straub, S.V., Meredith, A.L., Wilkerson, M.K., Aldrich, R.W., and Nelson, M.T. (2006). Local potassium signaling couples neuronal activity to vasodilation in the brain. Nat. Neurosci. *9*, 1397–1403.

Fox, P.T., and Raichle, M.E. (1986). Focal physiological uncoupling of cerebral blood flow and oxidative metabolism during somatosensory stimulation in human subjects. Pnas *83*, 1140–1144.

Fox, P.T., Raichle, M.E., Dence, C., and Mintun, M.A. (1988). Nonoxidative Glucose Consumption During Focal Physiologic Neural Activity. Science *241*, 462–464.

Girouard, H., Bonev, A.D., Hannah, R.M., Meredith, A., Aldrich, R.W., and Nelson, M.T. (2010). Astrocytic endfoot Ca2+ and BK channels determine both arteriolar dilation and constriction. Proc. Natl. Acad. Sci. U.S.a. *107*, 3811–3816.

Goldmann, E.E. (1909). Die äussere und innere sekretion des genden und gekranken Organismus im Licht der vitalen Färbung. *Beitr Klin Chix*. 64:192–265

Granger, A.J., Wang, W., Robertson, K., El-Rifai, M., Zanello, A., Bistrong, K., Saunders, A., Chow, B., Nunez, V., Gu, C., et al. (2019). Target-specific co-transmission of acetylcholine and GABA from a subset of cortical VIP+ interneurons. bioRxiv. 1–39.

Gross, P.M., Blasberg, R.G., Fenstermacher, J.D., and Patlak, C.S. (1987). The microcirculation of rat circumventricular organs and pituitary gland. Brain Research Bulletin *18*, 73–85.

Guemez-Gamboa, A., Nguyen, L.N., Yang, H., Zaki, M.S., Kara, M., Ben-Omran, T., Akizu, N., Rosti, R.O., Rosti, B., Scott, E., et al. (2015). Inactivating mutations in MFSD2A, required for omega-3 fatty acid transport in brain, cause a lethal microcephaly syndrome. Nat. Genet. *47.* 809-813

Hagan, N., and Ben-Zvi, A. (2014). The molecular, cellular, and morphological components of blood-brain barrier development during embryogenesis. Semin. Cell Dev. Biol. *38*, 7–15.

Hall, C.N., Reynell, C., Gesslein, B., Hamilton, N.B., Mishra, A., Sutherland, B.A., O'Farrell, F.M., Buchan, A.M., Lauritzen, M., and Attwell, D. (2014). Capillary pericytes regulate cerebral blood flow in health and disease. Nature *508*, 55–60.

Hamel, E. (2006). Perivascular nerves and the regulation of cerebrovascular tone. Journal of Applied Physiology *100*, 1059–1064.

Harel, T., Quek, D.Q.Y., Wong, B.H., Cazenave-Gassiot, A., Wenk, M.R., Fan, H., Berger, I., Shmueli, D., Shaag, A., Silver, D.L., et al. (2018). Homozygous mutation in MFSD2A, encoding a lysolipid transporter for docosahexanoic acid, is associated with microcephaly and hypomyelination. Neurogenetics 1–9.

Hatherell, K., Couraud, P.-O., Romero, I.A., Weksler, B., and Pilkington, G.J. (2011). Development of a three-dimensional, all-human in vitro model of the blood-brain barrier using mono-, co-, and tri-cultivation Transwell models. J. Neurosci. Methods *199*, 223–229.

Heistad, D.D., Marcus, M.L., Sandberg, S., and Abboud, F.M. (1977). Effect of sympathetic nerve stimulation on cerebral blood flow and on large cerebral arteries of dogs. Circulation Research *41*, 342–350.

Hill, R.A., Tong, L., Yuan, P., Murikinati, S., Gupta, S., and Grutzendler, J. (2015). Regional Blood Flow in the Normal and Ischemic Brain Is Controlled by Arteriolar Smooth Muscle Cell Contractility and Not by Capillary Pericytes. Neuron *87*, 95–110.

Hillman, E.M.C. (2014). Coupling mechanism and significance of the BOLD signal: a status report. Annu. Rev. Neurosci. *37*, 161–181.

Hrvatin, S., Hochbaum, D.R., Nagy, M.A., Cicconet, M., Robertson, K., Cheadle, L., Zilionis, R., Ratner, A., Borges-Monroy, R., Klein, A.M., et al. (2018). Single-cell analysis of experience-dependent transcriptomic states in the mouse visual cortex. Nat. Neurosci. *21*, 120–129.

Hsiao, E.Y., McBride, S.W., Hsien, S., Sharon, G., Hyde, E.R., McCue, T., Codelli, J.A., Chow, J., Reisman, S.E., Petrosino, J.F., et al. (2013). Microbiota Modulate Behavioral and Physiological Abnormalities Associated with Neurodevelopmental Disorders. Cell 1–25.

Huang, M., and Rorstad, O.P. (1983). Effects of vasoactive intestinal polypeptide, monoamines, prostaglandins, and 2-chloroadenosine on adenylate cyclase in rat cerebral microvessels. J. Neurochem. *40*, 719–726.

Huntley, M.A., Bien-Ly, N., Daneman, R., and Watts, R.J. (2014). Dissecting gene expression at the blood-brain barrier. Front Neurosci *8*, 355.

Iadecola, C. (2017). The Neurovascular Unit Coming of Age: A Journey through Neurovascular Coupling in Health and Disease. Neuron *96*, 17–42.

J R Pappenheimer (1951). Filtration, Diffusion and Molecular Sieving Through Peripheral Capillary Membranes. A Contribution to the Pore Theory of Capillary Permeability. American Journal of Physiology *167*, 1–34.

Ji, L., Zhou, J., Zafar, R., Kantorovich, S., Jiang, R., Carney, P.R., and Jiang, H. (2012). Cortical neurovascular coupling driven by stimulation of channelrhodopsin-2. PLoS ONE *7*, e46607.

Johnson, A.K., and Gross, P.M. (1993). Sensory circumventricular organs and brain homeostatic pathways. Faseb J. *7*, 678–686.

Jones, A.R., and Shusta, E.V. (2007). Blood–Brain Barrier Transport of Therapeutics via Receptor-Mediation. Pharm Res *24*, 1759–1771.

Karnovsky, M.J. (1967). The ultrastructural basis of capillary permeability studied with peroxidase as a tracer. J. Cell Biol. *35*, 213–236.

Kety, S.S., and Schmidt, C.F. (1948). The Nitrous Oxide Method For The Quantitative Determination Of Cerebral Blood Flow In Man: Theory, Procedure And Normal Values. J. Clin. Invest. *27*, 476–483.

Kim, B.J., Hancock, B.M., Bermudez, A., Cid, N.D., Reyes, E., van Sorge, N.M., Lauth, X., Smurthwaite, C.A., Hilton, B.J., Stotland, A., et al. (2015). Bacterial induction of Snail1 contributes to blood-brain barrier disruption. J. Clin. Invest. *125*, 2473–2483.

Kisler, K., Nelson, A.R., Montagne, A., and Zlokovic, B.V. (2017). Cerebral blood flow regulation and neurovascular dysfunction in Alzheimer disease. Nature Review Neuroscience *18*, 419–434.

Klein, A.M., Mazutis, L., Akartuna, I., Tallapragada, N., Veres, A., Li, V., Peshkin, L., Weitz, D.A., and Kirschner, M.W. (2015). Droplet barcoding for single-cell transcriptomics applied to embryonic stem cells. Cell *161*, 1187–1201.

Kuhnert, F., Mancuso, M.R., Shamloo, A., Wang, H.-T., Choksi, V., Florek, M., Su, H., Fruttiger, M., Young, W.L., Heilshorn, S.C., et al. (2010). Essential regulation of CNS angiogenesis by the orphan G protein-coupled receptor GPR124. Science *330*, 985–989.

Kuschinsky, W., and Wahl, M. (1975). Alpha-receptor stimulation by endogenous and exogenous norepinephrine and blockade by phentolamine in pial arteries of cats. Circulation Research *37*, 168–174.

Kwong, K.K., Belliveau, J.W., Chesler, D.A., Goldberg, I.E., Weisskoff, R.M., Poncelet, B.P., Kennedy, D.N., Hoppel, B.E., Cohen, M.S., and Turner, R. (1992). Dynamic magnetic resonance imaging of human brain activity during primary sensory stimulation. Pnas *89*, 5675–5679.

Lacroix, A., Toussay, X., Anenberg, E., Lecrux, C., Ferreirós, N., Karagiannis, A., Plaisier, F., Chausson, P., Jarlier, F., Burgess, S.A., et al. (2015). COX-2-Derived Prostaglandin E2 Produced by Pyramidal Neurons Contributes to Neurovascular Coupling in the Rodent Cerebral Cortex. J. Neurosci. *35*, 11791–11810.

Lafourcade, M., Larrieu, T., Mato, S., Duffaud, A., Sepers, M., Matias, I., De Smedt-Peyrusse, V., Labrousse, V.F., Bretillon, L., Matute, C., et al. (2011). Nutritional omega-3 deficiency abolishes endocannabinoid-mediated neuronal functions. Nat. Neurosci. *14*, 345–350.

Lee, J.H., Durand, R., Gradinaru, V., Zhang, F., Goshen, I., Kim, D.-S., Fenno, L.E., Ramakrishnan, C., and Deisseroth, K. (2010). Global and local fMRI signals driven by neurons defined optogenetically by type and wiring. Nature *465*, 788.

Lee, L.M., Boorman, L., Glendenning, E., Christmas, C., Sharp, P., Redgrave, P., Shabir, O., Bracci, E., Berwick, J., and Howarth, C. (2019). Key aspects of neurovascular control mediated by specific populations of inhibitory cortical interneurons. bioRxiv. 1–27.

Li, S., Koziol-White, C., Jude, J., Jiang, M., Zhao, H., Cao, G., Yoo, E., Jester, W., Morley, M.P., Zhou, S., et al. (2016). Epithelium-generated neuropeptide Y induces smooth muscle contraction to promote airway hyperresponsiveness. J. Clin. Invest. *126*, 1978–1982.

Liebner, S., Corada, M., Bangsow, T., Babbage, J., Taddei, A., Czupalla, C.J., Reis, M., Felici, A., Wolburg, H., Fruttiger, M., et al. (2008). Wnt/beta-catenin signaling controls development of the blood-brain barrier. J. Cell Biol. *183*, 409–417.

Lindauer, U., Leithner, C., Kaasch, H., Rohrer, B., Foddis, M., chtemeier, M.F.U., Offenhauser, N., Steinbrink, J., Royl, G., Kohl-Bareis, M., et al. (2009). Neurovascular coupling in rat brain operates independent of hemoglobin deoxygenation. Journal of Cerebral Blood Flow & Metabolism *30*, 757–768.

Lippmann, E.S., Al-Ahmad, A., Azarin, S.M., Palecek, S.P., and Shusta, E.V. (2014). A retinoic acid-enhanced, multicellular human blood-brain barrier model derived from stem cell sources. Sci. Rep. *4*, 4160.

Lippmann, E.S., Azarin, S.M., Kay, J.E., Nessler, R.A., Wilson, H.K., Al-Ahmad, A., Palecek, S.P., and Shusta, E.V. (2012). Derivation of blood-brain barrier endothelial cells from human pluripotent stem cells. Nat. Biotechnol. *30*, 783–791.

Liu, W.-Y., Wang, Z.-B., Zhang, L.-C., Wei, X., and Li, L. (2012). Tight junction in blood-brain barrier: an overview of structure, regulation, and regulator substances. CNS Neurosci Ther *18*, 609–615.

Longden, T.A., Dabertrand, F., Koide, M., Gonzales, A.L., Tykocki, N.R., Brayden, J.E., Hill-Eubanks, D., and Nelson, M.T. (2017). Capillary K+-sensing initiates retrograde hyperpolarization to increase local cerebral blood flow. Nat. Neurosci. *20*, 717–726.

Löscher, W., and Potschka, H. (2005). Role of drug efflux transporters in the brain for drug disposition and treatment of brain diseases. Prog. Neurobiol. *76*, 22–76.

Ma, J., Ayata, C., Huang, P.L., Fishman, M.C., and Moskowitz, M.A. (1996). Regional cerebral blood flow response to vibrissal stimulation in mice lacking type I NOS gene expression. Am. J. Physiol. *270*, H1085–H1090.

Martí, E., and Bovolenta, P. (2002). Sonic hedgehog in CNS development: one signal, multiple outputs. Trends in Neurosciences *25*, 89–96.

McDannold, N., Arvanitis, C.D., Vykhodtseva, N., and Livingstone, M.S. (2012). Temporary Disruption of the Blood–Brain Barrier by Use of Ultrasound and Microbubbles: Safety and Efficacy Evaluation in Rhesus Macaques. Cancer Res *72*, 3652–3663.

Mintun, M.A., Vlassenko, A.G., Rundle, M.M., and Raichle, M.E. (2004). Increased lactate/pyruvate ratio augments blood flow in physiologically activated human brain. Pnas *101*, 659–664.

Muldoon, L.L., Alvarez, J.I., Begley, D.J., Boado, R.J., Del Zoppo, G.J., Doolittle, N.D., Engelhardt, B., Hallenbeck, J.M., Lonser, R.R., Ohlfest, J.R., et al. (2013). Immunologic privilege in the central nervous system and the blood-brain barrier. J. Cereb. Blood Flow Metab. *33*, 13–21.

Mulligan, S.J., and MacVicar, B.A. (2004). Calcium transients in astrocyte endfeet cause cerebrovascular constrictions. Nature *431*, 195–199.

Nguyen, L.N., Ma, D., Shui, G., Wong, P., Cazenave-Gassiot, A., Zhang, X., Wenk, M.R., Goh, E.L.K., and Silver, D.L. (2014). Mfsd2a is a transporter for the essential omega-3 fatty acid docosahexaenoic acid. Nature *509*, 503–506.

Nielsen, K.C., Owman, C., and Sporrong, B. (1971). Ultrastructure of the autonomic innervation apparatus in the main pial arteries of rats and cats. Brain Res. *27*, 25–32.

Niewoehner, J., Bohrmann, B., Collin, L., Urich, E., Sade, H., Maier, P., Rueger, P., Stracke, J.O., Lau, W., Tissot, A.C., et al. (2014). Increased brain penetration and potency of a therapeutic antibody using a monovalent molecular shuttle. Neuron *81*, 49–60.

Nitta, T., Hata, M., Gotoh, S., Seo, Y., Sasaki, H., Hashimoto, N., Furuse, M., and Tsukita, S. (2003). Size-selective loosening of the blood-brain barrier in claudin-5-deficient mice. J. Cell Biol. *161*, 653–660.

Nizar, K., Uhlirova, H., Tian, P., Saisan, P.A., Cheng, Q., Reznichenko, L., Weldy, K.L., Steed, T.C., Sridhar, V.B., MacDonald, C.L., et al. (2013). In vivo stimulus-induced vasodilation occurs without IP3 receptor activation and may precede astrocytic calcium increase. J. Neurosci. *33*, 8411–8422.

O'Herron, P., Chhatbar, P.Y., Levy, M., Shen, Z., Schramm, A.E., Lu, Z., and Kara, P. (2016). Neural correlates of single-vessel haemodynamic responses in vivo. Nature *534*, 378–382.

Ogawa, S., Lee, T.M., Kay, A.R., and Tank, D.W. (1990). Brain magnetic resonance imaging with contrast dependent on blood oxygenation. Pnas *87*, 9868–9872.

Ogawa, S., Tank, D.W., Menon, R., Ellermann, J.M., Kim, S.G., Merkle, H., and Ugurbil, K. (1992). Intrinsic signal changes accompanying sensory stimulation: functional brain mapping with magnetic resonance imaging. Pnas *89*, 5951–5955.

Paes, K.T., Wang, E., Henze, K., Vogel, P., Read, R., Suwanichkul, A., Kirkpatrick, L.L., Potter, D., Newhouse, M.M., and Rice, D.S. (2011). Frizzled 4 is required for retinal angiogenesis and maintenance of the blood-retina barrier. Investigative Ophthalmology & Visual Science *52*, 6452–6461.

Paolinelli, R., Corada, M., Ferrarini, L., Devraj, K., Artus, C., Czupalla, C.J., Rudini, N., Maddaluno, L., Papa, E., Engelhardt, B., et al. (2013). Wnt activation of immortalized brain endothelial cells as a tool for generating a standardized model of the blood brain barrier in vitro. PLoS ONE *8*, e70233.

Pardridge, W.M. (2012). Drug transport across the blood–brain barrier. J. Cereb. Blood Flow Metab. *32*, 1959–1972.

Penfield, W. (1932). Intracerebral Vascular Nerves. Arch NeurPsych *27*, 30–44.

Posokhova, E., Shukla, A., Seaman, S., Volate, S., Hilton, M.B., Wu, B., Morris, H., Swing, D.A., Zhou, M., Zudaire, E., et al. (2015). GPR124 Functions as a WNT7-Specific Coactivator of Canonical β-Catenin Signaling. Cell Reports *10*, 123–130.

Powers, W.J., Hirsch, I.B., and Cryer, P.E. (1996). Effect of stepped hypoglycemia on regional cerebral blood flow response to physiological brain activation. Am. J. Physiol. *270*, H554–H559.

Purves, M.J. (1978). Do vasomotor nerves significantly regulate cerebral blood flow? Circulation Research *43*, 485–493.

Ransohoff, R.M., and Engelhardt, B. (2012). The anatomical and cellular basis of immune surveillance in the central nervous system. Nat. Rev. Immunol. *12*, 623–635.

Reese, T.S., and Karnovsky, M.J. (1967). Fine structural localization of a blood-brain barrier to exogenous peroxidase. J. Cell Biol. *34*, 207–217.

Roy, C.S., and Sherrington, C.S. (1890). On the Regulation of the Blood-supply of the Brain. J. Physiol. (Lond.) *11*, 85–158.

Samiotaki, G., Acosta, C., Wang, S., and Konofagou, E.E. (2015). Enhanced delivery and bioactivity of the neurturin neurotrophic factor through focused ultrasound-mediated blood-brain barrier opening in vivo. J. Cereb. Blood Flow Metab. *35*, 611–622.

Sander, J.D., and Joung, J.K. (2014). CRISPR-Cas systems for editing, regulating and targeting genomes. Nat. Biotechnol. *32*, 347–355.

Saunders, N.R., Daneman, R., Dziegielewska, K.M., and Liddelow, S.A. (2013). Transporters of the blood-brain and blood-CSF interfaces in development and in the adult. Mol. Aspects Med. *34*, 742–752.

Schinkel, A.H., Smit, J.J., van Tellingen, O., Beijnen, J.H., Wagenaar, E., van Deemter, L., Mol, C.A., van der Valk, M.A., Robanus-Maandag, E.C., and Riele, te, H.P. (1994). Disruption of the mouse mdr1a P-glycoprotein gene leads to a deficiency in the blood-brain barrier and to increased sensitivity to drugs. Cell *77*, 491–502.

Schinkel, A.H., Wagenaar, E., van Deemter, L., Mol, C.A., and Borst, P. (1995). Absence of the mdr1a P-Glycoprotein in mice affects tissue distribution and pharmacokinetics of dexamethasone, digoxin, and cyclosporin A. J. Clin. Invest. *96*, 1698–1705.

Segal, S.S. (2015). Integration and Modulation of Intercellular Signaling Underlying Blood Flow Control. J. Vasc. Res. *52*, 136–157.

Shen, Z., Lu, Z., Chhatbar, P.Y., O'Herron, P., and Kara, P. (2012). An artery-specific fluorescent dye for studying neurovascular coupling. Nat. Methods *9*, 273–276.

Siegenthaler, J.A., Sohet, F., and Daneman, R. (2013). "Sealing off the CNS": cellular and molecular regulation of blood-brain barriergenesis. Curr. Opin. Neurobiol. *23*, 1057–1064.

Silva, A.C., and Koretsky, A.P. (2002). Laminar specificity of functional MRI onset times during somatosensory stimulation in rat. Pnas *99*, 15182–15187.

Simpson, I.A., Carruthers, A., and Vannucci, S.J. (2007). Supply and demand in cerebral energy metabolism: the role of nutrient transporters. Journal of Cerebral Blood Flow & Metabolism *27*, 1766–1791.

Small, S.A. (2004). Quantifying cerebral blood flow: regional regulation with global implications. J. Clin. Invest. *114*, 1046–1048.

Sohet, F., Lin, C., Munji, R.N., Lee, S.Y., Ruderisch, N., Soung, A., Arnold, T.D., Derugin, N., Vexler, Z.S., Yen, F.T., et al. (2015). LSR/angulin-1 is a tricellular tight junction protein involved in blood-brain barrier formation. J. Cell Biol. *208*, 703–711.

Stenman, J.M., Rajagopal, J., Carroll, T.J., Ishibashi, M., McMahon, J., and McMahon, A.P. (2008). Canonical Wnt signaling regulates organ-specific assembly and differentiation of CNS vasculature. Science *322*, 1247–1250.

Stewart, P.A., and Wiley, M.J. (1981). Developing nervous tissue induces formation of blood-brain barrier characteristics in invading endothelial cells: a study using quail--chick transplantation chimeras. Dev. Biol. *84*, 183–192.

Sun, W., McConnell, E., Pare, J.-F., Xu, Q., Chen, M., Peng, W., Lovatt, D., Han, X., Smith, Y., and Nedergaard, M. (2013). Glutamate-dependent neuroglial calcium signaling differs between young and adult brain. Science *339*, 197–200.

Takano, T., Tian, G.-F., Peng, W., Lou, N., Libionka, W., Han, X., and Nedergaard, M. (2006). Astrocyte-mediated control of cerebral blood flow. Nat. Neurosci. *9*, 260–267.

Takata, N., Nagai, T., Ozawa, K., Oe, Y., Mikoshiba, K., and Hirase, H. (2013). Cerebral Blood Flow Modulation by Basal Forebrain or Whisker Stimulation Can Occur Independently of Large Cytosolic Ca2+ Signaling in Astrocytes. PLoS ONE *8*, e66525–e66526.

Tallini, Y.N., Brekke, J.F., Shui, B., Doran, R., Hwang, S.-M., Nakai, J., Salama, G., Segal, S.S., and Kotlikoff, M.I. (2007). Propagated Endothelial Ca2+ Waves and Arteriolar Dilation In Vivo. Circulation Research *101*, 1300–1309.

Tam, S.J., Richmond, D.L., Kaminker, J.S., Modrusan, Z., Martin-McNulty, B., Cao, T.C., Weimer, R.M., Carano, R.A.D., van Bruggen, N., and Watts, R.J. (2012). Death receptors DR6 and TROY regulate brain vascular development. Developmental Cell *22*, 403–417.

Tan, C.M.J., Green, P., Tapoulal, N., Lewandowski, A.J., Leeson, P., and Herring, N. (2018). The Role of Neuropeptide Y in Cardiovascular Health and Disease. Front. Physiol. *9*.

Tasic, B., Menon, V., Nguyen, T.N., Kim, T.K., Jarsky, T., Yao, Z., Levi, B., Gray, L.T., Sorensen, S.A., Dolbeare, T., et al. (2016). Adult mouse cortical cell taxonomy revealed by single cell transcriptomics. Nat. Neurosci. *19*, 335–346.

Tasic, B., Yao, Z., Graybuck, L.T., Smith, K.A., Nguyen, T.N., Bertagnolli, D., Goldy, J., Garren, E., Economo, M.N., Viswanathan, S., et al. (2018). Shared and distinct transcriptomic cell types across neocortical areas. Nature *563*, 72–78.

Tatemoto, K., Carlquist, M., and Mutt, V. (1982). Neuropeptide Y—a novel brain peptide with structural similarities to peptide YY and pancreatic polypeptide. Nature *296*, 659–660.

Tietz, S., and Engelhardt, B. (2015). Brain barriers: Crosstalk between complex tight junctions and adherens junctions. J. Cell Biol. *209*, 493–506.

Toth, P., Tarantini, S., Davila, A., Valcarcel-Ares, M.N., Tucsek, Z., Varamini, B., Ballabh, P., Sonntag, W.E., Baur, J.A., Csiszar, A., et al. (2015). Purinergic glio-endothelial coupling during neuronal activity: role of P2Y1 receptors and eNOS in functional hyperemia in the mouse somatosensory cortex. American Journal of Physiology - Heart and Circulatory Physiology.

Tran, C.H.T., Peringod, G., and Gordon, G.R. (2018). Astrocytes Integrate Behavioral State and Vascular Signals during Functional Hyperemia. Neuron 1–20.

Tsai, P.S., Kaufhold, J.P., Blinder, P., Friedman, B., Drew, P.J., Karten, H.J., Lyden, P.D., and Kleinfeld, D. (2009). Correlations of neuronal and microvascular densities in murine cortex revealed by direct counting and colocalization of nuclei and vessels. J. Neurosci. *29*, 14553–14570.

Tuma, P.L., and Hubbard, A.L. (2003). Transcytosis: crossing cellular barriers. Physiol. Rev. *83*, 871–932.

Uhlirova, H., Kılıç, K., Tian, P., Thunemann, M., Desjardins, M., Saisan, P.A., Sakadžić, S., Ness, T.V., Mateo, C., Cheng, Q., et al. (2016). Cell type specificity of neurovascular coupling in cerebral cortex. Elife *5*, e14315.

Urban, A., Rancillac, A., Martinez, L., and Rossier, J. (2012). Deciphering the Neuronal Circuitry Controlling Local Blood Flow in the Cerebral Cortex with Optogenetics in PV::Cre Transgenic Mice. Frontiers in Pharmacology *3*.

van Sorge, N.M., and Doran, K.S. (2012). Defense at the border: the blood–brain barrier versus bacterial foreigners. Future Microbiology *7*, 383–394.

Vanhollebeke, B., Stone, O.A., Bostaille, N., Cho, C., Zhou, Y., Maquet, E., Gauquier, A., Cabochette, P., Fukuhara, S., Mochizuki, N., et al. (2015). Tip cell-specific requirement for an atypical Gpr124- and Reck-dependent Wnt/β-catenin pathway during brain angiogenesis. Elife *4*.

Vanlandewijck, M., He, L., Mäe, M.A., Andrae, J., Ando, K., Del Gaudio, F., Nahar, K., Lebouvier, T., Laviña, B., Gouveia, L., et al. (2018). A molecular atlas of cell types and zonation in the brain vasculature. Nature *554*, 475–480.

Vein, A.A. (2008). Science and Fate: Lina Stern (1878–1968), A Neurophysiologist and Biochemist. Journal of the History of the Neurosciences *17*, 195–206.

Wang, Y., Cho, C., Williams, J., Smallwood, P.M., Zhang, C., Junge, H.J., and Nathans, J. (2018). Interplay of the Norrin and Wnt7a/Wnt7b signaling systems in blood-brain barrier and blood-retina barrier development and maintenance. Proc. Natl. Acad. Sci. U.S.a. *115*, E11827–E11836.

Wang, Y., Rattner, A., Zhou, Y., Williams, J., Smallwood, P.M., and Nathans, J. (2012). Norrin/Frizzled4 signaling in retinal vascular development and blood brain barrier plasticity. Cell *151*, 1332–1344.

Wilhelm, I., Fazakas, C., and Krizbai, I.A. (2011). In vitro models of the blood-brain barrier. Acta Neurobiol Exp (Wars) *71*, 113–128.

Willis, T., & Wren, C. (1664). Cerebri anatome: Cui accessit nervorum descriptio et usus. Londini: typis Tho. Roycroft, Impensis Jo. Martyn & Ja. Allestry.

Winkler, E.A., Nishida, Y., Sagare, A.P., Rege, S.V., Bell, R.D., Perlmutter, D., Sengillo, J.D., Hillman, S., Kong, P., Nelson, A.R., et al. (2015). GLUT1 reductions exacerbate Alzheimer's disease vasculo-neuronal dysfunction and degeneration. Nat. Neurosci. *18*, 521–530.

Wolf, T., Lindauer, U., Villringer, A., and Dirnagl, U. (1997). Excessive oxygen or glucose supply does not alter the blood flow response to somatosensory stimulation or spreading depression in rats. Brain Res. *761*, 290–299.

Xiao, G., and Gan, L.-S. (2013). Receptor-Mediated Endocytosis and Brain Delivery of Therapeutic Biologics. International Journal of Cell Biology *2013*, 1–14.

Yen, F.T., Roitel, O., Bonnard, L., Notet, V., Pratte, D., Stenger, C., Magueur, E., and Bihain, B.E. (2008). Lipolysis stimulated lipoprotein receptor: a novel molecular link between hyperlipidemia, weight gain, and atherosclerosis in mice. J. Biol. Chem. *283*, 25650–25659.

Yu, Y.J., and Watts, R.J. (2013). Developing therapeutic antibodies for neurodegenerative disease. Neurotherapeutics *10*, 459–472.

Zhao, Z., and Zlokovic, B.V. (2014). Blood-brain barrier: a dual life of MFSD2A? Neuron *82*, 728–730.

Zheng, P.-P., Romme, E., Spek, P.J.V.D., Dirven, C.M.F., Willemsen, R., and Kros, J.M. (2010). Glut1/SLC2A1 is crucial for the development of the blood-brain barrier in vivo. Ann. Neurol. *68*, 835–844.

Zhou, Y., and Nathans, J. (2014). Gpr124 controls CNS angiogenesis and blood-brain barrier integrity by promoting ligand-specific canonical wnt signaling. Developmental Cell *31*, 248–256.

Zhou, Y., Wang, Y., Tischfield, M., Williams, J., Smallwood, P.M., Rattner, A., Taketo, M.M., and Nathans, J. (2014). Canonical WNT signaling components in vascular development and barrier formation. J. Clin. Invest. *124*, 3825–3846.

Zlokovic, B.V. (2008). The blood-brain barrier in health and chronic neurodegenerative disorders. Neuron *57*, 178–201.

Zlokovic, B.V. (2011). Neurovascular pathways to neurodegeneration in Alzheimer's disease and other disorders. Nature Review Neuroscience *12*, 723–738.

Zonta, M., Angulo, M.C., Gobbo, S., Rosengarten, B., Hossmann, K.-A., Pozzan, T., and Carmignoto, G. (2003). Neuron-to-astrocyte signaling is central to the dynamic control of brain microcirculation. Nat. Neurosci. *6*, 43–50.

CHAPTER 2

Experimental Procedures

2.1 *In vivo* techniques

Animal models:

All mice were group housed in standard vivarium conditions, with *ad libitum* access to diet and water. Both males and females were used in this study. Wild-type Swiss-Webster mice (Charles River Laboratory; Strain 024) were used for postnatal BRB functionality assays. Day of birth was defined as postnatal day zero (P0). Wild-type C57BL/6J mice (Jackson Laboratory # 000664) were used to determine vesicular density between brain capillaries and arterioles. All the following mice were maintained on C57Bl/6J background: *Mfsd2a*$^{-/-}$ mice (Ben-Zvi et al., 2014) were used to determine precocious blood-retinal barrier formation and for validation of the Mfsd2a antibody in retinas. *Mfsd2a:CreER* (Chen et al., 2016) mice were used to determine endogenous Mfsd2a expression in CNS capillaries and arterioles. *BMX:CreER* (Ehling et al., 2013) mice were used to genetically target arterial endothelial cells. *Myh11:CreER* (Wirth et al., 2008) were used to genetically access mural cells. *NG2:DsRED* (Zhu et al., 2008) (JAX# 008241) were used to identify mural cells and to determine pericyte density and coverage during functional BRB development. *Ai14* (Madisen et al., 2010) (JAX# 007914) mice were used as a Cre-dependent reporter to express tdTomato. *Ai39* (Madisen et al., 2012) (JAX# 014539) were used to express halorhodopsin in a Cre-dependent manner. *Ai75* (Quina et al., 2017) (JAX# 014539) were used to express nuclear-localized tdTomato in a Cre-dependent manner. *Thy1:GCaMP6s* (Chen et al., 2013) (JAX# 024275) mice were used to monitor calcium dynamics in neurons as an indirect measurement for neural activity. *Cav1*$^{-/-}$ (Razani et al., 2001) (JAX# 007083) mice were used to determine precocious BRB development and to ablate caveolae in CNS arterioles. Cav1 floxed (Asterholm et al., 2012) mice were used to conditionally ablate *Cav1* and caveolae in a Cre-dependent manner. *Nos3*$^{-/-}$ (Shesely et al., 1996) (JAX#

002684) mice were used to determine defects in nitric oxide signaling for neurovascular coupling. *ROSA26: PhiC31* (Raymond and Soriano, 2007) (JAX# 007743) mice were used to remove the selection cassettes in mice that had genetic constructs flanked by attP and attB sites. A maximum of five adult mice was maintained in one cage. For postnatal, the litter and two adult mice were maintained in one cage. Mice were maintained on a 12 light/12 dark cycle. All animals were treated according to institutional and US National Institutes of Health (NIH) guidelines approved by the Institutional Animal Care and Use Committee (IACUC) at Harvard Medical School.

Generation of *ROSA26:LSL-Mfsd2a* transgenic mice:

The targeting vector contains a CAG promoter and loxP-3xSV40PA-loxP followed by mMfsd2a cDNA and WPRE-PolyA. A positive selection cassette, attB-PGKNeoR-attP, is located between the insertion and the 3' homologous arm which is 4.3 kb. The length of the 5' homologous arm is 1.1 kb. The targeting vector was electroporated into ES cells derived from F1 hybrid blastocyst of 129S6 x C57BL/6J. The G418 resistant ES clones were screened by nested PCR using primers outside the construct paired with primers inside the insertion cassette. The positive ES cell clones were used to generate chimeric mice by aggregating with 8-cell embryos of CD-1 strain. The attB-Neo-attP cassette was removed in mice by crossing the chimeras with R26PhiC31 females (JAX# 007743) backcrossed in C57BL/6J for 13 generations. The F1 pups were genotyped by PCR using primers set (5'- CCAAAGTCGCTCTGAGTTGT -3'); (5'- CCAGGTTAGCCTTTAAGCCT -3') and (5'- CGGGCCATTTACCGTAAGTT-3'). The PCR products are 250 bp for the wildtype allele and 329 bp for the mutant allele.

Cranial window surgery:

Six-week-old to four-month-old mice underwent a craniotomy, implantation of a sterile glass window (3.0 mm) and attachment of a customized titanium head-plate to the skull using dental cement (Metabond Parkell Inc.). Prior to the craniotomy, an intramuscular dose of Dexamethasone (120 mg•kg^{-1}) was administered. Mice were anesthetized with 3-5% Isoflurane and maintained at 1-2% Isoflurane for the duration of the craniotomy. The respiration rate and body temperature were continuously monitored throughout the procedure to ensure the appropriate level of anesthesia. A subcutaneous dose of the analgesic Ketoprofen (10 mg/kg) was administered at the onset of the procedure and was administered daily for two additional days after the craniotomy. A single dose of the local anesthetic Lidocaine (20 mg•kg^{-1}) / Bupivacaine (2.5 mg•kg^{-1}) was administered subcutaneously at the site the craniotomy. The center of the craniotomy over the somatosensory cortex was determined for each mouse in relation to the skull indentations bregma and lambda. Generally, 3.5 mm laterally from the midpoint between bregma and lambda along the sagittal suture was marked as the center of the craniotomy. Following the craniotomy and the window with headplate implantation, mice were observed for signs of pain and/or infection. Furthermore, mice were handled by the experimenter, habituated to head restraint and trained to run on the foam ball daily for three consecutive days. Sensory-evoked arteriolar dilation and capillary blood flow were imaged through a 3.0 mm diameter cranial window positioned over the somatosensory cortex in head-restrained mice with the freedom to walk on a bidirectional Styrofoam ball.

BRB permeability assay and retina immunohistochemistry

Neonatal pups and adults (8 -10 weeks old) were anesthetized with ketamine/xylazine at

10 µl/gram body weight. Sulfo-NHS-Biotin (Thermo Fisher Scientific; 21335), 3-kDa or 10-kDa dextran conjugated to Tetramethylrhodamine (Thermo Fisher Scientific; D3308 and D-1868, respectively), and bovine serum albumin conjugated to Alexa Fluor 555 (Thermo Fisher Scientific; A34786) were injected at 0.5 mg/g body weight for Sulfo-NHS-Biotin and 0.1 mg/g body weight for the rest of tracers as previously described (Armulik et al., 2010) into the left-ventricle with a 31 gauge, 0.3 cc insulin syringe. The heartbeat was monitored for a steady heartbeat that was continuous for 5 minutes. If the heartbeat stopped during the 5 minutes circulation, the animals were excluded due to poor circulation of the tracer. After 10 minutes of tracer circulation, both eyes were enucleated. Eyes were fixed briefly (5-10 minutes) in 4% PFA. Retinas were dissected out in 4% PFA to ensure dye fixation within the tissue. Retinas were fixed overnight in 4% PFA at 4ºC and washed in PBS three times for 5 minutes each the next day. Retinas were incubated in blocking buffer (10% normal goat serum, 3% bovine serum albumin, and 0.5% Triton X-100 in PBS) for 1 hour at room temperature. Isolectin GS-IB4 conjugated to Alexa-Fluor® 488 (Thermo Scientific; I21411) or the following primary antibodies: rabbit α-ERG1/2/3 rabbit(Abcam Cat# ab92513, RRID:AB_2630401), rabbit α-Mfsd2a (Cell Signaling Technology still under development, Cat# 14-87 Mfsd2a, RRID:AB_2617168, 1:200) and mouse α-Claudin-5, (Thermo Fisher Scientific Cat# 352588 Lot# RRID:AB_2532189, 1:400) were then incubated in blocking buffer overnight at 4ºC. Retinas were then washed in PBS three times for 5 minutes and incubated with the Alexa-Fluor® conjugated secondary antibodies (Thermo Fisher Scientific; 1:300) for 4 hours at room temperature. Retinas were washed in PBS three times for 10 minutes and flat-mounted with the vitreal surface facing up using Prolong Gold (Molecular Probe, 1747013).

Brain immunohistochemistry

Mice were anesthetized with ketamine/xylazine 10 µl/gram body weight via intraperitoneal injection and then mice were transcardially perfused with cold PBS and followed by cold 4% PFA. Brains and retinas were fixed by immersion in 4% PFA/PBS overnight at 4 °C. Next, brains and retinas were washed 3x in PBS. Brain sections were either cut as 50 µm sections on the vibratome or cryopreserved in 30% sucrose, frozen in TissueTek OCT (Sakura) and cut as 25 µm sections on the cryostat. For Mfsd2a and eNOS immunohistochemistry, mice were sacrificed via cervical dislocation. Brains were snap-frozen with liquid nitrogen and cut as 25 µm sections on the cryostat. Brain sections were fixed with chilled methanol for 10 minutes. Brain sections and retinas were blocked with 10% goat or donkey serum/5% BSA/PBST (0.5% Triton X-100) and stained overnight at 4 °C with the following primary antibodies at the indicated concentrations: α-Mfsd2a (1:200, Cell Signaling Technologies; RRID: AB_2617168) or α-Mfsd2a (generous gift from Dr. David Silver as used previously(Nguyen et al., 2014), α-SMA (1:1000, Sigma-Aldrich Cat# C6198, RRID:AB_476856), α-ICAM2 (1:200, BD Biosciences Cat# 553326, RRID:AB_394784), α-PECAM (1:200, BD Biosciences #553370; RRID: AB_394816), α-Claudin-5 (Thermo Fisher Scientific Cat# 34-1600, RRID:AB_2533157), α-eNOS (Abcam Cat# ab5589, RRID:AB_304967) followed by corresponding Alexa Fluor-conjugated secondary antibodies (1:500, Thermo Fisher Scientific) and hydrazide 633 (1:1000, Thermo Fisher Scientific). Tissues were mounted with ProLong Gold for imaging.

***In situ* NO detection**

This assay was previously adapted from (Jiang et al., 2012; Kanetsuna et al., 2007). Mice with deeply anesthetized with ketamine/xylazine. Mice were transcardially perfused with warm

(37°C) 50 mL PBS, then perfused with 50 mL warm PBS containing 10 μM DAF-2 (Thermo Fisher Scientific, D23842), 100 μM L-Arginine and 2 mM CaCl2. Next, mice were perfused with warm PBS again followed by 4% PFA. Brains and kidneys were harvested and fixed overnight in 4% PFA at 4°C. Tissues were sectioned on the vibratome (50 μm) and processed for immunostaining.

2.2 Imaging, Quantification, and Statistical Analysis

Two-Photon Microscopy:

Two-photon imaging was performed using a custom-built microscope equipped with a tunable Ti:Sapphire laser (MaiTai HP DS, Spectra-Physics) controlled by ScanImage 5.1 (Vidrio Technologies). The intensity of the femtosecond pulsed infrared beam was controlled by an electro-optical modulator (Conoptics Inc.) and passed through a pair of scan mirrors (Cambridge Technology) that enabled image acquisition at 30 Hz for a field of view of 1.0 mm^2 and 512x512 pixels. Control of image zoom was enabled by controlling the resonant scanner amplitude. The objective lens used was a 16x, 0.8 NA, water immersion from Nikon. Green and red fluorescence photons were separated using a custom-sized dichroic beamsplitter (580 BrightLine®, Semrock) and two custom-sized single-band bandpass filters (525/50 nm BrightLine®, 641/75 nm BrightLine®, Semrock). Fluorescence photons were collected using photomultiplier tubes (Hamamatsu).

Other light microscopes

Olympus FluoView FV1200 (20x, 0.75 N.A. and 40x, 1.4 N.A.) and Leica SP8 laser scanning confocal microscopes (20x, 0.75 N.A., 40x, 1.3 N.A., 63x 1.4 N.A.) and an Olympus VS 120 slide scanner (10x, 0.4 N.A.) were used for imaging retina flatmounts and brain sections. Images were processed using Adobe Photoshop, Illustrator, Olympus Fluoview and FIJI (NIH).

Transmission electron microscopy

EM imaging of adult and neonatal HRP injected retinas was carried out as described previously (Ben-Zvi et al., 2014). HRP (0.5 mg/g body weight Sigma Aldrich, HRP type II) was dissolved into 50 µl and 400 µl of PBS for pups and adults, respectively and injected into the retro-orbital sinus of deeply anaesthetized mice. After 15 or 30 minutes of HRP circulation for pups or adults, respectively, the contralateral eye of the sinus was enucleated. The eye was dissected immediately in 4% PFA and fixed by immersion in a 0.1 M sodium-cacodylate-buffered mixture (5% glutaraldehyde and 4% PFA) for 1 hour at room temperature followed by overnight fixation in 4% PFA at 4ºC. Following fixation, the tissue was washed three times and then overnight in 0.1 M sodium-cacodylate buffer. Retinas were incubated for 25 or 45 minutes for neonatal or adults, respectively, at room temperature in 0.05 M Tris-HCl pH 7.6 buffer, containing 5.0 mg per 10 ml of 3-39 diaminobenzidine (DAB, Sigma Aldrich) with 0.01% hydrogen peroxide. After DAB staining, the retinal vasculature could be visualized. The distal edge of the vasculature and proximal edge of optic nerve head were micro-dissected, and samples were lightly nicked to provide orientation to cut ultrathin sections. Samples were then postfixed in 1% osmium tetroxide and 1.5% potassium ferrocyanide, dehydrated, and embedded in epoxy resin. P8 and P10 *Cav-1*$^{-/-}$ and wildtype littermate retinas were processed as stated

above without HRP injections and fixed for 5 days in 0.5% glutaraldehyde in 4% PFA prepared in 0.1 mM phosphate buffer, pH 7.4 and without DAB staining. Retinas were washed three times and then overnight in 0.1 M sodium-cacodylate buffer.

Brains from adult mice were dissected and fixed by immersion in 5% glutaraldehyde/4% PFA/0.1 M sodium-cacodylate for two weeks at room temperature. Following fixation, brains were washed overnight in 0.1 M sodium-cacodylate. Coronal vibratome free-floating sections of 50 μm were collected. The cortex, particularly somatosensory and motor, were micro-dissected, post-fixed in 1% osmium tetroxide and 1.5% potassium ferrocyanide, dehydrated, and embedded in epoxy resin. Ultrathin sections of 80 nm were then cut from the block surface, collected on copper grids, and counter-stained with Reynold's lead citrate and examined under a 1200EX electron microscope (JEOL) equipped with a 2k CCD digital camera (AMT).

In vivo imaging of arteriolar dilation and analysis

Arterioles labeled with hydrazide were imaged at 800 nm with a field of view size of 200 μm x 200 μm (512x512 pixels, pixel size of 0.16 μm^2/pixel) at 30 Hz. Whisker stimulation (4 Hz, 5 s) was performed using a foam brush controlled by a servo motor under the control of Wavesurfer. Alexa Fluor 633 hydrazide (5 $mg \bullet kg^{-1}$) was intravenous injected into mice to visualize arterioles *in vivo* (Shen et al., 2012). Three technical trials were acquired and averaged for each field of view. 10-13 fields of view were acquired per imaging session. Three imaging sessions were collected on three separate days per mouse and arteriolar dilation responses were averaged across all three sessions for each mouse. To determine percent change in diameter relative to baseline, the movies were first filtered with a Gaussian blur and background subtracted with a rolling ball of 50. Five-line scans orthogonal to the arterioles were sampled to

generate kymographs. The two max intensity peaks (which represents the walls of the arterioles) were identified across the kymograph. The change in diameter of the arterioles was determined as ($diameter_{time}$ –$diameter_{baseline}$)/$diameter_{baseline}$. Diameter baseline was determined the mean diameter at all time points prior to the whisker stimulation. The change in max diameter was determined as the max value during the whisker stimulation. To determine latency onset to dilate, a line was fitted through 80% and 20% of max value. The latency onset to dilate is the time difference between the x-intercept of the line and the start of the whisker stimulation.

In vivo imaging of red blood cell velocity and analysis

Mice were intravenously injected with quantum dots 525 (Thermofisher) and hydrazide to unambiguously distinguish arterioles and capillaries *in vivo*. Hydrazide-negative capillaries were imaged with a field of view size of 200 μm x 200 μm (512x512 pixels, pixel size of 0.16 μm^2/pixel) at 610 Hz. Whisker stimulation (4 Hz, 5 s) was performed using a foam brush controlled by a servo motor under the control of Wavesurfer. Three technical trials were acquired and averaged for each field of view. Three imaging sessions were collected on three separate days per mouse and changes in capillary red blood cells velocity were averaged across all three sessions for each mouse. To determine percent change in velocity relative to baseline, the movies were first filtered with a Gaussian blur and background subtracted with a rolling ball of 50. Five-line scans parallel to the flow of red blood cells were sampled to generate kymographs. Using a published algorithm (Chhatbar and Kara, 2013) that uses a reiterative radon transform and edge detection filter, the change in velocity of red blood cells was determined as ($velocity_{time}$ - $velocity_{baseline}$)/$velocity_{baseline}$. Velocity baseline was determined the mean velocity at all time points prior to the whisker stimulation. The change in max velocity was determined as the max

value during the whisker stimulation. To determine latency onset to increase red blood cell velocity, a line was fitted through 80% and 20% of max value. The latency onset is the time difference between the x-intercept of the line and the start of the whisker stimulation.

Two-photon acute slice imaging

Acute coronal brain slices were prepared by deeply anesthetizing mice with isoflurane inhalation followed cardiac perfusion with ice-cold choline-based cut solution containing (in mM): 25 NaHCO3, 25 Glucose, 1.25 NaH2PO4, 7 MgCl2, 2.5 KCl, 0.5 CaCl2, 11.6 ascorbic acid, 3.1 pyruvic acid, 110 Choline chloride. After brain dissection and blocking, 300 μm slices were prepared in cut solution with a Leica VT1000s vibratome. Slices were then transferred for 30 minutes to recovery into a holding chamber containing 34° artificial cerebral spinal fluid (aCSF) containing (in mM): 125 NaCl, 2.5 KCl, 1.25 NaH2PO4, 25 NaHCO3, 11 glucose, 2 CaCl2, 1 MgCl2. During recovery, slices were incubated with ~ 2 μm Alexa Fluor™ 633 Hydrazide (ThermoFisher). Following recovery, slices were imaged while constantly perfused with room temperature aCSF. Choline cut solution and aCSF were constantly bubbled with 5% CO2/95% O2. Imaging was performed on a custom-built 2-photon microscope and images acquired with a custom version of ScanImage written in MATLAB (Mathworks). During imaging, arteries were constricted with 100 nM U46619 (Sigma-Aldrich) and dilated by acutely dissolving ~ 5 mg of DEA-NONOate (Cayman Chemical Company) into the 10 mL of recycling aCSF being perfused over the slice.

Permeability Index quantifications

All quantifications were performed blind with a self-written FIJI (NIH) macro. Six to eight 290 μm x 290 μm x 5 μm thick z-stack images of the vessels of distal and proximal regions of the primary plexus, six to eight 317 um x 317 um of deeper plexus and intermediate plexus at 3-5 μm thick z-stack images and six to eight 635 μm x 635 μm of *Mfsd2a*$^{-/-}$ and *Cav-1*$^{-/-}$ with their respective wildtype littermates per mouse retina were max Z-projected, filtered with a Gaussian blur and background subtracted via rolling ball method. Distal vessel images were acquired by aligning the field of view to capture the retinal tip cells and proximal images were acquired by aligning the field view slightly after the optic nerve head. The isolectin and tracer signals were auto-thresholded by the same method for all ages and genotypes. The area of the segmented vessel and the tracer were determined. The ratio of the area of the tracer and the area of the vessel was then calculated. A ratio of 1 means that the tracer and vessel area is the same, indicating a functional barrier. The average of the ratios from the six to eight images is considered one biological sample.

Smooth muscle cell coverage quantification

NG2:DsRED (or *CSPG4:DsRED*) were crossed to *Cav1*$^{-/-}$ mice. Cranial window surgery was performed over the barrel cortex of *Cav1*$^{+/+}$*; NG2:*^{DsRED}+ and *Cav1*$^{-/-}$*;NG2:*^{DsRED}+ mice. Mice were injected with Alexa Fluor 488 hydrazide (5 mg•kg^{-1}). ~30 arterioles (hydrazide+; DsRed+) per mice were imaged. A 100 μm intensity line profile was drawn perpendicularly to the contractile bands of the smooth muscle cells. Max peaks corresponding to individual smooth muscle were counted and the number of smooth muscle cells/100 μm length was determined.

Mean Vesicular Density and Functional Tight Junction Quantification

For all TEM quantifications, mean total vesicular density values were calculated from the number of vesicles per μm^2 of membrane for each image collected. All images were collected at 12000x magnification and analysis were performed blinded. Each density value (circle on the graphs) represents an individual vessel (capillary or arteriole). To determine the percentage of functional tight junctions, the number of tight junctions that halt the tracer at the luminal side without parenchymal leakage was counted and divided by the total number of tight junctions counted.

Pericyte density and coverage quantifications

Retinas from P5 NG2:DsRed mice were stained for ERG1/2/3 (endothelial nuclei marker) and isolectin. Images of four retinal leaflets per retina were acquired. Images were max Z-projected, filtered with a Gaussian blur and background subtracted via rolling ball method. To quantify pericyte density, the NG2:DsRed signal was also applied with a minimum filter to reduce weak signal in the processes of pericytes but retain high signals in the soma. 250 μm x 250 μm field of views were analyzed from 0 μm (slightly before the optic nerve head) to the distal vessels (up to 1750 μm). Images were then segmented for NG2:DsRed and ERG1/2/3 signals and particles were then counted to determine pericyte density (NG2:DsRed+/ERG+ particles). To quantify pericyte coverage which is displayed as NG2:DsRed area/Isolectin area, a minimum filter was not applied but instead, images were simply segmented for NG2:DsRed signal and Isolectin signal.

Statistical analyses

All statistical analyses were performed using Prism 7 (GraphPad Software). Two group comparisons were analyzed using an unpaired two-tailed Student's t-test. Multiple group comparisons were analyzed using a one-way ANOVA, followed by a post hoc Bonferroni analysis to correct for multiple comparisons. No data were excluded when performing statistical analysis. The standard error of the mean was calculated for all experiments and displayed as errors bars in graphs. Statistical details for specific experiments, including exact n values and what n represents, precision measures, statistical tests used, and definitions of significance can be found in the Figure Legends. Each circle on the graphs throughout the study represents an individual vessel (capillary or arteriole or smooth muscle cell). The same color of the circle represents vessels analyzed from the same mouse. Values are expressed as mean ± s.e.m.

References

Armulik, A., Genové, G., Mäe, M., Nisancioglu, M.H., Wallgard, E., Niaudet, C., He, L., Norlin, J., Lindblom, P., Strittmatter, K., et al. (2010). Pericytes regulate the blood-brain barrier. *468*, 557–561.

Asterholm, I.W., Mundy, D.I., Weng, J., Anderson, R.G.W., and Scherer, P.E. (2012). Altered mitochondrial function and metabolic inflexibility associated with loss of caveolin-1. Cell Metab. *15*, 171–185.

Ben-Zvi, A., Lacoste, B., Kur, E., Andreone, B.J., Mayshar, Y., Yan, H., and Gu, C. (2014). Mfsd2a is critical for the formation and function of the blood-brain barrier. Nature *509*, 507–511.

Chen, Q., Zhang, H., Liu, Y., Adams, S., Eilken, H., Stehling, M., Corada, M., Dejana, E., Zhou, B., and Adams, R.H. (2016). Endothelial cells are progenitors of cardiac pericytes and vascular smooth muscle cells. Nat Commun *7*, 12422.

Chen, T.-W., Wardill, T.J., Sun, Y., Pulver, S.R., Renninger, S.L., Baohan, A., Schreiter, E.R., Kerr, R.A., Orger, M.B., Jayaraman, V., et al. (2013). Ultrasensitive fluorescent proteins for imaging neuronal activity. Nature *499*, 295–300.

Chhatbar, P.Y., and Kara, P. (2013). Improved blood velocity measurements with a hybrid image filtering and iterative Radon transform algorithm. Front Neurosci *7*, 106.

Ehling, M., Adams, S., Benedito, R., and Adams, R.H. (2013). Notch controls retinal blood vessel maturation and quiescence. Development *140*, 3051–3061.

Jiang, R., Wang, S., Takahashi, K., Fujita, H., Fruci, C.R., Breyer, M.D., Harris, R.C., and Takahashi, T. (2012). Generation of a conditional allele for the mouse endothelial nitric oxide synthase gene. Genesis *50*, 685–692.

Kanetsuna, Y., Takahashi, K., Nagata, M., Gannon, M.A., Breyer, M.D., Harris, R.C., and Takahashi, T. (2007). Deficiency of Endothelial Nitric-Oxide Synthase Confers Susceptibility to Diabetic Nephropathy in Nephropathy-Resistant Inbred Mice. Am. J. Pathol. *170*, 1473–1484.

Madisen, L., Mao, T., Koch, H., Zhuo, J.-M., Berenyi, A., Fujisawa, S., Hsu, Y.-W.A., Garcia, A.J., Gu, X., Zanella, S., et al. (2012). A toolbox of Cre-dependent optogenetic transgenic mice for light-induced activation and silencing. Nat. Neurosci. *15*, 793–802.

Madisen, L., Zwingman, T.A., Sunkin, S.M., Oh, S.W., Zariwala, H.A., Gu, H., Ng, L.L., Palmiter, R.D., Hawrylycz, M.J., Jones, A.R., et al. (2010). A robust and high-throughput Cre reporting and characterization system for the whole mouse brain. Nat. Neurosci. *13*, 133–140.

Nguyen, L.N., Ma, D., Shui, G., Wong, P., Cazenave-Gassiot, A., Zhang, X., Wenk, M.R., Goh, E.L.K., and Silver, D.L. (2014). Mfsd2a is a transporter for the essential omega-3 fatty acid docosahexaenoic acid. Nature *509*, 503–506.

Quina, L.A., Harris, J., Zeng, H., and Turner, E.E. (2017). Specific connections of the interpeduncular subnuclei reveal distinct components of the habenulopeduncular pathway. Journal of Comparative Neurology *525*, 2632–2656.

Raymond, C.S., and Soriano, P. (2007). High-efficiency FLP and PhiC31 site-specific recombination in mammalian cells. PLoS ONE *2*, e162.

Razani, B., Engelman, J.A., Wang, X.B., Schubert, W., Zhang, X.L., Marks, C.B., Macaluso, F., Russell, R.G., Li, M., Pestell, R.G., et al. (2001). Caveolin-1 null mice are viable but show evidence of hyperproliferative and vascular abnormalities. J. Biol. Chem. *276*, 38121–38138.

Shen, Z., Lu, Z., Chhatbar, P.Y., O'Herron, P., and Kara, P. (2012). An artery-specific fluorescent dye for studying neurovascular coupling. Nat. Methods *9*, 273–276.

Shesely, E.G., Maeda, N., Kim, H.S., Desai, K.M., Krege, J.H., Laubach, V.E., Sherman, P.A., Sessa, W.C., and Smithies, O. (1996). Elevated blood pressures in mice lacking endothelial nitric oxide synthase. Pnas *93*, 13176–13181.

Wirth, A., Benyó, Z., Lukasova, M., Leutgeb, B., Wettschureck, N., Gorbey, S., Örsy, P., Horváth, B., Maser-Gluth, C., Greiner, E., et al. (2008). G12- G12-G13-LARG-mediated signaling in vascular smooth muscle is required for salt-induced hypertension. Nat. Med. *14*, 64–68.

Zhu, X., Bergles, D.E., and Nishiyama, A. (2008). NG2 cells generate both oligodendrocytes and gray matter astrocytes. Development *135*, 145–157.

CHAPTER 3

Gradual suppression of transcytosis governs functional blood-retinal barrier formation

Adapted from a publication in *Neuron* (March 22, 2017)

Gradual suppression of transcytosis governs functional blood-retinal barrier formation

Brian Wai Chow[1] and Chenghua Gu[1]

[1]Department of Neurobiology, Harvard Medical School, 220 Longwood Avenue, Boston, Massachusetts, 02115, USA

Correspondence: Chenghua_gu@hms.harvard.edu

3.1. Abstract

Blood-central nervous system (CNS) barriers partition neural tissues from the blood, providing a homeostatic environment for proper neural function. The endothelial cells that form blood-CNS barriers have specialized tight junctions and low rates of transcytosis to limit the flux of substances between the blood and the CNS. However, the relative contributions of these properties to barrier permeability are unknown. Here, by studying the formation of the functional blood-retinal barrier (BRB) in mice, we found that immature vessel leakage occurs entirely through bulk transcytosis and not via tight junctions. A functional barrier forms only when transcytosis is gradually suppressed during development. Therefore, the temporal regulation of transcytosis governs the development of a functional BRB. Mutant mice with elevated or reduced levels of transcytosis have delayed or precocious sealing of the BRB, respectively. These findings reveal that suppression of transcytosis is a principal contributor to establishing a functional barrier during normal development and provide new insights into developing therapeutic strategies for treating CNS diseases. This study also provides the first characterization of BRB formation and establishes the retinal vasculature as a tractable model system for studying blood-CNS barriers.

3.2. Introduction

CNS endothelial cells lining blood vessels form the blood-CNS barriers, which include the blood-brain barrier, blood-spinal cord barrier, and inner BRB (Engelhardt and Coisne, 2011). These cells have two properties that limit the passage of substances between the blood and the CNS parenchyma: 1) specialized tight junction complexes between CNS endothelial cells prevent paracellular flux; and 2) low rates of vesicular trafficking between the luminal and abluminal membrane, known as transcytosis, limit transcellular passage (Andreone et al., 2015; Chow and Gu, 2015; Raviola, 1977; Reese and Karnovsky, 1967; Zhao et al., 2015). Although tight junctions are thought to be the principal mechanism for establishing blood-CNS barriers, recent findings suggest that altered rates of transcytosis also influence barrier permeability (Ben-Zvi et al., 2014; Knowland et al., 2014). Barrier properties are not intrinsic to CNS endothelial cells, but rather are acquired from the neural environment during development (Blanchette and Daneman, 2015; Hagan and Ben-Zvi, 2015; Stewart and Wiley, 1981). However, it is not understood when and how specialized tight junctions and suppression of transcytosis occur, and what their relative contributions are in establishing a functional CNS barrier during development. Loss of barrier function is a hallmark of some CNS degenerative diseases (de Vries et al., 2012; Obermeier et al., 2013; Winkler et al., 2014; Zlokovic, 2008). Yet, a functional barrier is also a major obstacle for CNS drug delivery (Banks, 2016; Myles et al., 2005; Pardridge, 2012). Dissecting the relative roles of tight junctions and transcytosis in regulating barrier permeability and elucidating the basic principles governing the establishment of CNS barrier properties will enable targeted manipulations of the barrier during disease.

The retinal vasculature is well-suited to address many fundamental questions about CNS barriers. Physiologically analogous to the blood-brain barrier, the BRB regulates the optimal

milieu for phototransduction. Unlike the complex brain vascular network, the retinal vasculature has a relatively simple, stereotypic development and architecture, consisting of a three-tiered, two-dimensional plexus (Stone et al., 1995). Mouse retinal angiogenesis occurs shortly after birth. CNS endothelial cells invade the optic nerve head and expand radially along the vitreal surface from the center towards the periphery, forming the entire primary plexus by postnatal day 8 (P8) (**Figures 3.1**) (Fruttiger, 2007). Sprouts from the primary plexus then penetrate into the retina, forming the deeper plexus, followed by further sprouting to form the intermediate plexus (Raviola, 1977; Reese and Karnovsky, 1967).

In this chapter, we use the BRB as a model system to elucidate the relative contributions of tight junctions and transcytosis in regulating CNS barrier permeability during development. To our surprise, we found that functional tight junctions are already present when vessels first entered the CNS so the gradual suppression of transcytosis in CNS endothelial cells governs the development of a functional barrier.

3.3. Results

Functional BRB is formed gradually and is fully acquired by P10.

We first mapped the spatiotemporal formation of the functional BRB. To evaluate BRB permeability, we transcardially injected mice at several postnatal ages with Sulfo-NHS-Biotin (550 Da) or fluorescently-labeled, 10-kDa dextran tracer. A functional BRB, as observed in the adults, completely confines both tracers within the vasculature (**Supplementary Figure 1**). However, at P1, when blood vessels first enter the retina through the optic nerve head and are enshealthed by pericytes (**Supplementary Figure 2**), these budding vessels leaked both tracers into the retinal parenchyma (**Figure 3.2**),

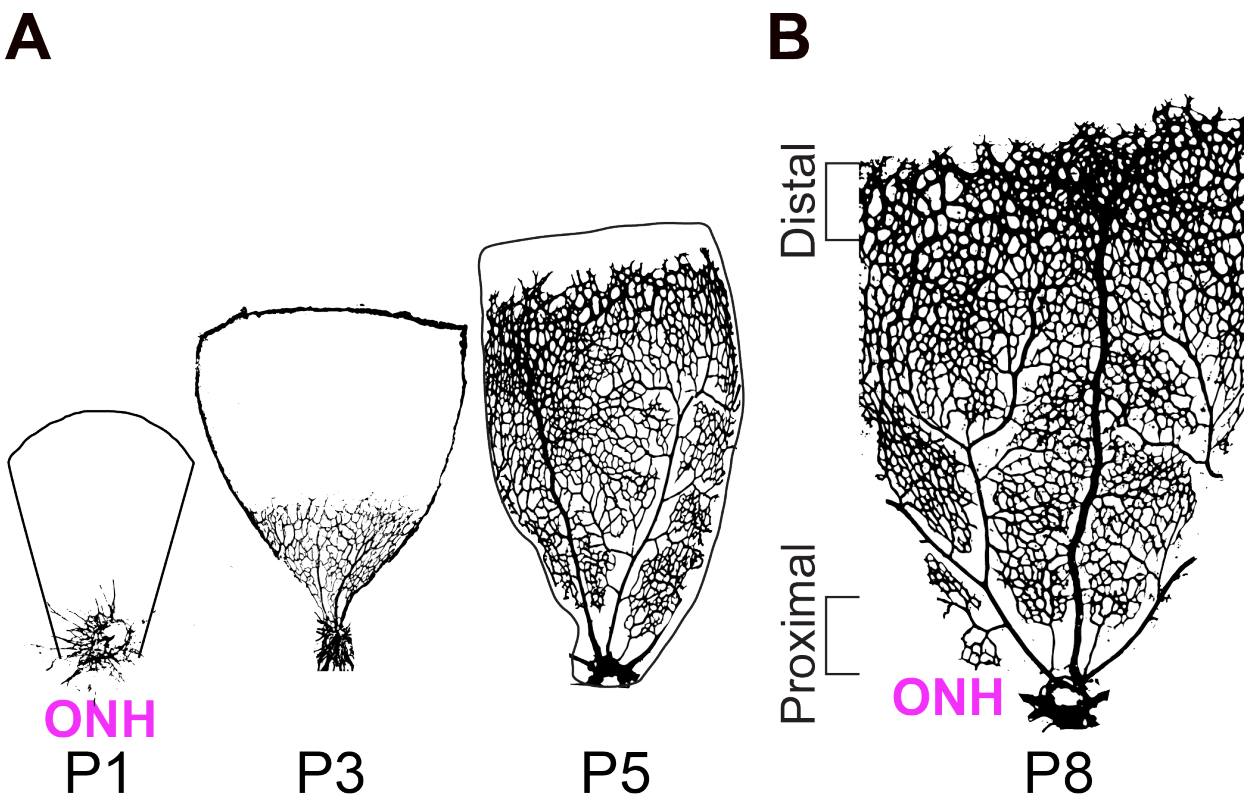

Figure 3.1. Spatiotemporal development of the mouse retinal vasculature. (**A-B**) Spatiotemporal development of the mouse retina primary plexus. (**A**)Vessel ingression at the optic nerve head (ONH) occurs at P1. Vessels then expand from the ONH to the retinal periphery during postnatal development. (**B**) Vessels reach the peripheral edge of the retina at P8. A spatiotemporal gradient of vessel maturation is observed: the vessels proximal to the ONH are more mature whereas the vessels distal to the ONH are nascent. P-Postnatal.

indicating that these developing vessels do not intrinsically have a functional barrier. In P3 (**Figure 3.2**) and P5 retinas (**Figure 3.3**), we observed that both tracers leaked into the parenchyma and were taken up by non-vascular cells near nascent vessels located distal to the optic nerve head (**Figure 3.2 and 3.3**), while both tracers were confined in the more mature vessels located proximal to the optic nerve head (**Figure 3.2 and 3.3**). Indeed, injecting Sulfo-NHS-Biotin, 3-kDa and 10-kDa dextran tracers at P5 (**Figure 3.3**), we found that a functional barrier is formed gradually in a proximal to distal fashion (Figure 3.3). At P8 and P9, although the angiogenic front reaches the retinal periphery, the nascent, distal vessels still exhibited leakage (**Figure 3.4**) whereas the mature, proximal vessels confined Sulfo-NHS-Biotin and 10-kDa dextran tracers (**Supplementary Figure 3).** At P10, both tracers were completely confined in all vessels of the primary plexus, including distal vessels (**Figure 3.4 and Supplementary Figure 3**). Thus, these data demonstrate that developing vessels are initially leaky, a functional barrier is formed gradually from proximal to distal, and the primary plexus acquires a functional BRB by P10.

We next examined when the functional BRB is established in the deeper plexus, which sprouts from the primary plexus between P7 and P12. Sprouting vessels of the deeper plexus showed leakage of both Sulfo-NHS-Biotin and 10-kDa-dextran tracers at P8 and P9 (**Supplementary Figure 4**). However at P10, when the deeper plexus vessels continue to sprout, both tracers were confined in newly formed vessels (**Supplementary Figure 4**). Finally, we investigated when the BRB becomes functional in the intermediate plexus, which sprouts from the deeper plexus between P12 and P17. At P12, sprouting nascent vessels, surprisingly, already confined both tracers; no leakage was observed at any ages examined (**Supplementary Figure 4).** Together, these data demonstrate that the developing retinal vasculature does not intrinsically

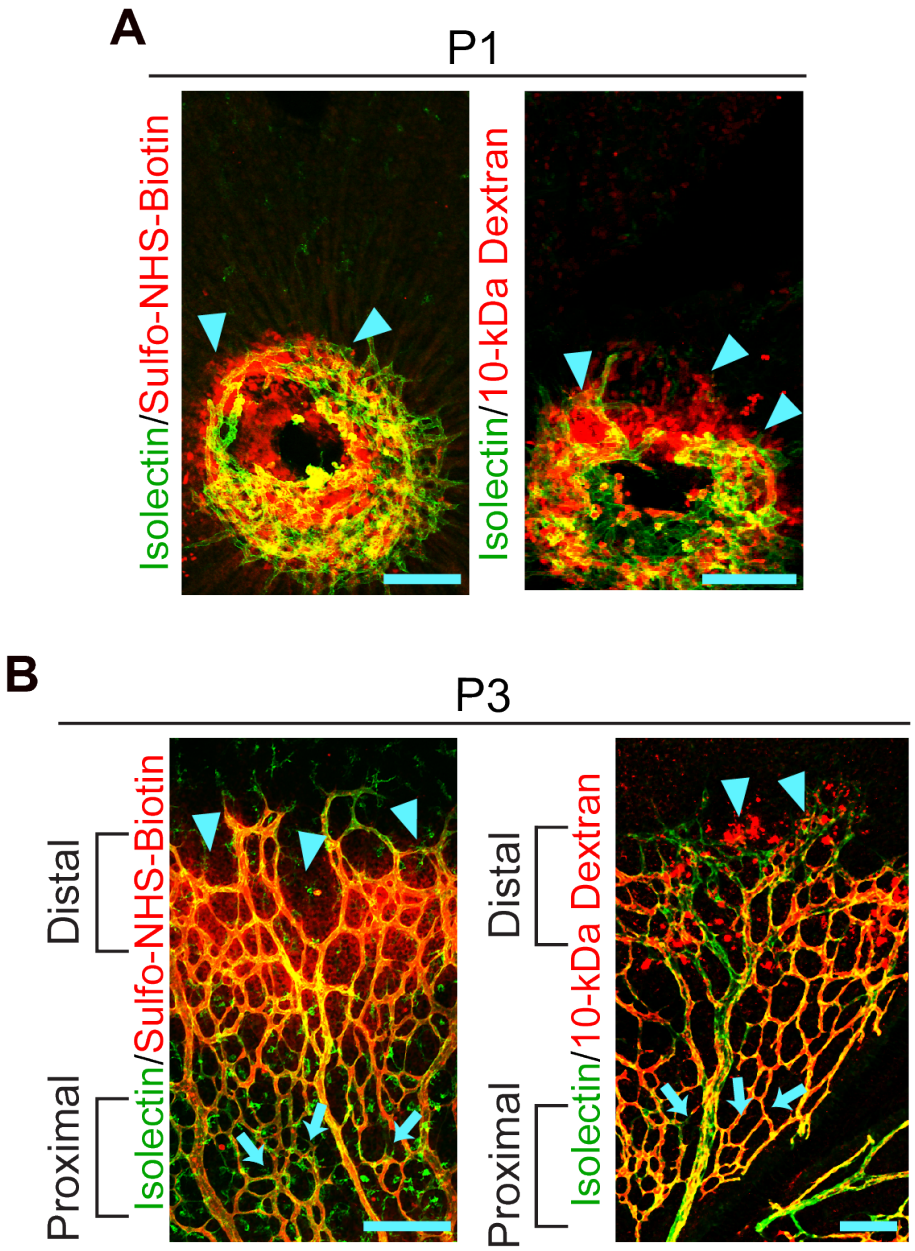

Figure 3.2. Spatiotemporal characterization of functional BRB formation. (A) In P1 retinas, when blood vessels (isolectin; green) first enter the retina, Sulfo-NHS-Biotin (left) and 10-kDa dextran (right) tracer (red) leakage is observed around budding vessels (arrowheads). **(B)** In P3 retinas, a gradient of barrier functionality is observed. More mature vessels proximal to the ONH confine tracer (arrows) whereas nascent vessels distal to the ONH leak tracer (arrowheads). Scale bar represents 100 μm for all panels.

Figure 3.3. Spatiotemporal characterization of functional BRB formation at P5. (**A-C**) Ticks represent distance in microns from the ONH. 0 is slightly before the ONH. (**D**) Permeability index of P5 retinas from tracer-injected pups reveals the functional BRB is gradually formed in a proximal to distal fashion. The permeability index is measured by the ratio of tracer-positive area over isolectin-positive area. A ratio greater than 1 indicates that the BRB is permeable and immature. A ratio of 1 indicates that the BRB is impermeable and hence mature. 250 μm^2 field of views were sampled and tiled starting from 0 to the angiogenic front. The average distance from the ONH to the angiogenic front at P5 is 1651 ± 288 μm. Data are mean ± s.e.m. (n = 5-6). Scale bar represents 100 μm for all panels.

Figure 3.3. (Continued)

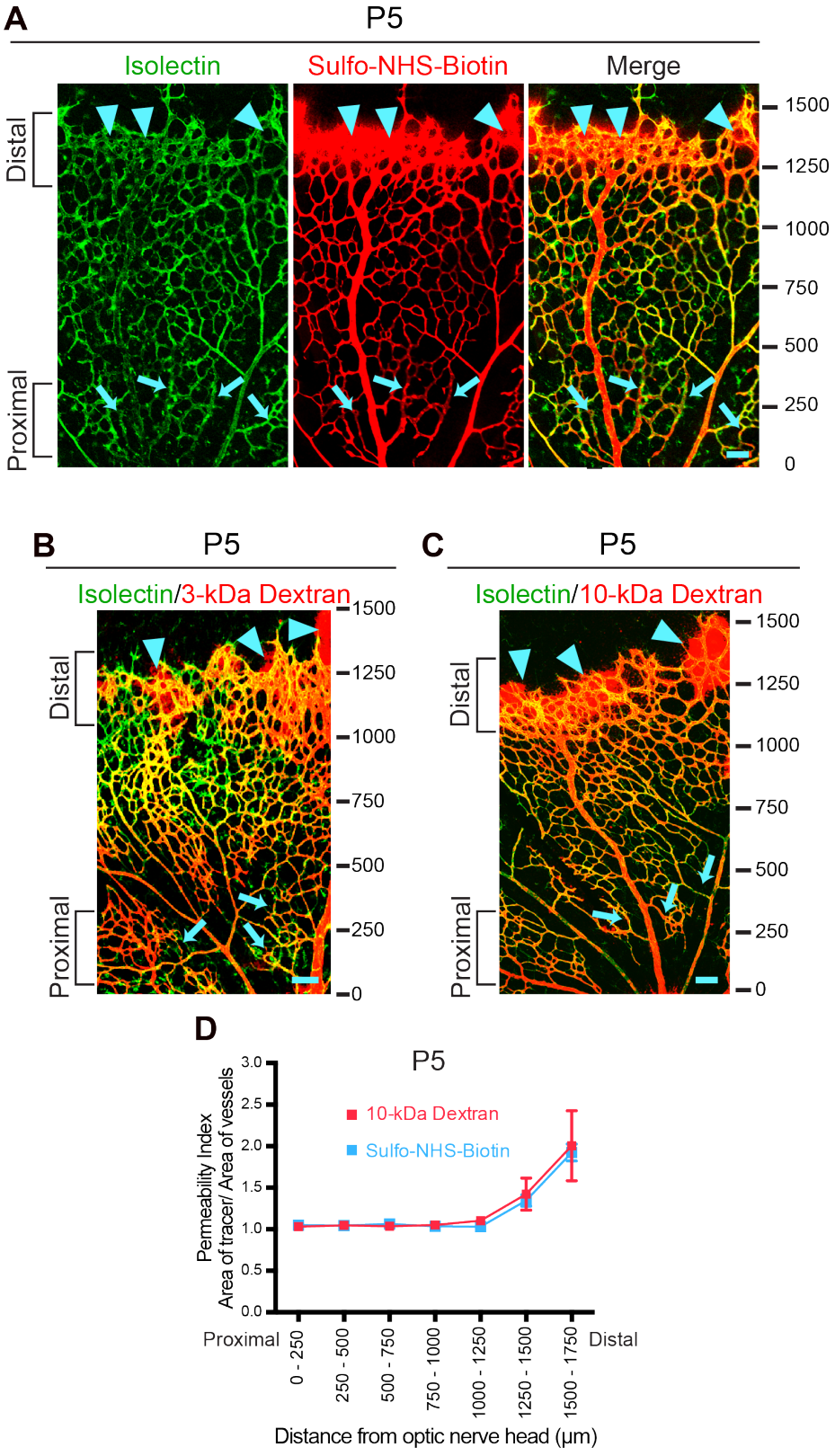

Figure 3.4. Functional BRB is developed by P10. (**A**) Higher magnification of distal vessels of the primary plexus show Sulfo-NHS-Biotin (top) and 10-kDa Dextran (bottom) tracer leakage at P8 and P9 (arrowheads). At P10, both tracers are confined in distal vessels (arrows). (**B**) Quantification of distal vessel permeability for Sulfo-NHS-Biotin and 10-kDa dextran throughout BRB development. Data are mean ± s.e.m. (n = 5-6 mice per age per tracer group, from 3 different litters). Statistical significance was determined by one-way ANOVA with a post-hoc Bonferroni multiple comparison adjustment, comparing the various neonatal ages with the adult in the respective Sulfo-NHS-Biotin and 10-kDa Dextran group. *, $P < 0.05$, ***, $P < 0.001$. Scale bar represents 100 μm for all panels.

Figure 3.4. (Continued)

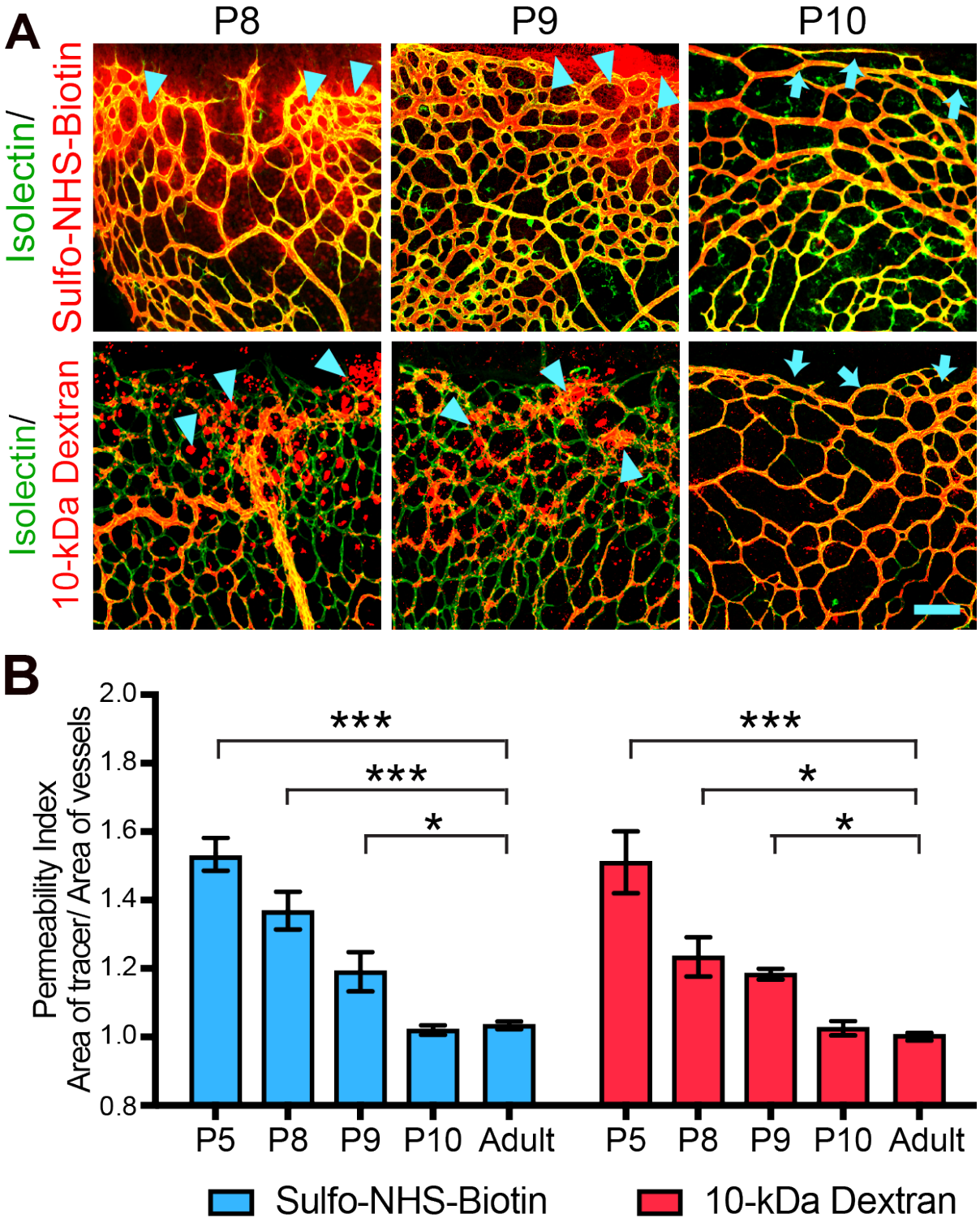

have a functional barrier but instead gradually acquires barrier properties. Once barrier properties are attained by P10, nascent vessels that have sprouted from existing vessels with a functional BRB will inherit and maintain these barrier properties. Thus, the three-tiered retinal vasculature acquires a functional BRB by P10.

At P1, budding CNS endothelial cells possess functional tight junctions but display bulk transcytosis

We next addressed the subcellular mechanisms underlying functional BRB development. We asked whether CNS endothelial cells form functional tight junctions and acquire low rates of transcytosis synchronously or sequentially to establish the functional BRB, and what the relative contribution of each property is to the regulation of BRB permeability. To evaluate the functionality of tight junctions and suppression of transcytosis at subcellular resolution, we injected horseradish peroxidase (HRP) intravenously at several ages and imaged the retina with transmission electron microscopy (EM). In the lung and heart vasculature where barrier properties are absent, luminal HRP leaks into the basement membrane and parenchyma both by passing through junctions, observed as HRP-filled tight junctions, and by high rates of transcytosis, evident as numerous HRP-filled intracellular vesicles (Ben-Zvi et al., 2014). However, in adult retinal endothelial cells, where barrier properties are present (Tuma and Hubbard, 2003), we observed that luminal HRP is halted sharply at electron-dense "kissing points" between endothelial cells where adjacent membranes are tightly apposed (**Figure 3.5**). Adult retinal endothelial cells also displayed a few HRP-filled vesicles relative to peripheral vessels, indicating that transcytosis is suppressed (**Figure 3.5**).

At P1, we observed tracer extravasation from budding vessels, indicating leaky vessels

Figure 3.5. At P1, budding CNS endothelial cells possess functional tight junctions but display bulk transcytosis whereas adult CNS endothelial cells have both functional tight junctions and suppression of transcytosis. As early as P1, budding CNS endothelial cells possess functional tight junctions but display bulk transcytosis. **(A and B)** EM of endothelial cells in the proximal retina of an HRP-injected adult mouse. (**A**) Specialized tight junctions are functional and prevent electron dense 3-3' diaminobenzidine (DAB) reaction product in the lumen from invading through the intercellular cleft (arrows). (**B**) Transcytosis was suppressed in endothelial cells as seen by negligible numbers of tracer-filled vesicles. Also shown is a magnification of the boxed areas. (**C** and **D**) EM of endothelial cells in the proximal retina from an HRP-injected P1 pup. (**C**) Tracer invades through the intracellular cleft between the endothelial cells but stops at junctions without invading to the abluminal side (arrows). (**D**) DAB reaction product filled the vesicles attached to the luminal membrane (arrows), in the cytoplasm (arrowheads) and near the abluminal membrane (asterisk). Also shown is a magnification of the boxed areas. (**E**) The percentage of functional tight junctions from the EM images (n = 5 mice per age; 15-20 vessels analyzed per mouse; number of tight junctions analyzed are displayed in parenthesis). (**F**) Number of tracer-filled vesicles in endothelial cells in P1 and adult mice. Data are presented as mean ± s.e.m. (n = 5 mice per age, each circle represents the average vesicular density from 15 – 20 vessels per mouse). Statistical significance was assessed by unpaired t-test. L – lumen, E – endothelial cell, Ab – abluminal. **, $P < 0.01$. Scale bar represents 100 nm in all panels.

Figure 3.5. (Continued)

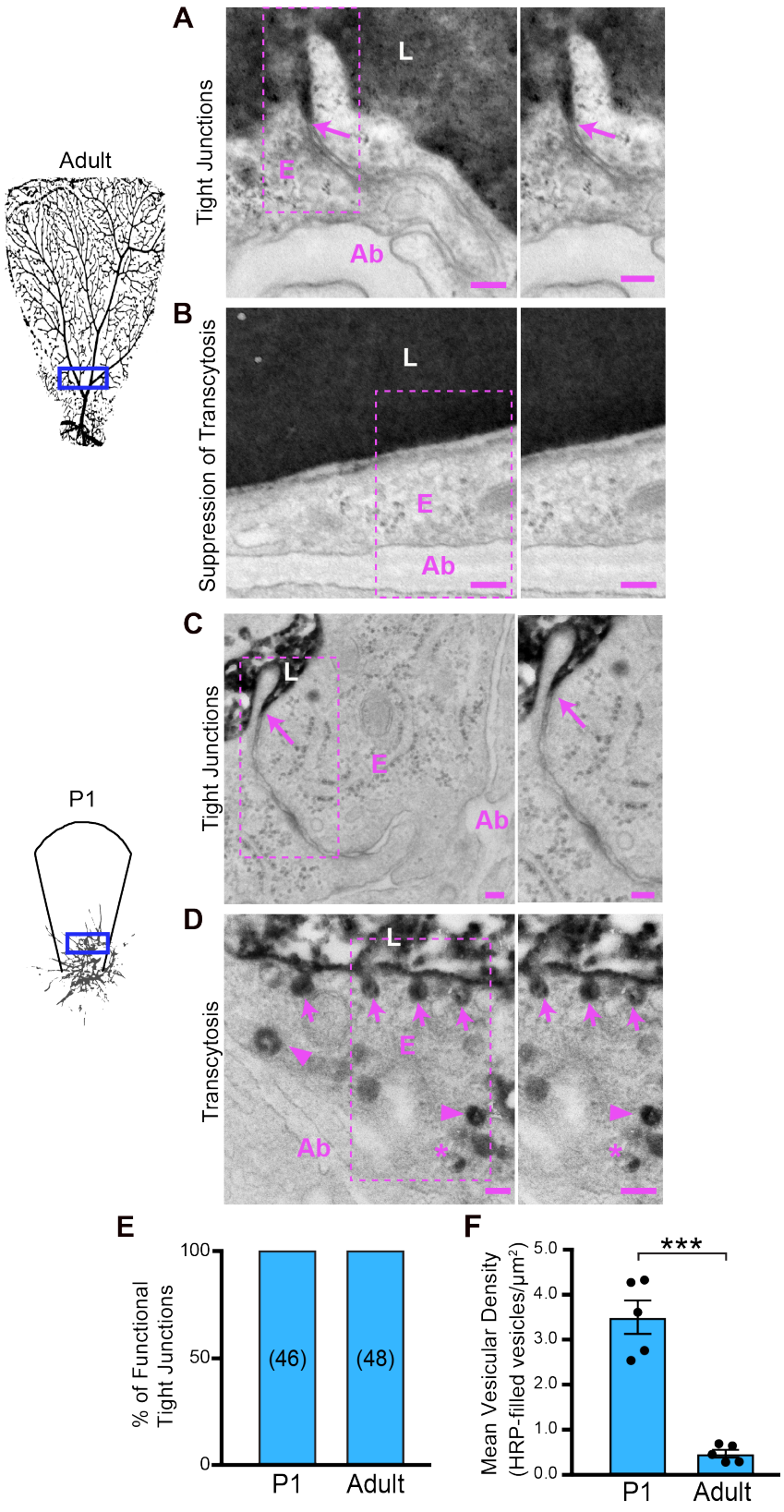

(**Figure 3.5**). Surprisingly, under EM, these CNS endothelial cells already had specialized tight junctions that halted the HRP at the "kissing points" (**Figure 3.5**), as observed in adult, mature CNS endothelial cells (**Figure 3.5**). However, these CNS endothelial cells had many HRP-containing vesicles, including luminal and abluminal membrane associated vesicles and cytoplasmic vesicles (**Figure 3.5**), similar to lung and heart endothelial cells where suppression of transcytosis is absent (Drab et al., 2001; Karnovsky, 1967; Razani et al., 2001). These results indicate that as early as vessel ingression at P1, functional tight junctions are present in budding CNS endothelial cells, but transcytosis has not been suppressed, suggesting that immature BRB leakiness is entirely due to uninhibited transcytosis.

Gradual suppression of transcytosis governs functional BRB formation

To test the hypothesis that suppression of transcytosis determines functional BRB development, we used EM to examine vesicular trafficking at later postnatal ages. At P5 and P8, in distal leaky vessels, many HRP-filled vesicles were observed (**Figure 3.6**) indicating that transcytosis has not been suppressed. However, in the proximal vessels that are impermeable to tracer, very few HRP-filled vesicles were observed, suggesting that suppression of transcytosis had occurred (**Supplementary Figure 5**). By P10, when all the retinal vessels have a functional BRB, negligible HRP-filled vesicles were observed in both distal and proximal vessels (**Figure 3.6 and Supplementary Figure 5**). Consistent with the observation at P1, functional tight junctions were present in all vessels, both proximal and distal, at all ages tested (**Figure 3.6 and Supplementary Figure 5**). These data demonstrate that a leaky, immature barrier is entirely due to high rates of bulk transcytosis in endothelial cells. A functional barrier is established days later, only after transcytosis is suppressed, which coincides with functional BRB development by

Figure 3.6. Gradual suppression of transcytosis governs the development of an impermeable, functional BRB. (**A**) At P5 and P8, many tracer-filled vesicles are observed at the luminal membrane (arrows), cytoplasm (arrowheads) and at the abluminal membrane (*****) in distal endothelial cells. At P10, distal endothelial cells contain negligible numbers of tracer-filled vesicles. (**B**) Number of tracer-filled vesicular densities in distal vessels at P5, P8 and P10. Data are shown as mean ± s.e.m. (n= 5 mice per age; each circle represents the average vesicular density from 15 – 20 vessels per mouse. Statistical significance was determined by one-way ANOVA with a post-hoc Bonferroni multiple comparison adjustment, comparing distal vessels of the various neonatal ages to distal vessels of adults. (**C)** EM of distal vessels from P5, P8 and P10 retinas reveals tracer product halts at tight junctions (arrows) at all ages. (**D**) Percentage of functional tight junctions from distal vessels. (n = 5 mice per age; 15-20 vessels analyzed per mouse; number of tight junctions analyzed are displayed in the bars). L – lumen, E – endothelial cells, Ab – abluminal, RBC- red blood cell. ***, $P < 0.001$. Scale bar represents 100 nm in all panels.

Figure 3.6. (Continued)

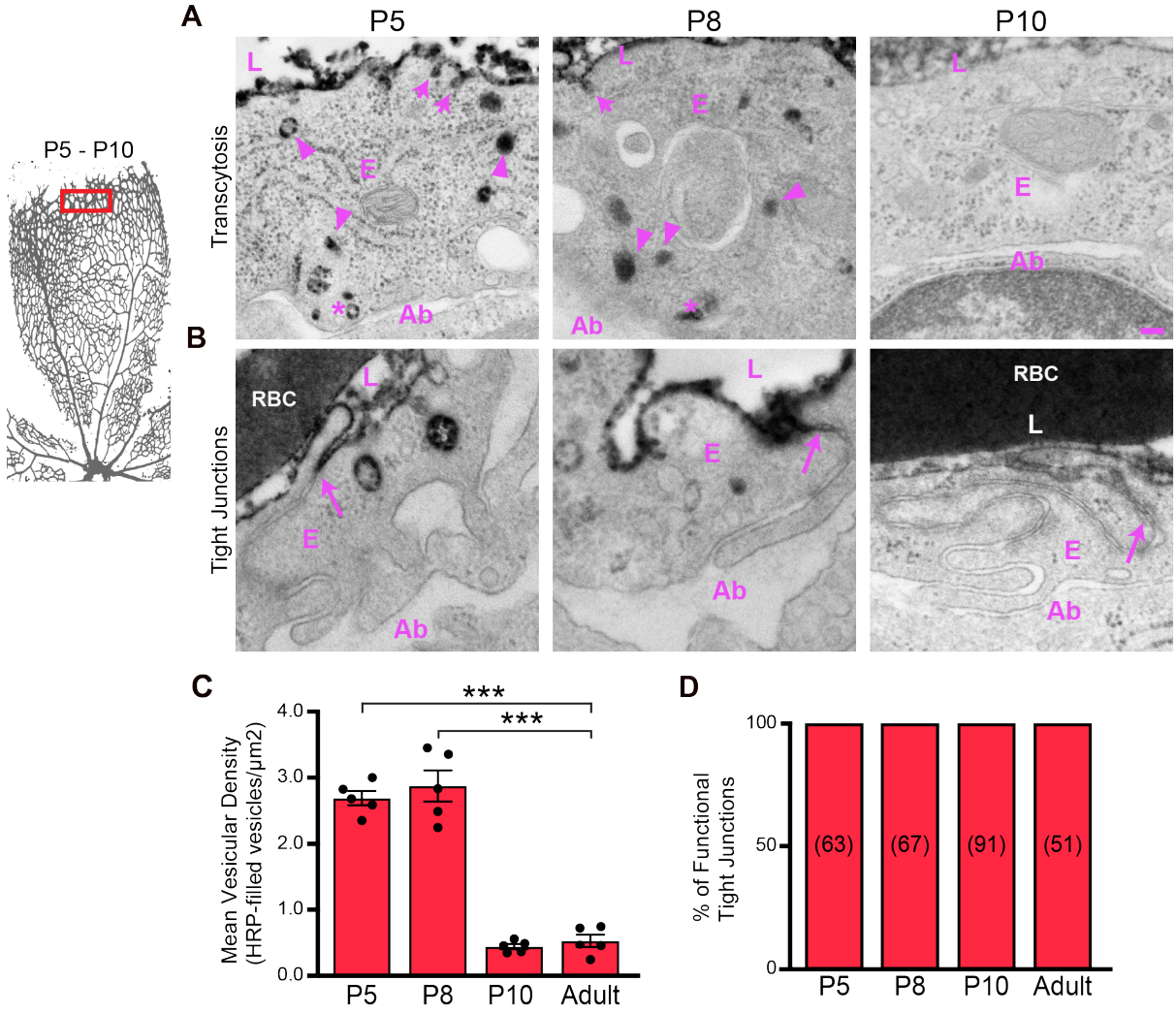

P10. Therefore, the spatiotemporal regulation of transcytosis indicates the development of a functional BRB.

Mfsd2a is essential to suppress transcytosis at the functional BRB

Given the significance of transcytosis in functional BRB formation, we next examined whether Mfsd2a, a known transcytosis regulator in blood-brain barrier formation (Ben-Zvi et al., 2014; Schubert et al., 2001), also plays a role in BRB formation. To test this hypothesis, we first intravenously injected HRP into *Mfsd2a*$^{-/-}$ mice and *Mfsd2a*$^{+/+}$ littermate controls and examine the retinas under EM. We found there is an increased HRP-filled vesicle density in the CNS endothelial cells of *Mfsd2a*$^{-/-}$ mice compared to *Mfsd2a*$^{+/+}$ littermate controls (**Figure 3.7**), whereas tight junctions remained functional (**Figure 3.7**). This phenotype is similar to what is observed in brain endothelial cells (Ben-Zvi et al., 2014). Thus, Mfsd2a plays a similar role at the BRB in suppressing transcytosis.

Mfsd2a expression correlates with functional BRB formation

We next examined Mfsd2a expression as a marker for suppressed transcytosis during BRB development by immunostaining retinas from dextran tracer-injected pups. At P7, Mfsd2a protein is only present in proximal, impermeable vessels but absent in distal, leaky vessels (**Figure 3.8**). In contrast, claudin-5 is fully present at the distal vessels (**Figure 3.8**). Importantly, Mfsd2a is absent from leaky, distal vessels during development (**Figure 3.8),** and only by P10, when the tracer is completely confined in the vessels, is Mfsd2a expression present at the distal vessels (**Figure 3.8**). Thus, the spatiotemporal expression of Mfsd2a correlates with the gradual suppression of transcytosis and the development of a functional BRB.

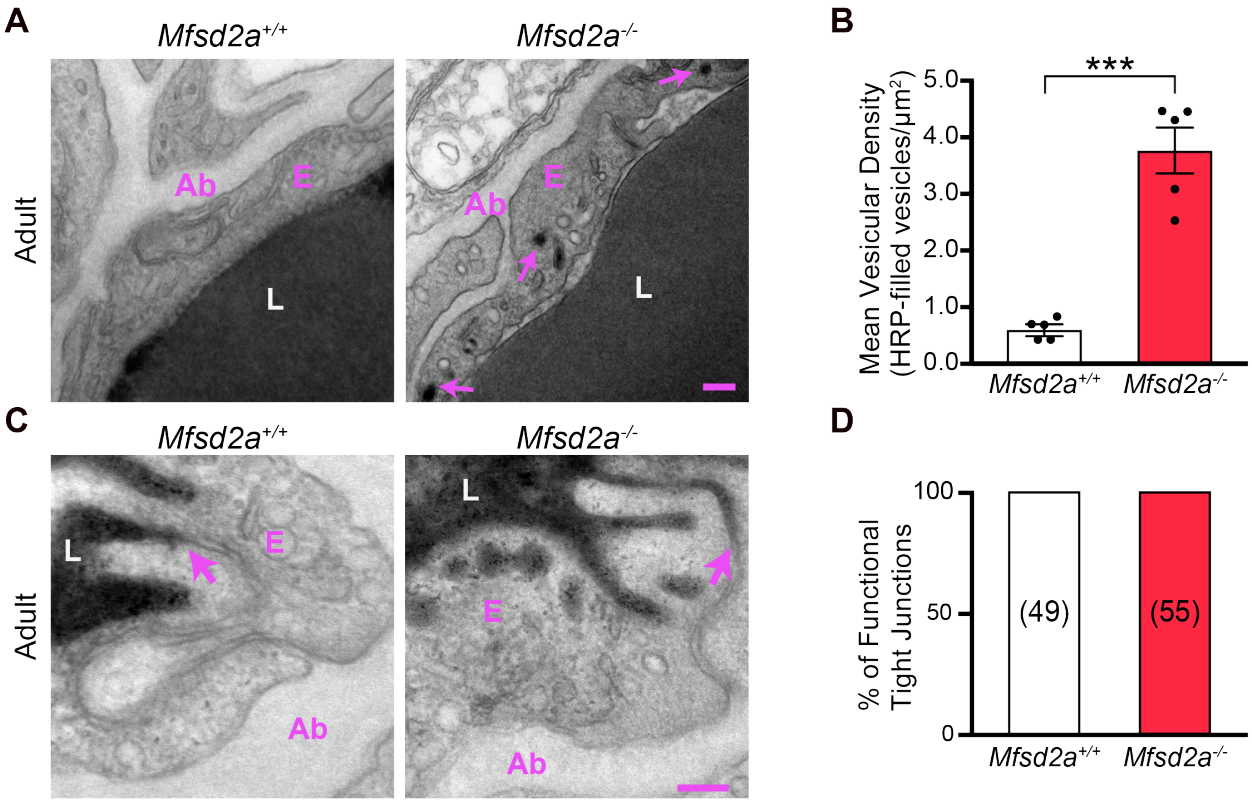

Figure 3.7. Mfsd2a is essential to suppress transcytosis in the BRB. (**A**) Transcytosis is increased in *Mfsd2a*$^{-/-}$ mice. Many tracer-filled vesicles (arrows) were observed in adult retinal endothelial cells from *Mfsd2a*$^{-/-}$ but not *Mfsd2a*$^{+/+}$ mice. (**B**) Quantification of HRP-filled vesicles in retinal endothelial cells from adult *Mfsd2a*$^{+/+}$ and *Mfsd2a*$^{-/-}$ mice. Data are shown as mean ± s.e.m. (n= 5 mice per genotype; each circle represents the average vesicular density from 18 – 20 vessels per mouse). Statistical significance was determined by unpaired t-test. (**C**) EM of the adult retina confirms that specialized tight junctions halt tracer product in both *Mfsd2a*$^{+/+}$ and *Mfsd2a*$^{-/-}$ adult mice (**D**) Quantification of functional tight junctions from *Mfsd2a*$^{+/+}$ and *Mfsd2a*$^{-/-}$ adult mice (n = 5 mice per genotype; 18-20 vessels analyzed per mouse; number of tight junctions analyzed are displayed in parenthesis). Scale bars represents 100 nm.

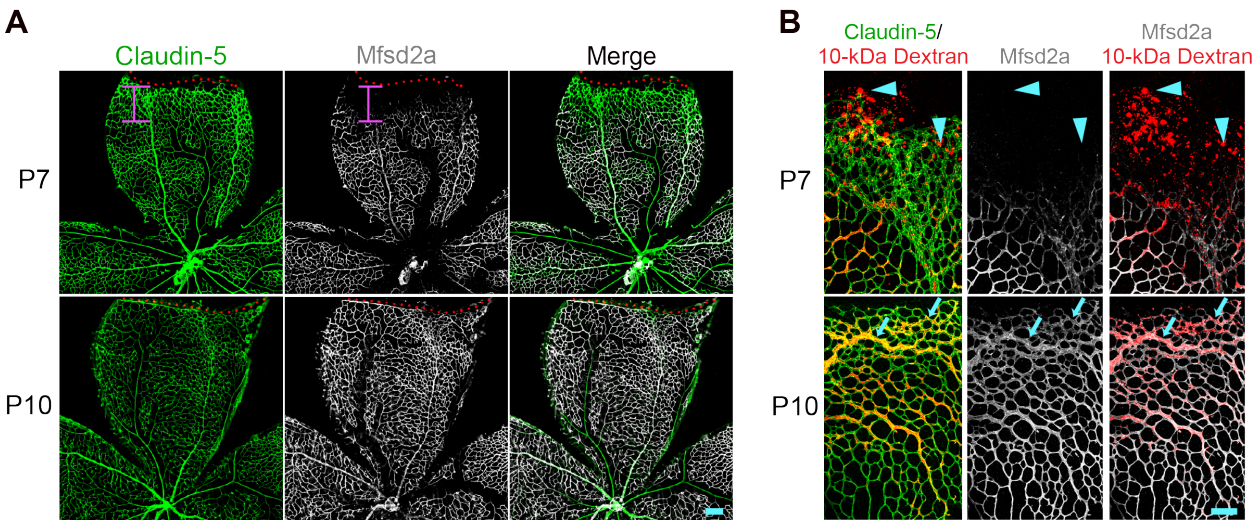

Figure 3.8. Mfsd2a expression correlates with functional BRB formation. (**A**) Immunostaining for Claudin-5 (green) and Mfsd2a (white) on P7 and P10 retinas shows the lack of Mfsd2a expression in nascent, distal vessels at P7. The red dash lines indicate the angiogenic front as determined by Claudin-5 expression, and the pink bar indicates the length from the angiogenic front to the appearance of Mfsd2a expression. In contrast to P7, Mfsd2a is expressed in the distal vessels at P10 (n= 5 mice per age). (**B**) Mfsd2a expression correlates with functional BRB formation. Immunostaining for Claudin-5 and Mfsd2a in retinas from 10-kDa dextran injected P7 and P10 mice shows that at P7, extravasation of tracer (arrowheads) occurs at nascent vessels where Mfsd2a is absent. At P10, tracer is confined (arrows) in distal vessels where Mfsd2a is expressed (n=5 mice per age). Scale bars represents 100 μm.

Elevated levels of transcytosis deter functional BRB formation

If the timing of the gradual suppression of transcytosis governs the development of a functional BRB, then altered regulation of transcytosis should affect functional BRB development. To test this idea, we examined the time course of functional BRB formation in two mutant mice with either elevated or attenuated transcytosis. First, we injected 10-kDa dextran tracers into *Mfsd2a*$^{-/-}$ mice and wild type littermates at P5, P10 and adult ages. In P5 *Mfsd2a*$^{+/+}$ wildtype mice, tracer leaked from distal vessels but was confined in proximal vessels (**Figure 3.9**). However, in P5 *Mfsd2a*$^{-/-}$ mice, tracer leaked from both distal and proximal vessels (**Figure 3.9**), similar to what we observed in P1 wildtype pups (**Figure 3.2**). Even at P10 and adulthood, this leaky phenotype persisted, indicating that failure to suppress transcytosis results in a incomplete formation of a functional BRB (**Supplementary Figure 6**).

Precocious suppression of transcytosis accelerates functional BRB formation

We next tested whether precocious suppression of transcytosis during development accelerates functional BRB formation. Among various transcytotic pathways, peripheral endothelial cells frequently utilize the caveolae-pathway (Armulik et al., 2010; Bell et al., 2010; Ben-Zvi et al., 2014; Daneman et al., 2010; Keskin et al., 2015; Sweeney et al., 2016; Winkler et al., 2011). *Caveolin-1 (Cav-1)* knockout mice lack caveolae vesicles throughout the endothelium (Stenman et al., 2008) but display normal tight junctions in CNS barriers (Junge et al., 2009; Wang et al., 2012; Ye et al., 2009; Zhou et al., 2014). EM analysis of distal retinal vessels from P8 and P10 *Cav-1*$^{+/+}$ wildtype retinas revealed decreased vesicular density from P8 to P10 (**Figure 3.10**). However, in *Cav-1*$^{-/-}$ mice, vesicular density was already low at P8 (**Figure 3.10**), indicating a precocious suppression of transcytosis in the BRB. To examine the impact of precocious suppression of transcytosis on functional BRB formation, bovine serum albumin (BSA), known

Figure 3.9. Elevated levels of transcytosis deter functional BRB formation. (**A**) Genetic ablation of *Mfsd2a* results in incomplete formation of the functional BRB. After intravenous injection of 10-kDa dextran in P5 *Mfsd2a*$^{+/+}$ and *Mfsd2a*$^{-/-}$ pups, tracer was confined (arrow) in proximal vessels (bottom) but leaked from distal vessels (top) in *Mfsd2a*$^{+/+}$ mice (arrowheads). In contrast, tracer leaked into the retinal parenchyma from both proximal and distal vessels in *Mfsd2a*$^{-/-}$ mice (arrowheads). (**H**) Permeability index from proximal and distal regions of P5 *Mfsd2a*$^{-/-}$ and *Mfsd2a*$^{+/+}$ littermates. Data are shown as mean ± s.e.m. (n=5 mice per genotype; each circle represents the average permeability from each mouse). Statistical significance was determined by unpaired t-test. ***, $P < 0.001$. Scale bars represents 100 μm.

Figure 3.9 (Continued)

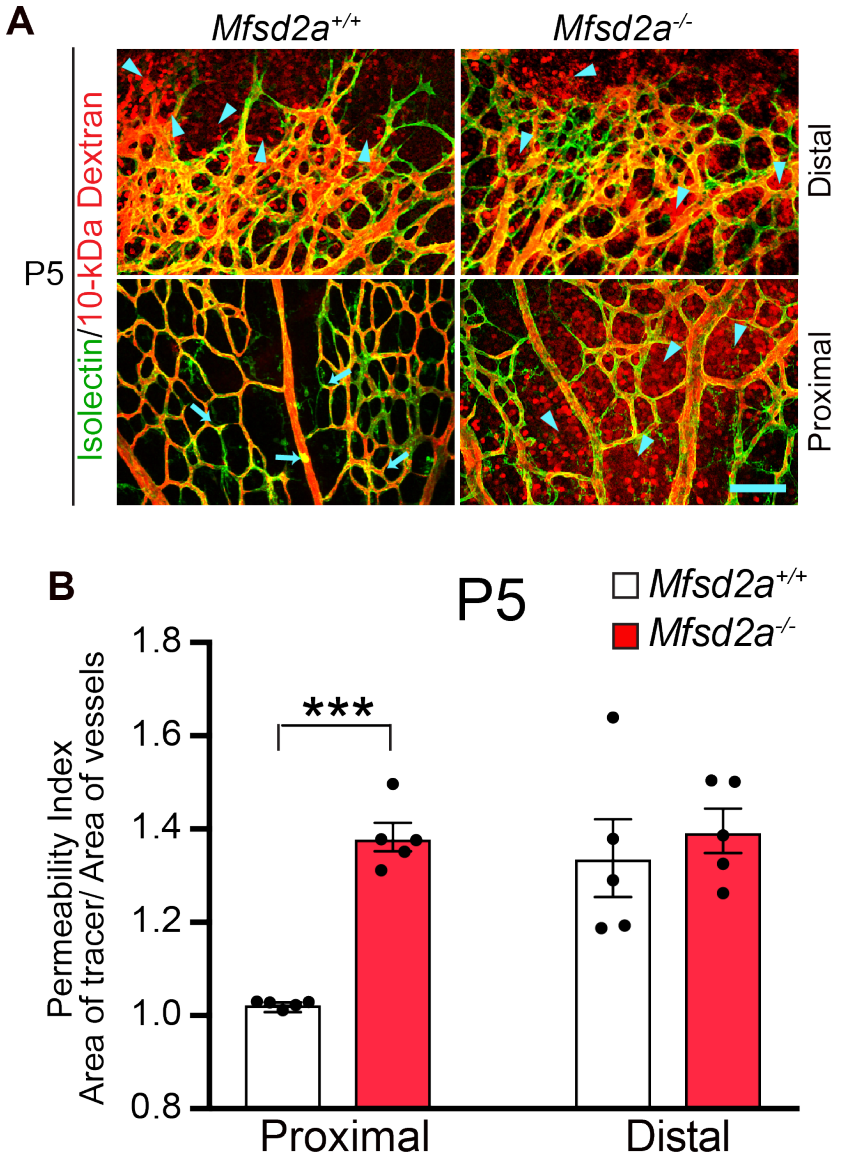

to be transported via caveolae vesicles in lung endothelial cells (Ulrich et al., 2016; Vanhollebeke et al., 2015), was injected intravenously in *Cav-1*$^{+/+}$ and *Cav-1*$^{-/-}$ mice at P8. In *Cav-1*$^{+/+}$ wildtype littermate mice, we observed BSA leakage into the retinal parenchyma from distal vessels (**Figure 3.11**) However, in *Cav-1*$^{-/-}$ mice, BSA was confined throughout the vasculature, indicating that a functional BRB had formed at P8 instead of P10 (**Figure 3.11**). This time shift in BRB impermeability demonstrates that precocious suppression of transcytosis results in an earlier formation of a functional BRB.

Discussion:

This study provides the first spatiotemporal characterization of functional BRB formation and establishes the BRB as a tractable model system for future study of CNS barriers. Using this system, we unexpectedly found that suppression of transcytosis is a principal contributor in the normal development of a functional barrier. We demonstrated that during BRB development, budding CNS endothelial cells already display functional tight junctions as early as vessel ingression but have not yet suppressed transcytosis. Thus, the leakiness of the developing retinal vasculature is entirely due to transcytosis. A functional BRB is established days later, only after transcytosis is gradually suppressed in BRB endothelial cells (**Supplementary Figure 7**). In contrast to the prevailing notion in the field emphasizing the role of tight junctions in barrier function, our findings support an emerging view that transcytosis also plays a key role in regulating CNS barrier permeability and indicate that while specialized tight junctions are intrinsic to retinal endothelial cells, suppression of transcytosis is induced by CNS environmental cues during development. Our findings revealed that CNS endothelial cells have a developmental program that actively inhibits transcytosis to ensure barrier function. Finally, unregulated BRB

Figure 3.10. Precocious suppression of transcytosis by genetically ablating caveolae vesicles. (**A**) Precocious suppression of transcytosis is observed in *Cav-1*$^{-/-}$ retinas. EM in distal vessels at P8 (top) reveals many vesicles associated with luminal (arrows) and abluminal membranes (*) and in the cytoplasm (arrowheads) in *Cav-1*$^{+/+}$ endothelial cells. *Cav-1*$^{-/-}$ endothelial cells have drastically reduced numbers of vesicles. At P10 (bottom), few vesicles are observed in both *Cav-1*$^{+/+}$ and *Cav-1*$^{-/-}$ distal vessels. (**B**) Quantifications of vesicles in distal vessels from *Cav-1*$^{+/+}$ and *Cav-1*$^{-/-}$ mice at P8 and P10. Data are presented as mean ± s.e.m. (n= 3 mice per age per genotype, 15-20 vessels analyzed per mouse). Statistical significance was determined by two-way ANOVA with a post-hoc Bonferroni multiple comparison adjustment. Scale bar represents 100 nm.

Figure 3.10 (Continued)

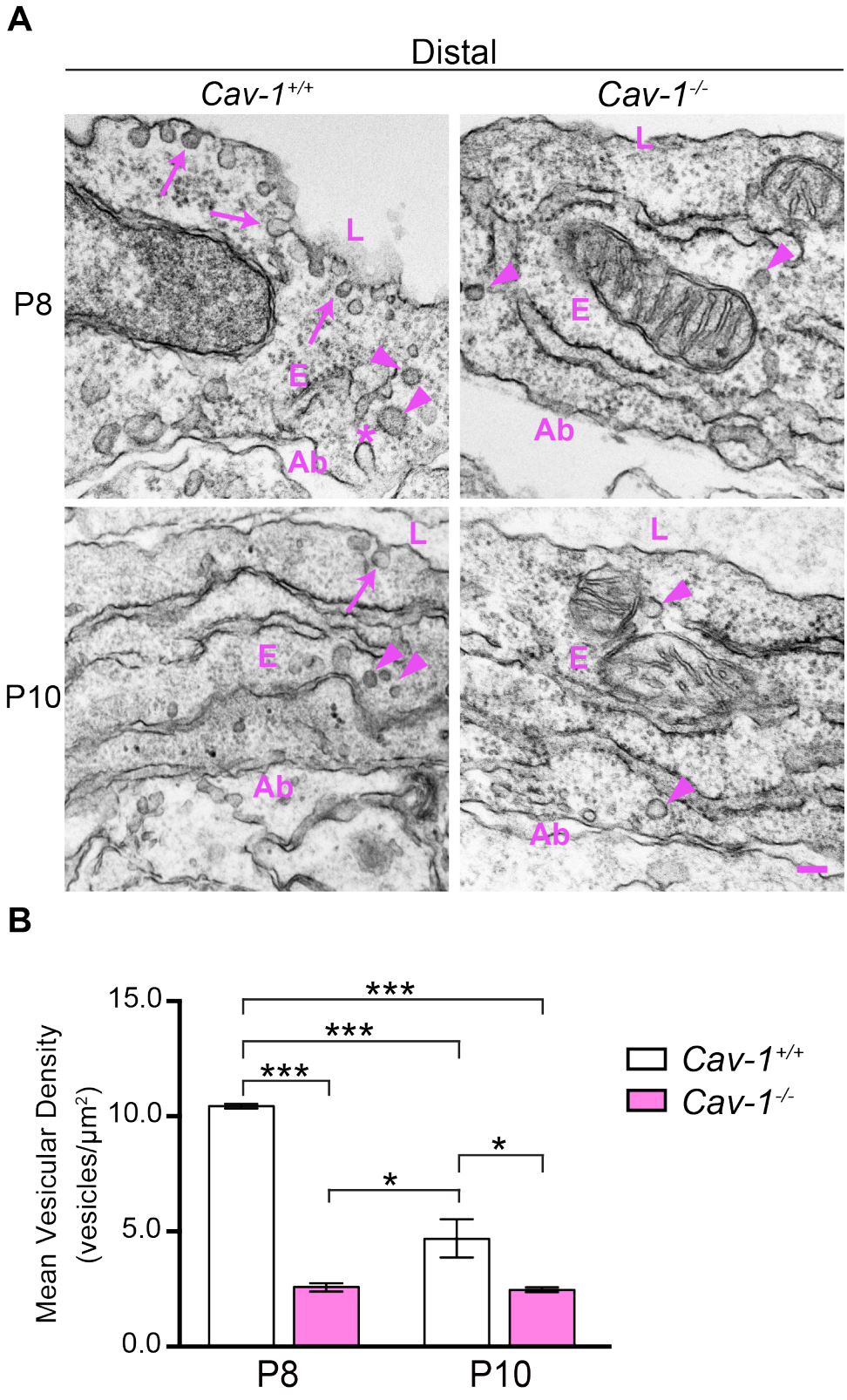

Figure 3.11. Precocious suppression of transcytosis by genetically ablating caveolae vesicles. (**A**) Intravenous injection of BSA (red) in P8 pups reveals tracer leakage in the retinal parenchyma from distal vessels of *Cav-1*$^{+/+}$ (arrowheads) but not *Cav-1*$^{-/-}$ mice. (**B**) Permeability index from distal regions of P8 *Cav-1*$^{+/+}$ and *Cav-1*$^{-/-}$ littermates. Data are presented as mean ± s.e.m. (n=3-4 mice per genotype). Statistical significance was determined by unpaired t-test. *, $P < 0.05$; **, $P < 0.01$; ***, $P < 0.001$. L – lumen, E – endothelial cells, Ab – abluminal. Scale bar represents 100 μm.

Figure 3.11 (Continued)

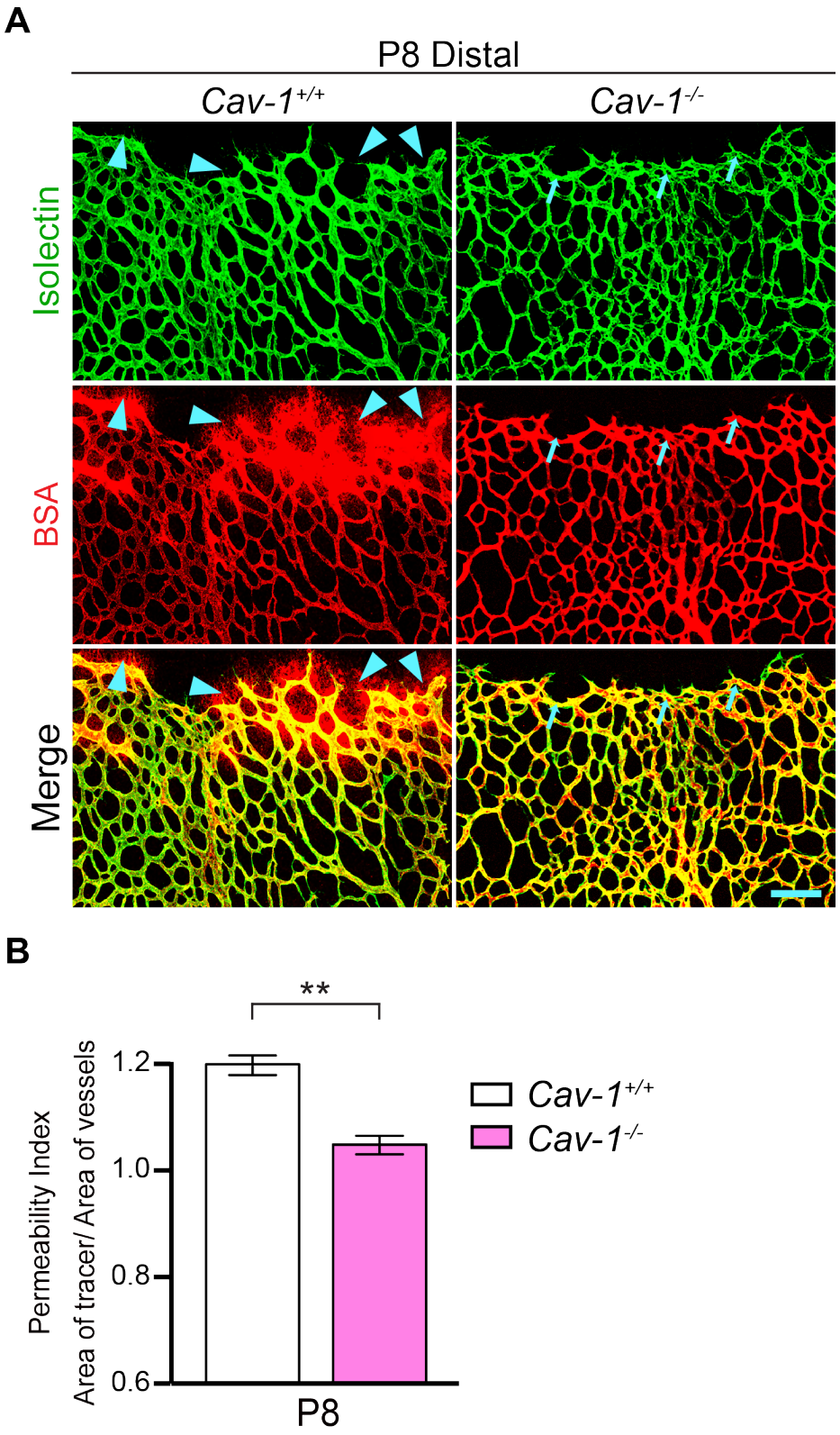

dysfunction is a pathological feature of many ocular diseases (Huberman et al., 2008). Our findings may offer insights to improving CNS drug delivery as manipulating transcytosis can transport different size cargos, including compounds less than 1kDa to large macromolecules. Furthermore, genes that regulate transcytosis can be targeted to repair CNS barriers to treat neurodegenerative diseases.

What are the molecular mechanisms that induce CNS endothelial cells to gradually suppress transcytosis to develop a functional BRB? Pericytes ensheathing CNS endothelial cells are the most promising candidates, as pericyte-deficient mice have leaky barriers in brain and retina, aberrant tight junctions, elevated transcytosis and reduced Mfsd2a protein at the blood-brain barrier (Armulik et al., 2010; Bell et al., 2010; Ben-Zvi et al., 2014; Daneman et al., 2010; Keskin et al., 2015; Sweeney et al., 2016; Winkler et al., 2011). Using *NG2:DsRed* reporter mice, which labels retinal mural cells, we examined pericyte coverage and density during BRB development and found that pericytes ensheath blood vessels at P1 (**Supplementary Figure 2**). In P5 retinas, we find about a 1:1 pericyte to endothelial cell ratio throughout the retina (**Supplementary Figure 8**), including distal, nascent leaky vessels where Mfsd2a protein is absent (**Supplementary Figure 9**). This suggests that the differentiation state of pericytes or inductive factors secreted from pericytes during development are likely the key mechanisms that induce CNS endothelial cells to suppress transcytosis for functional BRB formation. Indeed, the loss-of-function of two transcription factors, *foxc1* and *foxf2*, in CNS pericytes actually increases CNS pericyte density but still results in blood-brain barrier breakdown (Reyahi et al., 2015; Siegenthaler et al., 2013), suggesting that pericyte differentiation state but not necessarily pericyte coverage or density per se is important for blood-brain barrier integrity. Therefore, it is critical for future work to identify the pericyte-secreted factors that mediate the gradual

suppression of transcytosis for a functional BRB.

Canonical Wnt signaling is the best characterized signal for CNS angiogenesis and barrier formation (Stenman et al., 2008). In the retina, loss-of-function of the ligand (Norrin), receptor (Frizzled-4), co-receptors (Lrp5 and Tspan12) and downstream transcription factor (β-catenin), all result in impaired retinal angiogenesis and BRB breakdown (Junge et al., 2009; Wang et al., 2012; Ye et al., 2009; Zhou et al., 2014). Moreover, emerging evidence suggests that canonical Wnt signaling regulates tight junction function in CNS barriers, as loss-of-function of canonical Wnt signaling decreases Claudin-5 and increases PLVAP protein expression, resulting in opened junctions at the blood-brain barrier (Stan et al., 2012; Tran et al., 2016; Wang et al., 2012; Zhou et al., 2014). Whether canonical Wnt signaling also regulates the gradual suppression of transcytosis is not clear. On one hand, recent studies demonstrated canonical Wnt signaling is essential in the tip cells of nascent sprouts (Ulrich et al., 2016; Vanhollebeke et al., 2015) yet these nascent, distal vessels display bulk transcytosis and lack Mfsd2a during BRB development. But on the other hand, microarray analysis on retinas from canonical Wnt signaling deficient mice showed that Mfsd2a is downregulated (Chen et al., 2012). Therefore, while canonical Wnt signaling regulates functional tight junctions in BRB endothelial cells, it is imperative that future studies elucidate if canonical Wnt signaling also regulates the suppression of transcytosis.

It is intriguing that functional BRB formation and the shift in a homeostatic retinal microenvironment occurs by P10, a few days before mouse eyes open (Feller, 2009). Furthermore, it is notable that the timing of retinal barrier formation correlates with the development of the neural retina, particularly with retinal waves. Retinal waves are spontaneous neural activity in retinal ganglion cells during development, and are thought to refine visual

circuitry prior to eye-opening and the onset of sensory-evoked neural activity (Huberman et al., 2008). It will be interesting to investigate whether the temporal correlation of BRB development and retinal waves implies cross-talk between functional BRB formation and neural function. While the acquisition of barrier properties is dependent on inductive cues from the neural environment, it is unclear if neural activity, especially spontaneous activity during development, is involved in transmitting these inductive cues for BRB formation. Alternatively, the maturation of the BRB could influence the spatiotemporal formation of the retinal waves. Addressing if there is causal relationship between BRB formation and retinal waves could shift thought paradigms in both vascular biology and neurobiology.

Author Contributions

BW.C. and C.G. conceived the project and designed experiments.

B.W.C performed all experiments

B.W.C analyzed all data.

B.W.C and C.G. wrote the manuscript

References

Andreone, B.J., Lacoste, B., and Gu, C. (2015). Neuronal and vascular interactions. Annu. Rev. Neurosci. *38*, 25–46.

Armulik, A., Genové, G., Mäe, M., Nisancioglu, M.H., Wallgard, E., Niaudet, C., He, L., Norlin, J., Lindblom, P., Strittmatter, K., et al. (2010). Pericytes regulate the blood-brain barrier. *468*, 557–561.

Banks, W.A. (2016). From blood-brain barrier to blood-brain interface: new opportunities for CNS drug delivery. Nat Rev Drug Discov. *15,* 275-292.

Bell, R.D., Winkler, E.A., Sagare, A.P., Singh, I., LaRue, B., Deane, R., and Zlokovic, B.V. (2010). Pericytes control key neurovascular functions and neuronal phenotype in the adult brain and during brain aging. Neuron *68*, 409–427.

Ben-Zvi, A., Lacoste, B., Kur, E., Andreone, B.J., Mayshar, Y., Yan, H., and Gu, C. (2014). Mfsd2a is critical for the formation and function of the blood-brain barrier. Nature *509*, 507–511.

Blanchette, M., and Daneman, R. (2015). Formation and maintenance of the BBB. Mech. Dev. *138 Pt 1*, 8–16.

Chen, J., Stahl, A., Krah, N.M., Seaward, M.R., Joyal, J.-S., Juan, A.M., Hatton, C.J., Aderman, C.M., Dennison, R.J., Willett, K.L., et al. (2012). Retinal expression of Wnt-pathway mediated genes in low-density lipoprotein receptor-related protein 5 (Lrp5) knockout mice. PLoS ONE *7*, e30203.

Chow, B.W., and Gu, C. (2015). The Molecular Constituents of the Blood-Brain Barrier. Trends in Neurosciences *38*, 598–608.

Daneman, R., Zhou, L., Kebede, A.A., and Barres, B.A. (2010). Pericytes are required for blood-brain barrier integrity during embryogenesis. *468*, 562–566.

de Vries, H.E., Kooij, G., Frenkel, D., Georgopoulos, S., Monsonego, A., and Janigro, D. (2012). Inflammatory events at blood–brain barrier in neuroinflammatory and neurodegenerative disorders: Implications for clinical disease. Epilepsia *53*, 45–52.

Drab, M., Verkade, P., Elger, M., Kasper, M., Lohn, M., Lauterbach, B., Menne, J., Lindschau, C., Mende, F., Luft, F.C., et al. (2001). Loss of caveolae, vascular dysfunction, and pulmonary defects in caveolin-1 gene-disrupted mice. Science *293*, 2449–2452.

Engelhardt, B., and Coisne, C. (2011). Fluids and barriers of the CNS establish immune privilege by confining immune surveillance to a two-walled castle moat surrounding the CNS castle. Fluids Barriers CNS *8*, 4.

Feller, M.B. (2009). Retinal waves are likely to instruct the formation of eye-specific retinogeniculate projections. Neural Development 2009 4:1 *4*, 1.

Fruttiger, M. (2007). Development of the retinal vasculature. Angiogenesis *10*, 77–88.

Hagan, N., and Ben-Zvi, A. (2015). The molecular, cellular, and morphological components of blood–brain barrier development during embryogenesis. Semin. Cell Dev. Biol. *38*, 7–15.

Huberman, A.D., Feller, M.B., and Chapman, B. (2008). Mechanisms underlying development of visual maps and receptive fields. Annu. Rev. Neurosci. *31*, 479–509.

Junge, H.J., Yang, S., Burton, J.B., Paes, K., Shu, X., French, D.M., Costa, M., Rice, D.S., and Ye, W. (2009). TSPAN12 regulates retinal vascular development by promoting Norrin- but not Wnt-induced FZD4/beta-catenin signaling. Cell *139*, 299–311.

Karnovsky, M.J. (1967). The ultrastructural basis of capillary permeability studied with peroxidase as a tracer. J. Cell Biol. *35*, 213–236.

Keskin, D., Kim, J., Cooke, V.G., Wu, C.-C., Sugimoto, H., Gu, C., De Palma, M., Kalluri, R., and LeBleu, V.S. (2015). Targeting vascular pericytes in hypoxic tumors increases lung metastasis via angiopoietin-2. CellReports *10*, 1066–1081.

Knowland, D., Arac, A., Sekiguchi, K.J., Hsu, M., Lutz, S.E., Perrino, J., Steinberg, G.K., Barres, B.A., Nimmerjahn, A., and Agalliu, D. (2014). Stepwise recruitment of transcellular and paracellular pathways underlies blood-brain barrier breakdown in stroke. Neuron *82*, 603–617.

Myles, M.E., Neumann, D.M., and Hill, J.M. (2005). Recent progress in ocular drug delivery for posterior segment disease: emphasis on transscleral iontophoresis. Adv. Drug Deliv. Rev. *57*, 2063–2079.

Obermeier, B., Daneman, R., and Ransohoff, R.M. (2013). Development, maintenance and disruption of the blood-brain barrier. Nat. Med. *19*, 1584–1596.

Pardridge, W.M. (2012). Drug transport across the blood–brain barrier. Journal of Cerebral Blood Flow & Metabolism *32*, 1959–1972.

Raviola, G. (1977). The structural basis of the blood-ocular barriers. Experimental Eye Research *25 Suppl*, 27–63.

Razani, B., Engelman, J.A., Wang, X.B., Schubert, W., Zhang, X.L., Marks, C.B., Macaluso, F., Russell, R.G., Li, M., Pestell, R.G., et al. (2001). Caveolin-1 null mice are viable but show evidence of hyperproliferative and vascular abnormalities. J. Biol. Chem. *276*, 38121–38138.

Reese, T.S., and Karnovsky, M.J. (1967). Fine structural localization of a blood-brain barrier to exogenous peroxidase. J. Cell Biol. *34*, 207–217.

Reyahi, A., Nik, A.M., Ghiami, M., Gritli-Linde, A., Pontén, F., Johansson, B.R., and Carlsson, P. (2015). Foxf2 Is Required for Brain Pericyte Differentiation and Development and Maintenance of the Blood- Brain Barrier. Developmental Cell *34*, 19–32.

Schubert, W., Frank, P.G., Razani, B., Park, D.S., Chow, C.W., and Lisanti, M.P. (2001). Caveolae-deficient Endothelial Cells Show Defects in the Uptake and Transport of Albumin in Vivo. J. Biol. Chem. *276*, 48619–48622.

Siegenthaler, J.A., Choe, Y., Patterson, K.P., Hsieh, I., Li, D., Jaminet, S.-C., Daneman, R., Kume, T., Huang, E.J., and Pleasure, S.J. (2013). Foxc1 is required by pericytes during fetal brain angiogenesis. Biology Open *2*, 647–659.

Stan, R.V., Tse, D., Deharvengt, S.J., Smits, N.C., Xu, Y., Luciano, M.R., McGarry, C.L., Buitendijk, M., Nemani, K.V., Elgueta, R., et al. (2012). The diaphragms of fenestrated endothelia: gatekeepers of vascular permeability and blood composition. Developmental Cell *23*, 1203–1218.

Stenman, J.M., Rajagopal, J., Carroll, T.J., Ishibashi, M., McMahon, J., and McMahon, A.P. (2008). Canonical Wnt signaling regulates organ-specific assembly and differentiation of CNS vasculature. Science *322*, 1247–1250.

Stewart, P.A., and Wiley, M.J. (1981). Developing nervous tissue induces formation of blood-brain barrier characteristics in invading endothelial cells: a study using quail--chick transplantation chimeras. Dev. Biol. *84*, 183–192.

Stone, J., Itin, A., Alon, T., Pe'er, J., Gnessin, H., Chan-Ling, T., and Keshet, E. (1995). Development of retinal vasculature is mediated by hypoxia-induced vascular endothelial growth factor (VEGF) expression by neuroglia. Journal of Neuroscience *15*, 4738–4747.

Sweeney, M.D., Ayyadurai, S., and Zlokovic, B.V. (2016). Pericytes of the neurovascular unit: key functions and signaling pathways. Nat. Neurosci. *19*, 771–783.

Tran, K.A., Zhang, X., Predescu, D., Huang, X., Machado, R.F., Göthert, J.R., Malik, A.B., Valyi-Nagy, T., and Zhao, Y.-Y. (2016). Endothelial β-Catenin Signaling Is Required for Maintaining Adult Blood-Brain Barrier Integrity and Central Nervous System Homeostasis. Circulation *133*, 177–186.

Tuma, P.L., and Hubbard, A.L. (2003). Transcytosis: crossing cellular barriers. Physiol. Rev. *83*, 871–932.

Ulrich, F., Carretero-Ortega, J., Menéndez, J., Narvaez, C., Sun, B., Lancaster, E., Pershad, V., Trzaska, S., Véliz, E., Kamei, M., et al. (2016). Reck enables cerebrovascular development by promoting canonical Wnt signaling. Development *143*, 147–159.

Vanhollebeke, B., Stone, O.A., Bostaille, N., Cho, C., Zhou, Y., Maquet, E., Gauquier, A., Cabochette, P., Fukuhara, S., Mochizuki, N., et al. (2015). Tip cell-specific requirement for an atypical Gpr124- and Reck-dependent Wnt/β-catenin pathway during brain angiogenesis. Elife *4*.

Wang, Y., Rattner, A., Zhou, Y., Williams, J., Smallwood, P.M., and Nathans, J. (2012). Norrin/Frizzled4 signaling in retinal vascular development and blood brain barrier plasticity. Cell *151*, 1332–1344.

Winkler, E.A., Bell, R.D., and Zlokovic, B.V. (2011). Central nervous system pericytes in health and disease. Nat. Neurosci. *14*, 1398–1405.

Winkler, E.A., Sengillo, J.D., Sagare, A.P., Zhao, Z., Ma, Q., Zuniga, E., Wang, Y., Zhong, Z., Sullivan, J.S., Griffin, J.H., et al. (2014). Blood-spinal cord barrier disruption contributes to early motor-neuron degeneration in ALS-model mice. Proc. Natl. Acad. Sci. U.S.a. *111*, E1035–E1042.

Ye, X., Wang, Y., Cahill, H., Yu, M., Badea, T.C., Smallwood, P.M., Peachey, N.S., and Nathans, J. (2009). Norrin, frizzled-4, and Lrp5 signaling in endothelial cells controls a genetic program for retinal vascularization. Cell *139*, 285–298.

Zhao, Z., Nelson, A.R., Betsholtz, C., and Zlokovic, B.V. (2015). Establishment and Dysfunction of the Blood-Brain Barrier. Cell *163*, 1064–1078.

Zhou, Y., Wang, Y., Tischfield, M., Williams, J., Smallwood, P.M., Rattner, A., Taketo, M.M., and Nathans, J. (2014). Canonical WNT signaling components in vascular development and barrier formation. J. Clin. Invest. *124*, 3825–3846.

Zlokovic, B.V. (2008). The blood-brain barrier in health and chronic neurodegenerative disorders. Neuron *57*, 178–201.

CHAPTER 4

Caveolae in CNS arterioles mediate neurovascular coupling

Adapted from a manuscript in review (March 06, 2019)

Caveolae in CNS arterioles mediate neurovascular coupling

Brian W. Chow[1*], Vicente Nuñez[1*], Adam J. Granger[1,2], Karina Bistrong[1], Hannah L. Zucker[1], Payal Kumar[1], Bernardo L. Sabatini[1,2], Chenghua Gu[1]

[1]Department of Neurobiology, Harvard Medical School, 220 Longwood Ave, Boston, MA 02115, USA.

[2] Howard Hughes Medical Institute, Department of Neurobiology, Harvard Medical School, 220 Longwood Ave, Boston, MA 02115, USA.

Correspondence:

Chenghua Gu (chenghua_gu@hms.harvard.edu)

4.1 Abstract:

Proper brain function depends on neurovascular coupling, the process where local neural activation accelerates local blood flow to meet instantaneous changes in regional energy demand. Neurovascular coupling is the basis for functional brain imaging, and its impairment contributes to neurodegeneration. The underlying molecular and cellular mechanisms of neurovascular coupling remain poorly understood, although the conventional view is that neurons or astrocytes release vasodilatory factors directly onto smooth muscle cells (SMC) of arterioles to induce dilation and increase local blood flow. Here, using two-photon microscopy to simultaneously image neural activity and vascular dynamics in the barrel cortex of awake mice using sensory-evoked whisker stimulation, we found that arteriolar endothelial cells (aECs) play an active role in mediating neurovascular coupling. We found that unlike other vascular segments of ECs in the CNS, aECs have abundant caveolae. Acute genetic perturbations that eliminated caveolae in aECs, but not in adjacent SMCs, impaired neurovascular coupling. Strikingly, caveolae function in aECs is independent of the eNOS-mediated nitric oxide (NO) pathway. Ablation of both caveolae and eNOS completely abolished neurovascular coupling, whereas each single mutant exhibited partial impairment, revealing that caveolae-mediated pathway in aECs is a major contributor to neurovascular coupling. Our findings indicate that endothelial cells are essential for neurovascular coupling via a caveolae-dependent pathway.

4.2 Introduction:

To continuously compute neural activity for perception, motor movement, and cognition, the brain requires a continuous supply of blood (Iadecola, 2017). Despite representing only 2% of body mass, the brain uses 20% of the body's energy at rest (Sweeney et al., 2018). However, unlike other metabolically demanding organs such as the liver and skeletal muscles, the brain lacks significant energy storage (Zlokovic, 2008). To satisfy the brain's high metabolic consumption, the brain vasculature has evolved a unique function that is absent in the vasculature of peripheral organs. This unique function is known as neurovascular coupling, a process where increased local neural activation accelerates local blood flow to replenish nutrients and clear waste (Andreone et al., 2015; Iadecola, 2017). Neurovascular coupling is the basis for functional magnetic resonance imaging (fMRI), one of the few therapeutic armamentaria available to image the working human mind for research and diagnostics (Hillman, 2014). Impaired neurovascular coupling also contributes to neurodegeneration (Hernández et al., 2019; Iadecola, 2017; Sweeney et al., 2018; Zlokovic, 2008). Despite the importance of neurovascular coupling, the underlying molecular and cellular mechanisms are still unclear.

Neurovascular coupling begins with increased neural activity and ends with smooth muscle cell (SMC) relaxation, leading to arteriolar vasodilation and increased capillary blood flow (Cauli et al., 2014; Hillman, 2014; Kleinfeld et al., 2011). This process occurs rapidly, on the order of hundreds of milliseconds *in vivo* under physiological conditions (Chen et al., 2014; O'Herron et al., 2016; Shen et al., 2012). However, it is unclear how signals are transmitted from neurons to SMCs. The conventional view has been that during neural activity, neurons and astrocytes release vasodilatory signals directly onto SMCs to expand arteriolar diameter to increase blood flow (Attwell et al., 2010; Cauli et al., 2014; Kisler et al., 2017). Interestingly,

recent studies also indicate that blood vessels also play a role in neurovascular coupling (Chen et al., 2014; Longden et al., 2017).

Here, we demonstrate that CNS arteriolar endothelial cells (aECs) play an active role in mediating signals from neural activity to SMC relaxation during neurovascular coupling. We found that unlike other segments of endothelial cells in the CNS vasculature, aECs have abundant caveolae. We used *in vivo* two-photon microscopy for simultaneous measurement of neural activity and vascular dynamics, such as arteriolar vessel diameter and capillary blood flow, in the barrel cortex of awake mice stimulated with whisker stimulation. We found that acute genetic perturbations that eliminated caveolae in aECs, but not in adjacent SMCs, impaired neurovascular coupling. Moreover, caveolae function in aECs is independent of the eNOS-mediated nitric oxide (NO) pathway, and ablation of both caveolae and eNOS completely abolished neurovascular coupling, revealing that caveolae-mediated pathway in aECs is a major contributor to neurovascular coupling. Finally, we demonstrate that a molecular suppressor of caveolae, Mfsd2a, is absent in aECs and that ectopic expression of Mfsd2a specifically in aECs is sufficient to impair neurovascular coupling. Our findings indicate that neurovascular coupling is due to endothelial cells that actively mediate signals from neurons and astrocytes to SMCs via a caveolae-dependent pathway.

4.3 Result:

CNS arteriolar endothelial cells have abundant caveolae

Previously, we discovered that caveolae are actively suppressed in CNS capillary endothelial cells to ensure blood brain barrier integrity (Andreone et al., 2017; Ben-Zvi et al., 2014; Chow and Gu, 2017). Surprisingly, we found that not all segments of the CNS

endothelium suppress caveolae. Rather, we found that aECs have abundant caveolae (**Figure 4.1**), whereas capillary endothelial cells (cECs) have negligible numbers of caveolae (**Figure 4.1**). Under EM, CNS capillaries are identified by having 1) a smooth and circular lumen, 2) pericytes wrapped around the CNS cECs and 3) one basement membrane that is shared between cECs and pericytes (**Figure 4.1**) In contrast, CNS arterioles have strikingly different ultrastructure. CNS arterioles are identified by having 1) a ruffled lumen, 2) large and easily distinguishable SMCs that ensheathed the aECs and 3) two distinct basement membranes (**Figure 4.1**). Furthermore, we found that these abundant vesicles in aECs are caveolae because these vesicles are abolished in aECs in *caveolin-1* mutant mice *(Cav1$^{-/-}$)* (**Figure 4.2**). Cav1 is an obligatory component of caveolae, and *Cav1$^{-/-}$* mice lack caveolae in the endothelium (Andreone et al., 2017; Chow and Gu, 2017; Drab et al., 2001; Razani et al., 2001). Thus, CNS aECs have abundant caveolae. Interestingly, many caveolae are also present in SMCs that enshealth the aECs (**Figure 4.2**).

Caveolae are essential for neurovascular coupling

Given that we found caveolae are specifically abundant in aECs and CNS arterioles are the effectors that mediate vasodilation (Cauli et al., 2014; Hillman, 2014; Kleinfeld et al., 2011), we examined whether caveolae are important for neurovascular coupling using *Cav1$^{-/-}$* mice. To study neurovascular coupling *in vivo*, we optimized a two-photon microscope for simultaneous measurement of neural activity and vascular dynamics, including arteriolar vessel diameter and capillary blood flow, at single-vessel resolution in awake mice (**Supplementary Figure 10**). We focused on the barrel cortex, a well-characterized region of mouse somatosensory cortex that processes sensory input from the vibrissae (Hill et al., 2015; O'Connor et al., 2010). Sensory

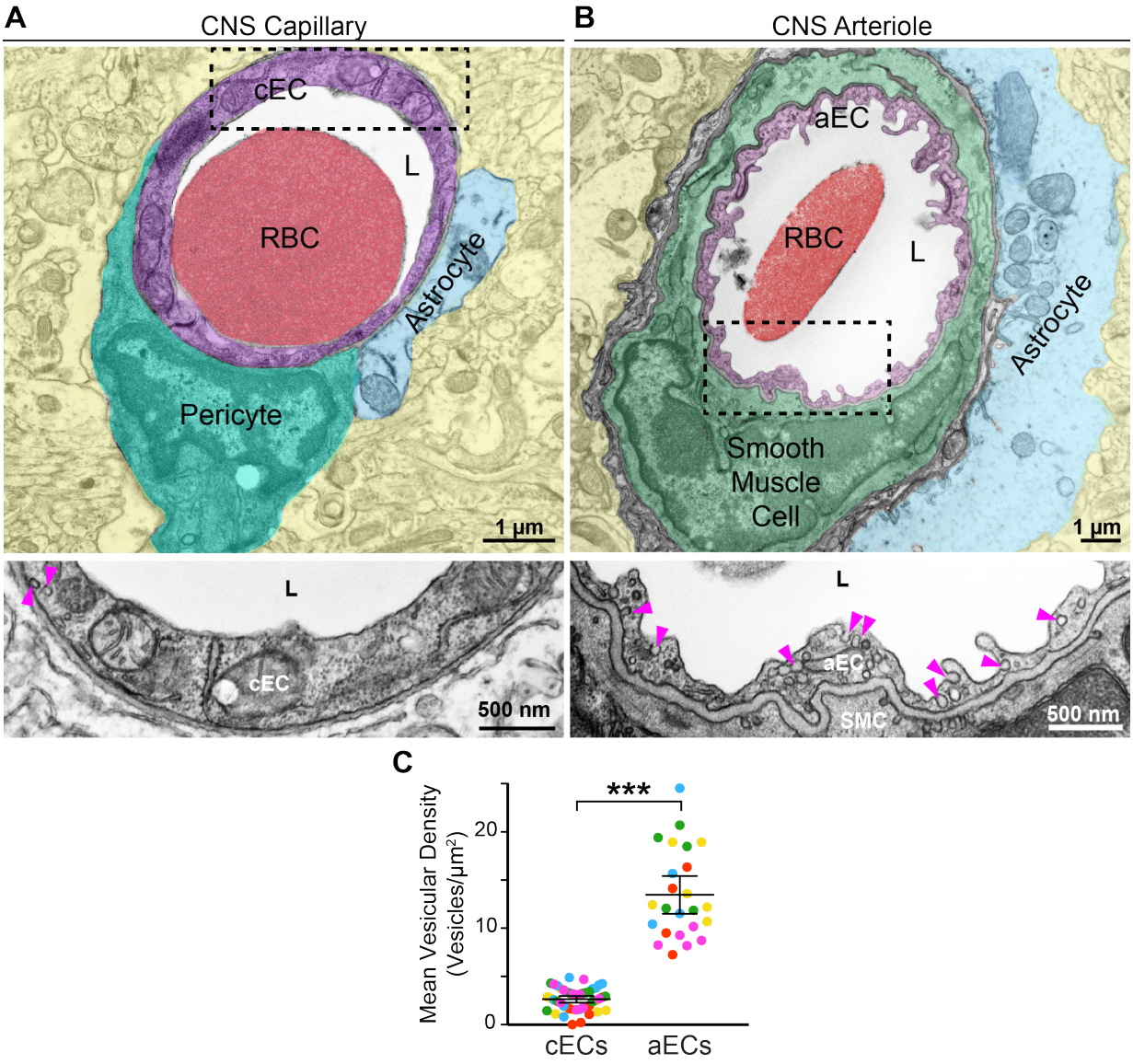

Figure 4.1. CNS arterioles have abundant vesicles. (A) EM image of a CNS capillary. Scale bar, 1 µm. Pseudo colors highlight different cells: cEC (purple), pericyte (teal), astrocyte end-foot (blue), red blood cell (RBC, red), lumen (L, white) and neuropil (yellow). Bottom shows an inverted, zoomed image of boxed area in cEC. Arrowheads point to vesicles. Scale bar, 500 nm. **(B)** EM image of a CNS arteriole. Scale bar, 1 µm. Pseudocolors highlight different cells: aEC (purple), smooth muscle cell (green), astrocyte end-foot (blue) and neuropil (yellow). Bottom shows a zoomed image of boxed area in aEC. Arrowheads point to vesicles. Scale bar, 500 nm. Statistical significance was determined by nested, unpaired, two-tailed t-test for (**C).**

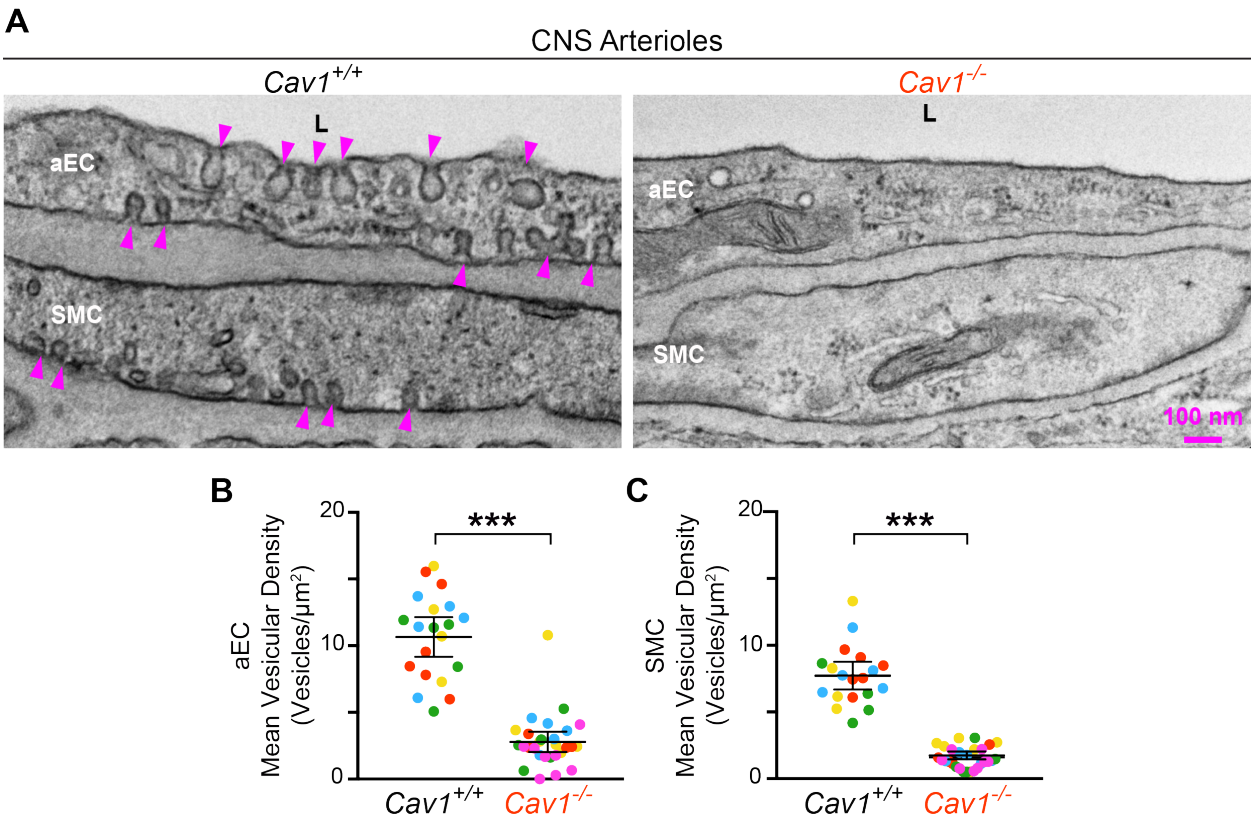

Figure 4.2. CNS arterioles have abundant caveolae. (A) EM images of aECs and SMCs from *Cav1*$^{+/+}$ and *Cav1*$^{-/-}$ mice. Arrowheads point to caveolae. SMC, smooth muscle cell. Scale bar, 100 nm. (**B and C**) Quantification of the mean vesicular density in aECs (**B**) and smooth muscle cells (**C**) between *Cav1*$^{+/+}$ (n=5 mice, 20 arterioles) and *Cav1*$^{-/-}$ mice (n=5 mice, 28 arterioles). Statistical significance was determined by nested, unpaired, two-tailed t-test for (**B,C**). Data shown as mean ± s.e.m. (***P<0.001).

stimulation via whisker brushing in awake mice evoked spatially and temporally patterned neural activity that can be imaged in the barrel cortex by intracellular calcium levels in mice expressing the calcium sensor GCaMP6 in neurons (*Thy1:*^{GCaMP6s}) (Kleinlogel et al., 2011) (**Supplementary Figure 10**). Hydrazide (Shen et al., 2012) and quantum dots were injected intravenously into *Thy1:*^{GCaMP6s} mice to visualize arterioles and image capillary blood flow, respectively. Upon whisker brushing, we observed a robust increase in the GCaMP signal in neurons, followed by increased arteriolar dilation and red blood cell velocity (measured by tracking movement of red blood cells, which are devoid of quantum dots) (**Supplementary Figure 10**).

Cav1$^{-/-}$ mice exhibited attenuated arteriolar dilation upon whisker stimulation whereas arterioles from wildtype *Cav1*$^{+/+}$ and heterozygous *Cav1*$^{+/-}$ mice dilated robustly (**Figure 4.3**). Importantly, the baseline diameter and latency to dilate were similar across the three genotypes (**Figure 4.3 and Supplementary Figure 11**). These results suggest that the absence of caveolae does not impair basal vessel tone and kinetics but specifically impairs the amplitude of sensory-evoked arteriolar dilation. Consistent with the attenuation of arteriolar vasodilation, capillary blood flow was also impaired in mutant *Cav1*$^{-/-}$ mice upon whisker stimulation compared to control mice (**Figure 4.4**), whereas baseline capillary velocity and kinetics were similar across genotypes (**Figure 4.4 and Supplementary Figure 11**). Moreover, the attenuated arteriolar dilation and capillary blood flow in mutant *Cav1*$^{-/-}$ mice was not due to impairment in sensory-evoked neural activity because similar GCaMP6s dynamics in neurons were observed in control and mutant mice (**Supplementary Figure 12**). Thus, these results demonstrate that caveolae are essential for optimal neurovascular coupling.

Figure 4.3. Caveolae are important for neurovascular coupling to promote arteriolar dilation. (A) Still frame images of neurovascular coupling in *Cav1*$^{+/+}$, *Cav1*$^{+/-}$ and *Cav*$^{-/-}$ mice using *in vivo* two-photon microscopy. Top images show hydrazide stained arterioles during baseline and whisker stimulation. White hashes outline the arterioles during baseline based on time= 0. Bottom images show the kymographs of the arteriolar dilation. The gray rectangle represents the time frame of whisker stimulation. **(B-D)** Quantification of change in arteriolar dilation (**B**) % max change in arteriolar dilation (**C**) and baseline diameter (**D**) (n= 5 mice, 196 arterioles), *Cav1*$^{+/-}$ (n= 5 mice, 191 arterioles) and *Cav1*$^{-/-}$ mice (n=5 mice, 194 arterioles). Statistical significance was determined by nested, one-way ANOVA with a post hoc Bonferroni multiple comparison adjustment for (**C,D**). Data shown as mean ± s.e.m. (***P<0.001, n.s., not significant).

Figure 4.3 (Continued)

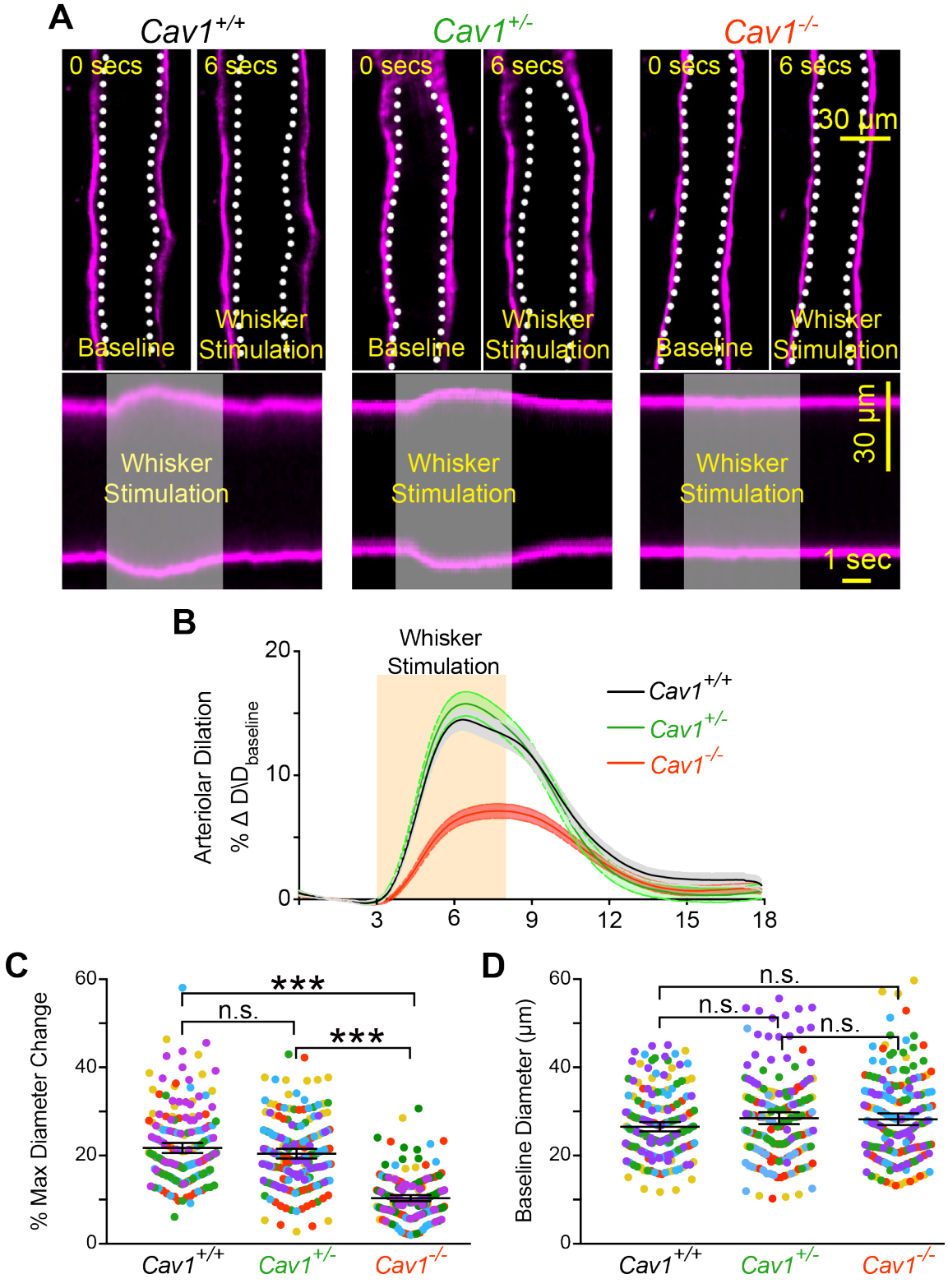

Figure 4.4. Caveolae are important for neurovascular coupling to promote increase capillary blood flow. (A) Kymographs of for *Cav1*$^{+/+}$, *Cav1*$^{+/-}$ and *Cav1*$^{-/-}$ mice. Left and right kymographs show during red blood cell flow during baseline and whisker stimulation, respectively. (**B-D**) Quantification of change in red blood cell velocity (**B**), % max change in red blood cell velocity (**C**) and baseline velocity (**D**) in *Cav1*$^{+/+}$ (n= 5 mice, 77 capillaries), *Cav1*$^{+/-}$ (n= 6 mice, 79 capillaries) and *Cav1*$^{-/-}$ mice (n=5 mice, 79 capillaries). Statistical significance was determined by nested, one-way ANOVA with a post hoc Bonferroni multiple comparison adjustment for (**C,D**). Data shown as mean ± s.e.m. (* P<0.05, **P<0.01, ***P<0.001, n.s., not significant)

Figure 4.4 (Continued)

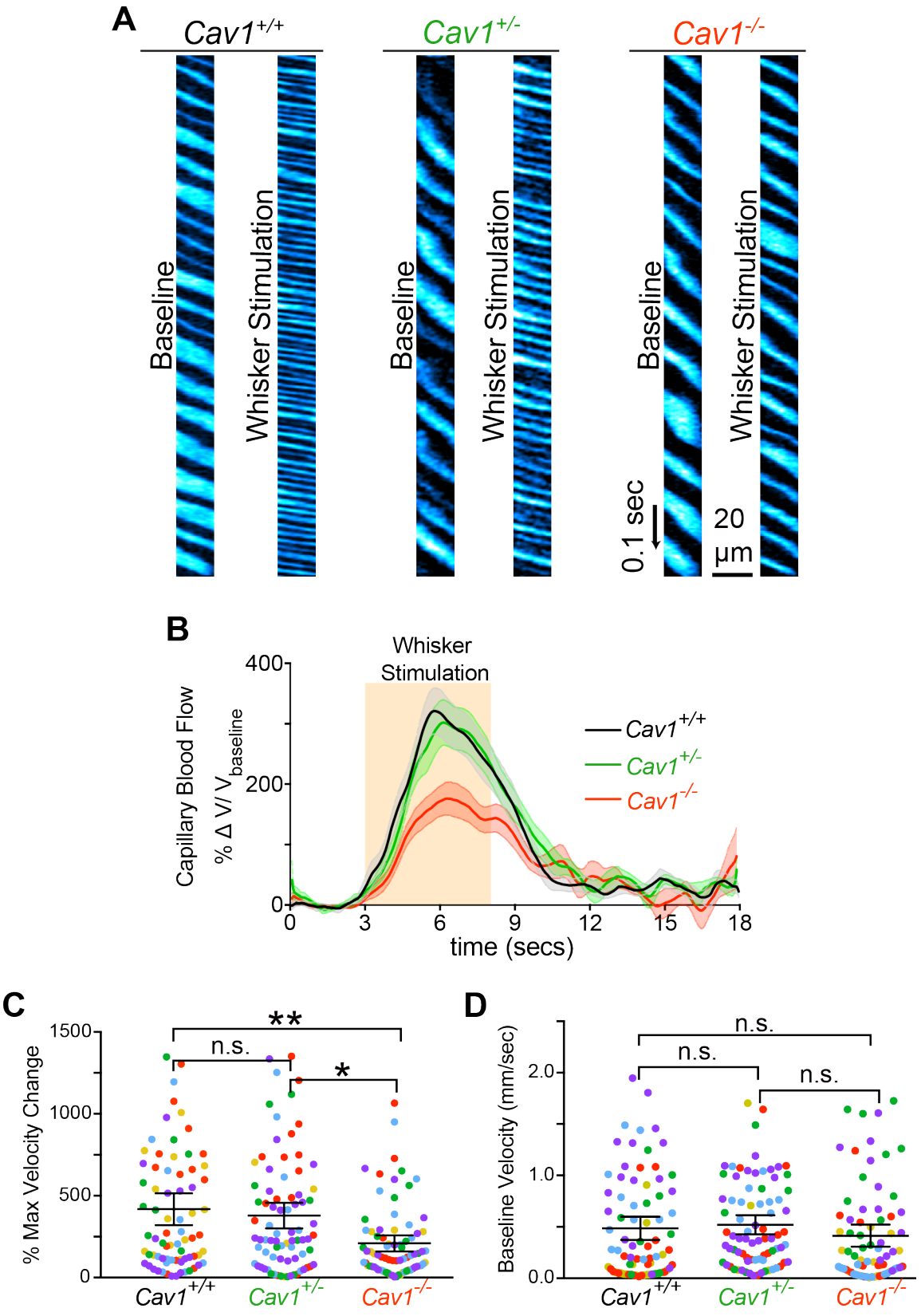

Because SMCs control arteriole dilation during neurovascular coupling (Cauli et al., 2014; Hillman, 2014; Kleinfeld et al., 2011), we next examined whether the attenuated neurovascular coupling in *Cav1*$^{-/-}$ mice is due to impaired integrity and function of SMCs. To visualize SMC morphology and vessel coverage, we intravenously injected Hydrazide into control *Cav1*$^{+/+}$*; NG2:*$^{DsRed+}$ and *Cav1*$^{-/-}$*; NG2:*$^{DsRed+}$ mice. NG2:DsRed is a reporter for SMCs, oligodendrocytes, and pericytes (Hill et al., 2015; Zhu et al., 2008). By quantifying of the number of DsRed+ cells on hydrazide+ arterioles, we established that there are normal coverage and morphology of SMCs in *Cav1*$^{-/-}$ mice compared to wildtype littermates (**Supplementary Figure 13**). To examine whether ablation of caveolae affects the ability of SMCs to respond to signals to contract and dilate, we imaged arteriolar diameter changes in acute brain slices under two-photon microscopy during delivery of pharmacological compounds to induce contraction and dilation. We found that SMCs in *Cav1*$^{-/-}$ mice displayed normal contraction compared to wildtype controls following administration of U46619, a thromboxane A2 receptor agonist (**Supplementary Figure 14**). When DEA-NONOate, a nitric oxide donor, was subsequently applied to the same vessel, we observed a similar level of dilation back to baseline as the wildtype controls (**Supplementary Figure 14**). These experiments demonstrate that the absence of caveolae impairs neurovascular coupling despite the presence of functionally normal SMCs.

Caveolae are specifically required in aECs but not SMCs for normal neurovascular coupling

Caveolae are present in both CNS aECs and SMCs (**Figure 4.1 and 4.2**). We next tested whether caveolae function in a cell-autonomous manner using acute, cell type-specific deletion of *Cav1* in adult mice. First, we crossed *BMX:*^{CreER} mice, a tamoxifen-inducible aEC-specific

driver line (Ehling et al., 2013) (**Supplementary Figure 15**) with *Cav1* floxed mice (*Cav1$^{fl/fl}$*) (Asterholm et al., 2012) to acutely ablate caveolae only in aECs. After tamoxifen treatment, Cav1 protein was present in both aECs and SMCs in *BMX:$^{CreER-}$;Cav1$^{+/fl}$* control mice, but was specifically lost in aECs but not in SMCs of *BMX:$^{CreER+}$;Cav1$^{-/fl}$* mutant mice (**Figure 4.5 A,C**). EM analysis shows that in the barrel cortex of mutant *BMX:$^{CreER+}$;Cav1$^{-/fl}$* mice, caveolae were ablated acutely in aECs but still present in SMCs, whereas abundant caveolae were present in both CNS aECs and SMCs in control *BMX:$^{CreER-}$;Cav1$^{+/fl}$* mice (**Figure 4.5 B,D**). Using our *in vivo* imaging paradigm, we found an attenuation of arteriolar dilation (**Figure 4.6**) and capillary blood flow (Figure 4.6 D,F) in *BMX:$^{CreER+}$;Cav1$^{-/fl}$* mutant mice upon whisker stimulation, similar to what was observed in the *Cav1$^{-/-}$* mutant mice (**Figure 4.3 and Figure 4.4**). Baseline and kinetics of arteriolar diameter and capillary blood flow were unaffected in tamoxifen-treated *BMX:$^{CreER+}$;Cav1$^{-/fl}$* mutant mice (**Figure 4.6 and Supplementary Figure 16**). Together, these experiments demonstrate caveolae in aECs are important for neurovascular coupling.

To test the role of SMC caveolae in neurovascular coupling, we crossed *Myh11:$^{CreER+}$* mice, a tamoxifen-inducible SMC-specific driver line (Wirth et al., 2008) (**Supplementary Figure 17**) to *Cav1* floxed mice to ablate acutely caveolae in SMCs. After tamoxifen treatment, we found that both Cav1 protein and caveolae were ablated successfully in SMCs but preserved in aECs in *Myh11:$^{CreER+}$;Cav1$^{-/fl}$* mutant mice (**Supplementary Figure 18).** However, in contrast to the attenuated neurovascular coupling observed in mice lacking Cav1 in aECs, no changes in arteriolar dilation and capillary blood flow after whisker stimulations were observed in mutants lacking Cav1 and caveolae in SMCs (**Supplementary Figure 19 and Supplementary Figure 20**). This result indicates that caveolae in SMCs play little, if any role, in neurovascular coupling.

Figure 4.5. Conditional deletion of caveolae specifically in CNS aECs. (A) Immunostaining of adult brain sections for endothelial cells (Icam2, green), smooth muscle cells (SMA, magenta) and Cav1 (red) from control (*BMX:^{CreER}-; Cav1$^{+/fl}$*) and aEC-specific conditional Cav1 mutant (*BMX:$^{CreER+}$; Cav1$^{-/fl}$*) mice. Arrow points to aEC. Scale bar, 15 μm. **(B)** EM images of CNS aECs and SMCs from control and aEC-specific conditional Cav1 mutant mice. Arrowheads point to caveolae. L, Lumen. aEC, arteriolar endothelial cells, SMC, smooth muscle cells. Scale bar, 100 nm. **(C)** Quantification of mean normalized immunofluorescence of Cav1 in aECs from control (n= 5 mice) and aEC-specific conditional Cav1 mutant mice (n=5 mice). **(D)** Quantification of the mean vesicular density in aECs and smooth muscle cells between control (n= 4 mice, 20 arterioles) and aEC-specific conditional Cav1 mutant mice (n=5 mice, 22 arterioles). Statistical significance was determined by Mann Whitney test for (**C**) and nested, unpaired, two-tailed t-test for (**D**). Data shown as mean ± s.e.m. (**,P<0.01, ***P<0.001, n.s., not significant).

Figure 4.5 (Continued)

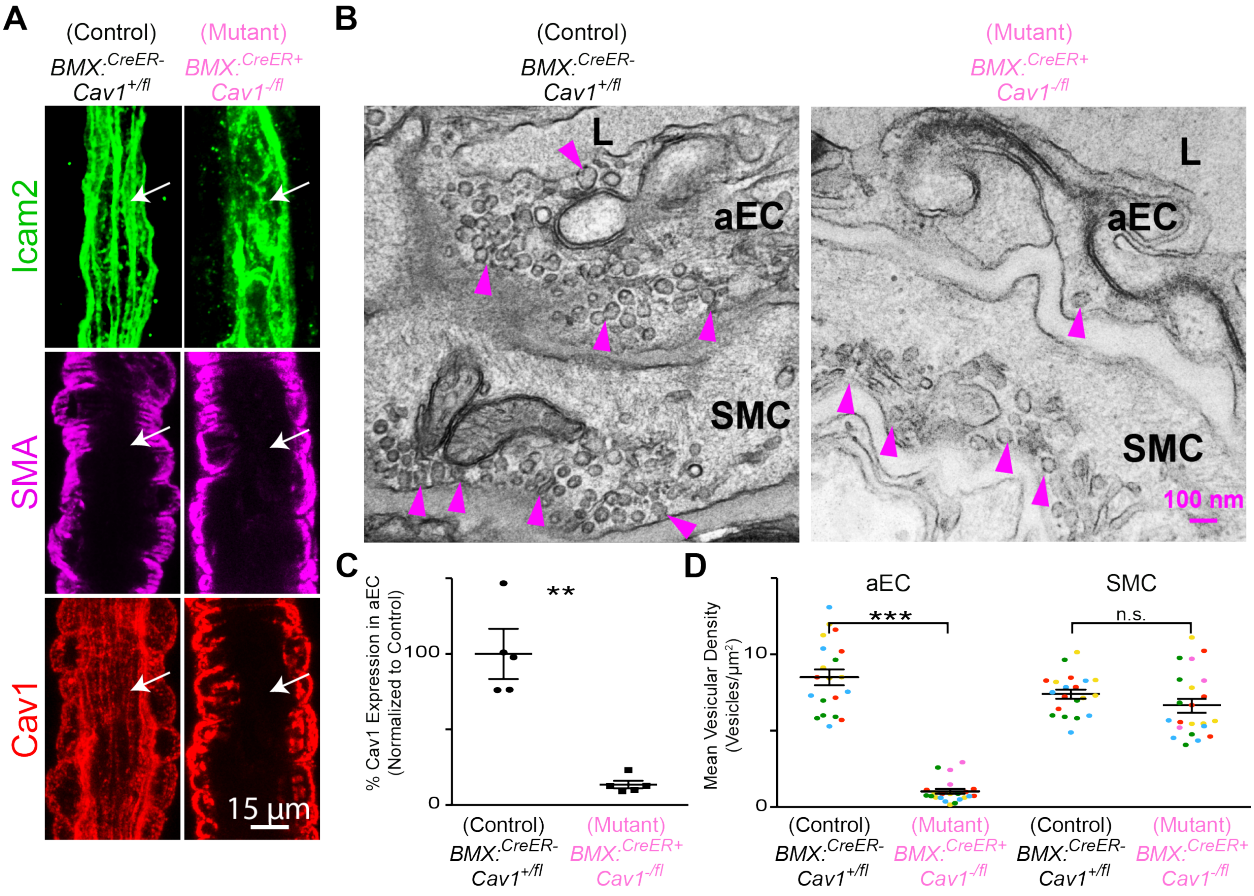

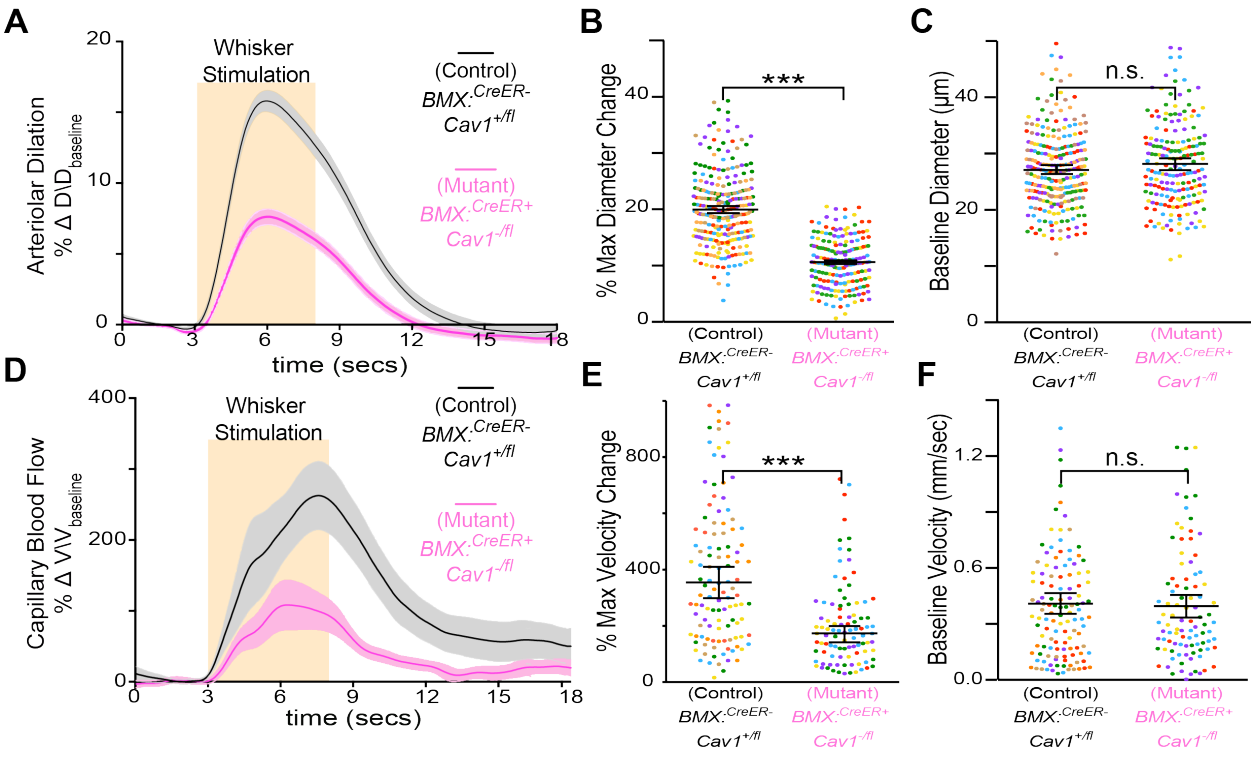

Figure 4.6. Caveolae in CNS aECs specifically are required for neurovascular coupling. (A-C) Quantification of change in arteriolar dilation (**A**), % max change in arteriolar dilation (**B**) and baseline diameter (**C**) in control (n= 7 mice, 260 arterioles) and aEC-specific conditional *Cav1* mutant mice (n= 5 mice, 193 arterioles). **(C-F)** Quantification of change in red blood cell velocity (**C**), % max change of red blood cell velocity (**E**) and baseline velocity (**F**) in control (n= 7 mice, 122 capillaries) and aEC-specific conditional *Cav1* mutant mice (n=5 mice, 94 capillaries). Statistical significance was determined by Mann Whitney test for (**c**) and nested, unpaired, two-tailed t-test for (**B,C,E,F**). Data shown as mean ± s.e.m. (**,P<0.01, ***P<0.001, n.s., not significant).

Caveolae in aECs mediate neurovascular coupling is independent of eNOS

Next, we examined how aECs utilize caveolae to mediate neurovascular coupling. Caveolae have been reported to mediate many functions, including transcytosis (Andreone et al., 2017; Chow and Gu, 2017; Knowland et al., 2014), serving as a membrane reservoir during mechanical stretch(Parton and del Pozo, 2013; Sinha et al., 2011), clustering receptors and ion channels (Balijepalli and Kamp, 2008), and mediating intracellular signaling as regulating kinase signaling (Parton, 2018; Sowa et al., 2001). We focused on nitric oxide (NO) signaling because NO is a major vasodilatory factor in neurovascular coupling (Kisler et al., 2017; Toth et al., 2015) and previous studies have reported that Cav1 interacts physically with endothelial NO synthase (eNOS/*nos3*) (García-Cardeña et al., 1997). We first examined whether eNOS and NO levels are altered in the absence of caveolae. We found similar levels of eNOS protein and NO in aECs between wildtype control and *Cav1*$^{-/-}$ mutant mice, whereas both eNOS protein and NO signal were absent in *eNOS*$^{-/-}$ mice (**Supplementary Figure 21 and Supplementary Figure 22**). To examine genetic interactions between *Cav1* and *eNOS*, we characterized neurovascular coupling in *Cav1*$^{-/-}$; *eNOS*$^{-/-}$ double mutant mice. We reasoned that if Cav1 and eNOS are in the same genetic pathway, the double mutants should phenocopy one of the single knockout mice, whereas if they are in separate and parallel pathways, the double knockout should have an additive phenotype of the two single knockout mice. With our *in vivo* imaging paradigm, *eNOS*$^{-/-}$ mice displayed attenuated arteriolar dilation and capillary blood flow upon whisker stimulus (**Figure 4.7**), neurovascular coupling defects that are similar to previously observed (Toth et al., 2015). Although each single *Cav1*$^{-/-}$ and *eNOS*$^{-/-}$ mutant alone exhibited partial impairment (34% and 53%, respectively)**,** strikingly, the *Cav1*$^{-/-}$; *eNOS*$^{-/-}$ double mutant mice completely lost

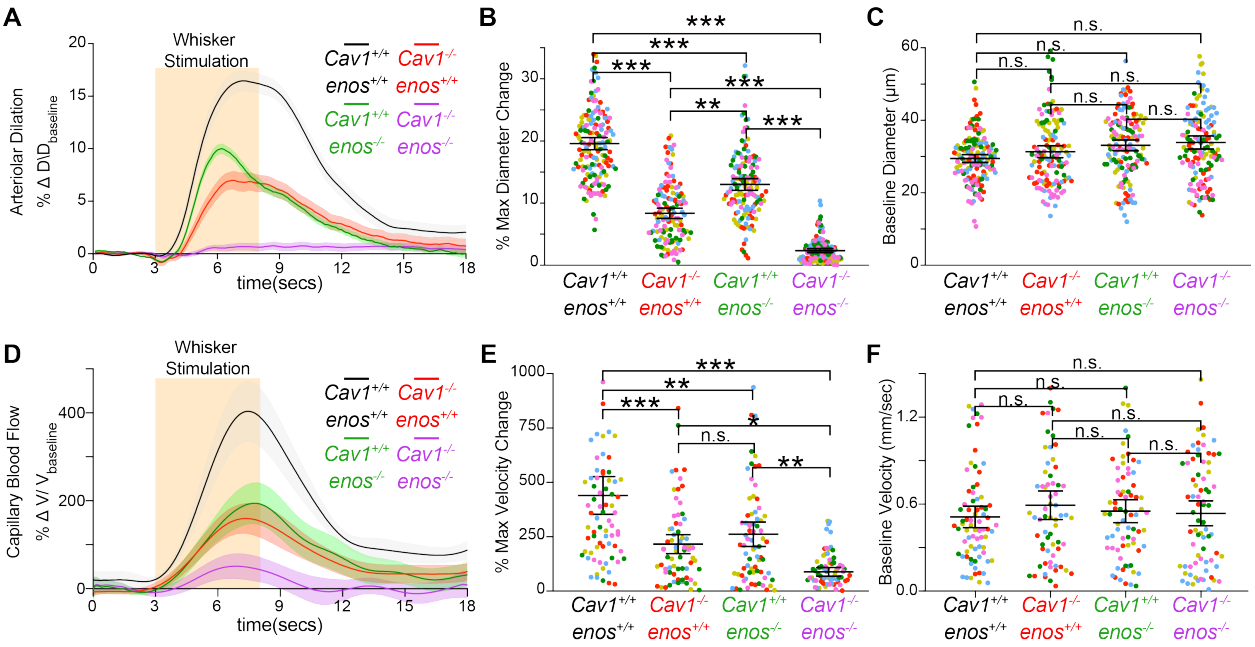

Figure 4.7. Caveolae in aECs mediate neurovascular coupling is independent of eNOS. (A-C) Quantification of change in arteriolar dilation (**A**), % max change in arteriolar dilation (**B**) and baseline diameter (**C**) in *Cav1*$^{+/+}$, *enos*$^{+/+}$ (n= 5 mice, 148 arterioles), *Cav1*$^{-/-}$, *enos*$^{+/+}$ (n= 5 mice, 128 arterioles), *Cav1*$^{+/+}$, *enos*$^{-/-}$ (n= 5 mice, 137 arterioles) and *Cav1*$^{-/-}$, *enos*$^{-/-}$ mice (n=5 mice, 139 arterioles). **(D-F)** Quantification of change in red blood cell velocity (**D**), % max change in red blood cell velocity (**E**) and baseline velocity (**F**) in *Cav1*$^{+/+}$, *enos*$^{+/+}$ (n= 5 mice, 76 capillaries), *Cav1*$^{-/-}$, *enos*$^{+/+}$ (n= 5 mice, 68 capillaries) and *Cav1*$^{+/+}$, *enos*$^{-/-}$ (n= 5 mice, 73 capillaries) and *Cav1*$^{-/-}$, *enos*$^{-/-}$ mice (n=5 mice, 74 capillaries). Statistical significance was determined by nested, one-way ANOVA with a post hoc Bonferroni multiple comparison adjustment for (**B,C,E,F**). Data shown as mean ± s.e.m. (*,P<0.05, **P<0.01,***P<0.001, n.s., not significant).

arteriolar dilation and red blood cell velocity enhancement was severely attenuated upon whisker stimulation (**Figure 4.7**). These results demonstrate that caveolae-mediated neurovascular coupling is independent of the NO pathway. Moreover, the caveolae-mediated pathway is at least as important as the NO pathway for neurovascular coupling.

Ectopic expression of Mfsd2a in aEC down-regulates caveolae and attenuates neurovascular coupling

We next asked why cECs have few caveolae whereas aECs have abundant caveolae. Previously, we discovered that Mfsd2a expression in CNS cECs actively suppresses caveolae formation and that this was necessary for blood-brain barrier integrity (Andreone et al., 2017; Ben-Zvi et al., 2014; Chow and Gu, 2017). In contrast, here we found that Mfsd2a protein was undetectable in aECs in both brain and retina (**Figure 4.8 and Supplementary Figure 23**). Consistent with this result, Mfsd2a transcript levels are also low in aECs compared to cECs (Vanlandewijck et al., 2018). Thus, CNS cECs robustly express Mfsd2a to suppress caveolae, whereas aECs lack Mfsd2a and are enriched in caveolae. We therefore examined whether ectopic expression of Mfsd2a specifically in CNS aECs is sufficient to suppress caveolae in aECs, and if so, our results so far predict that this suppression of caveolae in aECs would result in an attenuated neurovascular coupling.

To ectopically express Mfsd2a only in aECs, we generated a transgenic mouse where Mfsd2a expression is Cre-dependent (refer to as *R26:*$^{LSL\text{-}Mfsd2a}$*)* (**Supplementary Figure 24**) and crossed it to *BMX:*$^{CreER+}$. After tamoxifen treatment, Mfsd2a protein was expressed abundantly in aECs in brains from *BMX:*$^{CreER+}$*; R26:*$^{LSL\text{-}Mfsd2a/+}$ mice*,* whereas control, *BMX:*$^{CreER-}$*; R26:*$^{LSL\text{-}Mfsd2a/+}$ adult mice lacked Mfsd2a expression in brain arterioles (**Figure 4.9 and Supplementary Figure 25**). Moreover, under EM, caveolae density was reduced significantly in *BMX:*$^{CreER+}$*;*

Figure 4.8. CNS aECs have undetectable Mfsd2a expression (A) Immunostaining for all endothelial cells (Claudin-5, green), arterioles (hydrazide, magenta) and Mfsd2a (white) on wildtype adult brain sections demonstrates that Mfsd2a is not detectable in CNS arterioles. Blue hashes outline the hydrazide+ arterioles. Scale bar, 50 μm. **(B)** Immunostaining on adult brain sections for endothelial cells (Pecam1, green), smooth muscle cells (SMA, magenta) and Mfsd2a (white) from control and aEC-specific Mfsd2a overexpression mice. Scale bar, 50 μm.

Figure 4.8 (Continued)

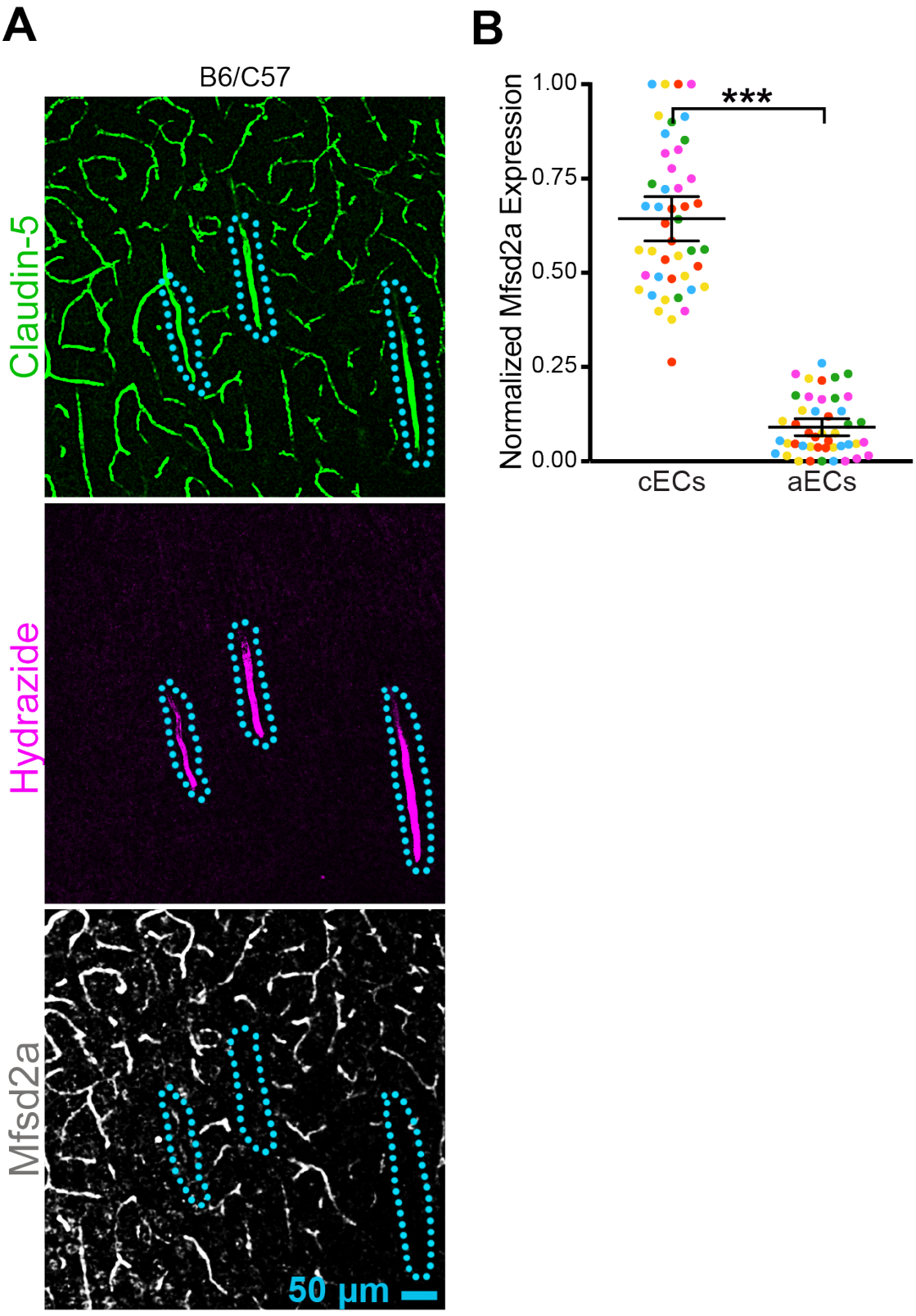

Figure 4.9. Ectopic expression of Mfsd2a in aECs downregulates. (A) Quantification of the normalized immunofluorescence of Mfsd2a in cECs (hydrazide-, Claudin-5+) and aECs (hydrazide+, Claudin-5+) (n= 5 mice, 45 images). **(B)** Quantification of mean normalized immunofluorescent of Mfsd2a in aECs from control (n= 4 mice, 40 images) and aEC-specific Mfsd2a overexpressing mice (n=5 mice, 51 images). **(C)** EM images of CNS aECs and SMCs from control and aEC-specific Mfsd2a overexpressing mice. Arrowheads point to caveolae. L, Lumen. SMC, smooth muscle cell. **(D)** Quantification of the mean vesicular density in aECs and smooth muscle cells between control (n= 3 mice, 20 arterioles) and aEC-specific Mfsd2a overexpression mice (n=3 mice, 22 arterioles) Scale bar, 500 nm. Statistical significance was determined by nested, unpaired, two-tailed t-test for (**B,D)** Data shown as mean ± s.e.m. (***P<0.001, n.s., not significant).

Figure 4.9 (Continued)

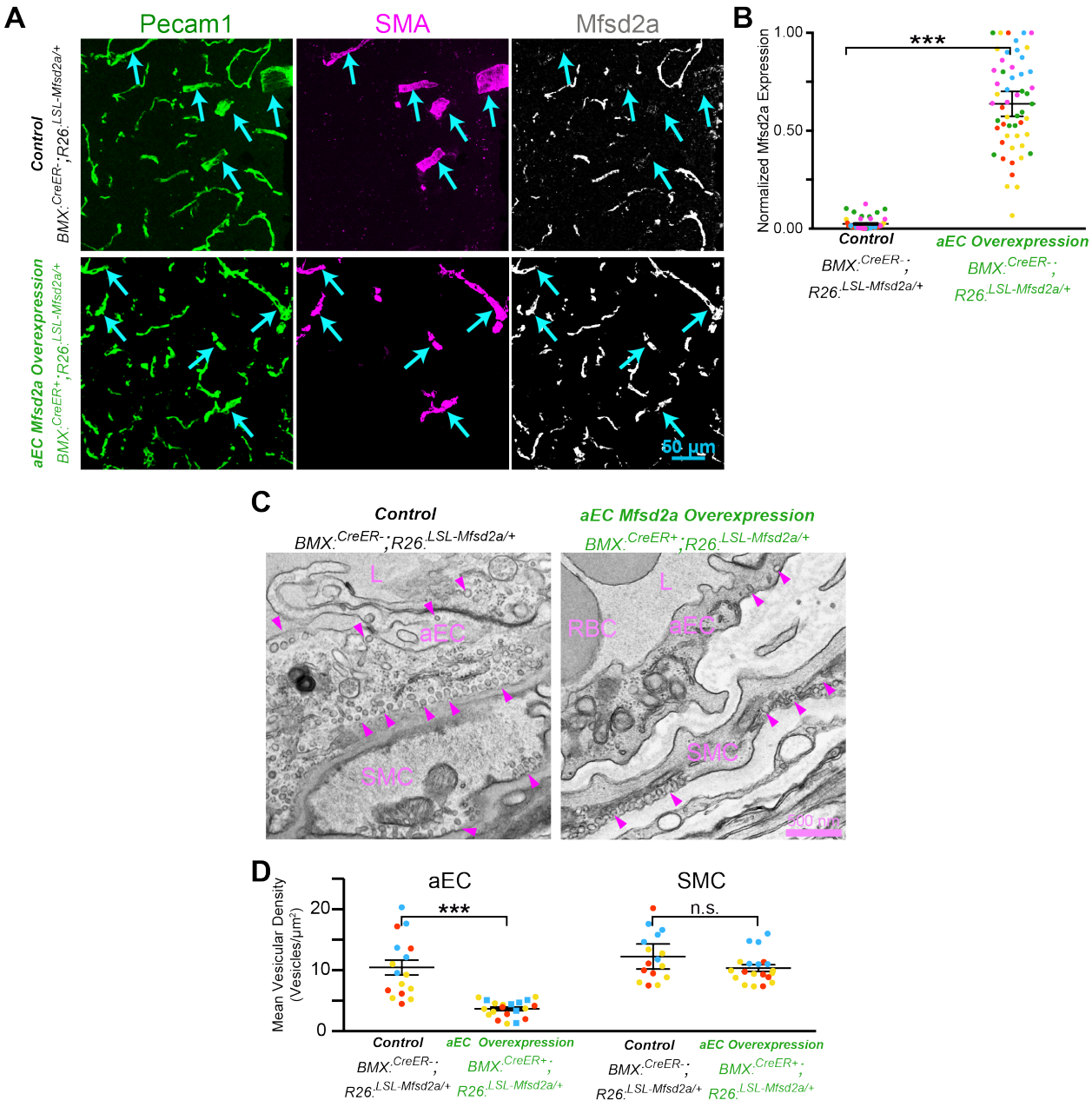

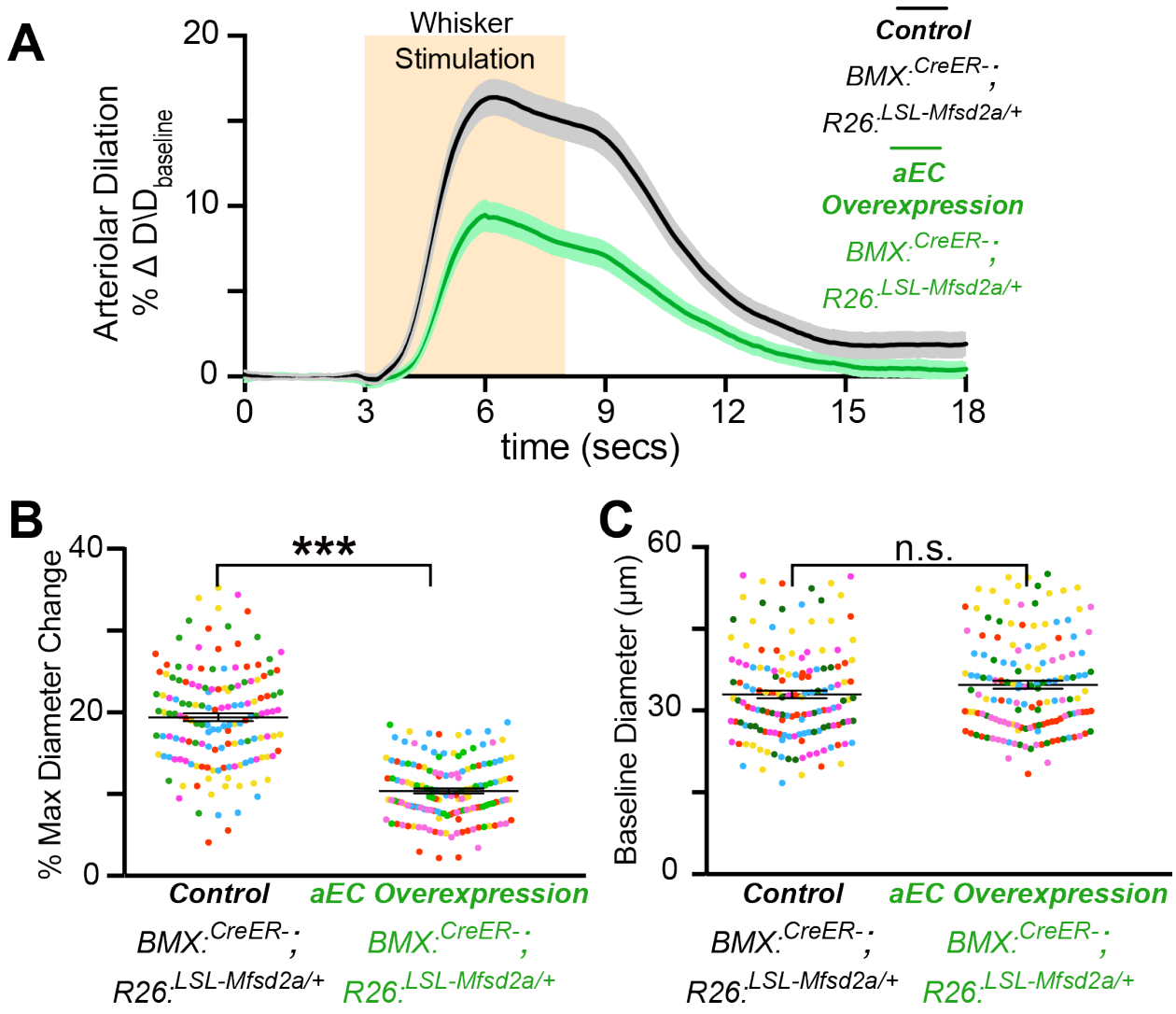

Figure 4.10. Ectopic expression of Mfsd2a in aECs downregulates caveolae. (A-C) Quantification of change in arteriolar dilation (**A**), % max change in arteriolar dilation (**B**) and baseline diameter (**C**) in control (n= 7 mice, 260 arterioles) and aEC-specific Mfsd2a overexpression mice (n= 5 mice, 193 arterioles). Statistical significance was determined by nested, unpaired, two-tailed t-test for (**B,C**). Data shown as mean ± s.e.m. (***P<0.001, n.s., not significant).

R26:$^{LSL\text{-}Mfsd2a/+}$ mice relative to control (**Figure 4.9).** Strikingly, *in vivo* imaging revealed an attenuation of arteriolar dilation upon whisker stimulation in mice with Mfsd2a overexpression in aECs (*BMX:*$^{CreER+;}$ *R26:*$^{LSL\text{-}Mfsd2a/+}$) relative to control mice (*BMX:*$^{CreER-;}$ *R26:*$^{LSL\text{-}Mfsd2a/+}$) (**Figure 4.10 and Supplementary Figure 26**). These experiments demonstrate that ectopic overexpression of Mfsd2a in CNS aECs is sufficient to reduce caveolae density and impair neurovascular coupling. Furthermore, inhibition of caveolae vesicles specifically in aECs in two different ways, by overexpression of Mfsd2a and by genetic deletion of Cav1, both resulted in attenuated neurovascular coupling, further demonstrating the importance of caveolae in CNS aECs for mediating neurovascular coupling.

4.4 Discussion:

We used natural stimuli under physiological conditions in awake mice while simultaneously measuring neural activity and vascular dynamics under two-photon microscopy to study mechanisms of neurovascular coupling. We discovered that caveolae in CNS aECs are important to mediate neurovascular coupling. In addition, we confirmed that the previously known eNOS pathway is also important for neurovascular coupling (Toth et al., 2015). However, we found that the caveolae-mediated pathway is independent of eNOS signaling. Given the spatiotemporal dynamics of neurovascular coupling and recent evidence that cECs are involved in sensing neural activity changes and are important for neurovascular coupling (Chen et al., 2014; Hillman, 2014; Longden et al., 2017), we envision that after sensing nearby increased neural activity, cECs relay this signal electrically to the upstream aECs and then aECs send vasodilatory cues to SMCs via a caveolae-dependent process. How caveolae carry out this

function and what caveolae mediate are still a mystery and will be an important next step to address for the field. Importantly, we found that perturbation of both caveolae- and eNOs-mediated pathways together completely abolished neurovascular coupling, whereas ablation of each pathway alone results in partial impairment. Thus, these findings reveal that the caveolae-mediated pathway is at least as important as the NO pathway for neurovascular coupling.

Our results demonstrate that CNS endothelial cells from different vascular segments exhibit heterogeneity at molecular, cellular, and functional levels. Here we show that this endothelial heterogeneity governs the two unique and important functions of the CNS vasculature: the blood-brain barrier and neurovascular coupling. We found capillary ECs express Mfsd2a, which suppresses caveolae to ensure blood-brain barrier integrity (Andreone et al., 2017; Ben-Zvi et al., 2014; Chow and Gu, 2017). In contrast, aECs lack Mfsd2a and concurrently have abundant caveolae, which are important for neurovascular coupling. We expect this kind of heterogeneity of endothelial cells exists broadly and that understanding this heterogeneity will advance our understanding of the diverse functions of endothelial cells in health and disease. Given that neurovascular coupling is impaired in various neurological disorders (Faraco et al., 2018; Hernández et al., 2019; Iadecola, 2017; Kisler et al., 2017; Zlokovic, 2008; 2011), future studies examining whether these differential molecular and cellular pathways are altered in diseases may provide insight for development of novel therapies.

Authors Contributions:

B.W.C and C.G conceived the project.

B.W.C, V.N and C.G designed experiments.

B.W.C and K.B performed the histology and electron microscopy experiments.

B.W.C, K.B and V.N performed cranial window surgeries.

B.W.C and V.N performed the *in vivo* two-photon imaging experiments.

A.J.G performed the *ex vivo* acute slice experiments.

H.Z performed preliminary experiments that were not included in the study.

V.N constructed the two-photon microscope.

B.W.C, V.N, A.J.G and P.K analyzed all data.

B.W.C. and C.G. wrote the manuscript, with feedback from all authors.

References:

Andreone, B.J., Chow, B.W., Tata, A., Lacoste, B., Ben-Zvi, A., Bullock, K., Deik, A.A., Ginty, D.D., Clish, C.B., and Gu, C. (2017). Blood-Brain Barrier Permeability Is Regulated by Lipid Transport-Dependent Suppression of Caveolae-Mediated Transcytosis. Neuron *94*, 581–594.e585.

Andreone, B.J., Lacoste, B., and Gu, C. (2015). Neuronal and vascular interactions. Annu. Rev. Neurosci. *38*, 25–46.

Asterholm, I.W., Mundy, D.I., Weng, J., Anderson, R.G.W., and Scherer, P.E. (2012). Altered mitochondrial function and metabolic inflexibility associated with loss of caveolin-1. Cell Metab. *15*, 171–185.

Attwell, D., Buchan, A.M., Charpak, S., Lauritzen, M., MacVicar, B.A., and Newman, E.A. (2010). Glial and neuronal control of brain blood flow. Nature *468*, 232.

Balijepalli, R.C., and Kamp, T.J. (2008). Caveolae, ion channels and cardiac arrhythmias. Prog. Biophys. Mol. Biol. *98*, 149–160.

Ben-Zvi, A., Lacoste, B., Kur, E., Andreone, B.J., Mayshar, Y., Yan, H., and Gu, C. (2014). Mfsd2a is critical for the formation and function of the blood-brain barrier. Nature *509*, 507–511.

Cauli, B., Zhou, X., Tricoire, L., Toussay, X., and Staiger, J.F. (2014). Revisiting enigmatic cortical calretinin-expressing interneurons. Front Neuroanat *8*, 52.

Chen, B.R., Kozberg, M.G., Bouchard, M.B., Shaik, M.A., and Hillman, E.M.C. (2014). A Critical Role for the Vascular Endothelium in Functional Neurovascular Coupling in the Brain. J Am Heart Assoc *3*, e000787–e000787.

Chow, B.W., and Gu, C. (2017). Gradual Suppression of Transcytosis Governs Functional Blood-Retinal Barrier Formation. Neuron *93*, 1325–1333.e3.

Drab, M., Verkade, P., Elger, M., Kasper, M., Lohn, M., Lauterbach, B., Menne, J., Lindschau, C., Mende, F., Luft, F.C., et al. (2001). Loss of caveolae, vascular dysfunction, and pulmonary defects in caveolin-1 gene-disrupted mice. Science *293*, 2449–2452.

Ehling, M., Adams, S., Benedito, R., and Adams, R.H. (2013). Notch controls retinal blood vessel maturation and quiescence. Development *140*, 3051–3061.

Faraco, G., Brea, D., Garcia-Bonilla, L., Wang, G., Racchumi, G., Chang, H., Buendia, I., Santisteban, M.M., Segarra, S.G., Koizumi, K., et al. (2018). Dietary salt promotes neurovascular and cognitive dysfunction through a gut-initiated TH17 response. Nat. Neurosci. *21*, 240–249.

García-Cardeña, G., Martasek, P., Masters, B.S., Skidd, P.M., Couet, J., Li, S., Lisanti, M.P., and Sessa, W.C. (1997). Dissecting the interaction between nitric oxide synthase (NOS) and

caveolin. Functional significance of the nos caveolin binding domain in vivo. J. Biol. Chem. *272*, 25437–25440.

Hernández, J.C.C., Bracko, O., Kersbergen, C.J., Muse, V., Haft-Javaherian, M., Berg, M., Park, L., Vinarcsik, L.K., Ivasyk, I., Rivera, D.A., et al. (2019). Neutrophil adhesion in brain capillaries reduces cortical blood flow and impairs memory function in Alzheimer's disease mouse models. Nat. Neurosci. *13*, 1.

Hill, R.A., Tong, L., Yuan, P., Murikinati, S., Gupta, S., and Grutzendler, J. (2015). Regional Blood Flow in the Normal and Ischemic Brain Is Controlled by Arteriolar Smooth Muscle Cell Contractility and Not by Capillary Pericytes. Neuron *87*, 95–110.

Hillman, E.M.C. (2014). Coupling mechanism and significance of the BOLD signal: a status report. Annu. Rev. Neurosci. *37*, 161–181.

Iadecola, C. (2017). The Neurovascular Unit Coming of Age: A Journey through Neurovascular Coupling in Health and Disease. Neuron *96*, 17–42.

Kisler, K., Nelson, A.R., Montagne, A., and Zlokovic, B.V. (2017). Cerebral blood flow regulation and neurovascular dysfunction in Alzheimer disease. Nature Review Neuroscience *18*, 419–434.

Kleinfeld, D., Blinder, P., Drew, P.J., Driscoll, J.D., Muller, A., Tsai, P.S., and Shih, A.Y. (2011). A guide to delineate the logic of neurovascular signaling in the brain. Front Neuroenergetics *3*, 1.

Kleinlogel, S., Feldbauer, K., Dempski, R.E., Fotis, H., Wood, P.G., Bamann, C., and Bamberg, E. (2011). Ultra-light-sensitive and fast neuronal activation with the Ca2+-permeable channelrhodopsin CatCh. Nat. Neurosci. *14*, 513–518.

Knowland, D., Arac, A., Sekiguchi, K.J., Hsu, M., Lutz, S.E., Perrino, J., Steinberg, G.K., Barres, B.A., Nimmerjahn, A., and Agalliu, D. (2014). Stepwise recruitment of transcellular and paracellular pathways underlies blood-brain barrier breakdown in stroke. Neuron *82*, 603–617.

Longden, T.A., Dabertrand, F., Koide, M., Gonzales, A.L., Tykocki, N.R., Brayden, J.E., Hill-Eubanks, D., and Nelson, M.T. (2017). Capillary K+-sensing initiates retrograde hyperpolarization to increase local cerebral blood flow. Nat. Neurosci. *20*, 717–726.

O'Connor, D.H., Peron, S.P., Huber, D., and Svoboda, K. (2010). Neural activity in barrel cortex underlying vibrissa-based object localization in mice. Neuron *67*, 1048–1061.

O'Herron, P., Chhatbar, P.Y., Levy, M., Shen, Z., Schramm, A.E., Lu, Z., and Kara, P. (2016). Neural correlates of single-vessel haemodynamic responses in vivo. Nature *534*, 378–382.

Parton, R.G. (2018). Caveolae: Structure, Function, and Relationship to Disease. Annu. Rev. Cell Dev. Biol. *34*, 111–136.

Parton, R.G., and del Pozo, M.A. (2013). Caveolae as plasma membrane sensors, protectors and organizers. Nat. Rev. Mol. Cell Biol. *14*, 98–112.

Razani, B., Engelman, J.A., Wang, X.B., Schubert, W., Zhang, X.L., Marks, C.B., Macaluso, F., Russell, R.G., Li, M., Pestell, R.G., et al. (2001). Caveolin-1 null mice are viable but show evidence of hyperproliferative and vascular abnormalities. J. Biol. Chem. *276*, 38121–38138.

Shen, Z., Lu, Z., Chhatbar, P.Y., O'Herron, P., and Kara, P. (2012). An artery-specific fluorescent dye for studying neurovascular coupling. Nat. Methods *9*, 273–276.

Sinha, B., Köster, D., Ruez, R., Gonnord, P., Bastiani, M., Abankwa, D., Stan, R.V., Butler-Browne, G., Vedie, B., Johannes, L., et al. (2011). Cells respond to mechanical stress by rapid disassembly of caveolae. Cell *144*, 402–413.

Sowa, G., Pypaert, M., and Sessa, W.C. (2001). Distinction between signaling mechanisms in lipid rafts vs. caveolae. Pnas *98*, 14072–14077.

Sweeney, M.D., Sagare, A.P., and Zlokovic, B.V. (2018). Blood-brain barrier breakdown in Alzheimer disease and other neurodegenerative disorders. Nat Rev Neurol *14*, 133–150.

Toth, P., Tarantini, S., Davila, A., Valcarcel-Ares, M.N., Tucsek, Z., Varamini, B., Ballabh, P., Sonntag, W.E., Baur, J.A., Csiszar, A., et al. (2015). Purinergic glio-endothelial coupling during neuronal activity: role of P2Y1 receptors and eNOS in functional hyperemia in the mouse somatosensory cortex. American Journal of Physiology - Heart and Circulatory Physiology *309*, H1837–H1845.

Vanlandewijck, M., He, L., Mäe, M.A., Andrae, J., Ando, K., Del Gaudio, F., Nahar, K., Lebouvier, T., Laviña, B., Gouveia, L., et al. (2018). A molecular atlas of cell types and zonation in the brain vasculature. Nature *554*, 475–480.

Wirth, A., Benyó, Z., Lukasova, M., Leutgeb, B., Wettschureck, N., Gorbey, S., Örsy, P., Horváth, B., Maser-Gluth, C., Greiner, E., et al. (2008). G12-G13|[ndash]|LARG|[ndash]|mediated signaling in vascular smooth muscle is required for salt-induced hypertension. Nat. Med. *14*, 64–68.

Zhu, X., Bergles, D.E., and Nishiyama, A. (2008). NG2 cells generate both oligodendrocytes and gray matter astrocytes. Development *135*, 145–157.

Zlokovic, B.V. (2008). The blood-brain barrier in health and chronic neurodegenerative disorders. Neuron *57*, 178–201.

Zlokovic, B.V. (2011). Neurovascular pathways to neurodegeneration in Alzheimer's disease and other disorders. Nature Review Neuroscience *12*, 723–738.

CHAPTER 5

Conclusions

The goal of my thesis work is to understand the two unique physiological functions of the CNS vasculature: blood-CNS barrier formation and neurovascular coupling. In this body of work, we advanced our understanding of the cellular and molecular mechanisms underlying both functions. Here, I highlight how our work has contributed to our understanding of the CNS vasculature and these two unique functions.

Angiogenesis and barriergenesis are independent developmental pathways

In the first part of my thesis, we identified a mechanism underlying blood-CNS barrier formation. Historical studies have identified that the blood-CNS barrier formation is not intrinsic to CNS endothelial cells but has to be induced by the nervous system. Interestingly, many developmental studies observed that CNS angiogenesis (vascular growth from pre-existing vessels) and barriergenesis (formation of the blood-CNS barrier) occur during the same developmental time period, raising questions whether these two processes are coupled. However, given that the development and architecture of the brain vasculature are complex, these questions have been difficult to address. We identified that these questions are readily addressable in a more tractable system: the retinal vasculature that forms the physiologically analogous blood-retinal barrier. In contrast to the brain vasculature, the retinal vasculature has a simple and well-characterized vascular development and architecture. Using the blood-retinal barrier, we mapped the formation of functional blood-retinal barrier and identified that the barrier forms gradually, with the most mature vessels forming the barrier first while the nascent vessels still lack a barrier. While this may suggest that angiogenesis and barriergenesis are coupled, we find that angiogenesis and barriergenesis are not necessarily linked. Indeed, the mouse retinal vasculature continues to develop past the third week after birth, but surprisingly, we find that blood-CNS

barrier is functional throughout the vasculature by one distinctive time point: P10. Thus, beyond P10, angiogenesis continues but these newly developing vessels have a functional barrier.

Many studies have tried to resolve if angiogenesis and barriergenesis are coupled. Indeed, previous studies have identified genes that are involved in both, including canonical Wnt signaling (Cho et al., 2017; Daneman et al., 2009; Stenman et al., 2008; Wang et al., 2012; Ye et al., 2009; Zhou and Nathans, 2014; Zhou et al., 2014) and PDGF:PDGFRB signaling (Armulik et al., 2005; 2010; Daneman et al., 2010) because disruption in these signaling pathways impairs both angiogenesis and barriergenesis. These studies prompted an interpretation that angiogenesis and barriergenesis are coupled. However, previous studies have also identified genes that only impair either angiogenesis or barriergenesis selectively and not both. For example, *Mfsd2a* (Ben-Zvi et al., 2014) and *Lsr* (Sohet et al., 2015) are genes that are involved in barrier formation during development, but the ablation of these genes did not impact angiogenesis. Concurrently, our study unequivocally demonstrates the notion that angiogenesis and barriergenesis are independent developmental programs.

Acquisition and contribution of tight junctions and suppression of transcytosis

Historical studies have identified that the two BBB properties that are induced by the nervous system onto CNS endothelial cells to confer barrier integrity are i) tight junction complexes and ii) suppression of transcytosis (Reese and Karnovsky, 1967; Stewart and Wiley, 1981). However, it has been unclear when these two properties manifest during development and what their relative contribution is to the integrity of the barrier. Again, this question has been difficult to address given the complexity of brain vascular development. It is difficult to determine unequivocally mature vessels from nascent vessels in the brain vasculature. In

contrast, in the retina, nascent vessels invade the optic nerve head and expand radially along the retina surface, resulting in an organization of the mature vessels located most proximal to the optic nerve head and nascent vessels most distal to the optic nerve head (Fruttiger, 2007). Using the blood-retinal barrier, we discovered that as soon as CNS vessels invade the retina, we find that these nascent CNS endothelial cells already form functional tight junctions but still display bulk transcytosis, resulting in the immature vessel leakage. As the CNS vessels expand along the retinal, these nascent vessels continue to have functional tight junctions and gradually suppress transcytosis. By P10, the most distal and nascent vessels have both functional tight junctions and suppression of transcytosis (Chow and Gu, 2017). These observations are consistent with previous attempts to address this question in the developing brains of opossum where their CNS vascularization occurs postnatally instead of *in utero* like most other mammalian species (Ek et al., 2006). Thus, we find that nascent CNS endothelial cells first form functional tight junctions and then gradually suppress transcytosis for functional blood-CNS barrier formation.

Inductive cues that determine gradual suppression of transcytosis

As mentioned in the former sections, various studies demonstrate that transcytosis does exist in CNS endothelial cells, but is actively suppressed to ensure functional CNS barrier (Andreone et al., 2017; Armulik et al., 2010; Ben-Zvi et al., 2014; Knowland et al., 2014). What could be the mechanism that induces CNS endothelial cells to suppress transcytosis? Canonical Wnt signaling is the most well-characterized signaling pathway for barrier induction. However, it is unclear whether Canonical Wnt signaling induces specialized tight junction formation or suppression of transcytosis, or possibly, both. Although not explicitly demonstrated, there are several indirect lines of evidence that Canonical Wnt signaling mediates specialized tight

junction formation. First, Norrin, the Wnt ligand for blood-retinal barrier formation, is present in the retina during vessel ingression, a time period where tight junctions are functional, yet transcytosis still occurs. Second, loss-of-function of Canonical Wnt signaling decreases protein expression of Claudin-5, a key tight junction molecule for barrier function (Nitta et al., 2003) and also increases protein expression of PLVAP, a molecule associated with fenestrated junctions (Herrnberger et al., 2014; Stan et al., 1999; 2012). Finally, a recent study suggests that loss-of-function of β-catenin, the downstream transcription factor that Canonical Wnt signaling converges on, results in open junctions at the blood-brain barrier (Tran et al., 2016). Thus, Canonical Wnt signaling seems to mediate specialized tight junction formation. However, it is unclear whether Canonical Wnt signaling also suppresses transcytosis in CNS endothelial cells. A microarray analysis on loss-of-function of LRP5 retinas suggest that Mfsd2a, the key suppressor of caveolae-mediated transcytosis is downregulated (Chen et al., 2012). However, because Canonical Wnt signaling also mediates angiogenesis and barriergenesis, it is unclear if the downregulation of Mfsd2a is due to a defective angiogenesis.

Pericytes are a important cell-type that induces CNS endothelial cells to suppress transcytosis. In pericyte-deficient mice, the barrier is defective due to elevated transcytosis (Armulik et al., 2010; Bell et al., 2010; Daneman et al., 2010). Furthermore, our lab identified that Mfsd2a is downregulated in pericyte-deficient mice (Ben-Zvi et al., 2014). However, our work demonstrates that pericyte coverage is not simply the determinant for suppression of transcytosis in CNS endothelial cells as pericytes are present in nascent vessels despite these nascent vessels still lack a function barrier and have yet to suppress transcytosis prior to P10 (Chow and Gu, 2017). Therefore, it is more likely that an inductive factor, either a secreted ligand or basement membrane, from pericytes is the mechanism to suppress transcytosis in CNS

endothelial cells. It is possible that pericytes could exhibit heterogeneity during BRB development. Interestingly, a recent study identified that Hey1, a basic helix-loop-helix (bHLH)-type transcriptional repressor, labels the pericytes on nascent vessels but not on mature vessels (Eilken et al., 2017). Could these Hey1+ pericytes lack key inductive factors for nascent CNS endothelial cell to form a functional BRB? Future work using lineage tracing and transcriptomic analysis on these Hey1+ pericytes might identify the inductive cues involved in BRB development.

Heterogeneity of caveolae vesicular density in CNS arterioles and capillaries

In the second story of my thesis, we made a surprising discovery that arteriolar endothelial cells are enriched in caveolae whereas capillary endothelial cells are sparse in caveolae. This suggests that different segments of the CNS vasculature utilize different genetic programs to differentially regulate caveolae density for distinct physiological functions. Indeed, we find that arteriolar endothelial cells lack Mfsd2a and are enriched in caveolae to mediate neurovascular coupling whereas capillary endothelial cells express Mfsd2a and have suppressed caveolae-mediated transcytosis to ensure functional blood-CNS barrier integrity (**Figure 5.1 and Figure 5.2**). Intriguingly, both the absence of Mfsd2a and the high caveolae density in CNS arteriolar endothelial cells would suggest that CNS arteriolar endothelial cells might have a high level of caveolae-mediated transcytosis and thus, not have a canonical blood-brain barrier. It will be interesting for future studies to examine whether tracer injection results in leakage from CNS arterioles.

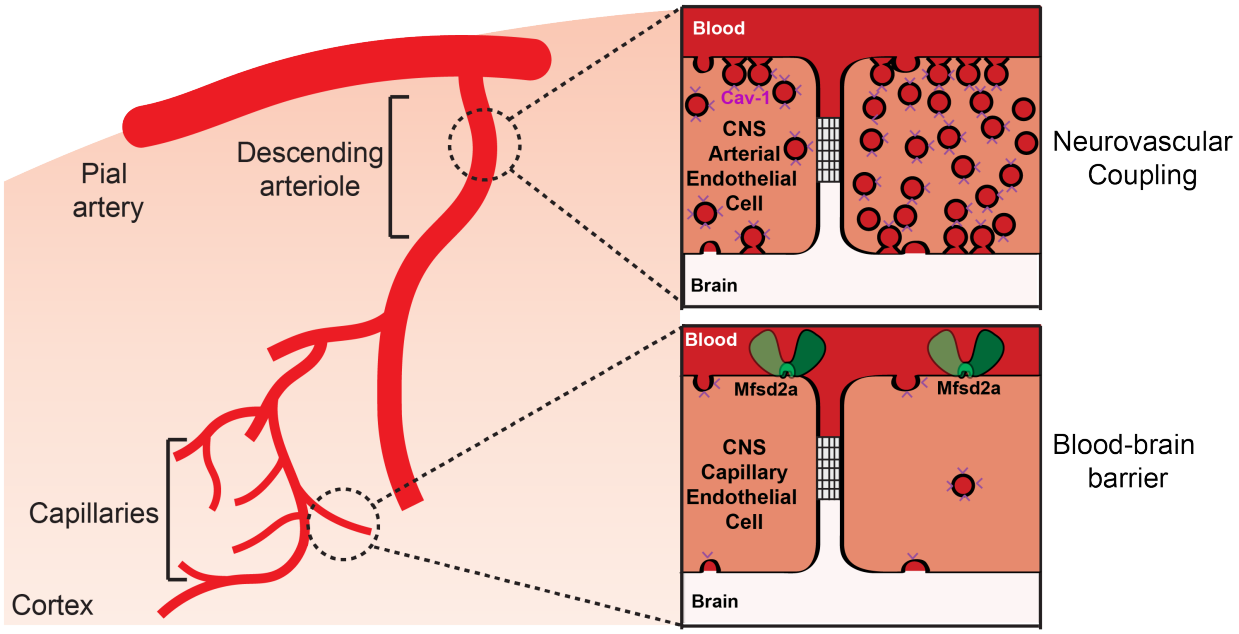

Figure 5.1. Heterogeneity of caveolae vesicular density across CNS vasculature. CNS capillaries have Mfsd2a and other genetic programs to deter caveolae formation and suppress transcytosis to ensure functional blood-brain barrier integrity whereas CNS arterioles lack Mfsd2a and concurrently, have high caveolae density to ensure optimal neurovascular coupling.

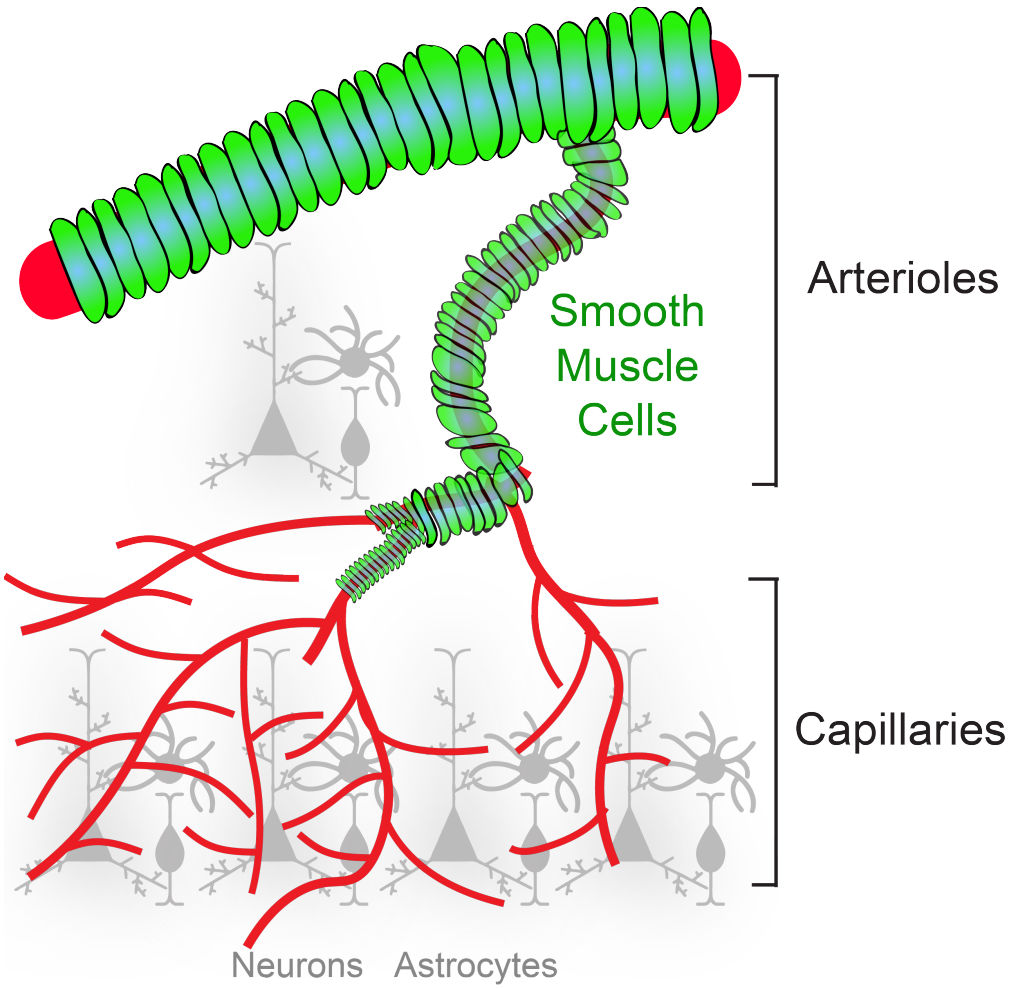

Figure 5.2. Cerebrovascular network anatomy places temporal and spatial constraints on neurovascular coupling. The brain's vascular network is composed of pial (superficial) arteries that descend into the parenchyma, narrowing and branching into penetrating arterioles and then branching to form capillaries. The capillaries represent the majority (more than 85%) of blood vessels in the brain and are intimately appose to neurons, including those in the deeper layers of the cortex that penetrating arterioles cannot reach. In contrast, only a small fraction (less than 10%) of blood vessels are arteries or arterioles, which provide limited spatial coverage in the brain. Importantly, neurovascular coupling depends on smooth muscle cells which have the contractile ability. However, only pial arteries and penetrating arterioles are ensheathed in smooth muscle cells, which relax to control arteriolar dilation.

What could be the mechanism that establishes this differential caveolae vesicular density in different segments of CNS endothelial cells? As mentioned before, pericytes are essential for Mfsd2a induction and suppression of transcytosis in CNS capillary endothelial cells. Interestingly, smooth muscle cells, instead of pericytes, wrap around arteriolar endothelial cells. Thus, smooth muscle cells may lack the key inductive cues to induce CNS arteriolar endothelial to suppress transcytosis and express Mfs2a. Thus, it would be imperative for future studies to mine the available transcriptome between smooth muscle cells and pericytes (Vanlandewijck et al., 2018) and identify these key inductive cues for blood-CNS barrier formation.

Arteriolar endothelial cells are essential for neurovascular coupling

While previous models have highlighted neurons, astrocytes, and mural cells as pivotal players for neurovascular coupling, only recently has the CNS endothelium has been demonstrated to play a role in neurovascular coupling (Chen et al., 2014; Longden et al., 2017) (**Figure 5.1**). Indeed, a recent study demonstrated that capillaries in deeper cortical layers sense neural activity and 'retrogradely' relay this information via an electrical propagation across the vascular network to dilate upstream arterioles (Longden et al., 2017). However, the mechanism of information transfer from capillary endothelial cells to arteriolar endothelial cells and finally to smooth muscle cells to dilate the arteries has been unclear. Here, we demonstrate for the first time that arteriolar endothelial cells play an integral role to mediate neurovascular coupling. Specifically, we found that arteriolar endothelial cells are abundant in caveolae. Ablation of caveolae specifically in arteriolar endothelial cells impairs neurovascular coupling whereas ablation of caveolae specifically in smooth muscle cells is dispensable for neurovascular coupling. Thus, our finding supports this emerging endothelium model in which capillary

endothelial cells sense neural activity and relay this information via an electrical hyperpolarization across the vascular network to upstream arteriolar endothelial cells (Chen et al., 2014; Longden et al., 2017). From here, we speculate that arteriolar endothelial cells communicate to smooth muscle cells via a caveolae-dependent mechanism to dilate and increase blood flow.

Arteriolar endothelial cells utilize caveolae independent of eNOS signaling

In the peripheral vasculature, early work reported that Cav1 protein interacts with endothelial nitric oxide synthases (eNOS) to generate nitric oxide (NO), a major vasodilatory factor (García-Cardeña et al., 1997) *in vitro*. Specifically, it has been demonstrated that Cav1 acts as a negative regulator for eNOS function and that removal of Cav1 results in eNOS hyperactivity and overdilation of vessels upon stimulus *ex vivo* (Bernatchez et al., 2011). Surprisingly, we find that in the CNS vasculature, genetic ablation of caveolae actually resulted in impaired dilation upon sensory-evoked neural activity. Furthermore, we found that eNOS protein level and activity in the CNS vasculature were similar between control and *Cav1*$^{-/-}$ mice. Finally, genetic deletion of both *Cav1*$^{-/-}$ and *eNOS*$^{-/-}$ revealed that these two genetic pathways are actually not epistatic for neurovascular coupling in the CNS vasculature as the double knockout mice did not phenocopy either of the single knockout mice. Instead, the double knockout mice had an additive phenotype of the two single knockouts. Furthermore, this additive phenotype resulted in near abolishment of neurovascular coupling, with negligible changes in arteriolar dilation and capillary blood flow upon sensory-evoked neural activity. Surprisingly, the double knockout mice overtly appear normal with no overt abnormalities in physical and behavior performance. It will be imperative for future studies to perform behavioral studies to determine

the significance of neurovascular coupling as this process has been linked to a myriad of neurological diseases and aging. However, rarely has anyone tested the significance of neurovascular coupling in health. The double knockout, or better yet, an inducible, arteriolar endothelial cell-specific conditional knockout of *Cav1* and *eNOS* could serve as an ideal model to test this question.

Finally, it is interesting to note that the single deletion of *Cav1* and the single deletion of *eNOS* both impair neurovascular coupling but single deletion of Cav1impairs arteriolar dilation to a larger extent. This suggests that the caveolae-mediated pathway is as important as the eNOS-mediated pathway for neurovascular coupling.

While we found that the caveolae and eNOS pathways are not epistatic, this still leaves the question of how arteriolar endothelial cells use caveolae to mediate neurovascular coupling? Currently, we are actively testing the hypothesis if caveolae in arteriolar endothelial cells could provide additional membrane to promote elasticity during arteriolar dilation. Given this hypothesis, it is conceivable that in the absence of caveolae, arteriolar endothelial cells lack the elasticity to dilate effectively upon neural activity. Furthermore, this hypothesis is consistent with the finding the Cav1 and eNOS are not epistatic. To test the hypothesis that arterioles lack elasticity for optimal vasodilation in the absence of caveolae, we will bypass neural activity and force arterioles to stretch by directly relaxing smooth muscle cells using optogenetics. If caveolae serve as a membrane reservoir to promote arteriolar dilation, then we expect that *Cav1* mutant mice will have impaired optogenetic-evoked arteriolar dilation relative to wildtype mice. Alternatively, if caveolae do not play a role as the membrane reservoir, then we expect *Cav1* mutant mice should display robust arteriolar dilation upon optogenetic-evoked arteriolar dilation with a magnitude similar to wildtype mice. In this case, this would suggest that caveolae in aECs

are essential to relay vasodilatory cues to smooth muscle cells. Thus, either outcome will be highly informative to understand the role of caveolae in aECs to mediate neurovascular coupling. Finally, note that this proposed experiment is conceptually different than the *ex vivo* acute brain slice experiment using NO donor to dilate smooth muscle cells in the absence of caveolae (**Supplementary Figure 14**). In the acute brain slice experiment, we assessed the signaling of smooth muscle cells to relax after contraction using Thromboxane agonist (U46619). Note that the dilation only returns back to the original baseline before contraction but not beyond the original baseline. Thus, this proposed experiment *in vivo* will test the dilation relative to the original baseline and not a contracted baseline.

An alternative hypothesis is that the abundant caveolae in arterial endothelial cells could mediate neurovascular coupling by coordinating proper gap junction communication as proposed in the peripheral vasculature (Saliez et al., 2008). However, the role of gap junctions in neurovascular coupling is quite elusive. Most vascular gap junction studies have been performed in the peripheral vasculature (Krüger et al., 2000; Kumai et al., 2000; Reaume et al., 1995; Saliez et al., 2008; Simon and McWhorter, 2003a) but very few studies have examined the role of gap junctions in the brain vasculature, especially in the context of neurovascular coupling. Furthermore, past studies that did examine the role of gap junctions in the vasomotion of the brain vasculature all used putative gap junction blockers (i.e heptanol, glycyrrhetinic acid and carbenoxolone) (Lagaud et al., 2002; Watanabe et al., 2018). However, repeated studies have demonstrated that putative gap junction blockers actually have non-gap junctional effects (Matchkov et al., 2004; Tare et al., 2002). These off-target effects include blocking ion channels such as $GABA_A$ receptors (Connors, 2012) and more pertinently, IK and SK channels expressed in the endothelium, which have been implicated in neurovascular coupling (Longden et al.,

2017). Thus, the role of gap junctions, as well as the identities of the connexins that form these gap junctions, in neurovascular coupling is actually elusive given that there are no studies to this date that have performed cell-type-specific genetic deletion of the various connexin genes and examine the impact on neurovascular coupling.

This is actually quite challenging given that there are 20 connexin genes identified in mouse (21 connexin genes in human) (Willecke et al., 2002) and connexin expression is not identical in all blood vessels in the body (Simon and McWhorter, 2003b). Adding more to this complexity, there are various connexin genes that 1) may play redundant functions (Simon and McWhorter, 2003b) and 2) are broadly expressed in various organs so genetic deletion often results in lethality to due to its requirement during development (Krüger et al., 2000; Kumai et al., 2000; Reaume et al., 1995; Simon and McWhorter, 2003b). The advent of various single-cell RNA sequencing of brain vasculature is a launching point and has provided clues to which connexin gene are expressed in the brain vasculature (Sabbagh et al., 2018; Tasic et al., 2018; Vanlandewijck et al., 2018). Interestingly and adding more to the complexity, there is heterogeneity in connexin expression across different segments of the CNS vasculature. Thus, to unequivocally understand the role of connexins and gap junction in neurovascular coupling, inducible, cell-type-specific deletion of putative connexin genes in different segments of the CNS vasculature would be required. Thus, it is imperative that future studies definitively elucidate which connexins are involved in gap junction communication and specifically, in which segments of the brain vasculature to mediate neurovascular coupling. After elucidating the role of connexins and gap junctions, it will be interesting to then address if caveolae are involved in gap junction communication for neurovascular coupling.

Outlook

In conclusion, my thesis work provides a new level of insight into the two unique functions of the CNS vasculature. We identified a common mechanism underlying blood-CNS barrier formation during development and then, identified a novel cell-type, the arteriolar endothelial cells, as essential to mediate neurovascular coupling. Future experiments that identify inductive cues for barrier formation or signals that mediate neurovascular coupling will open up new directions of investigation that are consistent with major goals and unanswered questions in the neurovascular field.

References

Andreone, B.J., Chow, B.W., Tata, A., Lacoste, B., Ben-Zvi, A., Bullock, K., Deik, A.A., Ginty, D.D., Clish, C.B., and Gu, C. (2017). Blood-Brain Barrier Permeability Is Regulated by Lipid Transport-Dependent Suppression of Caveolae-Mediated Transcytosis. Neuron *94*, 581–594.e585.

Armulik, A., Abramsson, A., and Betsholtz, C. (2005). Endothelial/pericyte interactions. Circulation Research *97*, 512–523.

Armulik, A., Genové, G., Mäe, M., Nisancioglu, M.H., Wallgard, E., Niaudet, C., He, L., Norlin, J., Lindblom, P., Strittmatter, K., et al. (2010). Pericytes regulate the blood-brain barrier. *468*, 557–561.

Bell, R.D., Winkler, E.A., Sagare, A.P., Singh, I., LaRue, B., Deane, R., and Zlokovic, B.V. (2010). Pericytes control key neurovascular functions and neuronal phenotype in the adult brain and during brain aging. Neuron *68*, 409–427.

Ben-Zvi, A., Lacoste, B., Kur, E., Andreone, B.J., Mayshar, Y., Yan, H., and Gu, C. (2014). Mfsd2a is critical for the formation and function of the blood-brain barrier. Nature *509*, 507–511.

Bernatchez, P., Sharma, A., Bauer, P.M., Marin, E., and Sessa, W.C. (2011). A noninhibitory mutant of the caveolin-1 scaffolding domain enhances eNOS-derived NO synthesis and vasodilation in mice. J. Clin. Invest. *121*, 3747–3755.

Chen, B.R., Kozberg, M.G., Bouchard, M.B., Shaik, M.A., and Hillman, E.M.C. (2014). A Critical Role for the Vascular Endothelium in Functional Neurovascular Coupling in the Brain. J Am Heart Assoc *3*, e000787–e000787.

Chen, J., Stahl, A., Krah, N.M., Seaward, M.R., Joyal, J.-S., Juan, A.M., Hatton, C.J., Aderman, C.M., Dennison, R.J., Willett, K.L., et al. (2012). Retinal expression of Wnt-pathway mediated genes in low-density lipoprotein receptor-related protein 5 (Lrp5) knockout mice. PLoS ONE *7*, e30203.

Cho, C., Smallwood, P.M., and Nathans, J. (2017). Reck and Gpr124 Are Essential Receptor Cofactors for Wnt7a/Wnt7b-Specific Signaling in Mammalian CNS Angiogenesis and Blood-Brain Barrier Regulation. Neuron *95*, 1056–1073.e5.

Chow, B.W., and Gu, C. (2017). Gradual Suppression of Transcytosis Governs Functional Blood-Retinal Barrier Formation. Neuron *93*, 1325–1333.e3.

Connors, B.W. (2012). Tales of a dirty drug: carbenoxolone, gap junctions, and seizures. Epilepsy Curr *12*, 66–68.

Daneman, R., Agalliu, D., Zhou, L., Kuhnert, F., Kuo, C.J., and Barres, B.A. (2009). Wnt/beta-catenin signaling is required for CNS, but not non-CNS, angiogenesis. Proc. Natl. Acad. Sci. U.S.A. *106*, 641–646.

Daneman, R., Zhou, L., Kebede, A.A., and Barres, B.A. (2010). Pericytes are required for blood-brain barrier integrity during embryogenesis. *468*, 562–566.

Eilken, H.M., Diéguez-Hurtado, R., Schmidt, I., Nakayama, M., Jeong, H.-W., Arf, H., Adams, S., Ferrara, N., and Adams, R.H. (2017). Pericytes regulate VEGF-induced endothelial sprouting through VEGFR1. Nat Commun *8*, 1574.

Ek, C.J., Dziegielewska, K.M., Stolp, H., and Saunders, N.R. (2006). Functional effectiveness of the blood-brain barrier to small water-soluble molecules in developing and adult opossum (Monodelphis domestica). J. Comp. Neurol. *496*, 13–26.

Fruttiger, M. (2007). Development of the retinal vasculature. Angiogenesis *10*, 77–88.

García-Cardeña, G., Martasek, P., Masters, B.S., Skidd, P.M., Couet, J., Li, S., Lisanti, M.P., and Sessa, W.C. (1997). Dissecting the interaction between nitric oxide synthase (NOS) and caveolin. Functional significance of the nos caveolin binding domain in vivo. J. Biol. Chem. *272*, 25437–25440.

Herrnberger, L., Hennig, R., Kremer, W., Hellerbrand, C., Goepferich, A., Kalbitzer, H.R., and Tamm, E.R. (2014). Formation of fenestrae in murine liver sinusoids depends on plasmalemma vesicle-associated protein and is required for lipoprotein passage. PLoS ONE *9*, e115005.

Knowland, D., Arac, A., Sekiguchi, K.J., Hsu, M., Lutz, S.E., Perrino, J., Steinberg, G.K., Ben A Barres, Nimmerjahn, A., and Agalliu, D. (2014). Stepwise Recruitment of Transcellular and Paracellular Pathways Underlies Blood-Brain Barrier Breakdown in Stroke. Neuron *82*, 603–617.

Krüger, O., Plum, A., Kim, J.S., Winterhager, E., Maxeiner, S., Hallas, G., Kirchhoff, S., Traub, O., Lamers, W.H., and Willecke, K. (2000). Defective vascular development in connexin 45-deficient mice. Development *127*, 4179–4193.

Kumai, M., Nishii, K., Nakamura, K., Takeda, N., Suzuki, M., and Shibata, Y. (2000). Loss of connexin45 causes a cushion defect in early cardiogenesis. Development *127*, 3501–3512.

Lagaud, G., Karicheti, V., Knot, H.J., Christ, G.J., and Laher, I. (2002). Inhibitors of gap junctions attenuate myogenic tone in cerebral arteries. American Journal of Physiology - Heart and Circulatory Physiology *283*, H2177–H2186.

Longden, T.A., Dabertrand, F., Koide, M., Gonzales, A.L., Tykocki, N.R., Brayden, J.E., Hill-Eubanks, D., and Nelson, M.T. (2017). Capillary K+-sensing initiates retrograde hyperpolarization to increase local cerebral blood flow. Nat. Neurosci. *20*, 717–726.

Matchkov, V.V., Rahman, A., Peng, H., Nilsson, H., and Aalkjaer, C. (2004). Junctional and nonjunctional effects of heptanol and glycyrrhetinic acid derivates in rat mesenteric small arteries. Br. J. Pharmacol. *142*, 961–972.

Nitta, T., Hata, M., Gotoh, S., Seo, Y., Sasaki, H., Hashimoto, N., Furuse, M., and Tsukita, S. (2003). Size-selective loosening of the blood-brain barrier in claudin-5-deficient mice. J. Cell Biol. *161*, 653–660.

Reaume, A.G., de Sousa, P.A., Kulkarni, S., Langille, B.L., Zhu, D., Davies, T.C., Juneja, S.C., Kidder, G.M., and Rossant, J. (1995). Cardiac malformation in neonatal mice lacking connexin43. Science *267*, 1831–1834.

Reese, T.S., and Karnovsky, M.J. (1967). Fine structural localization of a blood-brain barrier to exogenous peroxidase. J. Cell Biol. *34*, 207–217.

Sabbagh, M.F., Heng, J.S., Luo, C., Castanon, R.G., Nery, J.R., Rattner, A., Goff, L.A., Ecker, J.R., and Nathans, J. (2018). Transcriptional and epigenomic landscapes of CNS and non-CNS vascular endothelial cells. Elife *7*.

Saliez, J., Bouzin, C., Rath, G., Ghisdal, P., Desjardins, F., Rezzani, R., Rodella, L.F., Vriens, J., Nilius, B., Feron, O., et al. (2008). Role of caveolar compartmentation in endothelium-derived hyperpolarizing factor-mediated relaxation: Ca2+ signals and gap junction function are regulated by caveolin in endothelial cells. Circulation *117*, 1065–1074.

Simon, A.M., and McWhorter, A.R. (2003a). Decreased intercellular dye-transfer and downregulation of non-ablated connexins in aortic endothelium deficient in connexin37 or connexin40. J. Cell. Sci. *116*, 2223–2236.

Simon, A.M., and McWhorter, A.R. (2003b). Role of connexin37 and connexin40 in vascular development. Cell Communication and Adhesion *10*, 379–385.

Sohet, F., Lin, C., Munji, R.N., Lee, S.Y., Ruderisch, N., Soung, A., Arnold, T.D., Derugin, N., Vexler, Z.S., Yen, F.T., et al. (2015). LSR/angulin-1 is a tricellular tight junction protein involved in blood-brain barrier formation. J. Cell Biol. *208*, 703–711.

Stan, R.V., Kubitza, M., and Palade, G.E. (1999). PV-1 is a component of the fenestral and stomatal diaphragms in fenestrated endothelia. Pnas *96*, 13203–13207.

Stan, R.V., Tse, D., Deharvengt, S.J., Smits, N.C., Xu, Y., Luciano, M.R., McGarry, C.L., Buitendijk, M., Nemani, K.V., Elgueta, R., et al. (2012). The diaphragms of fenestrated endothelia: gatekeepers of vascular permeability and blood composition. Developmental Cell *23*, 1203–1218.

Stenman, J.M., Rajagopal, J., Carroll, T.J., Ishibashi, M., McMahon, J., and McMahon, A.P. (2008). Canonical Wnt signaling regulates organ-specific assembly and differentiation of CNS vasculature. Science *322*, 1247–1250.

Stewart, P.A., and Wiley, M.J. (1981). Developing nervous tissue induces formation of blood-brain barrier characteristics in invading endothelial cells: a study using quail--chick transplantation chimeras. Dev. Biol. *84*, 183–192.

Tare, M., Coleman, H.A., and Parkington, H.C. (2002). Glycyrrhetinic derivatives inhibit hyperpolarization in endothelial cells of guinea pig and rat arteries. American Journal of Physiology - Heart and Circulatory Physiology *282*, H335–H341.

Tasic, B., Yao, Z., Graybuck, L.T., Smith, K.A., Nguyen, T.N., Bertagnolli, D., Goldy, J., Garren, E., Economo, M.N., Viswanathan, S., et al. (2018). Shared and distinct transcriptomic cell types across neocortical areas. Nature *563*, 72–78.

Tran, K.A., Zhang, X., Predescu, D., Huang, X., Machado, R.F., Göthert, J.R., Malik, A.B., Valyi-Nagy, T., and Zhao, Y.-Y. (2016). Endothelial β-Catenin Signaling Is Required for Maintaining Adult Blood-Brain Barrier Integrity and Central Nervous System Homeostasis. Circulation *133*, 177–186.

Vanlandewijck, M., He, L., Mäe, M.A., Andrae, J., Ando, K., Del Gaudio, F., Nahar, K., Lebouvier, T., Laviña, B., Gouveia, L., et al. (2018). A molecular atlas of cell types and zonation in the brain vasculature. Nature *554*, 475–480.

Wang, Y., Rattner, A., Zhou, Y., Williams, J., Smallwood, P.M., and Nathans, J. (2012). Norrin/Frizzled4 signaling in retinal vascular development and blood brain barrier plasticity. Cell *151*, 1332–1344.

Watanabe, N., Sasaki, S., Masamoto, K., and Hotta, H. (2018). Vascular Gap Junctions Contribute to Forepaw Stimulation-Induced Vasodilation Differentially in the Pial and Penetrating Arteries in Isoflurane-Anesthetized Rats. Frontiers in Molecular Neuroscience *11*, 446.

Willecke, K., Eiberger, J., Degen, J., Eckardt, D., Romualdi, A., Güldenagel, M., Deutsch, U., and Söhl, G. (2002). Structural and functional diversity of connexin genes in the mouse and human genome. Biol. Chem. *383*, 725–737.

Ye, X., Wang, Y., Cahill, H., Yu, M., Badea, T.C., Smallwood, P.M., Peachey, N.S., and Nathans, J. (2009). Norrin, Frizzled-4, and Lrp5 Signaling in Endothelial Cells Controls a Genetic Program for Retinal Vascularization. Cell *139*, 285–298.

Zhou, Y., and Nathans, J. (2014). Gpr124 controls CNS angiogenesis and blood-brain barrier integrity by promoting ligand-specific canonical wnt signaling. Developmental Cell *31*, 248–256.

Zhou, Y., Wang, Y., Tischfield, M., Williams, J., Smallwood, P.M., Rattner, A., Taketo, M.M., and Nathans, J. (2014). Canonical WNT signaling components in vascular development and barrier formation. J. Clin. Invest. *124*, 3825–3846.

APPENDIX

Supplementary Figures

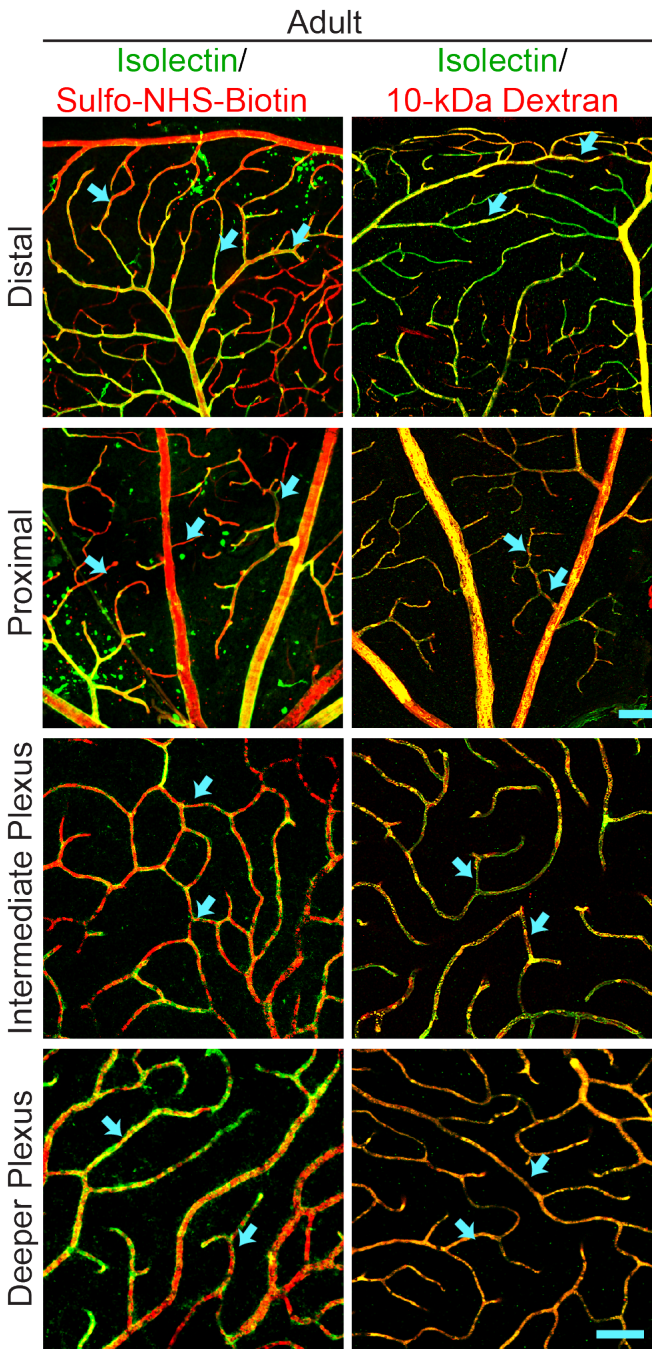

Supplementary Figure 1. Characterization of functional BRB in the adult retinal vasculature.

In a functional adult BRB, the vessels (isolectin; green) of the primary (1st and 2nd row), intermediate (3rd row) and deeper plexus (4th row) completely confines (arrow) both the Sulfo-NHS-Biotin (left) and 10-kDa dextran (right) tracers (red). Scale bar represents 50 μm.

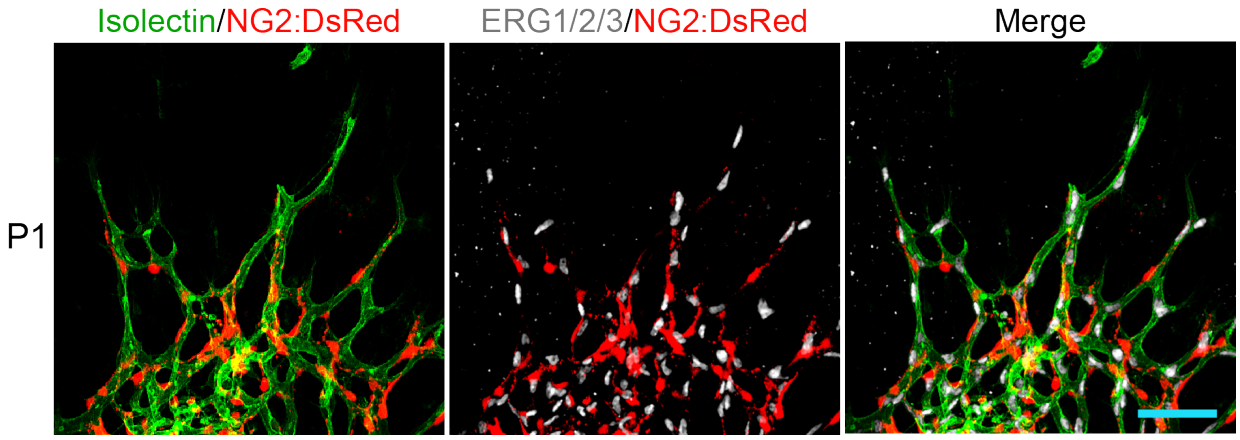

Supplementary Figure 2. Pericytes are present as soon as vessel ingression. A) As early as vessel ingression at P1, pericytes (NG2:DsRed; red) are already ensheathing budding CNS vessels (isolectin; green and ERG for endothelial nuclei; white). Scale bar represents 100 μm.

Supplementary Figure 3. Proximal, mature vessels form functional BRB before distal, nascent vessels. (A) Intravenous injections of Sulfo-NHS-Biotin (left) and 10-kDa dextran (right) tracer in postnatal mice demonstrate that the proximal vessels (green) already confine the tracer. Scale bar represents 50 μm. (**B**) Quantification of the permeability index of the proximal vessels. Data are presented as mean ± s.e.m. (n = 5-8 pups per age, from 3 different litters). Statistical significance was determined by one-way ANOVA, followed by post-hoc Bonferroni multiple comparison adjustment, comparing the various neonatal ages with the adult in the respective Sulfo-NHS-Biotin and 10-kDa dextran group. No significance was observed in the comparison of the proximal vessels.

Supplementary Figure 3 (Continued)

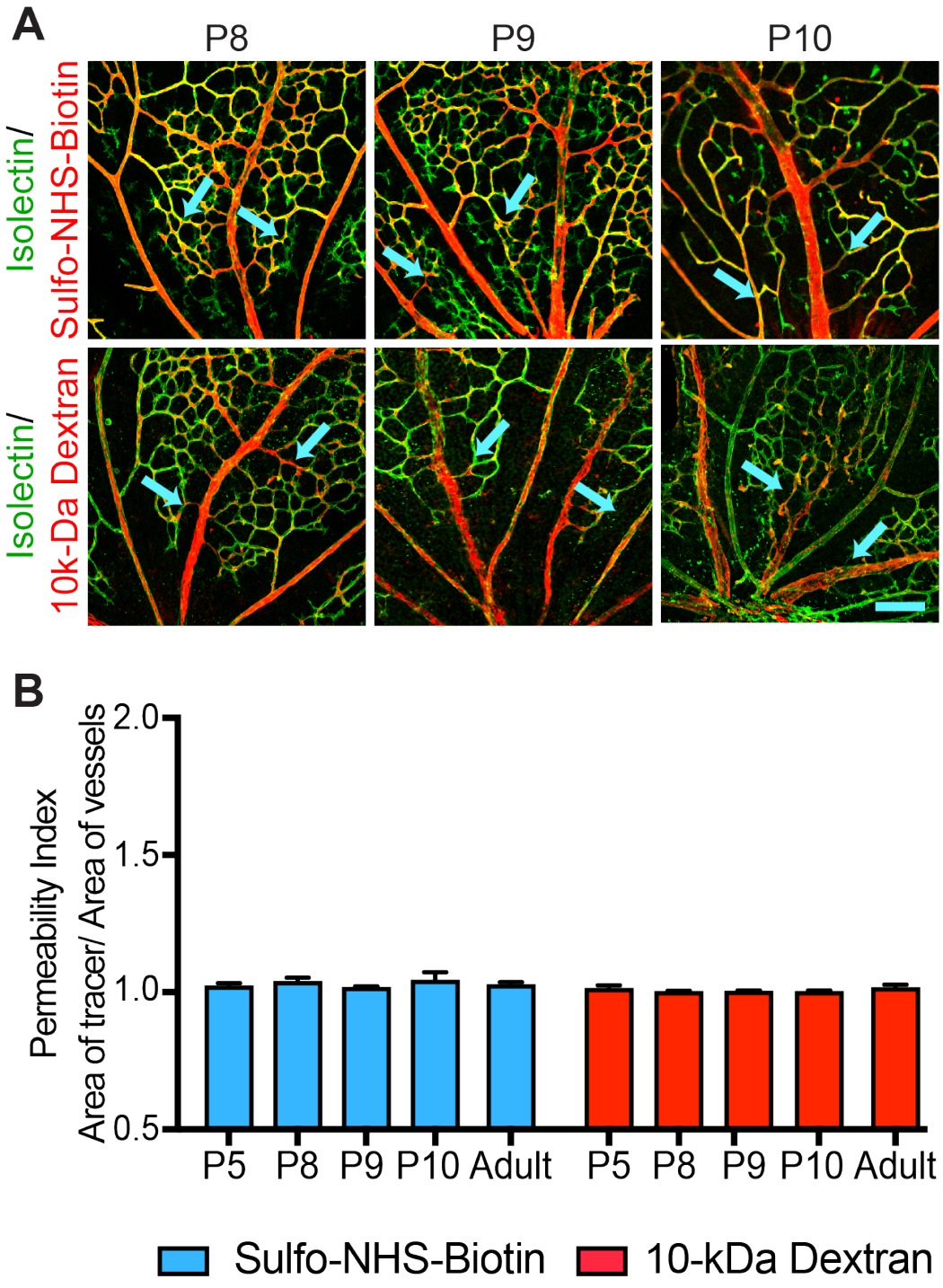

Supplementary Figure 4. Characterization of functional BRB in deeper plexus and intermediate plexus vessels. (A and C) Intravenous injections of Sulfo-NHS-Biotin and 10-kDa dextran tracer in postnatal mice demonstrate that sprouting deeper plexus vessels exhibit tracer leakage at P8 and P9 but not at P10. (**B**) Quantification of the permeability index of the deeper plexus vessels. Data are presented as mean ± s.e.m. (n = 5-8 pups per age, from 3 different litters). Statistical significance was determined by one-way ANOVA, followed by post-hoc Bonferroni multiple comparison adjustment, comparing the various neonatal ages with the adult in the respective Sulfo-NHS-Biotin and 10-kDa dextran group. (**C**) Sprouting intermediate plexus vessels completely confine the tracer as early as P12. (**D**) Quantification of the permeability index of the deeper plexus vessels. Data are presented as mean ± s.e.m. (n = 5-8 pups per age, from 3 different litters). Statistical significance was determined by one-way ANOVA, followed by post-hoc Bonferroni multiple comparison adjustment, comparing the various neonatal ages with the adult in the respective Sulfo-NHS-Biotin and 10-kDa dextran group. No significance was observed in the comparison of intermediate plexus vessels. *, $P < 0.05$, **, $P < 0.01$. ***, $P < 0.01$. Scale bar represents 50 μm for all panels.

Supplementary Figure 4. (Continued)

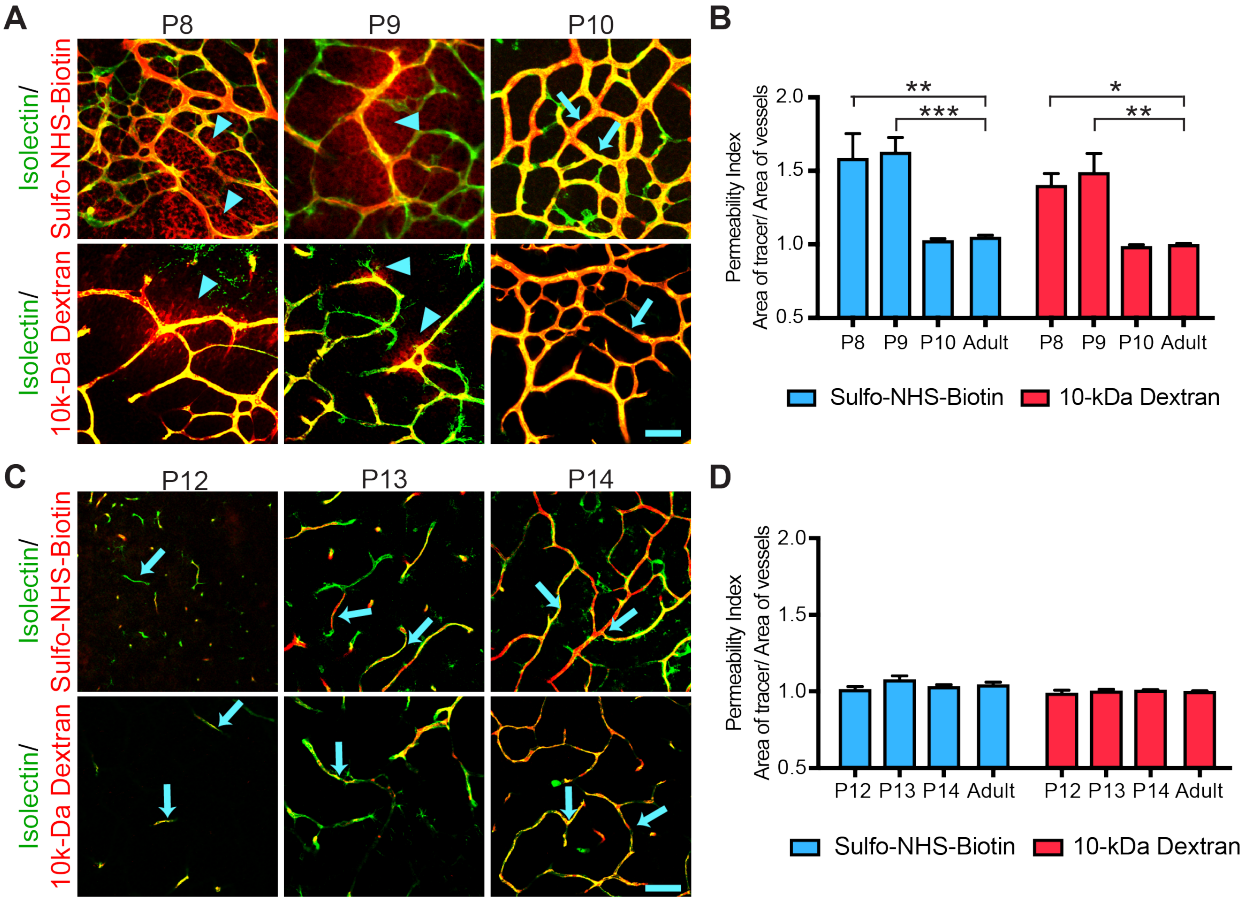

Supplementary Figure 5. EM analysis of Proximal Vessels at P5, P8, P10 and Adult. (**A)** P5 to P10 proximal endothelial cells already contain a negligible number of vesicles. **(B)** EM analysis of proximal vessels from P5, P8 and P10 retinas reveals tracer product halts abruptly at the tight junctions (arrows). (**C**) Quantifications of tracer-filled vesicular densities in the proximal endothelial cells at P5, P8 and P10. Data are presented as mean ± s.e.m. (n= 5 mice per age; each circle represents the average vesicular density from 15 – 20 vessels per mouse). Statistical significance was determined by one-way ANOVA, followed by post-hoc Bonferroni multiple comparison adjustment, comparing the proximal vessels of the various neonatal ages to the proximal vessels of the adult. No significant difference was observed in the comparisons of the proximal vessels. (**D**) Quantification of the number of tight junctions that halt the tracers at the luminal side without parenchymal leakage over the total number of tight junctions in proximal vessels. (n = 5 mice per age; 15-20 vessels analyzed per mouse; the number of tight junctions analyzed are displayed in the bars). The Adult data in Supplementary Figure 2C and S2D is the same as Figure 2E and 2F. L – lumen, E – endothelial cells, Ab – abluminal, RBC-red blood cell. ***, $P < 0.001$. Scale bar represents 100 nm for all panels.

Supplementary Figure 5 (Continued)

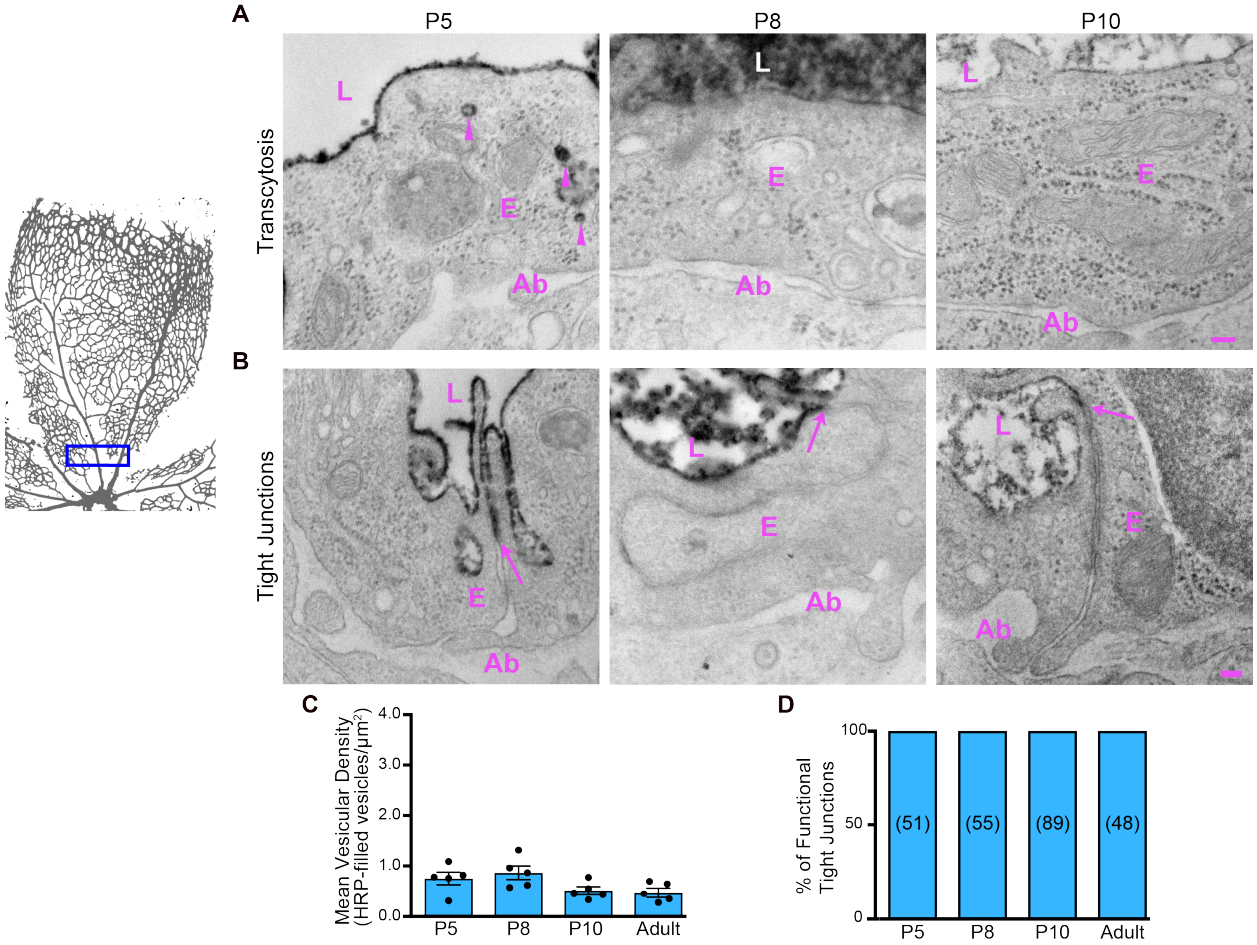

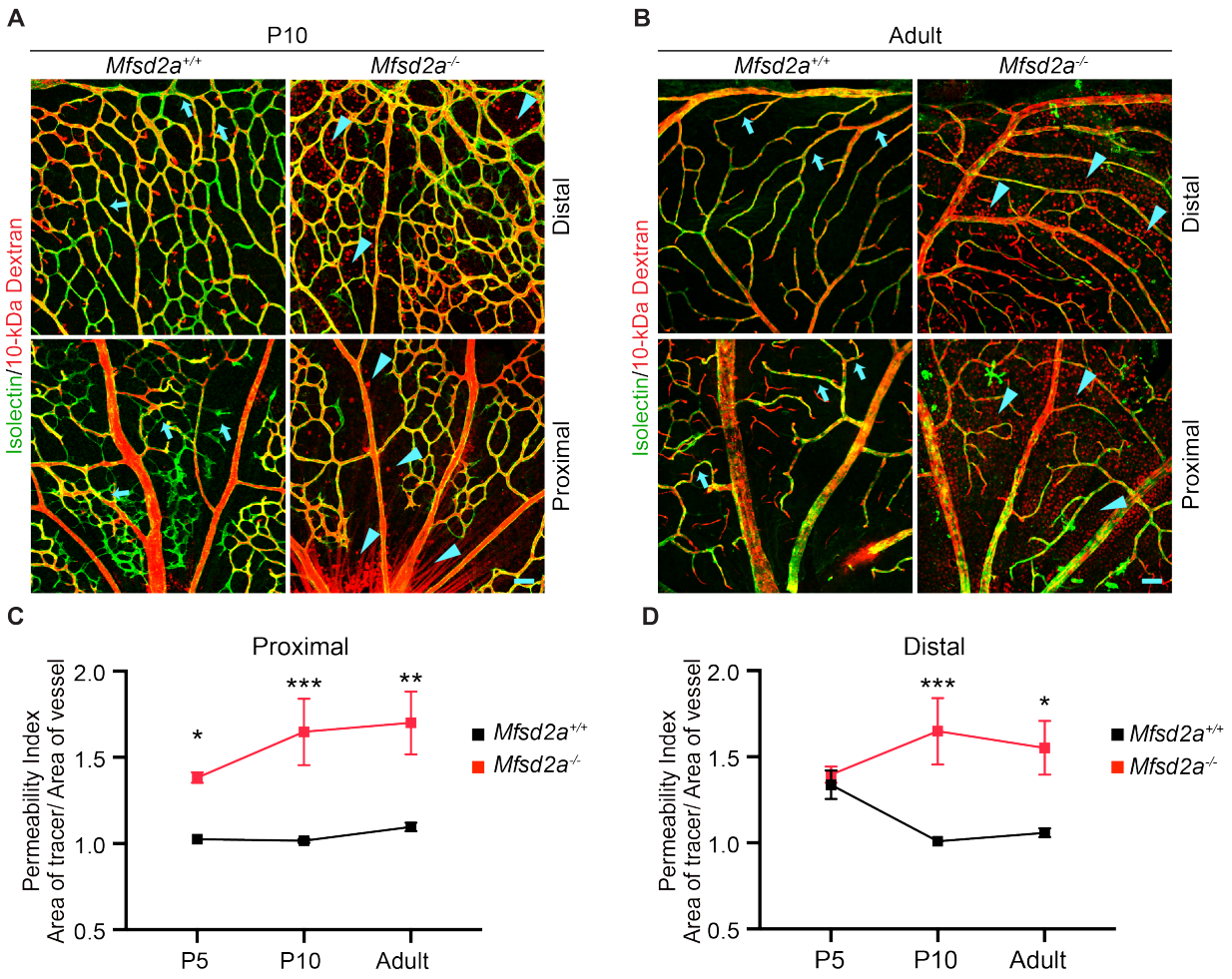

Supplementary Figure 6. Mfsd2a is essential for functional BRB formation. (A and B) Intravenous injection of tracer in P10 (A) and adult (B) *Mfsd2a*$^{+/+}$ mice results in confinement of the tracer throughout the vasculature (arrows) whereas tracer injection in *Mfsd2a*$^{-/-}$ mice results in tracer leakage into the retinal parenchyma (arrowheads) at both distal and proximal regions of the retina. **(C-D)** Quantification of the permeability of the **(C)** proximal and **(D)** distal vessels at P5, P10, and adult ages. Data are presented as mean ± s.e.m. (n = 5,6, and 4 for wildtype P5, P10 and adult respectively and n=5, 5 and 4 for *Mfsd2a*$^{-/-}$ P5, P10 and adult respectively). Statistical significance was determined by comparing *Mfsd2a*$^{-/-}$ and *Mfsd2a*$^{+/+}$ littermates at the respective age using two-way ANOVA, followed by post-hoc Bonferroni multiple comparison adjustment. *, $P < 0.05$, **, $P < 0.01$, ***, $P < 0.001$. Scale bar represents 50 μm for all panels.

Supplementary Figure 7. Illustration of the gradual suppression of transcytosis governs functional BRB formation. As early as vessel ingression at P1 (top), functional tight junctions are already formed to restrict paracellular flux between budding CNS endothelial cells. However, bulk transcytosis is present with many transcytotic vesicles in the endothelial cells, resulting in a leaky, immature barrier between the blood and retinal parenchyma. By P5 (middle), there is a spatiotemporal gradient of a functional BRB formation. The more mature, proximal vessels have both functional tight junctions and suppression of transcytosis to establish a functional barrier. However, the nascent, distal vessels have functional tight junctions but display bulk transcytosis, resulting in a leaky, immature barrier. By P10 (bottom), the entire retinal vasculature has functional tight junctions and suppressed transcytosis, resulting in a functional BRB throughout the vasculature.

Supplementary Figure 7 (Continued)

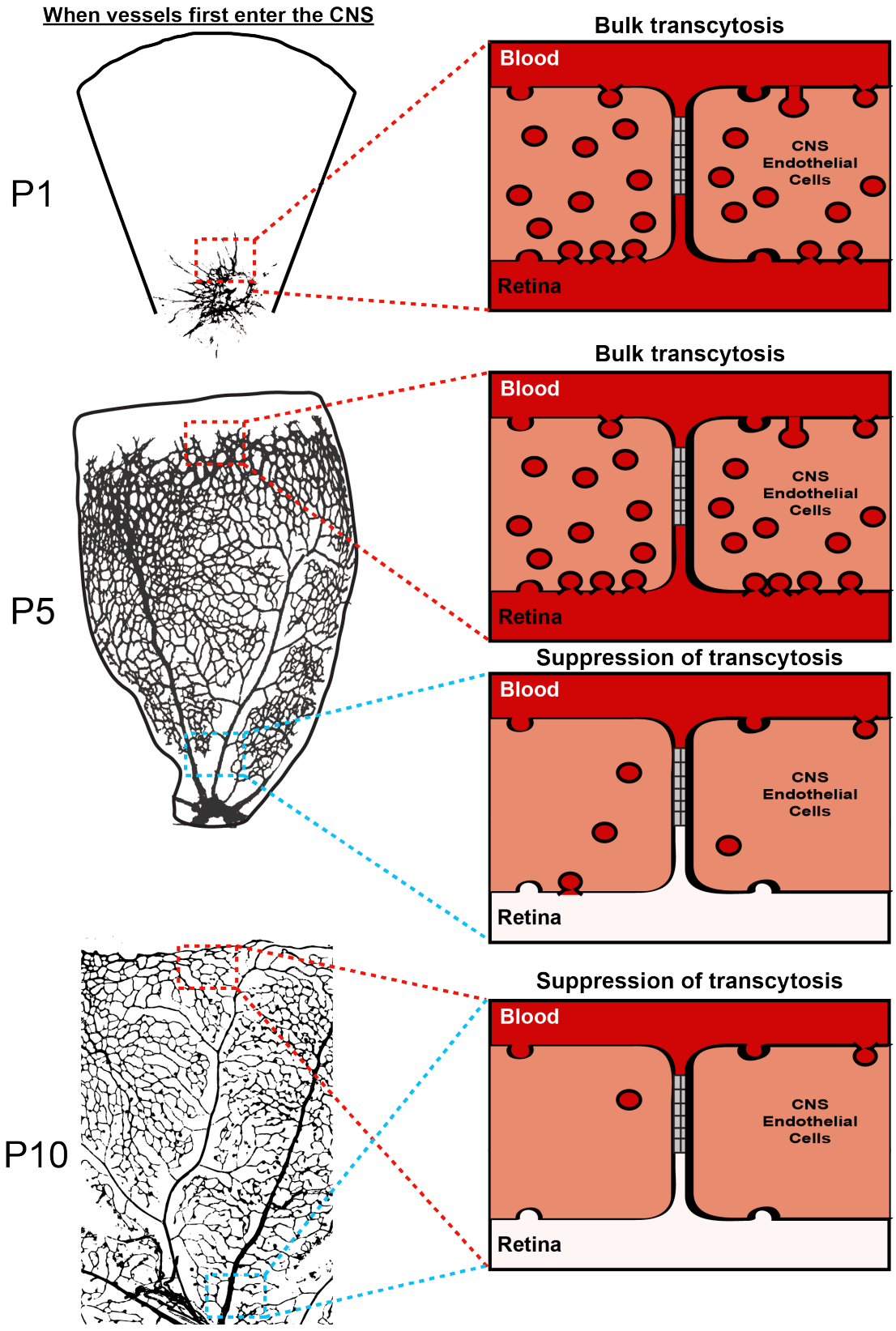

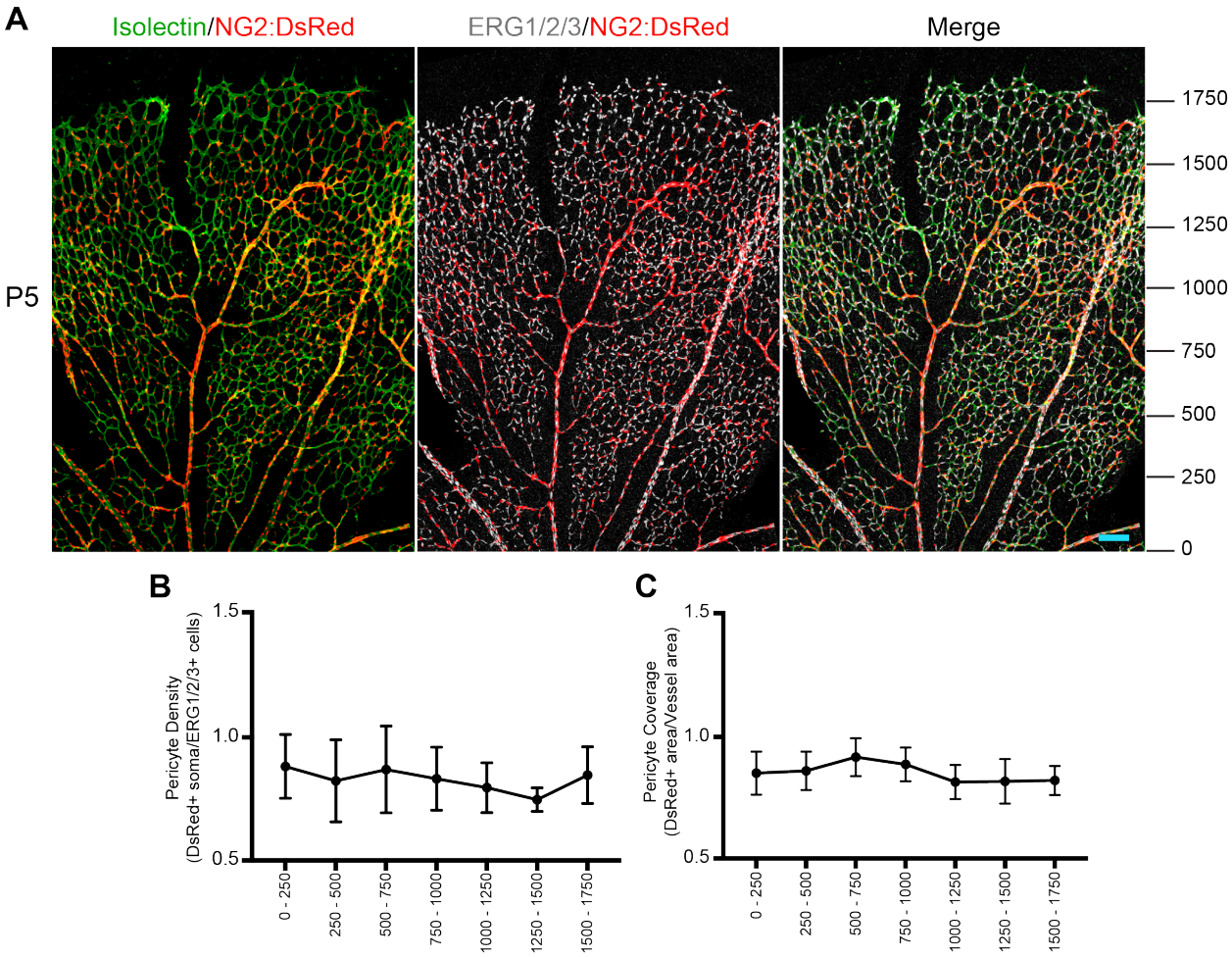

Supplementary Figure 8. Pericyte coverage is constant throughout the retina, including at the distal leaky vessels during BRB development. (**A**) At P5, pericyte density (**B**) NG2:DsRed+ (pericytes) soma/ ERG1/2/3+ cells (endothelial nuclei) and (**C**) pericyte coverage (NG2:DsRed area/Isolectin area) is around 1:1 throughout the retinal vasculature, including the distal, nascent vessels. Data are presented as mean ± s.e.m. (n = 5). The ticks in (**A**) represent the distance in microns from the ONH. 0 is set slightly before the ONH. Scale bar represents 100 μm.

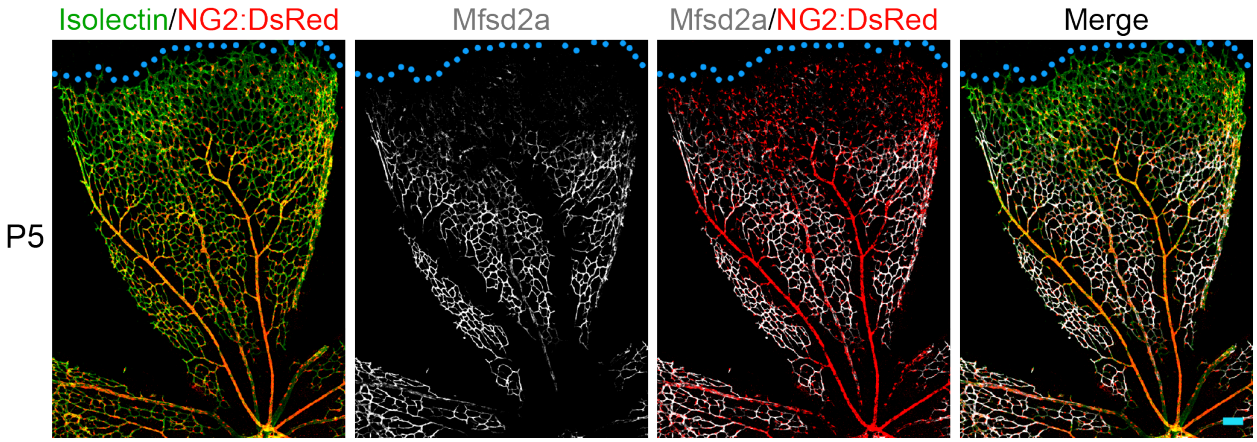

Supplementary Figure 9. Pericytes are present at nascent distal vessels even yet Mfsd2a is still absent at these vessels Pericytes are present in nascent, distal vessels yet Mfsd2a is absent in P5 retinas. The angiogenic front is outlined in blue (determined by isolectin staining). Scale bar represents 100 μm.

Supplementary Figure 10. *In vivo* two photon imaging for neurovascular coupling. (A) Setup of the two-photon microscope. Awake mice with cranial windows over the barrel cortex are head-fixed and allow to run on a foam ball. Whisker stimulator (arrow) is synchronized to image acquisition to evoke neural activity in barrel cortex. (**B)** Hydrazide injection in *Thy1:GCaMP6s* mice allows for simultaneous imaging of neural activity (green) and arteriolar dilation (magenta). Two-photon imaging of arterioles and neural activity (left) before and after (right) whisker stimulation. Hashes outline the baseline diameter at time = 0. (**C**) Quantification of change in arteriolar dilation (magenta) and GCaMP6 fluorescence (green). Yellow bar signifies the period of whisker stimulation. (**D**) Two-photon imaging of arterioles (magenta) and capillary blood flow (blue). After intravenous injection of quantum dots, the plasma is bright whereas the red blood cells are dark. (**E**) High magnification of a capillary in the red box in (**D**). Minimizing the image size increases the temporal resolution to ~610 Hz or 1.6 msec per frame. (**F)** Kymographs of capillary blood flow during baseline (left) and whisker stimulation (right). Kymograph were generated from the parallel line scan (red line) of the capillary blood flow in (**E**). (**G**) Quantification of change in red blood cell velocity. Yellow bar signifies the period of whisker stimulation. Scale bar is 50 μm in (**B,D**) and 5 μm in (**E**).

Supplementary Figure 10 (Continued)

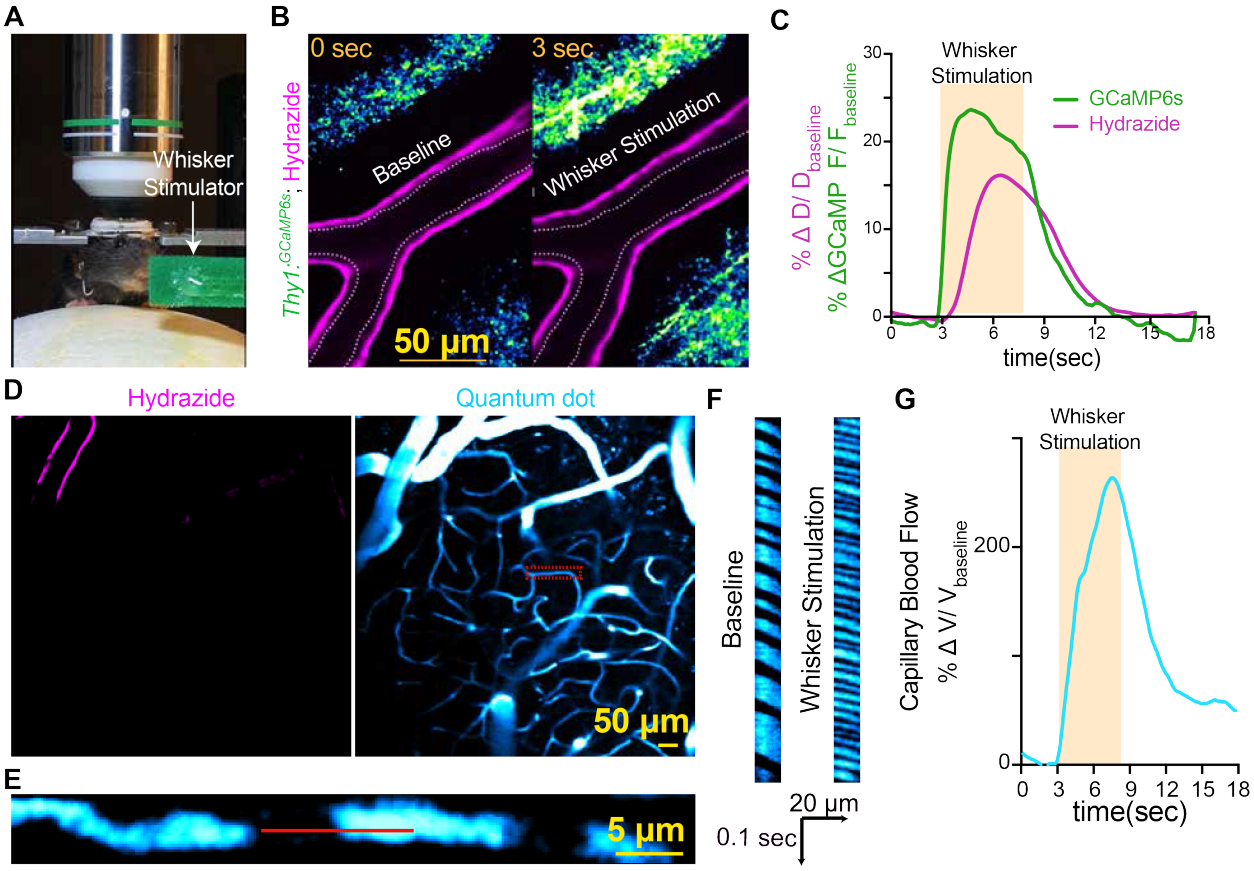

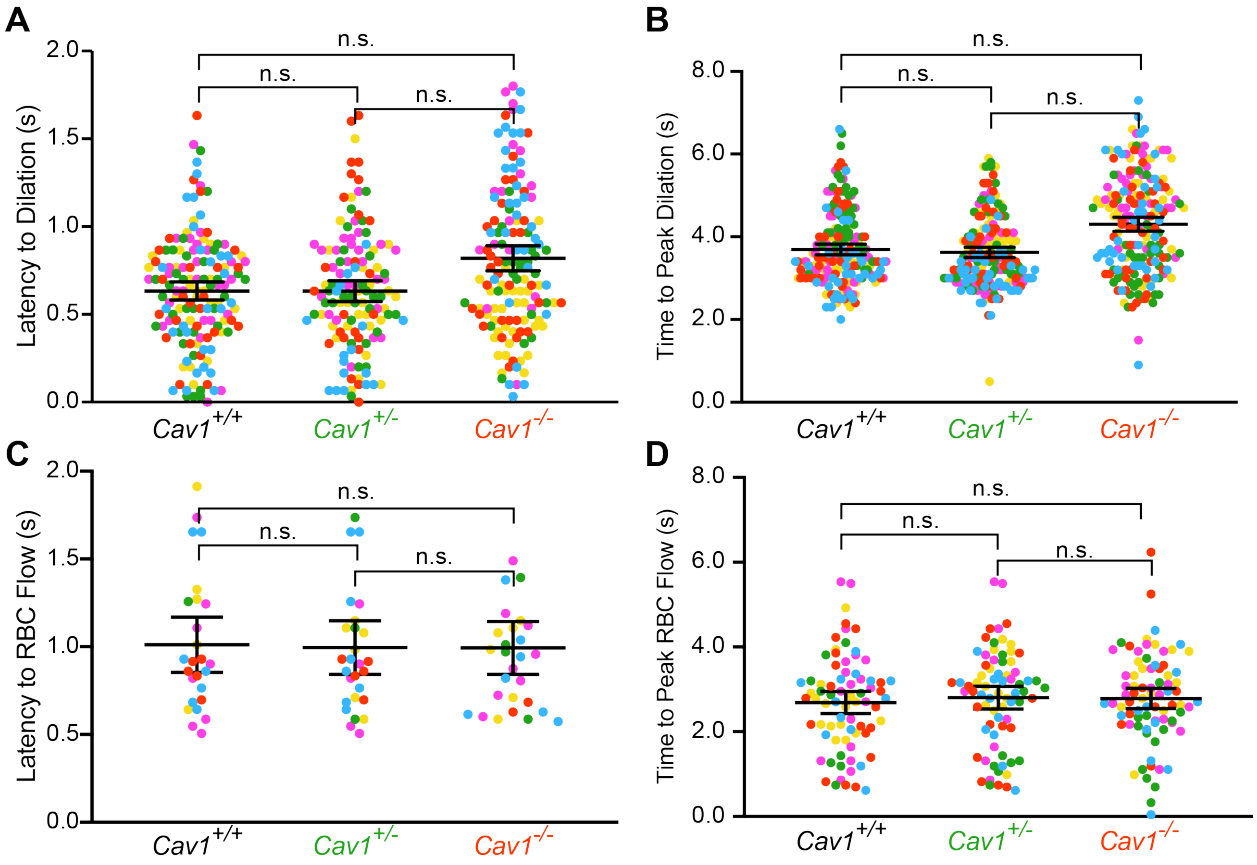

Supplementary Figure 11. Extended Data Fig. 2. *Cav1* knockout mice have normal neurovascular coupling kinetics. (**A,C)** Latency to changes in arteriolar dilation (**A**), and in capillary blood flow **(C)** in *Cav1*$^{+/+}$ (n=193 arteries, 40 capillaries, 5 mice), *Cav1*$^{+/-}$ (n= 123 arteries, 40 capillaries, 5 mice), *Cav1*$^{-/-}$ mice (n=153 arteries, 31 capillaries, 5 mice). Time to peak dilation (**B)** and time to peak RBC flow (**D)** in *Cav1*$^{+/+}$ (n=193 arteries, 40 capillaries, 5 mice), *Cav1*$^{+/-}$ (n= 123 arteries, 40 capillaries, 5 mice), *Cav1*$^{-/-}$ mice (n=153 arteries, 31 capillaries, 5 mice). Statistical significance was determined by nested, one-way ANOVA with a post hoc Bonferroni multiple comparison adjustment for (**A,B,C,D**). n.s., not significant.

Supplementary Figure 12. *Cav1* knockout mice have normal neural activity. (**A-C)** Quantification of change in neural activity via GCaMP6 fluorescence (**A**), % max change in GCaMP6s (**B**) and kinetics to peak change in GCaMPs (**C**) in *Cav1*$^{+/+}$*; Thy1:GCaMP6s* (n=78 neuropils, 5 mice) and *Cav1*$^{-/-}$*; Thy1:GCaMP6s* (n=78 neuropils, 5 mice). All data is mean ± s.e.m. Statistical significance was determined by a nested unpaired, two-tailed t-test for (**B,C)**. n.s., not significant.

Supplementary Figure 12 (Continued)

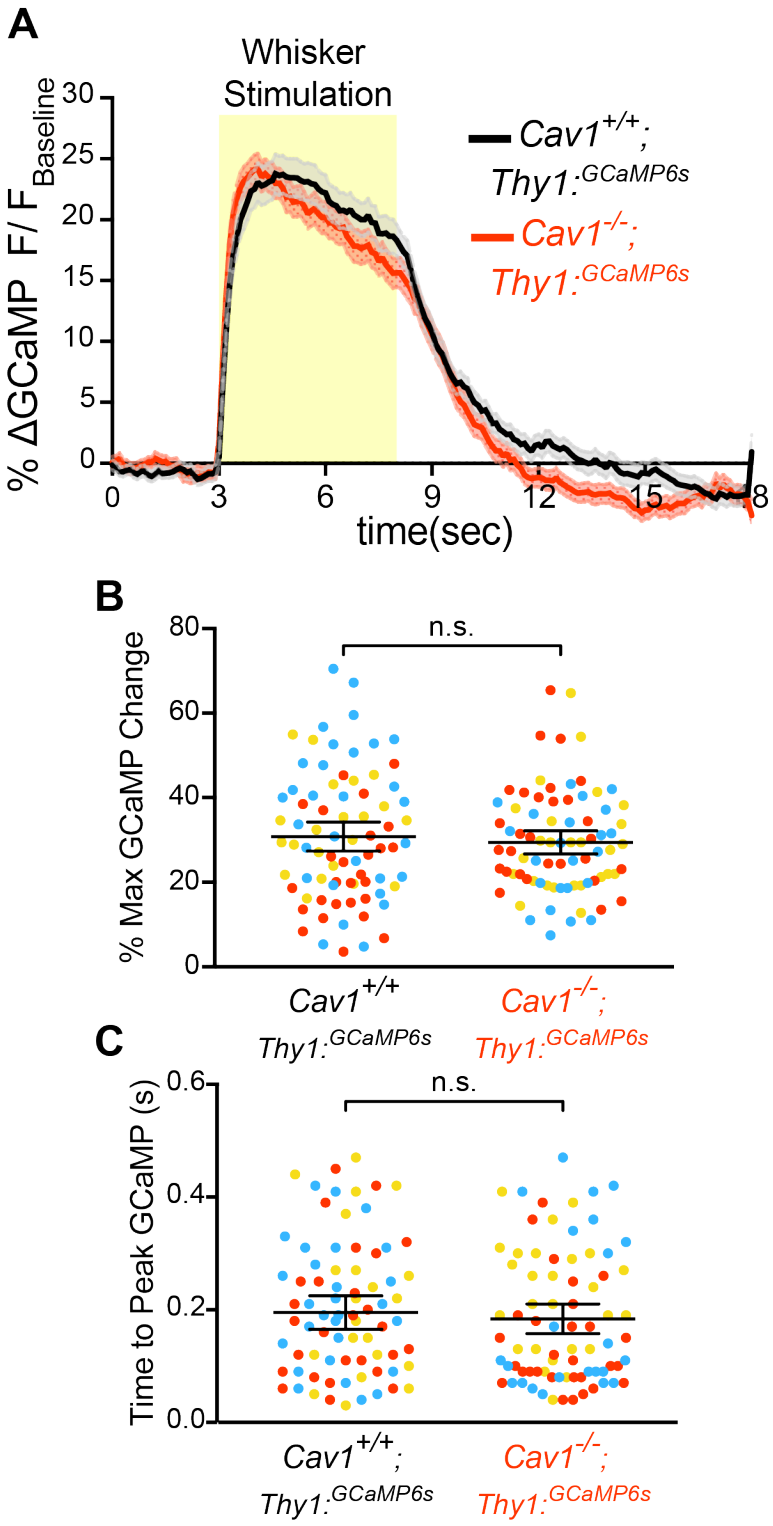

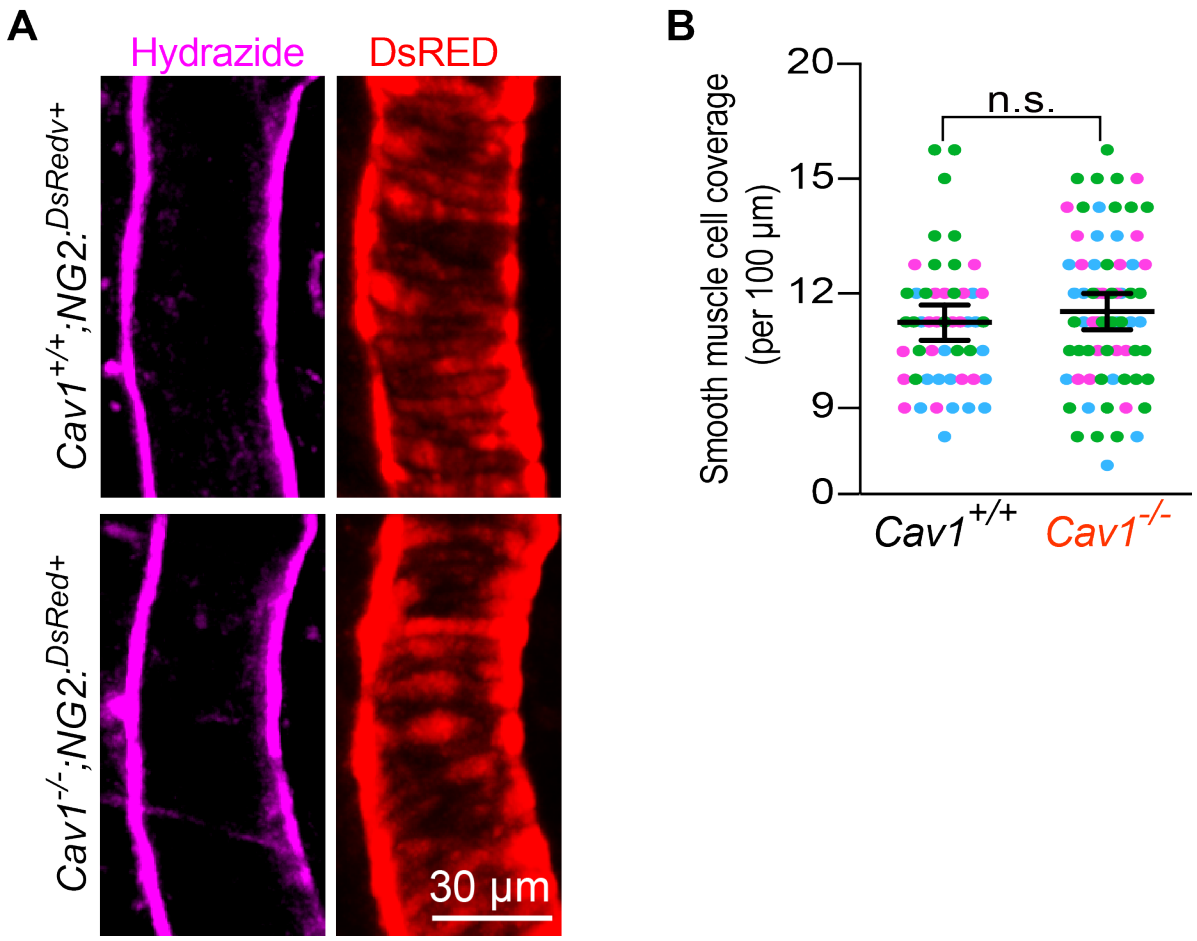

Supplementary Figure 13. *Cav1* mutant mice exhibit normal smooth muscle cell integrity. (**A)** *In vivo* two-photon microscopy images of hydrazide (purple) and DsRed (red) from *Cav1*$^{+/+}$, *NG2:*$^{DsRED+}$ *and Cav1*$^{-/-}$, *NG2:*$^{DsRED+}$ mice. Scale bar, 30 µm. (**B)** Quantification of DsRED+ smooth muscle cells per 100 µm as shown in (**A**) in *Cav1*$^{+/+}$ (n= 3 mice, 27 arterioles) and *Cav1*$^{-/-}$ (n= 3 mice, 28 arterioles). Statistical significance was determined by nested, unpaired, two-tailed t-test for (**B**). Data shown as mean ± s.e.m. (n.s., not significant).

Supplementary Figure 14. *Cav1* mutant mice exhibit normal smooth muscle cell signaling. (**A)** Still frame images of arterioles labeled with hydrazide in acute brain slices from *Cav1*$^{+/+}$ and *Cav1*$^{-/-}$ mice using two-photon microscopy. Left image shows arterioles during baseline, middle image shows during U46619 (thromboxane agonist) treatment and right image shows during DEA-NONOate (NO donor) treatment. White hashes outline the arterioles during baseline based on time =0. Scale bar is 30 μm. (**B-D)** Quantification of changes in arteriolar contraction by U46619 (arrow) and dilation back to baseline by DEA-NONOate (arrowhead). (**B)** Quantification of max arteriolar contraction by U46619 (**C)** and max arteriolar dilation relative to contracted baseline by DEA-NONOate (**D)** on acute brain slices from *Cav1*$^{+/+}$ (n= 5 mice, 19 arterioles) and *Cav1*$^{-/-}$ (n= 5 mice, 22 arterioles). Statistical significance was determined by nested, unpaired, two-tailed t-test for (**C,D**). Data shown as mean ± s.e.m. (n.s., not significant).

Supplementary Figure 14 (Continued)

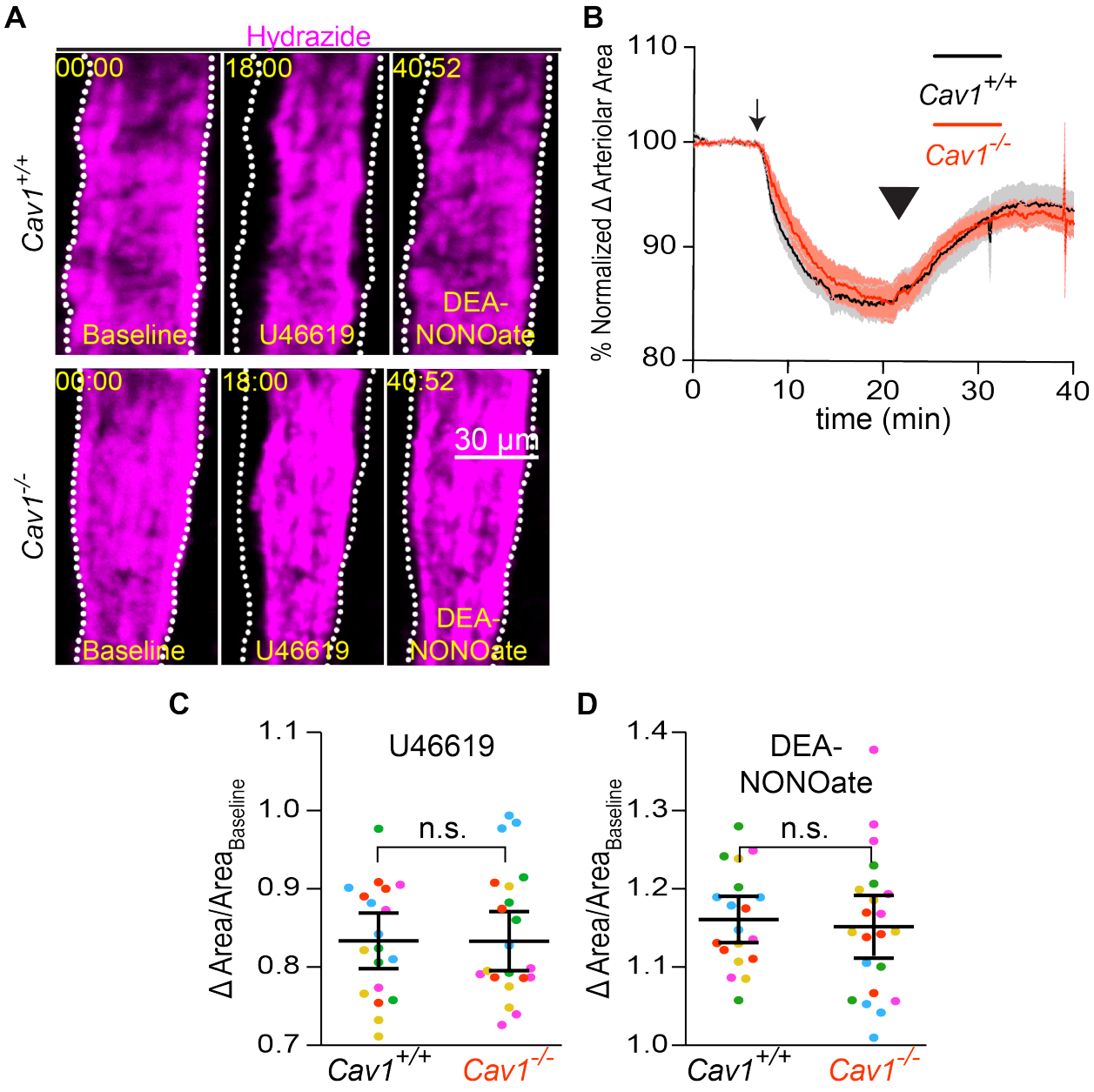

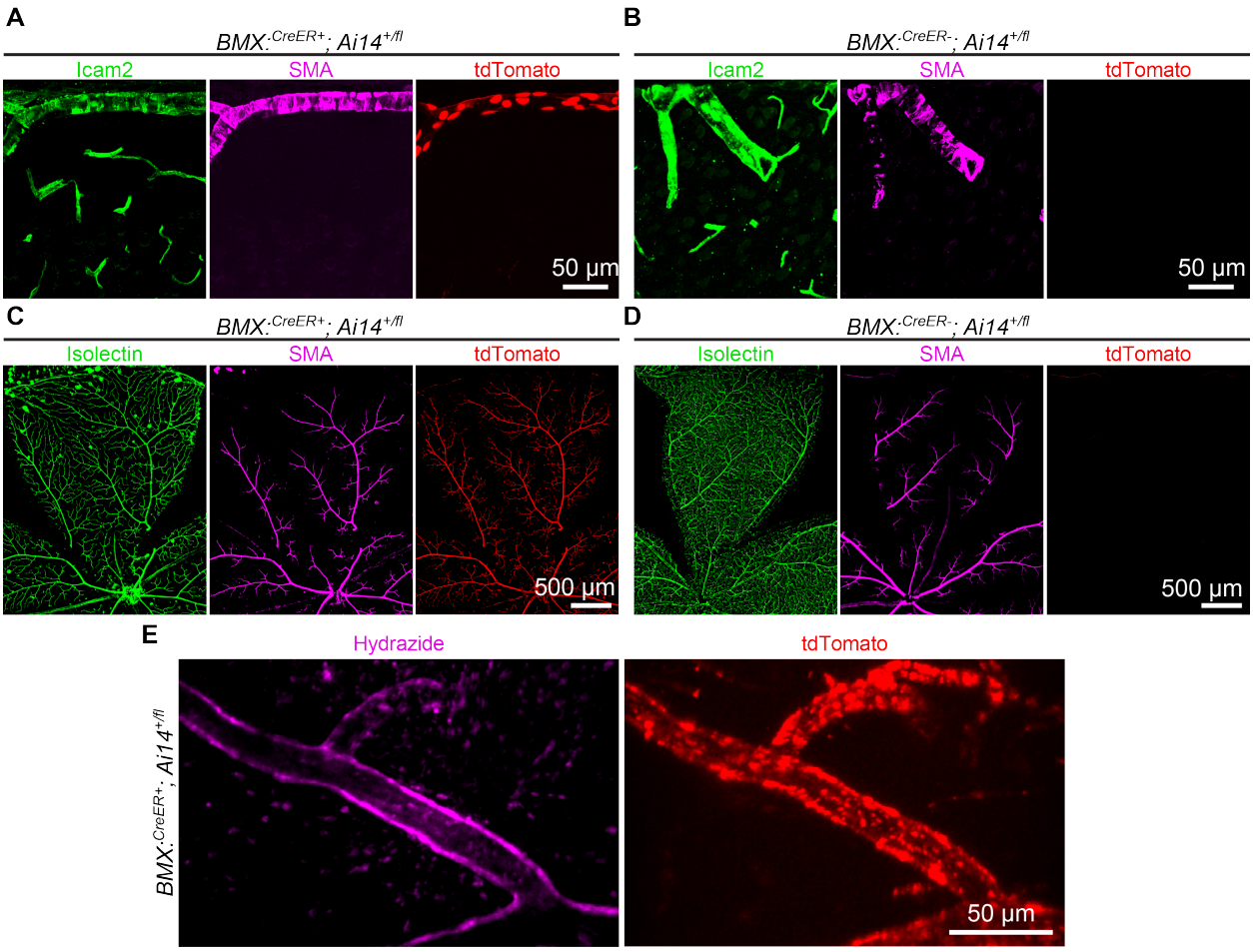

Supplementary Figure 15. *BMX:CreER* targets aECs. (A-B) Immunostaining on adult brain sections from tamoxifen-injected, reporter *BMX:*$^{CreER+}$*; Ai14*$^{+/fl}$ (**A**) and control *BMX:*$^{CreER-;}$ *Ai14*$^{+/fl}$ mice (**B**) for endothelial cells (Icam2, green) and arterioles (SMA, magenta). Endogenous Cre-dependent tdTomato is in red. Scale bar, 50 µm. **(C-D)** Immunostaining on adult retinas from tamoxifen-injected, reporter, *BMX:*$^{CreER+;}$ *Ai14*$^{+/fl}$ (**C**) and control, *BMX:*$^{CreER-;}$ *Ai14*$^{+/fl}$ mice (**D**) for endothelial cells (isolectin, green) and arterioles (SMA, magenta). Endogenous Cre-dependent tdTomato is in red. Scale bar, 500 µm. **(E)** *In vivo* two-photon imaging of endogenous tdTomato in reporter, *BMX:*$^{CreER+;}$ *Ai14*$^{+/fl}$ mice injected with hydrazide (magenta). Scale bar, 50 µm.

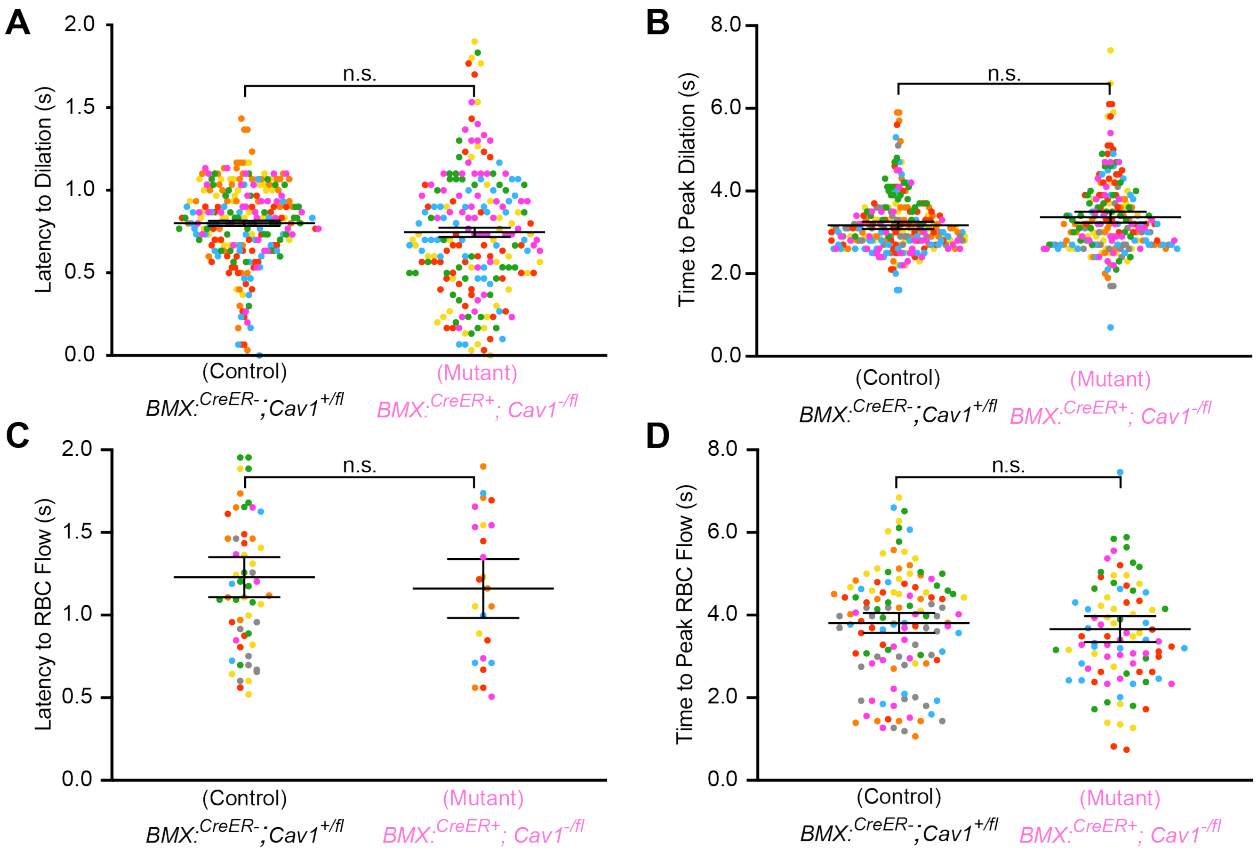

Supplementary Figure 16. *BMX:CreER* targets aECs. (A-B) Conditional aEC-specific *Cav1* knockout mice have normal neurovascular coupling kinetics. (A) Quantification of latency to changes in arteriolar dilation in control (*BMX:$^{CreER-}$; Cav1$^{+/fl}$*; n=7 mice, 234 arterioles) and aEC-specific conditional Cav1 mutant (*BMX:$^{CreER+}$; Cav1$^{-/fl}$*; n=5 mice; 202 arterioles) mice. **(B)** Quantification of time to peak arteriolar dilation in (*BMX:$^{CreER-;}$ Cav1$^{+/fl}$*; n=7 mice, 234 arterioles) and aEC-specific conditional Cav1 mutant (*BMX:$^{CreER+;}$ Cav1$^{-/fl}$*; n=5 mice; 202 arterioles) mice. **(C)** Quantification of latency to RBC flow in in (*BMX:$^{CreER-}$; Cav1+/fl*; n n=7 mice; 58 capillaries) and aEC-specific conditional Cav1 mutant (*BMX:$^{CreER+}$; Cav1-/fl*; n=5 mice; 25 capillaries) mice. **(D)** Quantification of time to peak RBC flow in (*BMX:$^{CreER-}$; Cav1$^{+/fl}$*; n=7 mice, 127 capillaries) and aEC-specific conditional Cav1 mutant (*BMX:$^{CreER+}$; Cav1$^{-/fl}$*; n=5 mice; 94 capillaries) mice. Statistical significance was determined by a nested unpaired, two-tailed t-test for (**A-D**). n.s., not significant.

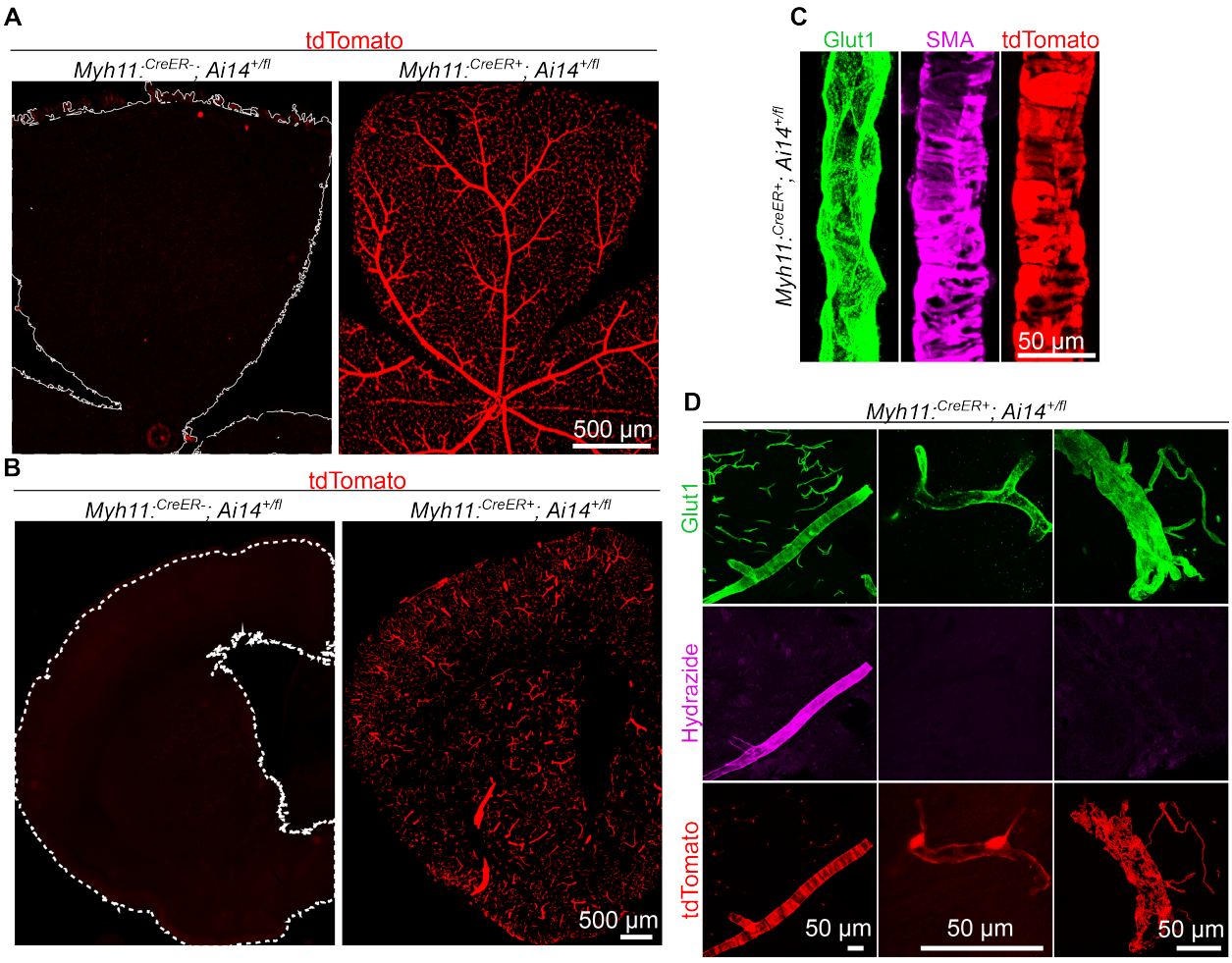

Supplementary Figure 17. *Myh11:CreER* targets mural cells, including smooth muscle cells. (A,B) Endogenous tdTomato signal (red) in adult retinas (**A**) and brain sections (**B**) from tamoxifen-injected control, *Myh11:*$^{CreER-;}$ *Ai14*$^{+/fl}$ and reporter, *Myh11:*$^{CreER+}$*; Ai14*$^{+/fl}$ mice. Scale bar, 500 µm. **(C)** Immunostaining on brain sections from reporter, *Myh11:*$^{CreER+}$*; Ai14*$^{+/fl}$ mice for (Glut1, green) and arterioles (SMA, magenta). Scale bar, 50 µm. (**D**) Immunostaining for Glut1 (green) and hydrazide (magenta) show that tdTomato signal is observed in all mural cells, including arteriolar smooth muscle cells (right column), capillary pericytes (middle column) and venular smooth muscle cells (left column). Scale bar, 50 µm.

Supplementary Figure 18. Generation of a conditional SMC-specific *Cav1* knockout (A) Immunostaining on brain sections for endothelial cells (Icam2, green), smooth muscle cells (SMA, magenta) and Cav1 (red) from control and SMC conditional Cav1 mutant mice. Scale bar, 15 μm. **(B)** EM images of CNS aECs and SMCs from control and SMC conditional *Cav1* mutant mice. Arrowheads point to caveolae. L, Lumen. aEC, arteriolar endothelial cells. SMC, smooth muscle cells. Scale bar, 100 nm. **(C)** Quantification of mean normalized immunofluorescene of Cav1 in SMCs from control (n= 5 mice) and SMC-specific conditional *Cav1* mutant mice (n=5 mice). **(D)** Quantification of the mean vesicular density in aECs and smooth muscle cells between control (n= 5 mice, 23 arterioles) and SMC conditional Cav1 mutant mice (n=5 mice, 22 arterioles). Statistical significance was determined by Mann Whitney test for (**C**) and a nested, unpaired, two-tailed t-test for (**D**). Data shown as mean ± s.e.m. (**,P<0.01, ***P<0.001, n.s., not significant).

Supplementary Figure 18 (Continued)

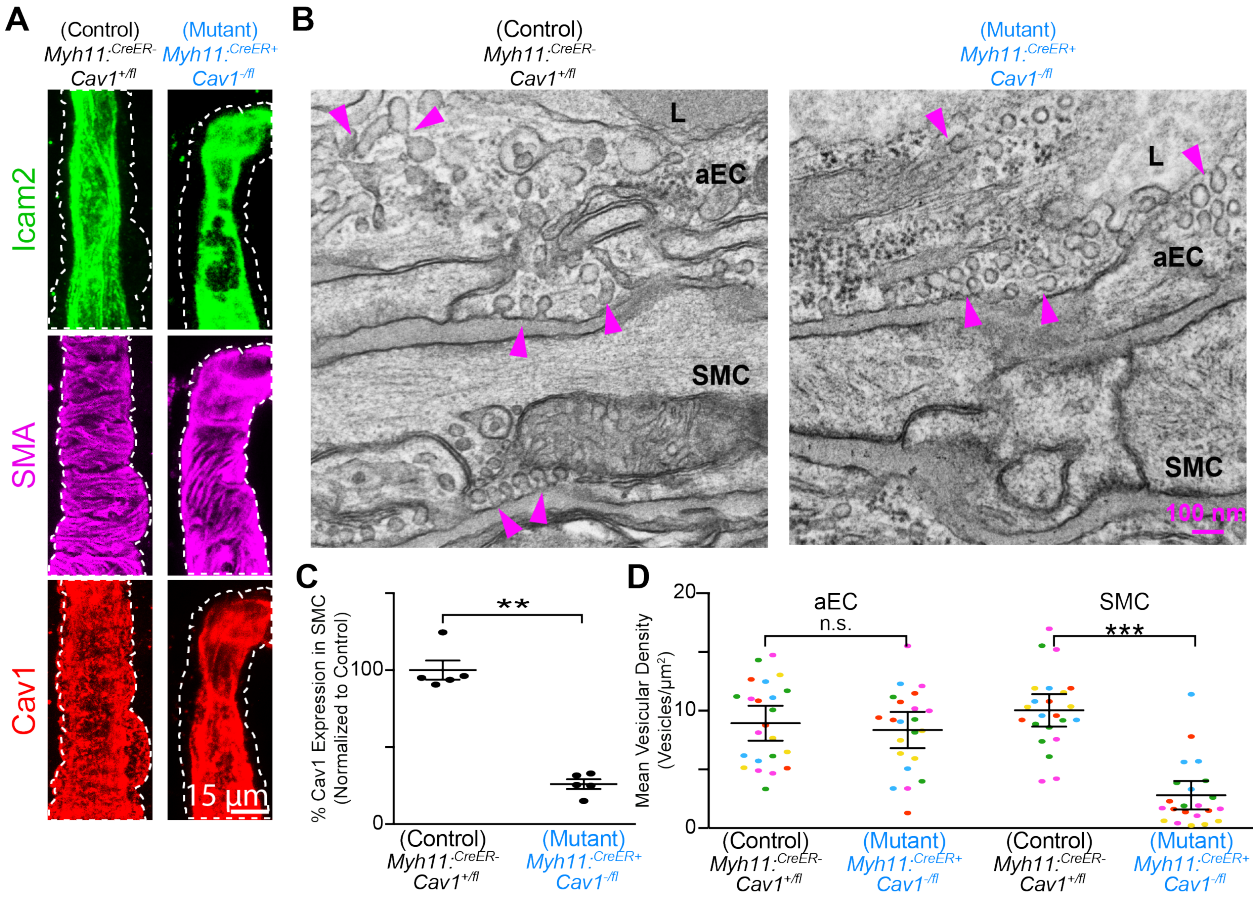

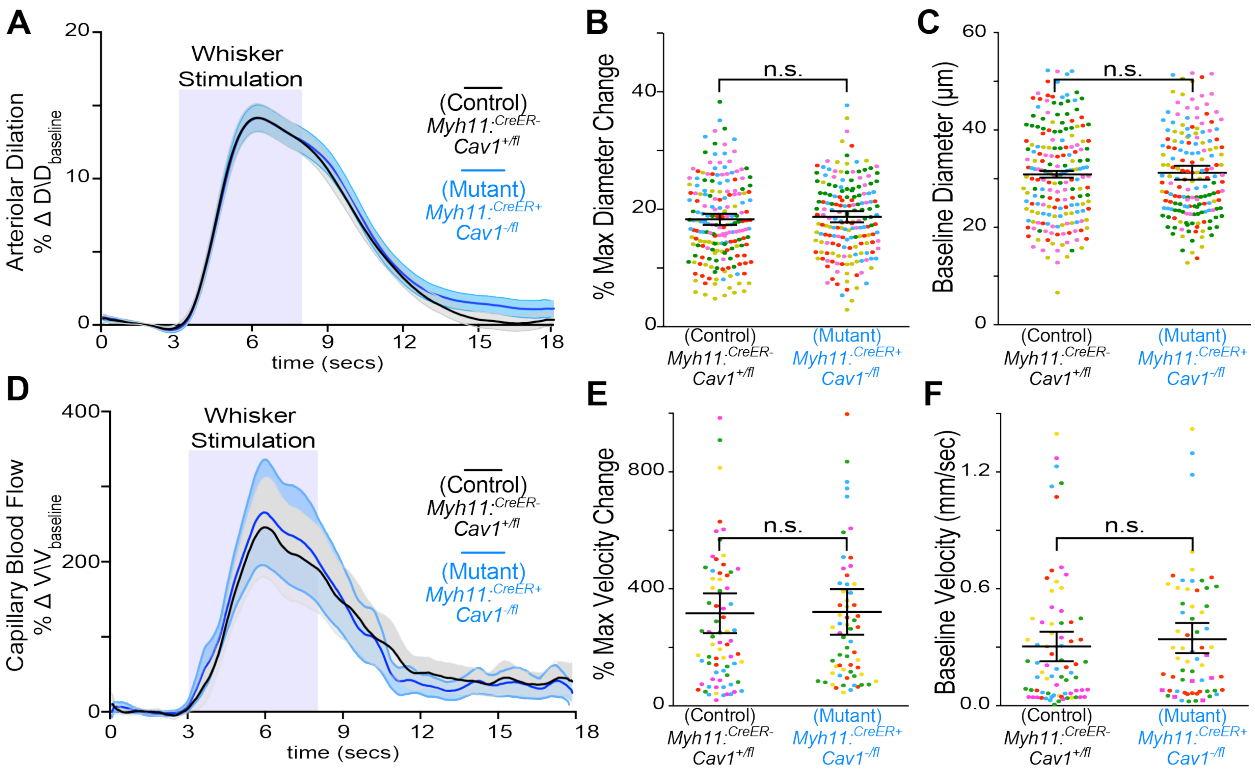

Supplementary Figure 19. Conditional SMC-specific *Cav1* knockout mice have normal neurovascular coupling (A-C) Quantification of change in arteriolar dilation (**A**), % max change in arteriolar dilation (**B**) and baseline diameter (**C**) in control (n= 7 mice, 193 arterioles) and SMC conditional *Cav1* mutant mice (n= 5 mice, 176 arterioles). **(D-F)** Quantification of change in red blood cell velocity (**D**), % max change in red blood cell velocity (**E**) and baseline velocity (**F**) in control (n= 7 mice, 75 capillaries) and SMC conditional Cav1 mutant mice (n=5 mice, 64 capillaries). Statistical significance was determined by a nested, unpaired, two-tailed t-test for (**B,C,E,F**). Data shown as mean ± s.e.m. (**,P<0.01, ***P<0.001, n.s., not significant).

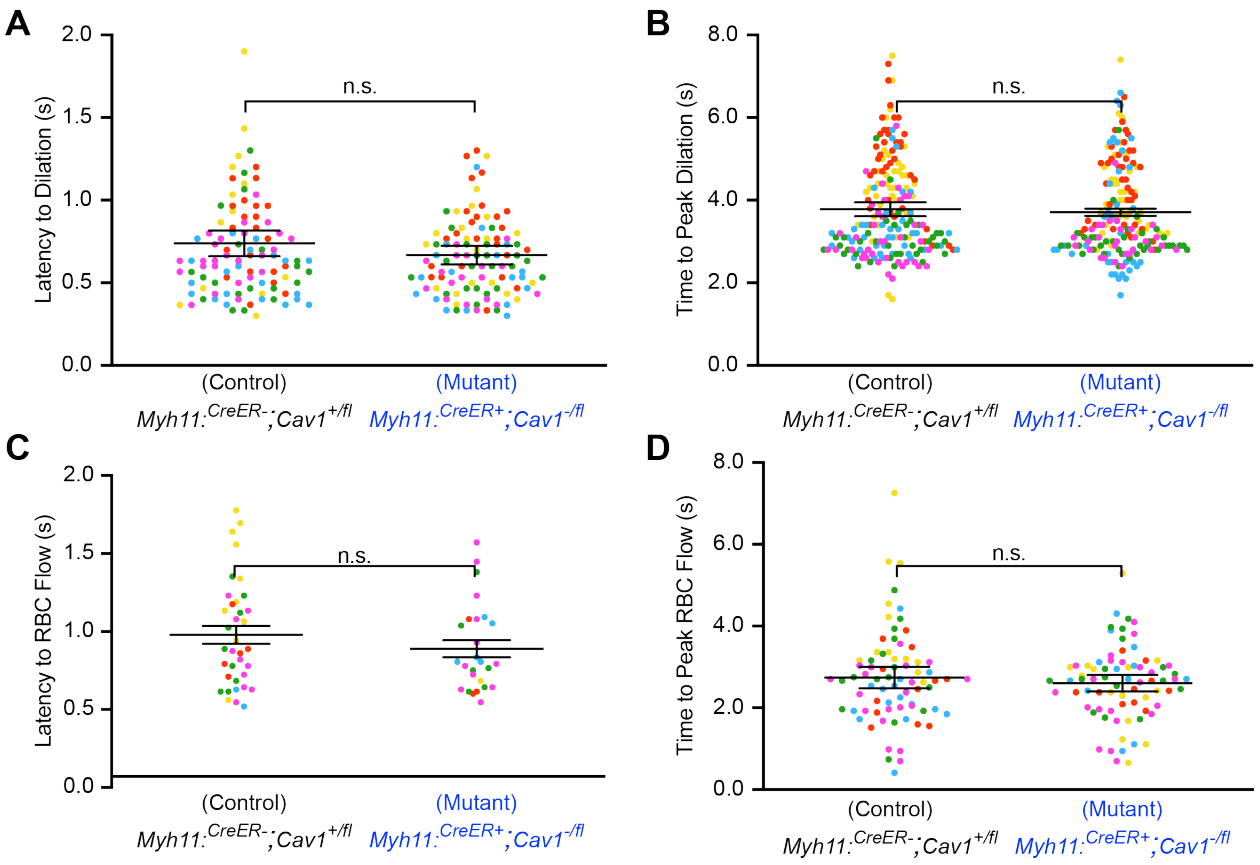

Supplementary Figure 20. Conditional SMC-specific *Cav1* knockout mice have normal neurovascular coupling kinetics. (A) Quantification of latency to changes in arteriolar dilation in control (*Myh11:$^{CreER-}$; Cav1$^{+/fl}$*; n=5 mice, 103 arterioles) and SMC conditional Cav1 mutant (*Myh11:$^{CreER+}$; Cav1$^{-/fl}$*; n=5 mice; 107 arterioles) mice. **(B)** Quantification of time to peak arteriolar dilation in (*Myh11:$^{CreER-}$; Cav1$^{+/fl}$*; n=5 mice, 193 arterioles) and SMC conditional Cav1 mutant (*Myh11:$^{CreER+}$; Cav1$^{-/fl}$*; n=5 mice; 180 arterioles) mice. **(C)** Quantification of latency to RBC flow in (*Myh11:$^{CreER-}$; Cav1$^{+/fl}$*; n=5 mice; 36 capillaries) and SMC conditional Cav1 mutant (*Myh11:$^{CreER+}$; Cav1$^{-/fl}$*; n=5 mice; 26 capillaries) mice. **(D)** Quantification time to peak RBC flow in (*Myh11:$^{CreER-}$; Cav1$^{+/fl}$*; n=5 mice; 75 capillaries) and SMC conditional Cav1 mutant (*Myh11:$^{CreER+}$; Cav1$^{-/fl}$*; n=5 mice; 75 capillaries) mice. Statistical significance was determined by a nested unpaired, two-tailed t-test for (**A-D**). n.s., not significant.

Supplementary Figure 21. *Cav1* mutant mice have normal levels of eNOS protein in CNS aECs. (A) Immunostaining on adult brain sections for endothelial cells (Pecam1, green), arterioles (SMA, magenta) and eNOS (cyan) from $Cav1^{+/+}$, $enos^{+/+}$, $Cav1^{-/-}$, $enos^{+/+}$ and $Cav1^{+/+}$, $enos^{-/-}$. Scale bar, 50 μm. **(B)** Quantification of eNOS immunofluorescene intensity as shown in (**A)** in aECs from $Cav1^{+/+}$, $enos^{+/+}$ (n= 3 mice, 35 images), $Cav1^{-/-}$, $enos^{+/+}$ (n= 3 mice, 35 images), and $Cav1^{+/+}$, $enos^{-/-}$ (n= 3 mice, 37 images). Statistical significance was determined by nested, unpaired, two-tailed t-test for (**B**). Data shown as mean ± s.e.m. (***P<0.001, n.s., not significant).

Supplementary Figure 21 (Continued)

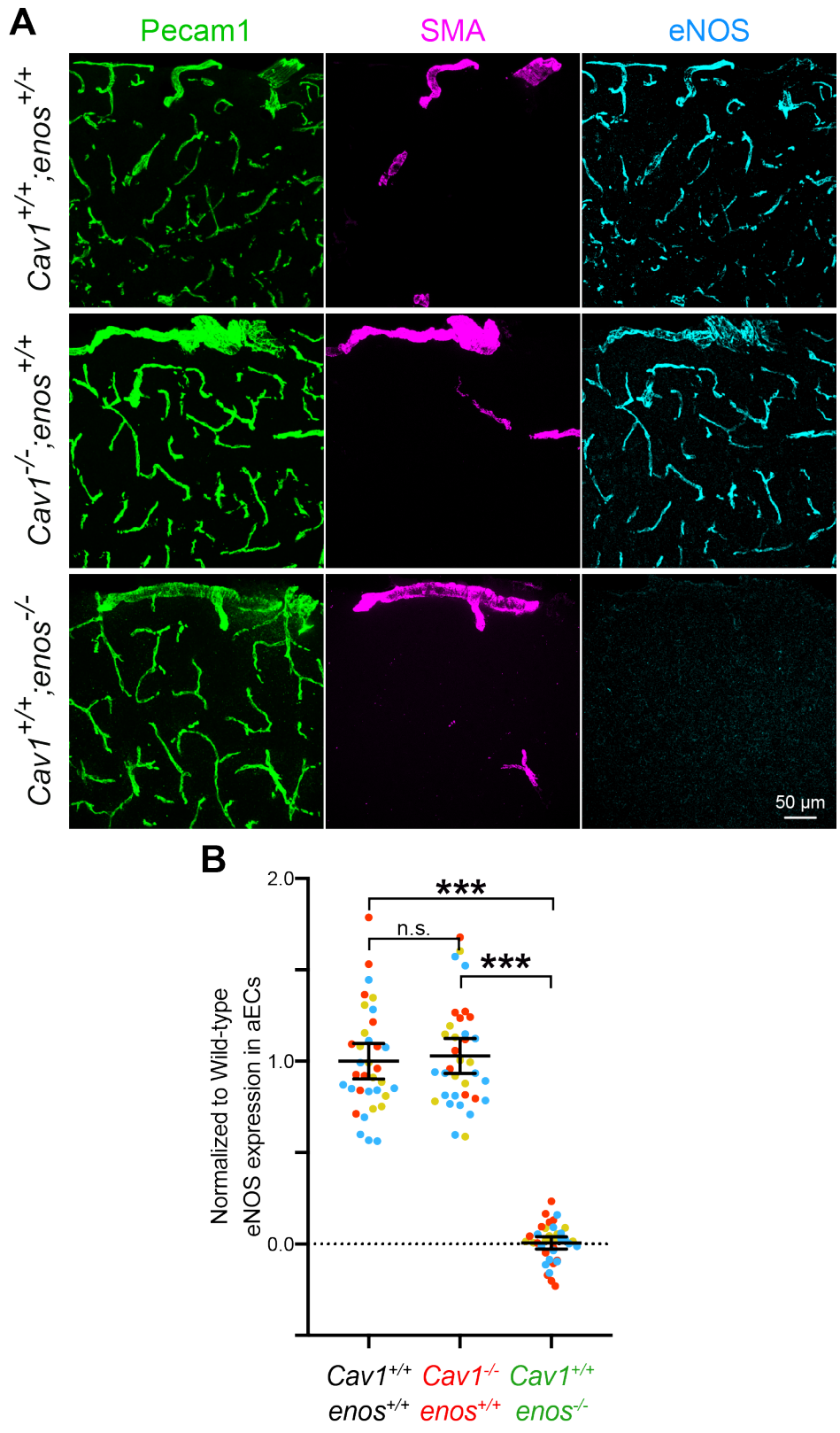

Supplementary Figure 22. *Cav1* mutant mice have normal levels of nitric oxide in CNS aECs. (A) Immunostaining on adult brain sections for endothelial cells (Pecam1, green) and arterioles (SMA, magenta) after *in vivo* perfusion of NO sensitive dye- DAF-2, yellow $Cav1^{+/+}$, $enos^{+/+}$, $Cav1^{-/-}$, $enos^{+/+}$, and $Cav1^{+/+}$, $enos^{-/-}$. Scale bar, 10 μm. **(B)** Quantification of DAF-2 intensity in aECs as shown in (**A)** from $Cav1^{+/+}$, $enos^{+/+}$ (n= 4 mice, 73 images), $Cav1^{-/-}$, $enos^{+/+}$ (n= 4 mice, 71 images), and $Cav1^{+/+}$, $enos^{-/-}$ (n= 4 mice, 64 images). Statistical significance was determined by nested, unpaired, two-tailed t-test for (**B**). Data shown as mean ± s.e.m. (***P<0.001, n.s., not significant).

Supplementary Figure 22 (Continued)

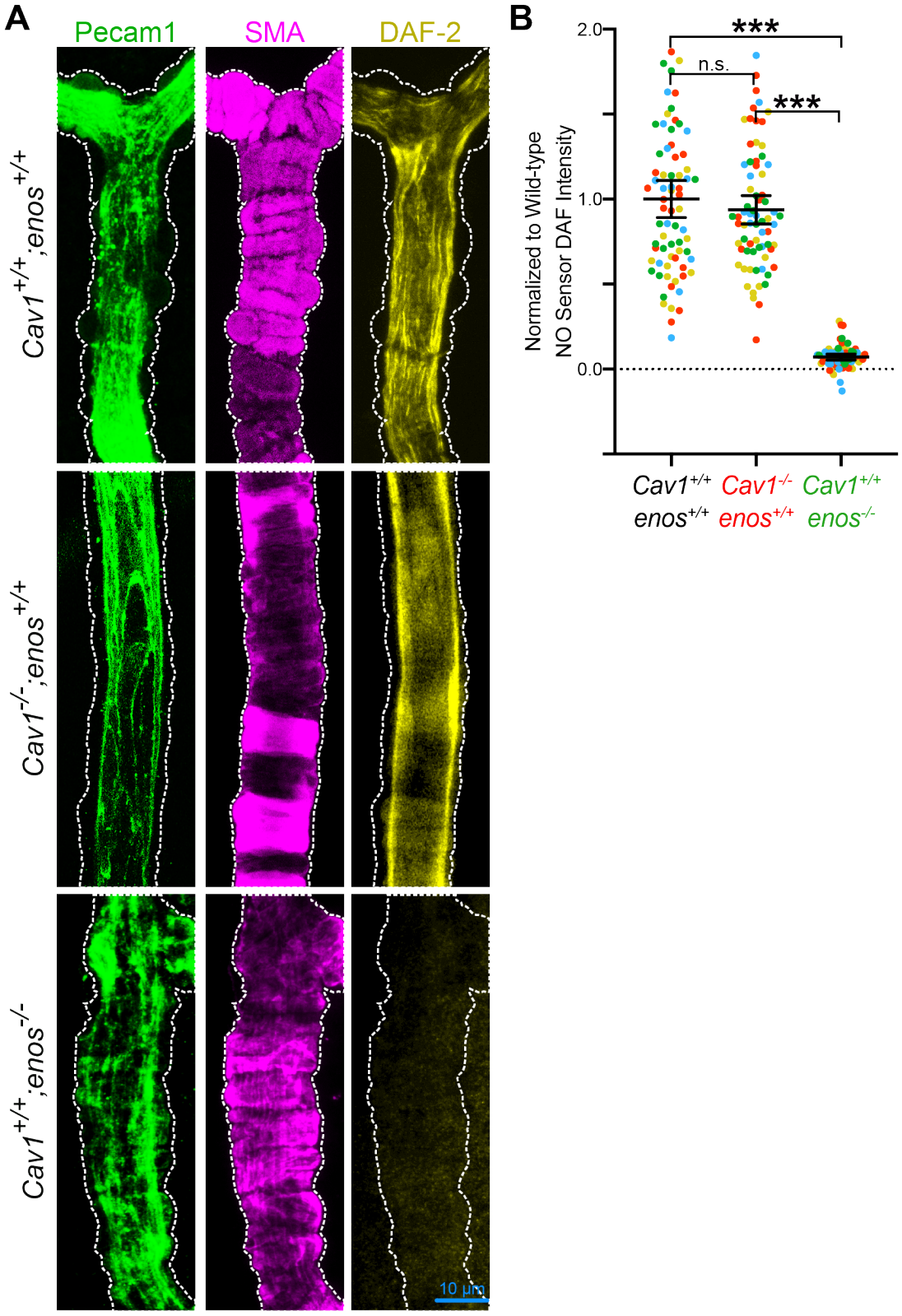

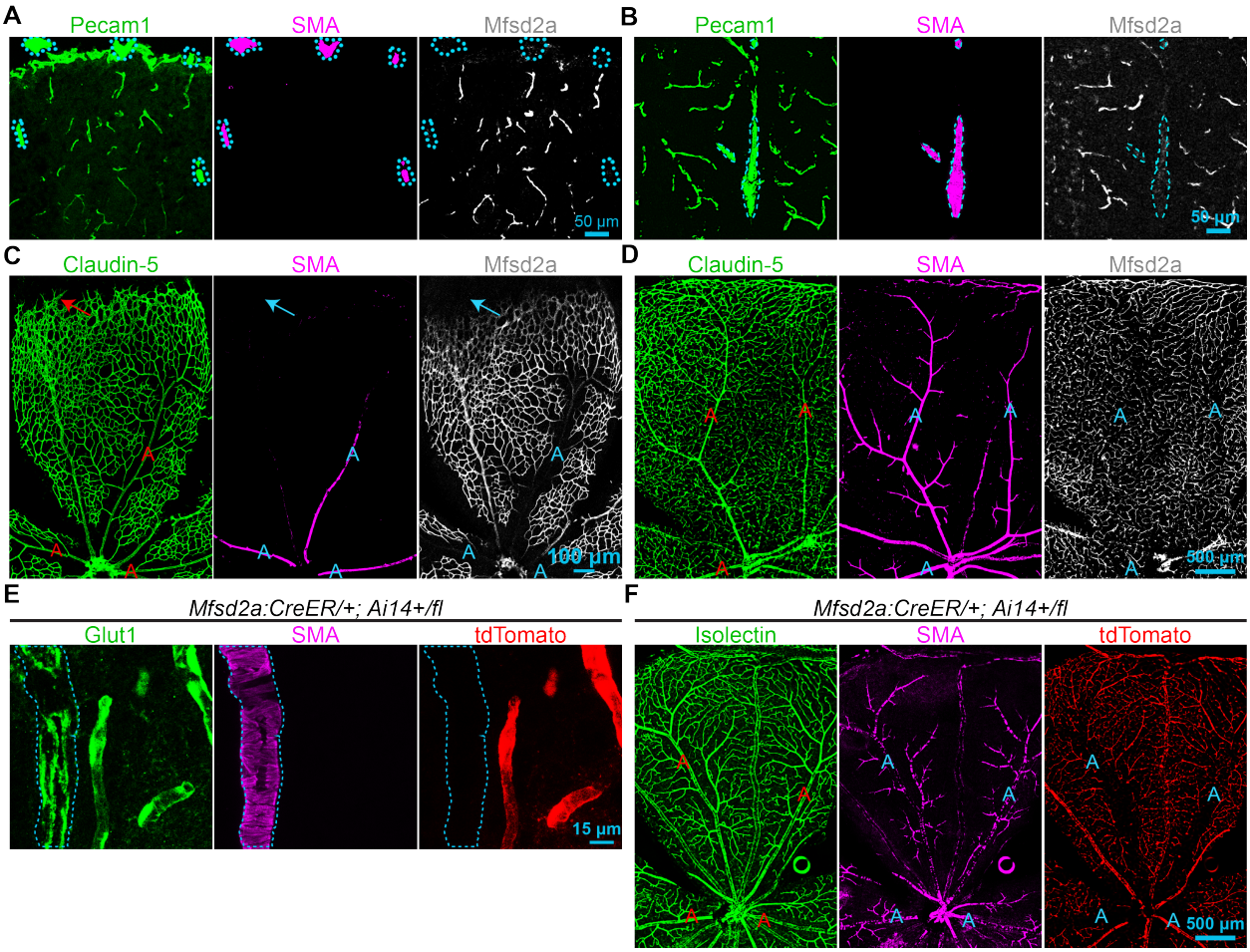

Supplementary Figure 23. Mfsd2a is undetected in CNS arterioles in brain and retina. **(A,B)** Immunostaining on P5 (**A**) and adult (**B)** brain sections for endothelial cells (Pecam1, green), smooth muscle cells (SMA, magenta) and Mfsd2a (white) from wildtype mice. Blue hashes outline SMA+ arterioles. Scale bar, 50 µm. **c,d,** Immunostaining on P5 (**C**) and adult (**D)** retina for endothelial cells (Claudin-5, green), smooth muscle cells (SMA, magenta) and Mfsd2a (white) from wildtype mice. A- arterioles. Scale bar, 100 and 500 µm respectively. Note that Mfsd2a is absent in nascent, distal vessel (arrows) in P5 retina in (**C**). **(E,F)** Tamoxifen-treated, adult knock-in Mfsd2a:$^{CreER+}$; Ai14$^{+/fl}$ reporter mice demonstrates that tdTomato is present in SMA+ arterioles but not SMA- capillaries in brain (**E)** and retina (**F**). Blue hashes and A- SMA+ arterioles. Scale bar in (**e**) and (**f**) is 15 and 500 µm respectively.

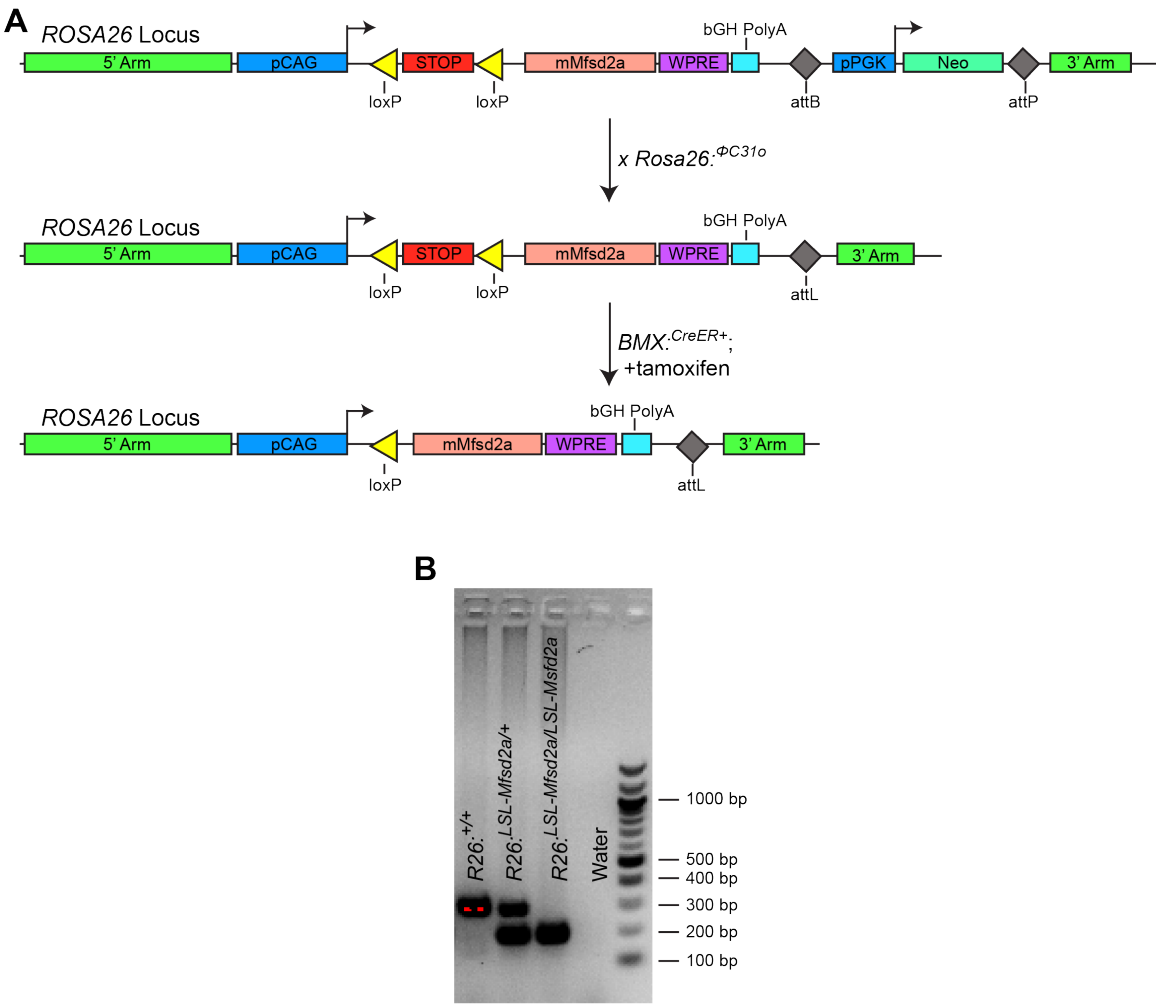

Supplementary Figure 24. Generation of a Cre-dependent Mfsd2a overexpression transgenic mouse. (A) Construct of the Cre-dependent Mfsd2a overexpression knocked-in the ROSA26 locus. Mating with *ROSA26:Φ C31* recombinase mice removes the neomycin selection cassette. Further mating with *BMX:CreER* and tamoxifen injection allows ecoptic overexpression of Mfsd2a in aECs. **(B)** PCR genotyping of Cre-dependent Mfsd2a overexpression mice.

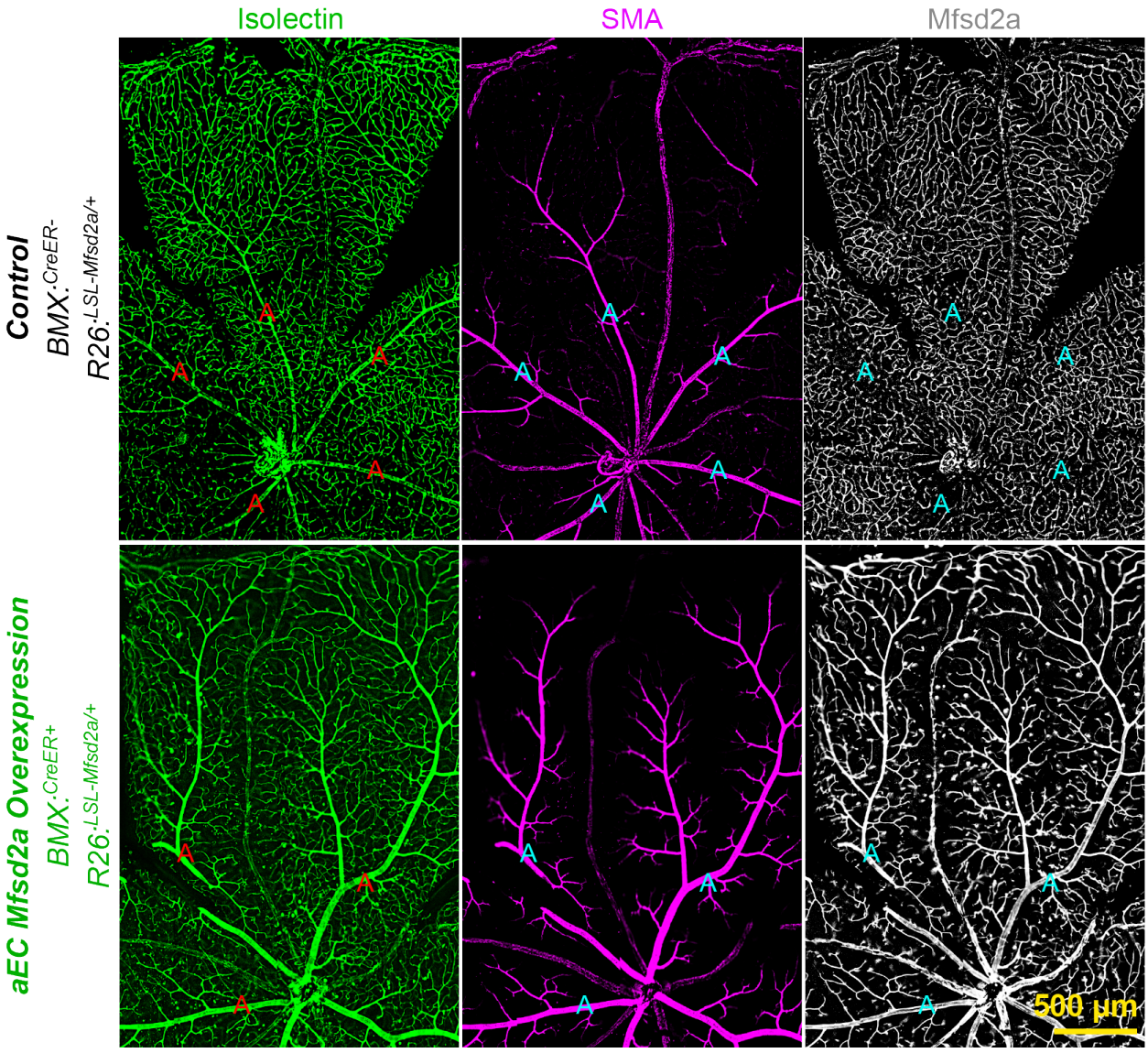

Supplementary Figure 25. Ectopic Mfsd2a overexpression in retinal arterioles. (A) Immunostaining on adult retinas for endothelial cells (isolectin, green), smooth muscle cells (SMA, magenta) and Mfsd2a (white) from control and aEC-specific Mfsd2a overexpression mice. Scale bar, 500 µm

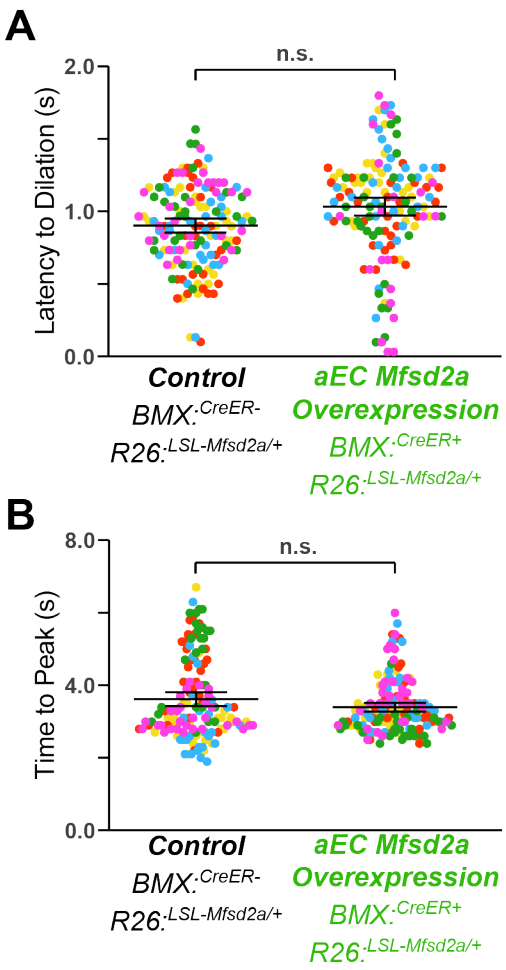

Supplementary Figure 26. Ectopic Mfsd2a overexpression in CNS arterioles does not impair neurovascular coupling kinetics. (A) Quantification of latency to changes in arteriolar dilation in control (*BMX:*$^{CreER-}$*; R26:*$^{LSL\text{-}Mfsd2a/+;}$ n=5 mice, 149 arterioles) and aEC-specific Mfsd2a overexpression (*BMX:*$^{CreER+}$*; R26:*$^{LSL\text{-}Mfsd2a/+;}$n=5 mice; 138 arterioles) mice. **(B)** Quantification of time to peak arteriolar dilation in (*BMX:*$^{CreER-}$*; R26:*$^{LSL\text{-}Mfsd2a/+;}$ n=5 mice, 149 arterioles) and aEC-specific conditional Cav1 mutant (*BMX:*$^{CreER+}$*; R26:*$^{LSL\text{-}Mfsd2a/+;}$n=5 mice; 138 arterioles) mice. Statistical significance was determined by a nested unpaired, two-tailed t-test for (**A,B**). n.s., not significant.